Fabrication and Characterization of Poly(methyl methacrylate) (PMMA) Nanocomposites with Organically Modified Montmorillonite (MMT) and Layered Double Hydroxides (LDHs)

A Dissertation Submitted to the
Indian Institute of Technology Guwahati
as Partial Fulfillment for the Degree of

DOCTOR of PHILOSOPHY

by

Manish Kumar

Roll No: 10610713

Department of Chemical Engineering

Indian Institute of Technology Guwahati

Guwahati – 781039, Assam, India

April 2016

STATEMENT

I hereby declare that the scientific matter embodied in this thesis entitled, "**Fabrication and Characterization of Poly(methyl methacrylate) (PMMA) Nanocomposites with Organically Modified Montmorillonite (MMT) and Layered Double Hydroxides (LDHs)**" is the outcome of the research work carried out by me under the supervision of Prof. G. Pugazhenthi, at the Department of Chemical Engineering, Indian Institute of Technology Guwahati, Guwahati, Assam, India, for the award of the degree of Doctor of Philosophy. To the best of my knowledge, the work delineated on this thesis is original and has not been submitted elsewhere for any degree of any other Institute or University.

In keeping with the scientific tradition, whatever work done by others has been utilized, due acknowledgement has been made.

IIT Guwahati
April 2016

Manish Kumar
Candidate

Dr. G. Pugazhenthi
Professor
Department of Chemical Engineering
Indian Institute of Technology Guwahati
Guwahati – 781039, Assam, India
Tel: +91- 361 2582264; Fax: +91 - 361 2582291
Email: pugal@iitg.ernet.in

CERTIFICATE

Certified that the work described in this thesis entitled "**Fabrication and Characterization of Poly(methyl methacrylate) (PMMA) Nanocomposites with Organically Modified Montmorillonite (MMT) and Layered Double Hydroxides (LDHs)**" by Mr. Manish Kumar, Department of Chemical Engineering, Indian Institute of Technology Guwahati has been carried out under my supervision and has not been submitted elsewhere for a degree.

April 2016

Prof. G. Pugazhenthi
Thesis supervisor
Department of Chemical Engineering
Indian Institute of Technology Guwahati
Guwahati – 781039, Assam, India

Dedicated To

A.P.J. Abdul Kalam,

My Parents

&

Beloved Sisters 'Archana' and 'Manupriya'

Acknowledgements

Though only my name appears on the cover of this dissertation, a great many people have contributed to its production. I owe my gratitude to all those people who have made this dissertation possible and because of whom my graduate experience has been one that I will cherish forever.

First of all, I wish to express my sincere gratitude and heartfelt thanks to my research supervisor, **Prof. G. Pugazhenthi**, for given me an opportunity to pursue this research work, and for his precious advice, continuous care, guidance, encouragement, and supervision of the research. I must acknowledge the unconditional freedom to think, plan, execute and express, that I was given in every step of my research work, while keeping faith and confidence on my capabilities. Through him I have learnt how to write a scientific article and enhance its quality, which have extensively contributed to the writing of my Ph.D. thesis. It has been a great privilege to work under a humble and genuine person like him.

Secondly, my gratitude goes to my doctoral committee, **Prof. Kaustubha Mohanty, Prof. Aloke Kumar Ghoshal, Dr. Venkatesh R. Prasanna**, Department of Chemical Engineering and **Dr. S. Senthilvelan**, Department of Mechanical Engineering for their periodic assessments of the findings of my research and their constructive suggestions, which helped me to improve my work pertaining to Ph.D. thesis. I am especially thankful to Dr. S. Senthilvelan for his valuable inputs and coherent suggestions which contributed enormously to enhance the quality of my research work.

I must express my sincere thanks to **Dr. Anil Verma, Dr. Pradeep Upadhyaya** and **Dr. Hitendra Nath Chaubey**, CIPET Lucknow for arranging the necessary documents required at the initial stage of doctoral work. I am also thankful to **Prof. Pallab Ghosh, Dr. Chandan Das, Dr. V.V. Goud** and **Dr. T.K. Mandal** for helping in various stages of research work.

I owe special thanks to **Dr. S. Kanagaraj**, Department of Mechanical Engineering for allowing me to work in Material Science Laboratory. I am thankful to **Dr. N. Shanmuga Priya** for helping in rheology analysis. I am also thankful to **S. Arun** and **Jiten Basumatary** for assisting in material compounding. It is my pleasure to work with **A. Murthuraja** in tribology laboratory. I must acknowledge **S. Narendren** from CoE-SUSPOL for assisting in water vapor transmission

rate (WVTR) test. I am also thankful to **Amit Kumar**, IICT Hyderabad for assisting in TGA analysis.

I would like to thank Central Instruments Facility and Analytical Lab Facility, Department of Chemical Engineering for providing the facilities to carry out DSC, TGA and XRD analysis. My special thanks to **Dr. Chandan Borghain** and **Dr. Kula Kamal Senapati**, Central Instruments Facility for lending help and cooperation whenever it was the need of the hour. I am grateful to the Centre of Excellence for Sustainable Polymers (CoE-SUSPOL), IIT Guwahati for providing the characterization facility of WVTR instrument. I also express my gratitude to DST, New Delhi for providing Powder X-Ray Diffraction analysis facility in our department through FIST grant Project# SR/FST/ETII-028/2010.

I acknowledge **MHRD**, New Delhi for the PhD fellowship that had allowed me to undertake this research. I must also thank **IITG** (for its national funding) and **DST, New Delhi** (for providing the international travel support) for giving me the opportunity to attend conferences and also meet so many interesting people from different quarters of the world.

I express my thanks to all the technical staffs of my department specially **Ms. Ritumoni Kalita, Mr. Dipak Kumar Barman, Dr. Lukumoni Borah, Mr. Pankaj Sekhar Baruah, Mr. Debajit Borah** and **Mr. Jayanta Kumar Mout** for their assistance during my experimental work. I would also like to thank **Mr. Sailen Das, Mr. Deep Jyoti Sinha** and **Mr. Bhagya Boro** for their support in various forms. My gratitude goes to **Dr. Mahesh Kumar Gagrai, Dr. Pankaj Tiwari** for kind help to attend the international conference. I am also thankful to **Anurag, Raunaq, Ajinkya, Rohan** for providing a pleasant stay in Salt Lake City, Utah.

My hearty gratitude also goes to the search engine Google Scholar and the developers of technical software: ORIGIN, WSxM, Microsoft. Without all these kits, it was impossible to finish the research work.

Special thanks to **Vijay, Samarshi, Vivek** and **Kelothu** for their co-operation in my research work. I was fortunate enough to get excellent lab mates like **Kanchapogu, Vinoth, Ashim, Mohan and Preethi** for their friendly support and timely assistance whenever needed. I am really grateful to my roommate **Mynah** (bird!) for sharing wonderful four years together.

Completing this work would have been all the more difficult were it not for the support and friendship provided by **Sanjib, Manna, Debashis, Debee Prasad, Dharamashi, Venubabu, Bisweswar, Sombhushan, Shailesh, Manish Poddar, Subhojit, Monika, Dharamdev, Nilanjan, Kishant, Ashim, Dipankar, Muthuraj Bala, Rajat, Rama Shankar, Rupesh, Chitta Ranjan Medhi, Satheeshkumar, Johnney, Biswajit, Satendra, Gedda Murali, Abhik, Siddharth,** among others. I am indebted to them. I am also thankful to my friends outside of campus, especially **Sandeep, Anup, Sanjay, Sunil** and **Mr. Shivkant,** IIT Delhi for their wishes and love throughout my studies.

I am forever indebted to my parents, **Sh. Ram Khilawan** and **Smt. Shiv Prabha** for their affections, support, blessings and endless patience. I would also acknowledge my sisters **Archana** and **Manupriya** for their constant encouragement and belief throughout my life. Many other people, not mentioned here but present in my soul, I greatly acknowledge their support to accomplish my doctoral study. Finally and foremost, I thank God for giving me the good times which I enjoyed and the bad times from which I learned many things. I remain thankful for the mental strength given to face adverse situations.

Manish Kumar

ABSTRACT

In comparison with conventional composites, polymer nanocomposites often exhibit a remarkable improvement in various properties such as enhanced mechanical properties, flame-retardance, thermal stability and decreased gas permeability even at lower loading of nanofillers. These improved properties can be achieved by a fine dispersion of nanofiller having a high aspect ratio within the polymer matrix. Poly (methyl methacrylate) (PMMA) is a hard, rigid and rather fragile thermoplastic material with an excellent transparency. However, its application is limited at elevated temperatures due to its relatively poor thermal stability. An effort has been made in the present research work to overcome this limitation by the fabrication of PMMA nanocomposites using organically modified montmorillonite (MMT) and layered double hydroxides (LDHs).

The initial part of the work addresses the preparation of PMMA nanocomposites using in-house made compatibilizer, maleic anhydride grafted PMMA (PMMA-g-MA) by melt intercalation in the presence of MMT clay modified with 15-35% octadecylamine and 0.5-5 wt.% aminopropyltriethoxysilane. PMMA nanocomposites containing 5 wt.% nanoclay (with and without compatibilizer) were prepared by melt intercalation technique using a single screw extruder. The obtained nanocomposites were characterized by X-Ray diffraction (XRD), Field emission scanning electron microscope (FESEM), Transmission electron microscopy (TEM), Thermogravimetric analysis (TGA), Differential scanning calorimetry (DSC), Dynamic mechanical analysis (DMA), Atomic force microscopy (AFM), tensile, flexural, and hardness test. The XRD traces and TEM images of the nanocomposites revealed the formation of intercalated PMMA nanocomposites. The research findings clearly pointed out that the thermal stability of the PMMA nanocomposites improved with the addition of nanoclay and compatibilizer. The PMMA nanocomposite prepared with compatibilizer (PMMA-5-G) displayed enhanced mechanical properties over neat PMMA as well as the nanocomposite synthesized without compatibilizer (PMMA-5). The maximum improvement of tensile strength, Young's modulus, flexural strength, flexural modulus and Shore-D hardness for the PMMA nanocomposite prepared with PMMA-g-MA was found to be 8, 98, 15, 21 and 13%, respectively, over neat PMMA. This investigation clearly demonstrated that the compatibilizer improved the distribution of clay as well as mechanical properties of the polymer.

Hence, in order to identify the best suitable compatibilizer for the PMMA nanocomposite system, the effect of three different compatibilizers, namely PP-g-MA, PE-g-MA and PS-g-MA on the properties of PMMA nanocomposite was examined. PMMA nanocomposites having 5 wt.% nanoclay (OMMT) and 5 wt.% of various compatibilizers were prepared by melt intercalation method using counter rotating twin screw extruder. PMMA nanocomposites prepared with various compatibilizers yielded the intercalated structure that was confirmed by XRD and TEM analyses. The TGA data demonstrated that the nanocomposites synthesized with compatibilizer exhibit enhanced thermal stability with

respect to neat PMMA. When 50% weight loss was selected as a point of comparison, the decomposition temperature of the nanocomposites prepared with PS-g-MA (named as PMMA-5-PS), PP-g-MA (named as PMMA-5-PP) and PE-g-MA (named as PMMA-5-PE) was found to be 32, 22, and 36 ^{o}C higher than that of neat PMMA, respectively. The PMMA nanocomposite synthesized with PS-g-MA displayed improved mechanical properties over PMMA-5-PP and PMMA-5-PE samples. The results clearly expressed that PS-g-MA compatibilizer promotes adequate interface adhesion between the nanoclay and polymer matrix. The maximum improvement of tensile strength, Young's modulus and hardness for the PMMA-5-PS nanocomposite over PMMA-5-PE sample was estimated to be 8, 2 and 26%, respectively.

Although the incorporation of compatibilizer improved the properties of PMMA/clay nanocomposites, the mechanical properties were not enhanced significantly. Therefore, the influence of novel nanofillers such as Co-Al LDH and Cu-Cr LDH on the properties of PMMA was investigated. Firstly, both LDHs were synthesized by co-precipitation method. The PMMA nanocomposites containing LDH content of 1-7 wt.% were fabricated by melt intercalation technique using PS-g-MA as a compatibilizer in twin screw extruder. The results suggested that PMMA/Co-Al LDH nanocomposites exhibited better properties over Cu-Cr LDH based nanocomposites. The maximum improvement in tensile, flexural and impact strength was achieved by the addition of 1 wt.% LDH in the PMMA matrix, which was found to be 22, 24 and 10 % higher for Co-Al LDH based nanocomposite over neat PMMA, respectively. The PMMA nanocomposite having 1 wt% Cu-Cr LDH showed around 18 and 21% improvement in tensile and flexural strength, respectively, over neat PMMA. The improved mechanical properties at lower loading of LDH are due to the strong interaction between the PMMA matrix and LDHs. TEM analysis further confirmed that the intercalated morphology was obtained at higher loading. At 50% weight loss, the PMMA/Co-Al LDH nanocomposites demonstrated the improved thermal degradation temperature by 31-35 ^{o}C over neat PMMA, while PMMA/Cu-Cr LDH nanocomposites displayed around 26-32 ^{o}C higher thermal stability over neat polymer. The enhanced thermal stability is due to the barrier effect of LDH layers which limit the emission of produced gases. The glass transition temperature (T_g) was enhanced by 5 and 3 ^{o}C for PMMA/Co-Al LDH and PMMA/Cu-Cr LDH nanocomposite, respectively. The confinement of polymer chains between the LDH layers and LDH surface-polymer interaction are the reasons for enhanced glass transition temperature. The thermal degradation activation energy evaluated by Coats-Redfern method and integral procedural decomposition temperature (IPDT) determined by Doyle's method substantiated that the thermal stability was higher for PMMA/Co-Al LDH nanocomposites over Cu-Cr LDH based samples. Criado method was used to analyze the thermal degradation mechanism of various samples. The results suggested that thermal degradation of both LDH based nanocomposites followed F1 reaction mechanism (random nucleation having one nucleus on individual particle, i.e. the identical probability of nucleation occurring at each active site)

at the initial stage and gradually moved toward A4 mechanism (nucleation and growth) at higher conversion. The rheological studies also demonstrated that the storage and loss modulus were increased as the frequency increased, however complex viscosity was reduced.

Furthermore, a facile solvent process method was employed for the preparation of different nanocomposites consisting of modified MMT clay, Co-Al LDH and Ni-Al LDH, using methylene chloride as a solvent. The XRD results demonstrated the intercalated morphology for PMMA/clay nanocomposites while for LDH based nanocomposites, no peak was observed, demonstrating the formation of exfoliated structure. However, TEM images revealed the partially exfoliated structures for different nanocomposites. The TGA result showed that all these nanocomposites exhibit a marked increase in the thermal stability with an increase in the nanofiller content. The maximum improvement of decomposition temperature for the PMMA nanocomposites was found to be 376 ^{o}C at 7 wt.% Ni-Al LDH content when 50% weight loss was taken as a point of comparison. All the nanocomposite materials were found to have a superior glass transition temperature relative to the neat PMMA and best result was obtained with Co-Al LDH. The water vapour transmission and water uptake capacity of PMMA nanocomposites decreased with an increase in the nanofiller loading. The optical clarity of PMMA/clay nanocomposites was close to the neat PMMA sample and also better than the LDH based nanocomposites. The improvement of thermal stability of nanocomposites was also confirmed by increasing the activation energies (E_a) and IPDT value, which also increased with increasing nanofiller loading. The reaction mechanism of thermal degradation of neat PMMA and respective nanocomposites was successfully predicted using Criado method. The obtained rheological data were fitted with various models and Einstein model best fitted the experimental values of storage modulus. Among the nanocomposites prepared by solvent blending method, PMMA/Ni-Al LDH nanocomposites demonstrated superior properties over Co-Al LDH and clay based nanocomposites. Overall, it can be concluded that the PMMA nanocomposite containing 1 wt.% Co-Al LDH prepared via melt intercalation technique exhibits better properties over other nanocomposites and neat PMMA.

Contents

List of Tables

List of Figures

Nomenclature

Abbreviations

APES	Aliphatic polyester
AFM	Atomic force microscopy
ASTM	American Society for Testing and Materials
CNT	Carbon nanotubes
CTAB	Cetyl trimethyl ammonium bromide
DMA	Dynamic mechanical analysis
DSC	Differential Scanning Calorimetry
E-AE-GMA	Glycidyl methacrylate ester
EGMA	Polyethylene-co-glycidyl methacrylate
EPDM	Ethylene propylene diene monomer
EPR-g-MA	Ethylene propylene rubber grafted with maleic anhydride
EVA	Ethyl vinyl acetate
EVA-g-MA	Ethylene vinyl acetate grafted with maleic anhydride
EVOH	Ethylene vinyl alcohol
FESEM	Field Emission Scanning Electron Microscopy
FTIR	Fourier Transmission Infra-Red Spectroscopy
HDPE	High density polyethylene
iPP	Isotactic polypropylene
LDH	Layered Double Hydroxide
LDPE	Low density polyethylene
LLDPE-g-MA	Maleic anhydride-grafted linear low density polyethylene
MAH	Maleic anhydride

MAH-g-EPDM	Maleic anhydride grafted ethylene propylene diene monomer
MMA	Methyl methacrylate
MMT	Montmorillonite
MWCNT	Multi-walled carbon nanotubes
OMMT	Organo-modified-Montmorillonite
PET	Polyethylene terephthalate
PMA	Poly methyl acrylate
PMMA	Polymethyl methacrylate
PMMA-g-MA	Polymethyl methacrylate grafted maleic anhydride
PMMA-g-PE	Polymethyl methacrylate grafted polyethylene
PMMA-g-PP	Polymethyl methacrylate grafted polypropylene
PMMA-g-PS	Polymethyl methacrylate grafted polystyrene
PNQASs	Phosphorous nitrogen containing quaternary ammonium salts
POE-g-MA	Ethylene-octene copolymer grafted with maleic anhydride
PP	Polypropylene
PPC	Polypropylene carbonate
PP-g-MA	Polypropylene grafted with maleic anhydride
PS	Polystyrene
SAN-g-MAH	Poly(styrene-grafted-acrylonitrile)-maleic anhydride
SEM	Scanning Electron Microscopy
TEM	Transmission Electron Microscopy
TGA	Thermo gravimetric analysis
XNBR	Carboxylated nitrile rubber
XRD	X-Ray Diffraction

Notations

α	Fractional Conversion
β	Rate of Heating
k	Rate Constant
θ	Diffraction Angle
T_{max}	Maximum Degradation Temperature
A	Pre-Exponential Factor
E_a	Activation Energy
n	Order of Reaction
R	Gas Constant
nm	Nanometer
λ	Cu-Kα Radiation Wavelength
T_g	Glass Transition Temperature
G'	Storage Modulus
G"	Loss Modulus
tan δ	Loss Factor
η^*	Complex Viscosity
ω	Angular Frequency
τ	Shear Stress
η	Viscosity
γ	Shear Rate

Chapter 1

Introduction and Literature Review

This chapter presents a brief summary of the basic fundamentals, terminologies and applications of polymer nanocomposites along with the basis of the problem chosen in this work. The advantage of polymer nanocomposites over conventional composites is highlighted. State of art on the preparation and characterization of polymer nanocomposites and their applications have been discussed in details. Subsequently, the history of various nanofiller used as reinforcements in the PMMA matrix is elaborated. Thereafter, the objectives of the thesis have been summarized followed by the organization of present work.

1.1 INTRODUCTION

Composites are combinations of two materials in which one of the materials, called the reinforcing phase, is in the form of fibers, sheets, or particles, are embedded in the other materials called the matrix phase. The reinforcing material and the matrix material can be metal, ceramic, or polymer. Reinforcing materials are generally strong with low density while the matrix is usually a ductile, or tough, material. The composites are generally designed and fabricated to combine the strength of the reinforcement with the toughness of the matrix to achieve a combination of desirable properties not available in any single material.

When one of the constituent phases has one dimension less than 100 nm they are called as nanocomposites. The main idea behind the nanocomposites is to enhance the properties and improve the characteristics of the materials. Polymer-clay nanocomposites consist of clay nanolayers dispersed in a polymer matrix, which exhibit enhanced thermal and mechanical properties, improved barrier properties and reduced flammability (Ray et al., 2003). These enhanced properties are realized only when clay particles are well dispersed in the polymer matrix.

1.2 HISTORICAL DEVELOPMENT OF POLYMER NANOCOMPOSITES

The development of polymer/clay nanocomposites began in the late 1930s with work of Prof. E.A. Hauser on latex system and the technology for producing highly dispersible organo bentonite was developed by Jordan et al., in 1940s. In the 1960s, the J.M. Huber Corporation began the work on the development of functional, silica-modified kaolin. These materials provided significant improvements in the mechanical properties of elastomers and had found wide spread use in commercial sector in spite of high cost (Chaiko, 2006).

The real revolution came in 1985, when Nylon/montmorillonite clay nanocomposites (PNC) were first developed in Toyota Central R & D lab (Okada et al., 2006). The new concept of PNC expanded the fields of polymer science and led to new applications for automotive, electric and food packaging industries. Passenger cars equipped with a PNC part were launched in 1989. Since then, extensive worldwide research is going on involving PNC not only in the industrial sector but also in the academic field.

1.3 SELECTION OF POLYMER

Poly(methyl methacrylate) (PMMA) is an important amorphous thermoplastic with desirable properties, including clarity (the transparency is close to the ultraviolet region and also the infrared), chemical resistance, good moldability, protection against ultraviolet radiation, good weatherability, high strength and dimensional stability (Bamfor et al., 1975; Silva et al., 2008; Mark, 1985). PMMA is resistant to many inorganic reagents, aliphatic hydrocarbons, nonpolar solvents and acidic and alkaline solutions (Gross et al., 2007). However, PMMA has limitations in its thermal stability and mechanical-dynamical properties at higher temperatures. One way to improve the performance of polymers is the addition of nanoparticles such as clays, silica or carbon nanotubes to the polymer matrix (Etiene et al., 2007; Kashiwagi et al., 2008). Nanocomposites based on layered smectite clays as the reinforcing part of the matrix often exhibit improved mechanical properties. Usually, PMMA nanocomposites offer a potential for reduced gas permeability, improved physical performance, and increased heat resistance often without a sacrifice in optical clarity. The structure of PMMA is illustrated in Figure 1.1.

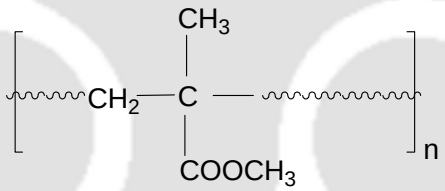

Figure 1.1 Structure of PMMA

1.4 SELECTION OF FILLERS

The filler is the dispersed phase, which normally bears the majority of stress. A reinforcing agent is the strong, stiff integral component, which is incorporated into the matrix to achieve desired properties. The fillers can improve mechanical properties, especially the modulus; they modify the electrical characteristics, change the density, improve the fire resistance, and reduce smoke evolution on burning. The compatibility between filler and polymer, aspect ratio (ratio between length and breadth of the filler) of nanoparticle and interaction between two phases of the system (filler and polymer), which is related to the contact surface, have great impact on the dispersion of nanoparticle in the polymer matrix.

Nanoscale materials are defined as substances where at least one dimension is less than approximately 100 nanometers. Nanomaterials are broadly classified into three categories depending on the dimensions of dispersed particles (Chrissafis and Bikiaris, 2011). Figure 1.2 illustrates the various types of nanoscale materials.

(a) *Nanoparticles*: When the three dimensions of particulates are in the order of nanometers, they are called isodimensional nanoparticles. They include spherical nanoparticles, nanogranules and nanocrystals.

(b) *Nanotubes*: When two dimensions are in the nanometer scale and the third is larger, forming an elongated structure, they are generally called 'nanotubes' or nanofibers/nanorods and they include carbon nanotubes (CNTs), silica and titanium nanotubes, cellulose whiskers, etc.

(c) *Nanolayers*: The particulates which are characterized by one dimension in nanometer scale are nanolayers/nanosheets. In this case, the filler is present in the form of sheets of one to few nanometer thick to hundreds to thousands nanometers long, such as clays (layered siliactes), layered double hydroxides (LDHs), etc.

The most extensively used nanoparticle in PNC is second and third type. The aspect ratio of nanoparticle and interaction between two phases of the system (filler and polymer) has great impact on the dispersion of nanoparticle in the polymer matrix. Besides the aspect ratio of the nanoparticle, other aspect has to be taken into consideration in PNC synthesis, which is compatibility between the filler and polymer. This is generally favored through the use of organically modified layered silicates and the way of dispersion of filler in the polymer matrix by using ultrasonication or by vigorous stirring.

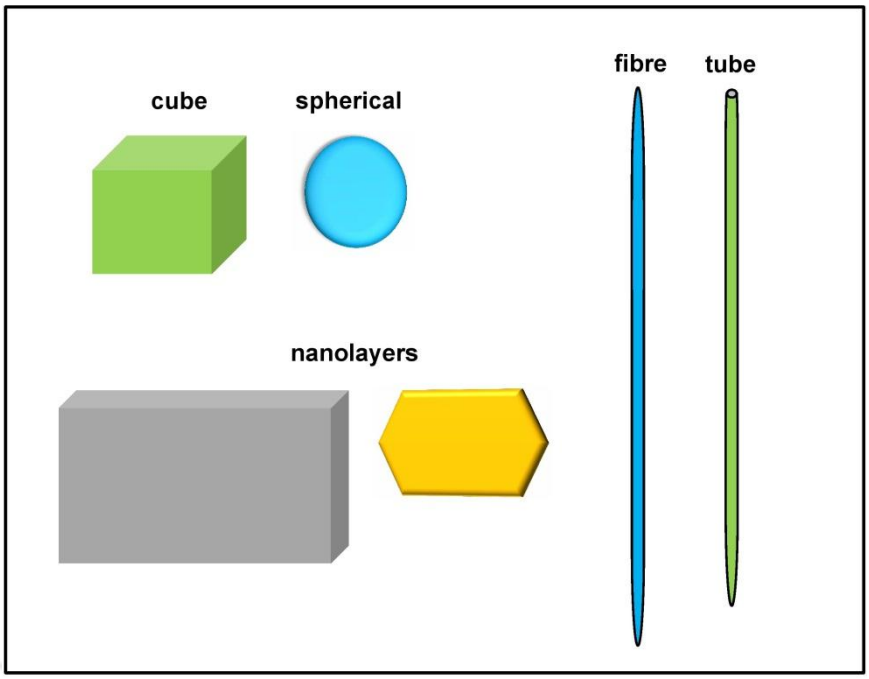

Figure 1.2 Various types of nanoscale materials

1.4.1 Clay

Clay consists mainly one the most abundant elements in the earth crust: silicon, which is chemically bonded to oxygen, thus forming silica $[SiO_4]^{4-}$. The layered silicates commonly used in nanocomposites belong to a larger structural family known as the 2:1 phyllosillicate or smectite clays (Fahim Uddin, 2008). The crystal lattice consists of two-dimensional layers of tetrahedral silica sheets fused to an edge-shared octahedral alumina-magnesia sheet (see Figure 1.3). Sheets are present in the form of stacks, which lead to a regular Van der Waals gap between the interlayer or gallery of the clay platelets, called as basal spacing. Different nomenclatures used are 1:1, (in which one tetrahedral sheet is linked to an octahedral sheet known as a dimorphic clay mineral) and 2:1 (when one octahedral sheet is sandwiched between two tetrahedral silicate sheets called trimorphic clay mineral). The most often used clays are montmorillonite (MMT), $M_x(Al_{4-x}Mg_x)Si_8O_{20}(OH)_4$ and hectorite, $M_x(Mg_{6-x}Li_x)Si_8O_{20}(OH)_4$. The 2:1 layered silicates have a characteristic layer thickness of 1 nm and lateral dimensions that vary from 25 nm to several micrometers depending on the particular silicate. Two types of charges are present in the clay platelets: (i) permanent charges produced by '*isomorphic substitutions'* which are negative and (ii) induced charges or charges depending upon pH, mainly originating by breaking bonds found at superficial

ends of clay that generate positive charge. The negative charges are counter balanced by alkali or alkaline earth cations such as Li^+, Na^+, K^+, Ca^{2+}, or Mg^{2+}, which are situated in the interlayer. As a result of the strong interaction between layers due to Van der Waals attraction, layers are stacked together. The compensating cations which are absorbed on the clay surface can be exchanged for other cations. Hence, they are called exchangeable cations of the clay (Giannelis et al., 1996). The amount per unit weight of the clay is the cationic exchange capacity (CEC).

Monovalent cations such as Li^+ or Na^+ make the clay hydrophilic, whereas Cu^{2+} flocculates the clay. Binding strength study of alkylammonium compounds on montmorillonite has shown a decrease in binding strength in the sequence: $R_3NH^+ > R_2NH_2^+ > RNH_3^+$, as a result, quaternary ammonium salts are the most common cations to be exchanged with the clays. Clays on the whole are lyophobic, but only smectite clays such as *montmorillonite* and *hectorite* have some lyophilic/hydrophilic properties. Clay minerals may be divided into four major groups, mainly in terms of the variation in the layered structure. These include the kaolinite group, montmorillonite/smectite, illite and the chlorite group. Kaolinite group is $Al_2Si_2O_5(OH)_4$, and general formula of MMT is $(Na,Ca)(Al,Mg)_2.(Si_4O_{10})(OH)_2.nH_2O$. The general formula of illite is $(K,H)Al_2(Si,Al)_4O_{10}[(OH)_2.(H_2O)]$. Chlorite group is not considered as clays and is placed in a separate group of phyllosillicate.

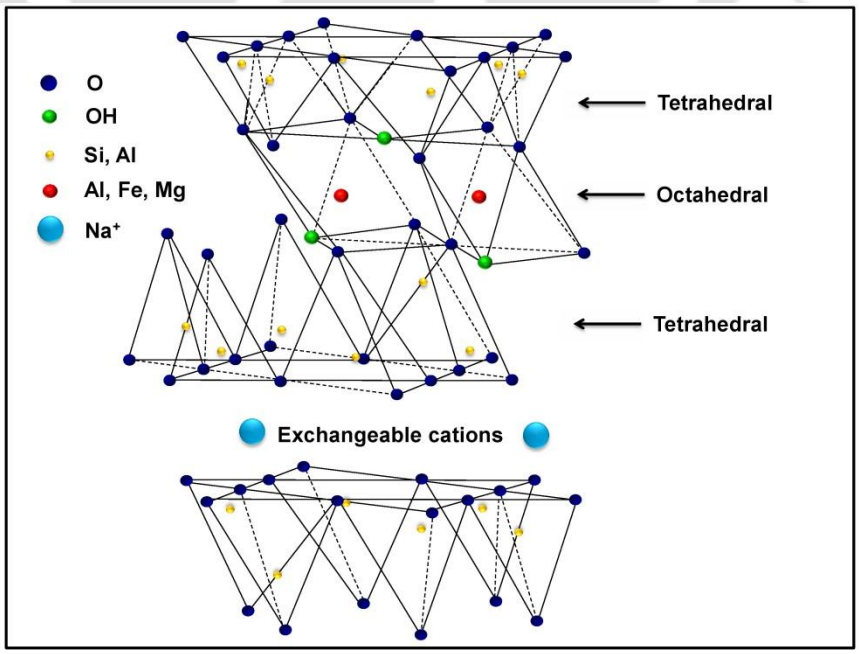

Figure 1.3 Idealized structure of Montmorillonite clay

1.4.2 Layered Double Hydroxide

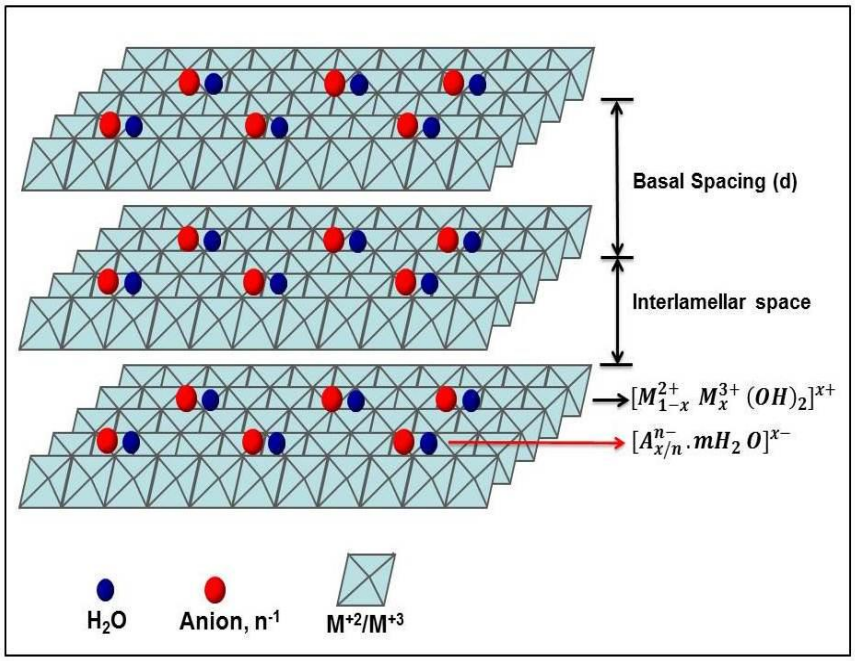

Figure 1.4 Structure of LDH

Layered double hydroxide (LDH) is mineral and synthetic materials with positively charged brucite type layers of mixed metal hydroxide (see Figure 1.4). LDHs are layered crystalline materials having exchangeable anions located in the interlayer spaces (Cavani et al., 1991; Constantino et al., 1995; Newman et al., 1998). Layered double hydroxides are also known as anionic clays: mineral of this family is hydrotalcite (Mg-Al-CO_3). The general chemical formula for these materials is $[M^{2+}_{1-x}M^{3+}_{x}(OH)_2]^{x+}A^{n-}_{x/n}.mH_2O$, where M^{2+} is a divalent cations (Ca^{2+}, Mg^{2+}, Zn^{2+}, Co^{2+}), M^{3+} is a trivalent cations (Al^{3+}, Cr^{3+}, Fe^{3+}), A^{m-} represents the interlayer anions (NO_3^-, Cl^-, CO_3^{2-}), m is the number of interlayer water and X(=M^{2+}/(M^{2+} + M^{3+})) is the layer charge density of LDH.

Organic adjustment of layered double hydroxides is essential prior to its application in the polymer matrix for preparing PNCs. The exfoliated or intercalated PNC preparation depends on the compatibility of LDH with polymer. LDHs are hydrophilic in nature and it must be made organophillic (hydrophobic) to become compatible with most host polymers that are hydrophobic in nature. LDH will only disperse and phase separate in the polymer matrix without modification. The substitution of the inorganic ions between the clay gallery by organic ions (surfactant, intercalant) overcomes this problem. Longer surfactant chain length and higher charge density of LDH will force clay layers to move

further apart making it easier for polymer chains to penetrate within the LDH layers. This helps to form exfoliated nanocomposite structure.

1.4.3 Advantages of LDH

- The different variety of LDHs can be synthesized in the laboratory by co-precipitation method with high chemical purity, homogenous structure and tunable chemical composition. (Feitkneeht et al., 1942; Miyata, 1977).
- LDHs have technological importance in catalysis, separation technology, optics, medical science and nanocomposite materials engineering.
- LDH containing magnesium and aluminium are biocompatible and have been used as an antacid and antipepsin agent.
- LDH are reactive materials that undergo endothermic decomposition producing metal oxide residue. This property helps improving thermal and flame retardancy of polymer matrix more efficiently.
- Ni-Al LDH is used for bacteriophage removal in water treatment and filtration application. Ni-Al LDH modified electrode is used as biosensor (Park et al., 2005).

1.5 DIFFERENT POLYMER MATRICES USED FOR NANOCOMPOSITES

1.5.1 Thermoplastic based nanocomposites

Many thermoplastic based nanocomposites were made by inserting nanoparticle in the polymer matrices. The thermoplastic polymer used for this type of nanocomposites includes biodegradable polymer, polyamide, polyacrylonitrile, polybutylene, polycarbonate, polyethylene, polyethylene copolymer, polymethyl methacrylate, polymethyl pentane, polyphenylene oxide, polyphenylene sulfide, polypropylene, polystyrene, polysulfone, polyvinyl chloride, etc (Chrissafis and Bikiaris, 2011).

1.5.2 Thermosetting based nanocomposites

Different thermosetting resins have been used for the preparation of nanocomposites by introducing nanoparticles into the matrix. These types of resins include urea and melamine formaldehyde, bismalemide (BMI), polyester (thermosetting), vinylester, cyanate ester, polyimide (thermosetting), polyurethane, epoxy resin, etc (Chrissafis and Bikiaris, 2011; Mittal, 2008).

1.6 ROLE OF COMPATIBILIZER

Compatibilizers are also commonly known as coupling agent that work as an interfacial agent to facilitate the bonding between the polymer and nanofiller, immiscible polymer blends. Various researchers made an attempt (Chow et al., 2005; Lim et al., 2006) to modify the polymer matrix with various grafting agents (EPR-g-MA, PP-g-MA) to improve the degree of dispersion i.e. exfoliation and intercalation and the compatibility of the nano filler into the polymer matrix. As a result, the interfacial tension between the filler and matrix is reduced.

1.7 METHODS OF PREPARATION

Various methods are employed for the preparation of polymer nanocomposites. Among those methods, in-situ polymerization, solvent blending and melt compounding are widely used. Among these three methods, last two methods directly insert polymer into the clay/LDH galleries, while the first method inserts monomers followed by polymerization in the galleries.

1.7.1 In-situ polymerization method

In this method, layered silicate is swollen within the liquid monomer, or a monomer solution so as the polymer formation can occur in between the intercalated sheets. Polymerization can be initiated either by heat or radiation. It can also be done by the diffusion of a suitable initiator or catalyst fixed through cationic exchange inside the interlayer before the swelling step by the monomer. This technique was used by the Toyota research team to realize nylon 6 based nanocomposites from caprolactum (Li et al., 2013; Wang et al., 2012).

1.7.2 Solvent blending method

This is a two- stage process in which, at first, the layered silicate is firstly exfoliated into single layers using a solvent (in which the polymer is soluble). It is well known that such layered silicates, owing to the weak forces that stack the layers together can be easily dispersed in an adequate solvent. Then the polymer added to the nanoclay solvent mixture that absorbs onto the delaminated sheets. When the solvent is evaporated or the mixture precipitated, the sheets reassemble and sandwich the polymer giving rise to intercalated or exfoliated structure depending on the extent of penetration (Du et al., 2007).

1.7.3 Melt-intercalation method

The layered silicate is mixed with the polymer matrix in the molten state, in either static or flow conditions. Under these conditions and if the layer surfaces are sufficiently compatible with the chosen polymer, the polymer chains spread from the molten mass into the silicate galleries to form either intercalated or delaminated hybrids according to the degree of penetration. This method has great advantages over either in-situ polymerization or solvent blending. First, this method is environmentally benign due to the absence of organic solvents. Secondly, it is compatible with current industrial process, such as extrusion and injection molding. The melt intercalation method allows the use of polymers, which are previously not suitable for in-situ polymerization or solvent blending (Wang et al., 2011; Du et al., 2007).

1.8 TYPES OF NANOCOMPOSITES

Depending on the strength of interfacial interactions between the polymer matrix and layered silicate (modified or not), three different types of PNC are thermodynamically achievable as shown in Figure 1.5.

1.8.1 Conventional structure

This type of morphology occurs when the miscibility between the polymer matrix and the filler does not support favorable interactions to overcome the thermodynamic consideration leading the clay layers to collapse. The microcomposite, thus resulted under such circumstances is referred as phase separated composites. The properties of such phase separated composites are rather hardly ever enhanced or may reduce after the reinforcement (Morgan and Gilman, 2003).

1.8.2 Intercalated structure

In intercalated nanocomposites, the insertion of a polymer matrix into the layered silicate structure occurs in a crystallographically regular fashion, regardless of the clay to polymer ratio. Intercalated nanocomposites are normally intercalated by a few molecular layers of polymer. The intercalation increases the basal spacing between the clay sheets, as the diffraction peak shifted to lower angle ($2\theta^{o}$) detected by XRD (Morgan and Gilman, 2003).

1.8.3 Exfoliated structure

The exfoliated nanocomposites are formed by extensive polymer penetration and silicate delamination (nanoparticle layer). In this, the ordered structure is not preserved and the individual platelets are randomly dispersed in the polymer matrix and diffraction peak cannot be detected by XRD. Usually, the clay content of an exfoliated nanocomposite is much lower than intercalated nanocomposite (Morgan and Gilman, 2003).

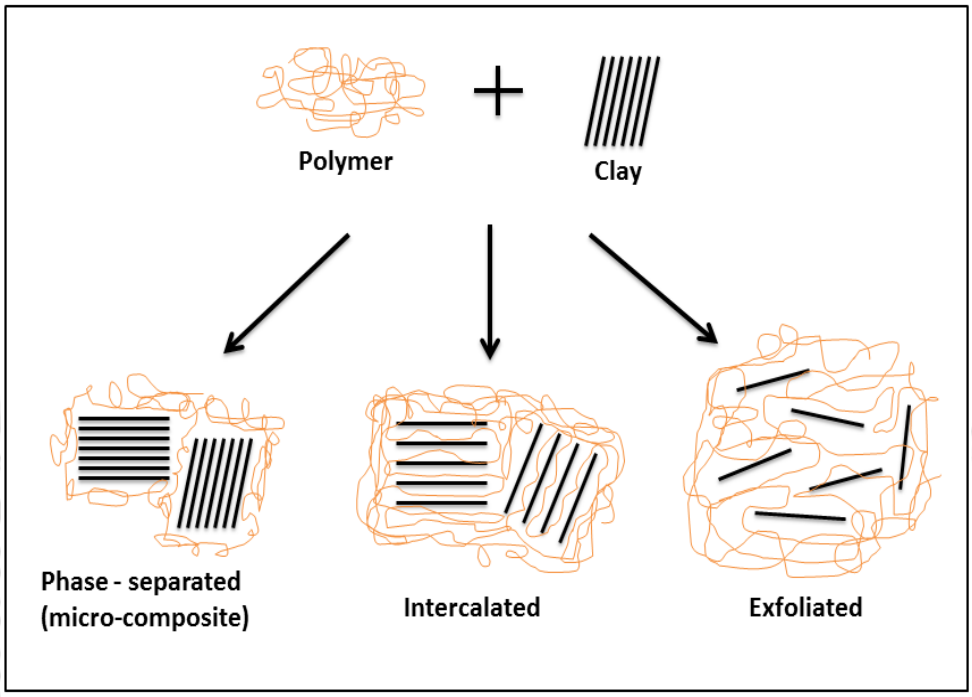

Figure 1.5 Different types of polymer nanocomposites

1.9 PROPERTIES OF POLYMER NANOCOMPOSITES

PNC typically contain 2-10% loading on weight basis, yet property improvements can equal an exceed traditional composites containing 20-35% mineral or glass. Some of the properties are given below:

- Improved mechanical properties including strength, modulus and dimensional stability.
- Greater thermal stability.
- Excellent flame retardancy.
- Decreased gas, water and hydrocarbon permeability due to tortuous path created by fillers when dispersed in the polymer matrix.

- Lower density and similar recyclability.
- Improved electrical conductivity.
- Enhanced physical properties.
- Increase in melt strength.

1.10 APPLICATIONS OF POLYMER NANOCOMPOSITES

A wide range of potential applications of polymer nanocomposites are discussed by various researchers as shown in Figure 1.6 (Garcés et al., 2000; Ahmadi et al., 2004; Kurahatti et al., 2010; Wei et al., 2011). Some of them are mentioned below:

- Enhanced gas barrier characteristics have found the use of nanocomposites in food packaging industry. Examples include packaging for processed meat, cheese, confectionary and boil in the bag foods. Extrusion coating application with paper board is used in fruit juice and dairy industry.
- Automotive and industrial applications are extensive. Mirror housing on various vehicle types, handles and engine cover are few examples of application.
- Used as impellers and blades for vacuum cleaner and cover for portables electronic equipment such as mobile phone cover.
- Polymer nanocomposites can be used for aerospace application.
- Filler incorporation at nano-levels has significant impact on the transparency and haze characteristics of film.
- It has high flame retardant characteristics, so it can be used for high temperature application such as internal combustion engine.
- This material can be used in fuel tank and fuel line in the car to reduce fuel loss.
- LDH based nanocomposites containing magnesium and aluminium is biocompatible and used as an antacid and anti-pepsin agent.
- LDH based nanocomposites acts as soluble inorganic vector for different genes and DNA biomolecules.

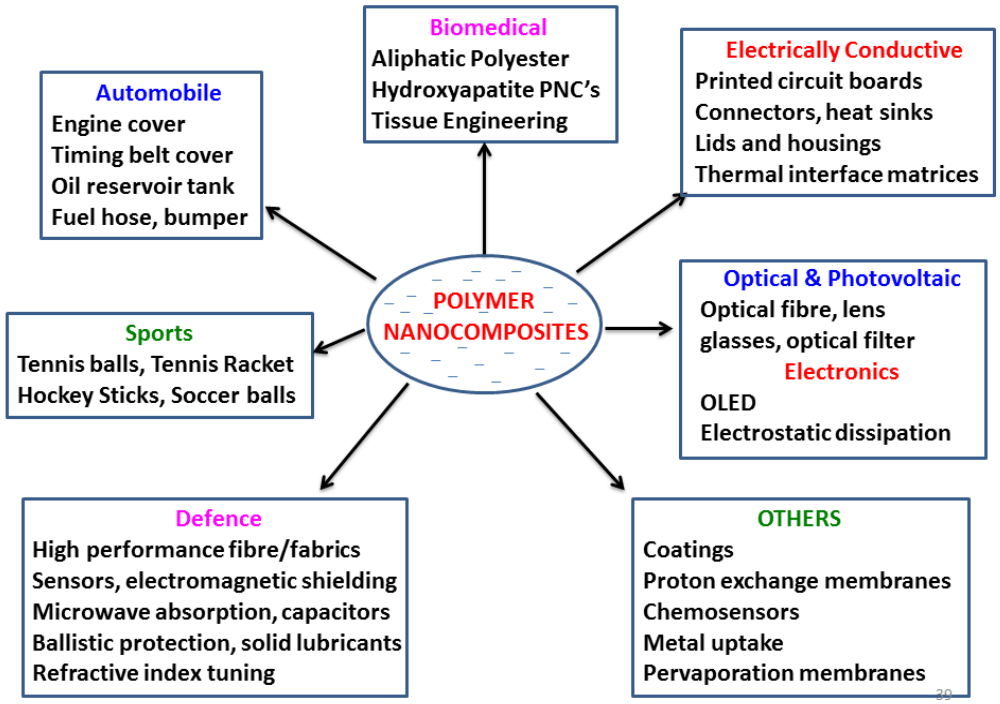

Figure 1.6 Applications of polymer nanocomposites

1.11 LITERATURE SURVEY

1.11.1 PMMA/clay nanocomposites

The PMMA and PS nanocomposites were prepared using lipophilized smectic clay by in-situ free radical polymerization method (Okamoto et al., 2000). The clays were modified with two different modifiers i.e. oligo-(oxypropylene)-, diethyl-, methyl-ammonium chloride (SPN), and methyl-trioctil-ammonium chloride (STN). The d-spacing of these nanocomposites was examined by XRD and TEM analysis. The d-spacing for the solid SPN and STN obtained by XRD measurements was 4.20 and 1.81 nm, respectively. The XRD results suggested that the PMMA nanocomposites were intercalated structures, which were further confirmed by the TEM images. It was also noted that the flocculation takes place owing to the hydroxylated edge-edge interaction of silicate layers. The storage modulus (G') in the glassy region below T_g was 57% (for PS/SPN) and 34% (for PMMA/STN) higher in the nanocomposites compared to the systems without clays.

Laachachi et al., (2009) reported the preparation of PMMA nanocomposites. They compared the role of boehmite (AlOOH) and alumina (Al_2O_3) in the thermal stability and flammability of the polymer matrix. PMMA/AlOOH and PMMA/Al_2O_3 nanocomposites were prepared by melt blending technique with different loading of filler. It was observed that the prepared nanocomposites exhibited higher thermal stability and fire resistance in comparison with pure PMMA. It was also found that improvement in thermal stability of PMMA seems to be higher in the case of Al_2O_3 than for AlOOH. Greater reduction in pHRR (peak heat release rate) was observed with PMMA/AlOOH 20% and PMMA/Al_2O_3 15% samples.

In order to achieve exfoliated structure, a novel method has been employed to prepare PMMA/clay nanocomposites by in-situ polymerization of MMA in the presence of triethylaluminum modified MMT-k10 clay (Cui et al., 2008). The exfoliated structure of the nanocomposites was identified by the XRD and TEM. The TEM images confirmed that clay layers were disorderly distributed in the polymer matrix. The glass transition temperature (T_g) was improved by 0.5 to 4.5 ^oC for different nanocomposites. The PMMA nanocomposites were found to retain 80% transparency, which is important for optical application. Thermal stability was also enhanced by 45-58 ^oC at 5 wt.% weight loss as a point of comparison. The storage modulus of nanocomposites was 20 -54% higher than that of neat PMMA. The tensile properties were also significantly increased as the amount of clay increased. The tensile strength of nanocomposites was up to 70 MPa for 7.26 wt.% of clay content, and the tensile modulus exhibited a 20% higher value than that of neat PMMA.

Huang et al., (2013) synthesized five different kinds of phosphorous-nitrogen containing quaternary ammonium salts (PNQASs) for the modification of clay and studied the influence of different PNQASs modifiers on the flammability properties of PMMA/MMT nanocomposites prepared by in-situ polymerization technique. The XRD spectra exhibited that all the PMMA nanocomposites have exfoliated structure except for the PMMA/Na-MMT and PMMA/PAAB-MMT nanocomposites. From the TEM analyses, it was confirmed that PMMA/PHAB-MMT sample has better dispersed clay layers than the PMMA/Na-MMT, PMMA/CTAB-MMT, PMMA/PAAB-MMT, PMMA/PAEAC-MMT and PMMA/PAHAC-MMT compositions. The different nanocomposites demonstrated 3 to 23 ^oC improvement in thermal degradation temperature when 20% weight loss is considered as point of references. The peak heat releasing rate was recorded to be 34% lower for PMMA/PAEAC-MMT compared to pure PMMA. The DMA results suggested that PMMA/PHAB-MMT sample has the highest storage modulus and improvement in T_g value of 8 ^oC over other samples.

PMMA/layered silicate nanocomposites produced via melt intercalation technique were reported by Mohanty et al., (2010) and the influence of different layered silicates on the morphological, thermal and mechanical properties was studied. They have used different types of organoclays such as Closite 30B (C30B), Closite 20A (20A) and Bentone 109 (B109) for the preparation of nanocomposites. In order to improve the interfacial adhesion between organoclays and PMMA matrix, the later had been modified by maleic anhydride. The intercalated structures of different nanocomposites were identified by XRD analysis; however the TEM analysis confirmed that partially exfoliated layers of clay were present in the PMMA matrix. At 10% weight loss, the thermal stability was increased by 5 to 27 ^{o}C for different nanocomposites. The tensile properties elucidated that tensile strength and modulus of PMMA/C30B (5%) nanocomposites were 22 and 35% higher over pristine PMMA, respectively. The flammability property of different nanocomposites was also enhanced by 25 to 36 mm/min.

Organically modified nanoclay was incorporated in the PMMA matrix through melt-extrusion process (Unnikrishnan et al., 2011). Three different organoclay modifiers with varying hydrophobicity (single tallow vs. ditallow) were investigated. Both XRD and TEM analyses identified the presence of partially intercalated and exfoliated nanocomposites structures after the reinforcement of the filler in the PMMA matrix. The TGA analyses suggested that thermal stability was enhanced by 3 to 16 ^{o}C at 50% weight loss ($T_{50\%}$). The activation energy was also improved by 23 kJ/m for PMMA/C30B sample over pure PMMA. The reinforcement also led to the improvement in the tensile modulus by 36% for PMMA/3% C10A sample; however tensile strength and impact strength were reduced for all the compositions. The rate of burning was noticed in the following order: PMMA/C93A > PMMA/C10A > PMMA/C30B > PMMA.

Fu et al., (2006) reported the preparation of PMMA/clay nanocomposites by solvent co-precipitation method, which was later used for microcellular foams. In this work, they investigated the effect of nanoclay on the mechanical properties of PMMA/clay nanocomposites foams. PMMA nanocomposite with only 0.5 wt% of well dispersed montmorillonite nanoclay showed considerable improvement of mechanical properties, especially in elastic modulus, tensile strength, elongation at break with an increase of 24%, 54% and 97%, respectively. However, with further increased load of clay (0.5 wt.%) in the nanocomposites, the mechanical properties decreased due to the agglomeration of excessive

nanoclay. The agglomerated nanoclay promoted stress concentration in the PMMA matrix and therefore decreased the tensile strength and elongation at break.

A series of PMMA/MMT nanocomposites containing (1-10 wt.%) of Cloisite 15A modified with N,N'-dimethyl, dehydrogenated tallow quaternary ammonium salt was prepared by bulk polymerization and melt compounding method (Krajnc and Šebenik, 2008). The properties of nanocomposites containing same compositions prepared by two methods were compared. It was observed that PMMA nanocomposites prepared by melt compounding method had highly oriented structure with lower d-spacing values compared to bulk polymerization. The enhanced PMMA penetration between the MMT layers and degradation of organic modifier at 200 ^{o}C were the two main reasons for lower interlayer spacing as noticed in melt compounded samples. Both reasons led to the fracture of melt compounded nanocomposites on the MMT-polymer interface. The enhanced T_g (5-10 ^{o}C) and thermal stability (5-16 ^{o}C) were also noticed for bulk polymerized nanocomposites.

A variety of nanocomposites were synthesized by bulk polymerization of MMA as well as by extrusion of PMMA (Ratinac et al., 2006). Various types of nanoclays were employed for the fabrication of nanocomposites i.e. commercial and lab-synthesized clay by different modifying agents. The influence of organoclay and processing parameters on the structure of PMMA/clay nanocomposites was examined. From the result, it was observed that quaternary-alkyl ammonium surface modification of MMT dramatically improved polymer intercalation and the dispersion of clay at the microscale in bulk-polymerized PMMA. It was also found that incorporation of a polymerizable modifier in an organoclay significantly increased the exfoliation and polymer intercalation during polymerization of MMA. The presence of excess modifier in the organoclays improved the nanoscale and microscale structures of bulk-polymerized PMMA nanocomposites. It was also noticed that PMMA nanocomposites prepared by extrusion produced better structures than bulk polymerization.

In a separate contribution, Laachachi et al., (2009) investigated the effect of ZnO and organomodified montmorillonite (MMT) clay on thermal degradation of poly(methyl methacrylate) nanocomposites. The PMMA nanocomposites were prepared by melt blending method using different loading of nanofiller (2, 5 and 10 wt.%). The XRD result revealed that exfoliated and intercalated structure were obtained at lower (2%) and higher (3, 5%) loading, respectively. However, TEM analyses provided the partially exfoliated/intercalated morphology even for 2 wt.% loading. The PMMA/ZnO nanocomposites exhibited two

contrary effects, under oxidative medium, a catalytic effect at lower loading in PMMA matrix and stabilizing effect at higher loading. The PMMA/OMMT nanocomposites stabilized the thermal degradation of PMMA in both oxidative and inert atmosphere.

The organophilic montmorillonite (OMMT) was synthesized by cationic exchange between Na-MMT and cetyltrimethylammonium bromide (CTAB) in aqueous solution (Wei'an et al., 2003). Thereafter, the PMMA/OMMT nanocomposites were prepared by γ-ray irradiation polymerization. The FTIR results exhibited the characteristic peak of C-H stretching that was recorded at 2850 and 2919 cm^{-1} for CTAB. Both XRD and TEM analyses confirmed the presence of intercalated nanocomposites after the incorporation of OMMT in PMMA. The TGA results suggested that thermal stability can be quickly gained at 3 wt.% OMMT, however at higher loading (10 wt.%), thermal stability does not increase quickly. The nanocomposites also demonstrated an increase in storage modulus and T_g as suggested by DMA results.

Zhang et al., (2009) synthesized PMMA-mesoporous silica nanocomposites by in-situ batch emulsion polymerization of methyl methacrylate in the presence of large pore MSU-F silica. The sample containing 5 wt.% silica demonstrated an increase of onset decomposition temperature (temperature at 10% weight loss) of 41 ^oC in comparison to pure PMMA. The glass transition temperature of the PMMA/MSU-F(5%) sample was also enhanced by 9.3 ^oC. The storage modulus was increased by 80% at 100 ^oC. Substantial improvements in tensile strength, (+50%) and modulus (+72%) were achieved with PMMA/MSU-F(10%). The sample prepared by compression molding exhibited less improvement in thermal stability, glass transition temperature and mechanical properties with respect to in situ batch emulsion polymerization.

In the work reported by Zhu et al., (2002), three different kinds of ammonium salts were utilized to organically modify the sodium MMT (Cloisite Na^+) clay. The PMMA nanocomposites with these clays were prepared by bulk-polymerization technique. The XRD and TEM analysis confirmed that the PMMA-Bz16 nanocomposites have intercalated structures whereas PMMA-Allyl16 and PMMA-VB16 exhibited mixed intercalated-exfoliated nature. The TGA results indicated that the thermal degradation temperature of different compositions was enhanced by 39 to 43 ^oC at 50% weight loss. The lowest peak heat release rate (PHRR) was recorded for PMMA-Bz16 sample; however the PMMA-Allyl16 nanocomposite exhibited 29% higher tensile strength over pristine PMMA.

PMMA nanocomposites with organically modified montmorillonite (PMMA/OMMT) prepared via solution intercalation method were reported by Yamagata et al., 2012. Two different kinds of OMMT (NZ70 and NX) modified with quaternary alkylammmonium ions were reinforced into the PMMA matrix to prepare the nanocomposites. From the XRD results, it was found that the peak related to d_{001} was shifted to lower 2θ, implying the expansion or partial exfoliation of silicate layers. The TEM images also exhibited that clay layers were well dispersed in the polymer matrix although some aggregates were also noticed. The flexural modulus of the PMMA/OMMT nanocomposites increased favorably with an increasing amount of OMMT and found maximum at 4 wt.%. Similarly, toughness was also enhanced for nanocomposites containing NX, especially at 1 and 2 wt.%. The enhancement in the reinforcement of nanocomposites may be due to shear deformation and stress transfer to silicate platelets. The results also suggested that the use of NX with a highly hydrophobic grade has the potential to improve the properties of PMMA/OMMT nanocomposites.

PMMA/MMT nanocomposites were synthesized by in-situ polymerization using ethanol and acetonitrile as solvent (Valandro et al., 2013). Two different kind of organmontmorillonite (SWy-1-C8-Mt and SWy-1-C16-Mt) were prepared by ion-exchange process and used in different loadings (1, 3 and 5%). The XRD results demonstrated that intercalated as well as exfoliated structures were obtained for different nanocomposites. It was also noticed that clay mineral loading and the solvent used for the preparation of polymer-clay nanocomposites have direct influence on the morphological structures. The different nanocomposites were exposed to UV light at 40 ^{o}C for photooxidative degradation followed by size exclusion chromatography (SEC). The different compositions exhibited a significant decrement in number average molecular weight (M_n) after 15-20 h of irradiation. The SEC suggested that pure PMMA and nanocomposites were degraded by random chain scissions. It was also found that most of the samples prepared in acetonitrile showed lower degradation rate coefficient; however, for pure PMMA, it was 6 times larger than polymer nanocomposites. It was also found that nanocomposites with higher loadings showed slow rates of oxidation.

In order to improve the compatibility between polymer matrix and clay platelets, pristine Na^+ MMT clay was modified using cocoamphodipropionate (K2). Three different kinds of organoclay such as CL42-K2, CL120-K2 and CL88-K2 were synthesized by Tsai et al., (2013). Thereafter the respective clays were dispersed in the PMMA matrix via in-situ free radical polymerization and the influence of various loadings of clays on the morphological

and thermal properties of PMMA investigated. The XRD results clearly indicated that layered materials were well dispersed in polymer matrix as no diffraction peaks were observed corresponding to clay. The nanocomposites with 3 and 5% loading containing CL120-K2 and CL88-K2 clay displayed exfoliated morphology. When 5% weight loss (T_d) was considered as point of comparison, it was found that the thermal decomposition temperature of PMMA/CL88-K2 5 wt.% was about 55% higher than pure PMMA. The exfoliated nanocomposites (PMM/CL120-K2 5wt.%) exhibited 26 ^oC improved T_g over pure PMMA, which resulted from the strong interactions between the clay layers and polymer chains.

A mica-like K fluorohectorite clay with two aspect ratio (~55 and ~620) was utilized for the fabrication of PMMA nanocomposites via melt-compounding process by Fischer et al., (2012). The impact of mica-like clay on the mechanical behaviour of PMMA/clay nanocomposites was studied. These synthetic PMMA/clay nanocomposites were compared with natural bentone clay based nanocomposites. It was noticed that with the addition of novel clay, tensile modulus and fracture toughness of PMMA/clay were significantly increased compared to pure PMMA. For synthetic clay nanocomposite, tensile modulus was increased by 11% at 4 wt.% clay loading. Similarly, the fracture toughness was enhanced by 25% and 66% for low aspect ratio clay and high aspect ratio clay based nanocomposites, respectively at 4 wt.% clay loading. The incorporation of bentone clay led to an increase in tensile modulus but tensile strength and fracture roughness were considerably reduced. It was also found that elongation at break reduced for both, synthetic and bentone clay based nanocomposites. The bentone and synthetic clay nanocomposites demonstrated 65% and 24% reduction in elongation at break, respectively, with 4 wt.% clay loading. The SEM morphology stated that bentone clay formed large agglomerate whereas the synthetic clay was well dispersed in the polymer matrix.

The effect of quaternary ammonium salt and MMT on the PMMA nanocomposites was examined by Huskic et al., 2012. The PMMA nanocomposites were synthesized by one-step in situ solution polymerization method using MMT modified with cetyl-trimethylammonium bromide (CTMAB). It was observed that small amount of CTMAB reduces the molar mass (M_w and M_n) of PMMA nanocomposites. The ^1H NMR confirmed the different functional group in the PMMA nanocomposites. The signals for methoxy and methyl groups of PMMA were found at 3.6 and 0.8-1.3 ppm, respectively. The formation of intercalated nanocomposites was further verified by XRD and TEM analyses. The T_g results suggested

that glass transition temperature was found to be lower for nanocomposites containing modified MMT with respect to non-modified MMT. The thermal stability was also enhanced by the addition of modified MMT (up to 3 wt.% loading).

The different loading (1-10 wt.%) of sodium MMT was reinforced into the PMMA matrix and the morphological and optical characteristics were examined out by Yeom et al., 2004. The PMMA/MMT nanocomposites were synthesized by emulsion polymerization method. The XRD results suggested that d_{001} peak (interlayer spacing) of clay was intensively suppressed by the PMMA/clay nanocomposites. The TEM also reflected highly dissociated silicate layers in the polymer matrix. As the loading increased, the storage modulus was also enhanced well below the T_g of the different PMMA nanocomposites. The T_g of neat PMMA was recorded as 118 ^oC, whereas for different nanocomposites, it was found between 142 to 150 ^oC. UV/VIS measurement showed slightly higher absorbance for nanocomposites as compared to neat PMMA, however it was well below the transparency limit, representing that nanocomposites formation under emulsifier-free condition is highly favorable to reduce the UV/VIS absorbance.

In order to improve the dispersion of silica nanoparticles in the PMMA matrix, the silanol groups were functionalized with methacrylate groups. Thereafter, the PMMA/silica nanocomposites with and without modified silica were prepared by in-situ free radical polymerization method (Kalajahi et al., 2013). The TGA results proposed that thermal decomposition temperature was improved by the addition of silica nanoparticles in the polymer matrix and it was higher for modified nanocomposites than pristine ones. The highest T_g was obtained at 7wt.% silica content, while T_g value of modified nanocomposites was higher than pristine nanocomposites. It was also observed that the addition of filler content alters the kinetics of polymerization and increases the conversion up to 7 wt.% clay loading. Table 1.1 summarizes the literature of PMMA/MMT nanocomposites based on the modifier involved.

Table 1.1 Classification of literature based on various modifiers used for modification of clays

Authors	Polymer matrix	Nanofiller	Modifier	Method of preparation	Remarks
Huang *et al.*, 2013	PMMA	MMT	phosphorous-nitrogen containing quaternary ammonium salts (PNQASs)	in-situ polymerization	(i) Exfoliated structure obtained as suggested by TEM. (ii) At 20% weight loss, thermal degradation temperature was enhanced by 2 to 33 ^{o}C.
Cui *et al.*, 2008	PMMA	MMT-k10 clay	triethylaluminum	in-situ polymerization	(i) Nanocomposites retained 80% transparency. (ii) At 5% weight loss, thermal stability was improved by 45 to 58 ^{o}C.
Valandro *et al.*, 2013	PMMA	OMMT	octyltrimethylammonium bromide (C8) and hexadecyltrimethylammonium bromide (C16)	in-situ polymerization	(i) Number average molecular weight (M_n) was significantly reduced after 15-20 hours, when exposed to UV light.
Tsai *et al.*, 2013	PMMA	MMT	cocoamphodipropionate (K2)	in-situ polymerization	(i) Exfoliated morphology obtained. (ii) Thermal degradation temperature was improved by 55%. (iii) T_g was enhanced by 26 ^{o}C.
Huskic *et al.*, 2012	PMMA	MMT	cetyl-trimethylammonium bromide	in-situ polymerization	(i) Intercalated structure was confirmed by XRD and TEM. (ii) Modified MMT demonstrated lower T_g than unmodified MMT. (iii) CTMAB reduced the molar mass of nanocomposites.
Fischer *et al.*, 2012	PMMA	Bentone 38 and Mica-like clay	Alkyl ammonium chains	melt compounding	(i) Tensile modulus was increased by 11%. (ii) Fracture toughness was improved by 66% for high aspect ratio mica-like clay.
Laachachi *et al.*, 2009	PMMA	boehmite and alumina		melt blending	(i) Peak heat release rate (pHRR) was reduced for AlOOH (20%) and Al_2O_3 (15%) based nanocomposites.

Authors	Polymer matrix	Nanofiller	Modifier	Method of preparation	Remarks
Mohanty *et al.*, 2010	PMMA	Cloisite 30B, Cloisite 20A and Bentone 109	methyl tallow bis-2 hydroxyethyl ammonium, dimethyl dihydrogenated tallow ammonium and 2-methyl dehydrogenated tallow ammonium ion	melt intercalation	(i) Partially exfoliated structure as suggested by TEM. (ii) At 10% weight loss, thermal degradation temperature was enhanced by 2 to 33 ^{o}C. (iii) Improvement in tensile strength (22%) and modulus (35%) observed for PMMA/C30B nanocomposite.
Unnikrishnan *et al.*, 2011	PMMA	Cloisite 30B, Cloisite 10A and Cloisite 93A	methyl tallow bis-2 hydroxyethyl quaternary ammonium salt, dimethyl benzyl hydrogenated tallow quaternary ammonium salt and methyl dihydrogenated tallow quaternary ammonium salt	melt intercalation	(i) Partially exfoliated structure obtained as suggested by XRD and TEM. (ii) Tensile modulus was improved by 36% for PMMA/C10A nanocomposite. (iii) At 20% weight loss, thermal stability was improved by 3 to 16 ^{o}C.
Laachachi *et al.*, 2008	PMMA	ZnO and Cloisite 30B	methyl tallow bis-2 hydroxyethyl quaternary ammonium salt	melt blending	(i) Partially exfoliated/intercalated structure for clay based nanocomposite as suggested by TEM.
Zhu *et al.*, 2002	PMMA	MMT	hexadecylallyldimethyl ammonium chloride (Allyl16), hexadecylvinylbenzyldimethyl ammonium chloride (VB16) and hexadecylvinylbenzyldimethyl ammonium chloride (Bz16)	Bulk polymerization	(i) Intercalated structure for PMMA-Bz16 nanocomposite. (ii) At 50% weight loss, thermal degradation temperature was improved by 39 to 43 ^{o}C. (iii) Tensile strength was enhanced by 29% for PMMA-Allyl 16 nanocomposite.
Ratinac *et al.*, 2006	PMMA	Cloisite 93A, Cloisite 30B and Bentonite	methyl dehydrogenated-tallow ammonium and bis-2-hydroxyethyl methyl tallow ammonium	bulk polymerization and melt compounding	(i) Extrusion produced samples exhibited better morphology than bulk method.

Authors	Polymer matrix	Nanofiller	Modifier	Method of preparation	Remarks
Krajnc and Šebenik, 2008	PMMA	Cloisite 15A	N,N'-dimethyl, dehydrogenated tallow quaternary ammonium salt	bulk and suspension polymerization	(i) T_g (5-10 ^oC) and thermal stability (5-16 ^oC) improved for bulk polymerized nanocomposites.
Okamoto *et al.*, 1999	PMMA and PS	smectic clay	oligo-(oxypropylene)-, diethyl-, methyl-ammonium chloride (SPN) and methyl-trioctil-ammonium chloride (STN)	free radical polymerization	(i) Intercalated structure obtained as suggested by XRD and TEM. (ii) Storage modulus was improved for PS (57%) and PMMA (34%) based nanocomposites.
Wei'an *et al.*, 2003	PMMA	OMMT	cetyltrimethylammonium bromide	γ-ray irradiation polymerization	(i) Intercalated structure obtained. (ii)Thermal stability was increased rapidly at lower loading (3wt.%).
Yamagata *et al.*, 2012	PMMA	OMMT	quaternary alkylammmonium ions	solution	(i) Partially exfoliated structure obtained. (ii) Flexural modulus was found to be maximum at 4wt.%
Fu *et al.*, 2006	PMMA	clay		solvent co-precipitation	(i) Elastic modulus, tensile strength, elongation at break increased by 24%, 54% and 97%, respectively.
Kalajahi *et al.*, 2013	PMMA	Silica		in-situ polymerization	(i) Thermal stability and T_g found maximum at 7wt.% loading.
Yeom *et al.*, 2014	PMMA	MMT		emulsion	(i) T_g was enhanced by 27 ^oC as suggested by DMA. (ii) UV/VIS absorbance was reduced.

1.11.2 Polymer/clay nanocomposites using compatibilizer

The effect of maleic anhydride-grafted ethylene vinyl acetate (EVA-g-MA) and maleic anhydride-grafted linear low density polyethylene (LLDPE-g-MA) compatibilizers on the morphological, thermal and crystallization behaviour of ethylene vinyl alcohol (EVOH)/clay nanocomposites was investigated by Artzi et al., 2003. The nanocomposites were fabricated by melt-blending method containing various content of compatibilizer (1, 5 and 10 wt.%). The XRD data suggested that all the nanocomposites possessed intercalated structure. SEM micrographs also confirmed that EVA-g-MA compatibilizer provided better dispersion of clay over LLDPE-g-MA as the later had bigger particle size. The crystallization temperature was lower for compatibilized nanocomposites compared to uncompatibilized and pure polymer. From the DMA analysis, it was observed that both storage modulus and T_g were reduced with an increase in compatibilizer loading. The TGA results proposed that the thermal stability was found to be highest at 10 wt.% loading of compatibilizer for both the nanocomposites. At 50% weight loss, the EVA-g-MA and LLDPE based nanocomposites containing 15wt.% clay exhibited around 50 and 43 ^{o}C, respectively higher decomposition temperature over pure polymer.

Hwang et al., (2006) prepared the low density polyethylene (LDPE)/aliphatic polyester (APES)/organoclay ternary nanocomposites through melt intercalation method using two different kinds of organoclays (Cloisite 20A and Cloisite 30B). The effect of a compatibilizer, polyethylene-graft-maleic anhydride (PE-g-MAH), on the properties of the ternary nanocomposites was investigated. From the XRD analysis, it was found that all the nanocomposites exhibited intercalated structures with and without grafting agent. However, the degree of intercalation for LDPE/APES/Cloisite 30B hybrids was higher than the LDPE/APES/Cloisite 20A nanocomposites. The AFM results suggested that the silicate particles in the nanocomposites were finely dispersed in the matrix with an average length from 0.1 to 1 mm for both organoclays. The LDPE/APES/organoclay nanocomposites showed higher tensile properties than the corresponding LDPE/APES blends for both type of organoclays. It was also observed from the SEM analysis that the LDPE/APES/Cloisite 30B nanocomposite showed fine particle-like morphology over Cloisite 20A based nanocomposites. The rheological study also suggested that at 1 rad/sec, the storage modulus of LDPE/APES/Cloisite hybrids 30B was 58% higher than the LDPE/APES/Cloisite 20A nanocomposite

A terpolymer of ethylene, acrylic ester, and glycidyl methacrylate ester (E-AE-GMA) was used as compatibilizer to improve the interaction between poly(trimethylene terephthalate) (PTT) and organically treated MMT using torque rheometer (Favaro et al., 2009). The FTIR analysis confirmed the various functional groups present in the nanoclay and compatibilizer. The XRD results suggested that only intercalated morphology was obtained without compatibilizer. However, with the addition of compatibilizer, both intercalated and exfoliated structure was obtained for different nanocomposites, which were verified by TEM. The thermal degradation was improved for all nanocomposites by 3-14 ^{o}C as suggested by TGA analysis.

In the work reported by Wang et al., (2009), three different kinds of compatibilizers (PP grafted with maleic anhydride (PP-g-MA), ethylene-octene copolymer grafted with MA (POE-g-MA), and ethylene-vinyl acetate copolymer grafted with MA (EVA-g-MA)) were used as compatibilizers to investigate the influence of interfacial interaction on the crystallization and mechanical properties of polypropylene (PP)/nano-$CaCO_3$ composites**.** PP nanocomposites were prepared by melt-intercalation technique. The good compatibility between PP chain in PP-g-MA and PP matrix improved the dispersion of nano-$CaCO_3$ particles, favored the nucleation effect of nano-$CaCO_3$ and increased the tensile strength and modulus. However, it reduced the ductility and impact strength of composites. The partial compatibility between POE in POE-g-MA and PP matrix had little effect on crystallization and mechanical properties of PP/nano-$CaCO_3$ composites. The poor compatibility between EVA in EVA-g-MA and PP matrix retarded the nucleation effect of nano-$CaCO_3$, and reduced the tensile strength, modulus, and impact strength.

Hellati et al., (2010) studied the role of compatibilizer, SEBS-MAH (styrene ethylene/butylene styrene block copolymer grafted with maleic anhydride) on the morphological and mechanical properties of blends i.e. polyethylene terephthalate with isotactic polypropylene (PET/iPP) and high density polyethylene (PET/HDPE) blends. The results revealed that PET was incompatible with both iPP and HDPE. However, the presence of compatibilizer, SEBS-MAH allowed the compatibilization between them. The addition of clay (3-5%) induced hardness in the PET/iPP and PET/HDPE blends.

The PP/Mg_2Al LDH nanocomposites were prepared by the direct melt-intercalation method using maleic anhydride grafted polypropylene (PP-g-MA) as a compatibiilizer (Lonkar et al., 2011). The XRD results revealed that morphology was shifted from intercalated to partially

exfoliated with an increase in compatibilizer content. The XRD results were further supported by TEM analysis, where higher intergallery spacing was observed with highly compatibilized nanocomposites. The DSC results displayed that the melting temperature (T_m) was marginally improved by 2 ^oC. However, crystallization temperature was enhanced by 11 ^oC as compared to pure PP. The TGA results also revealed that maximum degradation temperature (T_{max}) was improved by 44 ^oC over pure polymer. From the mechanical analysis, it was found that tensile strength, modulus, flexural modulus, izod impact strength were improved by 30, 25, 35 and 7%, respectively at 10 wt.% content of compatibilizer. Similarly, the oxygen gas permeability was reduced by 29% over pure PP.

Manjhi and Sarkhel, (2011) studied the influence of MAH-g-EPDM (maleic anhydride grafted ethylene propylene diene monomer) on the properties of kaolin reinforced EPDM rubber. EPDM-kaolin composites containing various quantity of maleated EPDM were prepared by mixing on two roll mill. The FTIR analysis confirmed the presence of different functional groups in the composites. The cross-linking density was increased with the addition of filler due to interfacial and intertubular interaction between EPDM and filler. Similarly, the hardness was also increased with increasing the filler concentration. It was also observed that tensile modulus was increased as the concentration of kaolin filler increased from 0 to 20 phr. From the SEM, it was observed that the fillers distributed homogenously with increasing the compatbilizer. The rheological study also suggested that optimum curing time increases with increasing compatibilizer concentration without decreasing torque value.

Various weight loadings of MWCNT (2-6 wt.%) were added in the PP nanocomposites prepared using two different grades of MA-g-PP via melt-blending process (Ezat et al., 2012). From the mechanical analysis, it was observed that the addition of compatibilizer results in enhanced tensile and flexural modulus due to well dispersion of CNT in polymer matrix. It was also noticed that tensile strength decreased in the presence of low molecular weight MA-g-PP. The DSC results demonstrated that the crystallization temperature was enhanced by 5-6 ^oC at 2 wt.% loading of filler. The morphological analysis carried out using SEM revealed that the dispersion of CNT was improved and also decreased the size of aggregation in the presence of MA-g-PP with high grafting level.

The influence of three compatibilizers, poly(styrene-*grafted*-acrylonitrile)-maleic anhydride (SAN-g-MAH), polyethylene-*co*-glycidyl methacrylate (EGMA) and maleic anhydride (MAH) on the mechanical, thermal, morphological and rheological properties of

poly(propylene carbonate)(PPC)/poly(methyl methacrylate) (PMMA) blends prepared by melt blending was investigated by Yoo et al., (2013). It was observed that tensile strength improved with the addition of compatibilizer up to 5 phr and found maximum for SAN-g-MAH compatibilizer over EGMA and MAH compatibilizer. The droplet size of the dispersed phase (PMMA) also reduced with the addition of compatibilizer. The glass transition temperature (T_g) was also enhanced by 6 ^oC at 5 phr of SAN-g-MAH. The shift in T_g indicated that compatibility was improved between PPC and PMMA. The TGA analysis implied that thermal degradation temperature was enhanced by 9 ^oC, when 50% weight loss as taken as reference. The increase in complex viscosity of the blend also indicated that interaction increased between the two components i.e. PPC and PMMA.

The polypropylene nanocomposites prepared with dimethyldioctadecylammonium modified MMT were evaluated for their mechanical and gas permeation properties (Mittal, 2008). Three different kinds of compatibilizers i.e. PP-g-MA1, PP-g-MA2 and PP-b-PPG were used to improve the compatibility between the polymer and filler. The XRD results elucidated that all the nanocomposites exhibits intercalated structures. The oxygen permeability test showed that 2 wt.% compatibilizer (PP-g-MA2) was optimum to reduce the gas permeation for PP/OMMT 3% sample. Calorimetric study revealed that melting and crystallinity behaviour was remained unchanged even at 8% addition of PP-g-MA2. The tensile modulus was found to be maximum (40% higher than pure PP) at 2 wt.% content of PP-g-MA2 compatibilizer.

Basson and Reenen, (2012) studied the effect of two compatibilizer (PP-g-MA and EvOH) on the properties of poly(propylene)-pine wood composites. They found that joint compatibilizers of PP-g-MA and EvOH, provided better control over the hardness to impact properties of composite materials. It was also observed that some of the properties improved depending upon the ratio between PP-g-MA and EvOH used. Table 1.2 summarize the classification of literature based on compatibilizers.

Table 1.2 Classification of literature based on compatibilizer

Authors	Polymer matrix	Nanofiller	Compatibilizer	Method of preparation	Remarks
Artzi *et al.*, 2003	EVOH	Nanomer-1.30E clay	EVA-g-MA LLDPE-g-MA	melt blending	(i) Intercalated structure obtained. (ii) At 50% weight loss, thermal stability was improved by 50 ^{o}C for nanocomposite containing EVA-g-MA.
Hwang *et al.*, 2006	low density polyethylene (LDPE)/aliphatic polyester (APES)	Cloisite 20A and Cloisite 30B	PE-g-MAH	melt intercalation	(i) Intercalated structure as suggested by XRD. (ii) Storage modulus was increased by 58% for Cloisite 30B based nanocomposites.
Favaro *et al.*, 2009	poly(trimethylene terephthalate) (PTT)	OMMT	E-AE-GMA	melt blending	(i) Both intercalated and exfoliated structure. (ii) Thermal stability was enhanced by 3-14 ^{o}C.
Wang *et al.*, 2009	PP	nano-$CaCO_3$	PP-g-MA, POE-g-MA and EVA-g-MA	melt intercalation	(i) PP-g-MA increased the tensile strength and modulus over other compatibilizer.
Hellati *et al.*, 2010	(PET/iPP) and (PET/HDPE) blends	Bentonite clay	SEBS-MAH	melt blending and compression molding	(i) Hardness was increased by 60% for PET/iPP blends containing 5% clay. (ii) PET became compatible with iPP and HDPE, in the presence of compatibilizer.
Lonkar *et al.*, 2011	PP	Mg_2Al	PP-g-MA	melt intercalation	(i) Exfoliated structure obtained. (ii) Tensile strength, modulus, flexural modulus, impact strength improved by 30, 25, 35 and 7%, respectively. (iii) Oxygen gas permeability was reduced by 29%.
Manjhi and Sarkhel, 2011	EPDM rubber	kaolin	MAH-g-EPDM	compression molding	(i) Cross-linking density and hardness was increased with an increase in kaolin loading.

Authors	Polymer matrix	Nanofiller	Compatibilizer	Method of preparation	Remarks
Ezat *et al.*, 2012	PP	MWCNT	MA-g-PP	melt compounding	(i) Aggregation was reduced in the presence of compatibilizer. (ii) Crystalline temperature of nanocomposite was improved by 5-6 ^{o}C over pure polymer.
Yoo *et al.*, 2013.	poly(propylene carbonate)(PPC)/ poly(methyl methacrylate) (PMMA)		SAN-g-MAH, EGMA and MAH	melt blending	(i) T_g was improved by 6 ^{o}C. (ii) Thermal stability was enhanced by 9 ^{o}C.
Mittal, 2007	PP	OMMT	PP-g-MA1, PP-g-MA2 and PP-b-PPG	compounding followed by compression molding	(i) Intercalated structure was obtained. (ii) Tensile modulus was increased by 44%.
Basson and Reenen, 2012	PP	pine wood	PP-g-MA and EvOH	melt mixing	(i) Hardness and impact strength was improved by the combination of both compatibilizers.

1.11.3 Polymer/Layered Double Hydroxide Nanocomposites

PP/LDH nanocomposite and PP/MMT nanocomposites were synthesized using melt-intercalation technique and the properties of these composites were compared (Ding et al., 2006). The XRD and TEM analyses showed that the PP/LDH nanocomposites had an exfoliated structure and the ZnAl LDH layers were well dispersed at molecular level in the PP matrix. The TGA and DMA data demonstrated that the PP/LDH nanocomposites possessed higher thermal stability as compared to pristine PP and PP/MMT nanocomposites, especially at high temperature range. The XPS and FTIR results showed that the photo-oxidation mechanism of PP in the PP/LDH materials was much lower than that of PP and PP/MMT samples, indicating better UV stability of PP/LDH nanocomposites.

Trujillano et al., (2006) prepared LDH with the hydrotalcite-like structure, containing Cu (II) and Al (III) in the layers and different alkyl sulphonates in the interlayer and characterized them by XRD, FTIR and TGA analysis. The LDH was prepared by direct synthesis through coprecipitation using NaOH as precipitation agent. The sharp XRD peak recorded at 2θ value of 12 ^{o}C corresponding to (003) plane of a hydrotalcite structure. From the width of the brucite-like, the interlayer spacing calculated was 0.27 nm, indicating that the carbonate anions were located with their molecular plane parallel to the brucite-like layers. They reported that after surfactant modification, the diffraction of basal planes shifted towards lower diffraction angle, which was expected from the molecular size of the surfactants.

It was observed from the XRD and TEM analysis that the exfoliated ZnAl LDH layers were well distributed in the polystyrene matrix (Ding and Qu, 2006). The completely exfoliated morphology were obtained even at 10 and 20 wt.% of LDH loadings in the PS nanocomposites, which were prepared by emulsion and suspension polymerization. The FTIR spectra confirmed the various function groups in the nanocomposites. The stretching vibration of sulfate of SDS was found at 1218 and 1247 cm^{-1}. When 50% weight loss was selected as a reference, the PS nanocomposite having 5 wt.% LDH, prepared by emulsion method, displayed about 28 ^{o}C higher thermal degradation temperature over neat polymer.

Ethyl vinyl acetate (EVA) nanocomposites with sodium dodecyl sulfate modified Mg-Al LDH was prepared through solution intercalation method by Kuila et al., (2007). The XRD analysis showed that (003) peak corresponding to LDH shifted to lower 2θ value, indicating the formation of intercalated nanocomposites. However, TEM micrograph exhibited the presence of partially exfoliated Mg-Al LDH layers along with the stacked crystallites in the

EVA matrix. The tensile strength and elongation at break for the EVA nanocomposite containing 1 wt.% LDH increased by 42% and 5%, respectively over neat polymer.

Du et al., (2007) prepared Nylon 6/Mg-Al LDH nanocomposite by melt intercalation of nylon 6 into the part of organo modified Mg-Al LDH interlayer. The XRD analysis demonstrated that high LDH loading made the LDH layer difficult to exfoliate. An increase of 12 ^{o}C in crystallization temperature compared to pure nylon 6 was noticed by adding 5 wt% of Mg-Al (H-DS). The thermal degradation temperature of nanocomposite with 5 wt.% loading (NC-5) was 19.7 ^{o}C lower than that of pure nylon 6. The peak heat release rate (pHRR) values decreased significantly for the NC-5 sample having 5 wt.% of Mg-Al (H-DS).

Mg-Al LDH modified with sodium 1-decasulfonate ($C_{10}H_{21}SO_3Na$) was incorporated into ethylene propylene diene terpolymer (EPDM) and carboxylated nitrile rubber (XNBR) by Pradhan et al., (2008). Both the elasotmers had widely different polarities and functional groups. The nanocomposites were compounded by internal mixer followed by compression molding press at 150 ^{o}C and 100 kN pressure. The XRD results demonstrated that intercalated structures were present in different nanocomposites. TEM micrographs suggested that the Mg-Al LDH were more efficiently exfoliated in XNBR/LDH samples, while in the EPDM nanocomposites, the LDH layers were distributed in soft cluster form at 5 wt.% loading. The XNBR samples (17.83 MPa) exhibited higher tensile strength as compared to EPDM nanocomposites (3.25 MPa). Similarly, the tensile modulus and elongation were also increased. It was also observed that LDH particle promoted strain-induced crystallization in XNBR/LDH nanocomposites.

Qiu et al., (2005) made exfoliated polystyrene (PS)/Zn-Al LDH nanocomposite by in-situ atom transfer radical polymerization. When 50% weight loss was considered as a point of reference in the TGA profile, the decomposition temperature of PS/Zn-Al LDH nanocomposite was about 45 ^{o}C higher than that of pure PS.

The influence of two different nanofillers, i.e. adipate-LDH (A-LDH) and 2-methyl-2-propene-1-sulfonate-LDH (S-LDH) on the physical, thermal, mechanical and fire retardancy properties of unsaturated polyester (UP) was investigated by Pereira et al., (2009). The XRD result suggested that intercalated morphology was obtained for different nanocomposites. It was found from the physical appearance that A-LDH based nanocomposites demonstrated homogenous distribution of nanofiller, and the UP/S-LDH nanocomposites had aggregates in polymer matrix. The mechanical study revealed that the addition of organo-LDH, reduced the

flexural strength. A significant reduction in flammability by 46% was also reported for unsaturated polyester nanocomposites filled with 1 wt.% A-LDH.

Ca-Al LDH modified with benzoate anions (LDH-B) (1-7.5 wt.%) was impregnated into poly(styrene-co-methyl methacrylate) matrix by in-situ polymerization process (Matusinović et al., 2009). The XRD results indicated that the layered structure of Ca-Al LDH disappeared in the nanocomposite due to the disordering. However, the TEM micrographs revealed that alternating matrix-particle region appear in the form of intercalated nanocomposite structure. The DSC measurements exhibited slightly diminished value of T_g over PS-PMMA copolymer. It was also observed that thermal degradation temperature was increased by 10-26 ^oC for different nanocomposites at 50% weight loss.

The structural and thermal properties of PS/Co-Al LDH nanocomposites were investigated by Krishna and Pugazhenthi (2011). The nanocomposites with various content of LDH were prepared by solvent blending method. TEM and XRD analysis verified the formation of exfoliated nanocomposites up to 5 wt.% LDH content. The thermal degradation temperature of PS nanocomposite containing 5 wt.% Co-Al LDH was found to be 12 ^oC higher than that of pure PS when 50% weight loss was selected as a point of comparison. The glass transition temperature of PS nanocomposite was about 14 ^oC higher than that of pure PS.

The thermal degradation behavior of polypropylene/organically modified Co-Al LDH (PP/Co-Al-LDH) was studied via TGA analysis by Wang et al., (2011). The different compositions of PP/Co-Al-LDH nanocomposites were prepared by melt compounding method. The thermal degradation activation energies of the PP/Co-Al-LDH nanocomposite were determined via Friedman and Flynn-Waal-Ozawa methods. The effect of Co-Al-LDH concentration (1.5-6.0 wt.%) on the thermal properties was investigated. The results clearly pointed out that the activation energies of the nanocomposites were higher than pure PP at the same weight loss. Two methods demonstrated similar trend of change of activation energy with change in conversion (α).

PP/LDH nanocomposites were synthesized by one step reverse micro emulsion method (Wang et al., 2012). Melt rheology of the prepared nanocomposites showed a reduced storage modulus (G') and loss modulus (G") value when the LDH loading is low (less than 2 wt.%). The reduced G' and G" were attributed to the enhanced mobility of confined polymer chains at the PP-LDH interface. When the LDH loading increased from 2 to 16 wt.%, both storage and loss modulus gradually increased. For PP/LDH nanocomposites, damping factor

increased with increasing LDH loading up to 1.5 wt.%, then it started to decrease with further addition of LDH. This was due to LDH nanoparticle that restricts the relative motion of polymer chains, making the nanocomposite stiffer. Complex viscosity clearly followed the trend of storage and loss modulus of PP/LDH nanocomposites.

The exfoliated nanocomposite based on Mg-Al LDH and PMMA was prepared by exfoliation/adsorption process (Li et al., 2003). They found that, decomposition temperature of PMMA/LDH nanocomposites corresponding to 5 wt.% weight loss was 288.5 ^{o}C, which was 149 ^{o}C higher than that of pure PMMA (140 ^{o}C). The temperature corresponding to the maximum rate of weight loss was 367.2 ^{o}C and 337.2 ^{o}C for pure PMMA and PMMA/LDH nanocomposite.

Chen and Qu (2005) reported the improved thermal and mechanical properties for PMA/Zn-Al LDH nanocomposites over pure polymer. The intercalated nanocomposite was formed by in-situ polymerization of methyl acrylate with organomodified Zn-Al-LDH. The tensile strength of PMA/Zn-Al LDH nanocomposite was enhanced to 3.81 MPa, compared to the pure PMA (0.46 MPa). When, 10% weight loss was taken as the reference point for comparison, the decomposition temperature of PMA, PMA/OZn-Al-LDH nanocomposite and PMA/OZn-Al-LDH micro composite samples were 325, 342 and 324 ^{o}C, respectively.

The disorderly exfoliated PMMA/LDH nanocomposite was prepared by in-situ bulk polymerization (Wang et al., 2006). They found that at 5% weight loss, the decomposition temperature of PMMA/LDH 5 was about 90 ^{o}C higher than that of pristine PMMA. The glass transition temperature was 22 ^{o}C higher for disorderly exfoliated PMMA/LDH nanocomposite than that of pure PMMA (105 ^{o}C). The tensile modulus of this nanocomposite was enhanced with increased LDH-U content. An increase of LDH-U content from 3 to 5 wt.% enhanced the tensile modulus from 38% to 80% (1.38 GPa to 1.8 GPa). The degradation activation energy of pristine PMMA was 160 kJ/mol, whereas for disorderly exfoliated LDHs/PMMA nanocomposite, it was in the range of 200-240 kJ/mol.

Manzi-Nshuti et al., (2009) investigation revealed that XRD analysis of PMMA/Ca_3Al LDH and PMMA/Ca_3Fe LDH showed exfoliated structure of nanocomposites. TEM analysis was also performed to confirm the nanocomposite structure. It was revealed that at lower magnification, PMMA/Ca_3Fe LDH 5 showed agglomeration in polymer matrix. Higher magnification showed that LDHs were seen in group not as individual layers. The TEM analysis of other PMMA/LDH nanocomposites showed mixed morphology (both intercalated

and exfoliated) at higher magnification. When 10% weight loss was considered as a point of comparison, PMMA/Ca_3Al LDH10 and PMMA/Ca_3Fe LDH10 showed significant improvement in thermal stability (28 ^oC and 37 ^oC compared to pure PMMA).

Nyambo et al., (2009) worked on the effect of organic modification of LDH. Organic treatment of LDH helped to improve structural, thermal and fire retardancy properties of PMMA/LDH nanocomposite. TEM micrographs suggested that nanocomposites formation was seen in modified LDH, whereas unmodified MgAl-CO_3, MgAl-NO_3 and calcined LDH gave micro-composite structure. Organic modification of MgAl-CO_3 gave 51% reduction in peak Heat Release Rate (pHRR) value of its nanocomposites. On the other hand, unmodified Mg-Al CO_3, Mg-Al NO_3 and calcined LDH gave only 30% reduction in PHRR value of its composites. This analysis clearly indicated the improved fire retardant property due to organic modification of LDH. TGA analysis also exhibited higher thermal decomposition value for PMMA/organo modified Mg-Al LDH nanocomposites when compared with PMMA composites. Table 1.3 summarize the literature review on LDH based polymer nanocomposites.

Table 1.3 Classification of literature on LDH based polymer nanocomposites

Authors	Polymer matrix	Nanofiller	Modifier	Method of preparation	Remarks
Ding *et al.*, 2006	PP	Zn-Al LDH and MMT	sodium dodecyl sulfate	melt intercalation	(i) Exfoliated structure as suggested by XRD and TEM. (ii) PP/LDH nanocomposites had better thermal stability over MMT based compositions.
Trujillano *et al.*, 2006		Cu-Cl LDH	octylsulphonate, octanebenzenesulphonate, dodecylbenzenesulphonate, and octadecanesulphonate	coprecipitation	(i) Interlayer spacing of LDH was increased after modification.
Ding and Qu, 2006	PS	Zn-Al LDH	sodium dodecyl sulphate	emulsion and suspension polymerization	(i) Exfoliated structure. (ii) At 50% weight loss, thermal degradation was improved by 28^{o}C.
Kuila *et al.*, 2007	EVA	Mg-Al LDH	sodium dodecyl sulfate	solution intercalation	(i) Intercalated structure obtained. (ii) Tensile strength was increased by 42%.
Du *et al.*, 2007	Nylon 6	Mg-Al LDH	sodium dodecyl sulfate	melt intercalation	(i) Intercalated structure obtained. (ii) Crystallization temperature was improved by 12^{o}C. (iii) Thermal degradation temperature was enhanced by 19^{o}C.
Pradhan *et al.*, 2008	EPDM and XNBR	Mg-Al LDH	1-decasulfonate	compression molding	(i) Intercalated structure obtained. (ii) Tensile strength was improved for XNBR (17.83 MPa) over EPDM (3.25) nanocomposites.
Qiu *et al.*, 2005	PS	Zn-Al LDH	sodium dodecyl sulfate	in-situ polymerization	(i) At 50% weight loss, decomposition was improved by 45^{o}C.

Authors	Polymer matrix	Nanofiller	Modifier	Method of preparation	Remarks
Pereira *et al.*, 2009	unsaturated polyester	adipate-LDH (A-LDH) and 2-methyl-2-propene-1-sulfonate-LDH (S-LDH)		sonication followed by curing	(i) Intercalated structure. (ii) Flammability was reduced by 46%.
Matusinović *et al.*, 2009	poly(styrene-co-methyl methacrylate)	Ca-Al LDH	benzoate anions	in-situ polymerization	(i) Intercalated structure. (ii) At 50% weight loss, thermal degradation temperature was improved by 26 ^{o}C.
Krishna and Pugazhenthi, 2013	PS	Co-Al LDH	sodium dodecyl sulfate	solvent blending	(i) Exfoliated structure. (ii) T_g was increased by 14^{o}C. (iii) Thermal stability was enhanced by 12 ^{o}C.
Wang *et al.*, 2011	PP	Co-Al LDH	DBS	melt compounding	(i) Activation energy was enhanced with increase in LDH loading.
Wang *et al.*, 2012	PP	Mg-Al LDH	dodecyl sulfate	micro emulsion polymerization	(i) Storage and loss modulus was increased with increase in loading. (ii) Damping factor was reduced at higher loading.
Li *et al.*, 2003	PMMA	Mg-Al LDH	glycine	exfoliation/adsorption process	(i) Exfoliated structure. (ii) At 5% weight loss, thermal stability was improved by 9^{o}C.
Chen and Qu, 2005	Poly methyl acrylate (PMA)	Zn-Al LDH	sodium dodecyl sulfate	in-situ polymerization	(i) Intercalated structure. (ii) Tensile strength was improved from 0.46 MPa (PMA) to 3.81MPa (PMA nanocomposites).

Authors	Polymer matrix	Nanofiller	Modifier	Method of preparation	Remarks
Wang *et al.*, 2006	PMMA	LDH-U	10 - undecenoate	in-situ polymerization	(i) Exfoliated structure. (ii) T_g was enhanced by 22 ^oC. (iii) Tensile modulus was improved from 1.38 GPa (PMMA) to 1.80 GPa (PMMA nanocomposites).
Manzi-Nshuti *et al*., 2009	PMMA	Ca_3Al LDH and Ca_3Fe LDH	10 - undecenoate	in-situ polymerization	(i) Both intercalated and exfoliated. (ii) At 10% weight loss, thermal stability of Ca_3Al LDH, Ca_3Fe LDH was improved by 28 and 37 ^oC, respectively.
Nyambo *et al.*, 2009	PMMA	MgAl-CO_3, MgAl-NO_3 and calcined LDH	benzene phosphate	melt blending	(i) pHRR was reduced by 51% for modified MgAl-CO_3 based nanocomposites. (ii) Unmodified LDH exhibited 30% decline in pHRR.

1.12 OUTCOME OF LITERATURE REVIEW

- The extensive literatures survey clearly indicated that the incorporation of modified MMT has improved the mechanical and thermal properties of PMMA nanocomposites. However, none of the earlier researchers reported the effect of MMT modified with octadecylamine.
- The addition of compatibilizer enhanced the compatibility between the polymer matrix and nanofiller and as a result, the properties of nanocomposites increased. Therefore, the role of compatibilizer needs to be identified for the PMMA/clay nanocomposite systems.
- It is also noticed that very few researchers attempted the fabrication of PMMA/LDH nanocomposites. Hence, there is need to explore the properties of PMMA/LDH nanocomposites fabricated by melt-intercalation as well as solvent blending methods.
- Solvent blending method has advantage over melt intercalation, as the former gives the exfoliated structure with improved properties. Therefore, the preparation of PMMA nanocomposites by solvent blending method needs to be studied and the results need to be compared with melt-intercalation technique.

1.13 OBJECTIVES OF THE THESIS

The main objectives of the doctoral work are framed as follows:

- Fabrication and characterization of PMMA/OMMT nanocomposites by melt intercalation technique.
- Role of different compatibilizers on the properties of PMMA/OMMT nanocomposites.
- Fabrication and characterization of PMMA/Co-Al and PMMA/Cu-Cr LDH nanocomposites by melt intercalation method.
- Preparation and characterization of PMMA/OMMT, PMMA/Ni-Al LDH and PMMA/Co-Al LDH nanocomposites via solvent blending method.

1.14 ORGANIZATION OF DOCTORAL THESIS

The doctoral thesis is organized in following chapter as follows:

Chapter 1 elaborates introduction and literature review.

Chapter 2 addresses the fabrication and characterization of PMMA/OMMT nanocomposites by melt intercalation technique using single screw extruder. The properties of PMMA/OMMT nanocomposites were evaluated by X-ray diffraction (XRD), transmission electron microscopy (TEM), thermogravimetric analysis (TGA), Fourier transform infrared spectroscopy (FTIR), Field emission scanning electron microscopy (FESEM), dynamic mechanical analysis and mechanical properties measurement.

Chapter 3 presents the influence of different compatibilizers on the properties of PMMA/clay nanocomposites fabricated by melt intercalation technique.

Chapter 4 deals with the development of PMMA nanocomposites containing Co-Al LDH and Cu-Cr LDH by melt intercalation method. The different properties such as flammability, rheology and degradation kinetics are also discussed.

Chapter 5 describes the preparation and characterization of PMMA/OMMT, PMMA/Ni-Al LDH and PMMA/Co-Al LDH nanocomposites via solvent blending method.

Chapter 6 presents the summary of the inference drawn from the present research work and provides some suggestion towards future direction of research.

Chapter 2

Fabrication and Characterization of PMMA/OMMT Nanocomposites by Melt Intercalation Technique

This work reports the preparation of PMMA nanocomposites using in-house made compatibilizer, maleic anhydride grafted PMMA (PMMA-g-MA) by melt intercalation in the presence of nanoclay modified with 15-35% octadecylamine and 0.5-5 wt.% aminopropyltriethoxysilane. PMMA nanocomposites containing 5 wt.% nanoclay (with and without compatibilizer) were prepared by melt intercalation technique using a single screw extruder. The structural, thermal and mechanical properties of the prepared nanocomposites were investigated. The structural properties of the polymer nanocomposites were examined by the X-ray diffraction (XRD), Field emission scanning electron microscope (FESEM) and Transmission electron microscopy (TEM). The thermal properties were characterized by differential scanning calorimetry (DSC) and thermogravimetric analysis (TGA). The results clearly indicated that thermal stability is influenced by the presence of nanoclay and compatibilizer. The PMMA nanocomposite prepared with compatibilizer displays enhanced mechanical properties over neat PMMA and the nanocomposite synthesized without compatibilizer.

*** The part of this work has been published in **Composite Interfaces**, 2014, 21, 819-832, **Nanocomposites,** 2016, 2, 109-116.

2.1 INTRODUCTION

PMMA nanocomposites reinforced with various nanofillers, such as clay, carbon nanotubes, LDH are evidenced to reveal a noteworthy balance of properties in terms of mechanical, thermal and barrier effects (Li et al., 2003; Costache et al., 2006; Ratinac et al., 2006; Oral et al., 2009; Tsai et al; 2009; Dortmans et al., 2013). Laachachi et al., (2009) reported that the PMMA nanocomposites containing variable loading of boehmite (AlOOH) and alumina (Al_2O_3) fillers developed by melt blending method displayed around 17-35 ^oC higher thermal stability over pure PMMA. PMMA/alumina nanocomposites prepared by Singh et al., (2007) revealed that the presence of alumina nanoparticles improved the impact strength of the nanocomposite by 84% compared to pure polymer. Kiersnowski et al., (2013) synthesized PMMA nanocomposites using MMT modified with (3-acrylamidepropyl) trimethylammonium chloride via emulsion and *in situ* polymerization method. The results indicated that the emulsion polymerization was more effective for deflocculating and intercalating the clay particles with polymer matrix, leading to better thermal stability over in-situ polymerization method. PMMA/OMMT nanocomposites prepared by bulk polymerization and melt compounding method were reported by Kranjnc et al., (2009). The results clearly indicated that the nanocomposites prepared via melt compounding showed ~11 ^oC higher glass transition temperature (T_g) with respect to bulk compounding method at 10 wt.% loading of filler. Brostow et al., (2010) have studied the influence of clay content on the tribilogical behaviour of PMMA-brazilian clay nanocomposites. The dynamic friction of the nanocomposite increased with an increase in the clay content that results higher wear rate compared to pure polymer. In the study of Meneghetti et al., (2006), the nanocomposite samples synthesized via emulsion polymerization demonstrated around 18 ^oC higher T_g when compared with pure PMMA and the sample prepared by *in situ* polymerization displayed about 10 ^oC lower T_g value than the emulsion polymerization. Sahoo et al., (2007) investigated the fabrication of PMMA/MMT nanocomposites by emulsion-free polymerization technique, and the nanocomposites showed better fire-retardant properties than the pure polymer. Methyl methacrylate oligomerically-modified clay was used by Zheng et al., (2005) to produce PMMA/clay nanocomposites by melt compounding. They noticed that the clay was homogenously dispersed in polymer matrix, demonstrating good compatibility with methyl-methacrylate. PMMA/silica nanocomposites with 70 wt.% of silica content exhibited better hardness and thermal stability (Liu et al., 2005). Kuan et al., (2008) have reported that thermal stability of PMMA composites increased about 84 ^oC by

the incorporation of expandable graphite. It is well documented in the literature that the modifier used in the clays also plays a key role in determining the final properties of polymer nanocomposites. Recently, Mohanty et al., (2010) developed PMMA nanocomposites using MMT clay (Cloisite) modified with various chemicals/modifiers including methyl tallow bis-2-hydroxyethyl ammonium (C30B), dimethyl-dihydrogenated tallow ammonium (C20A). The results suggested that the PMMA nanocomposites prepared using clay modified with methyl tallow bis-2-hydroxyethyl ammonium (PMMA/C30B) demonstrated significantly improved mechanical properties than that of PMMA/ C20A.

The objective of this study is to examine the effect of nanoclay which is modified by octadecylamine and compatibilizer, PMMA-g-MA on the properties of PMMA nanocomposites prepared by melt blending technique. The structural, thermal and mechanical properties of the nanocomposites are evaluated using various techniques.

2.2 EXPERIMENTAL

2.2.1 Materials

PMMA (IG 840) used in this study was a commercial product from LG Polymers, South Korea. The melt flow index (MFI at 230 ^{o}C) and specific gravity of PMMA are 5.8 g/10 min and 1.18, respectively. Nanoclay (Nanomer 1.31 PS, MMT clay modified with 15-35% octadecylamine and 0.5-5 wt.% aminopropyltriethoxysilane) was purchased from Sigma-Aldrich, USA. Methanol was procured from Merck India Ltd. Benzoyl peroxide and maleic anhydride were supplied by Loba Chemie Pvt. Ltd. Xylene was obtained from Rankem, RFCL Limited India. All the materials were used as received, without further purification.

2.2.2 Synthesis of PMMA-g-MA

The procedure adopted for the synthesis of maleic-anhydride grafted PMMA was reported elsewhere (Kakati et al., 2012). PMMA (50 g) was first dissolved in 500 mL of xylene at 100 ^{o}C. When the PMMA was completely dissolved, 4 g of maleic anhydride (mixed into minimum quantity of isopropyl alcohol) and 0.4 g of benzoyl peroxide was added in the previous solution with continuous stirring. Then the resulting solution was heated at 100 ^{o}C for 7 h. Finally, the grafted PMMA was precipitated in methanol and the obtained powder was known as PMMA-g-MA that was used as a compatibilizing agent in the blending of nanoclay with PMMA.

2.2.3 Preparation of PMMA nanocomposites

PMMA nanocomposites containing organically modified nanoclay was prepared by melt blending method. Before melt intercalation, PMMA pellets and nanoclay were dried in a vacuum oven at 80 ^{o}C and 65 ^{o}C, respectively for 12 h. PMMA nanocomposites containing 5 wt.% nanoclay (with and without compatibilizer) were prepared by melt intercalation technique in a single screw extruder (Make: Neoplast Engineering Pvt. Ltd., Ahmedabad, India; Model : SSE = 25; L/D=25). The processing temperature was maintained at 150, 200, 210, 220, and 210 ^{o}C for the feed zone, metering zone, compression zone, adapter zone and die-head, respectively. The rotation speed was set at 100 rpm. In a typical experiment, 90 wt.% of PMMA, 5 wt.% nanoclay and 5 wt.% PMMA-g-MA were fed into the extruder, and the obtained extrudate was quenched in water at room temperature. Subsequently, the extrudate was cut into pellets and then oven-dried before being injection moulded (Texair JTS 40 semi-automatic injection moulding machine) at 215-235 ^{o}C to make specimens for mechanical testing. Hereafter, the nanocomposites prepared with 5 wt.% nanoclay and 5 wt.% PMMA-g-MA are referred as PMMA-5-G, while the nanocomposite prepared with 5 wt.% nanoclay (without PMMA-g-MA) is referred as PMMA-5. The composition of the nanocomposites is listed in Table 2.1.

Table 2.1 Composition and TGA results for neat PMMA and its nanocomposites

Sample Name	PMMA (wt %)	Clay Loading (wt%)	PMMA-g-MA (wt%)	Temperature ($T_{10\%}$) at 10% weight loss (^{o}C)	Temperature ($T_{50\%}$) at 50% weight loss (^{o}C)
Neat PMMA	100	-	-	343.6	371.1
PMMA-5	95	5	-	351.0	381.6
PMMA-5- G	90	5	5	350.6	381.9

2.2.4 Characterization Techniques

2.2.4.1 XRD Analysis

The XRD profile of nanoclay and various PMMA nanocomposite samples was done under air at room temperature, using the AXS D8 ADVANCE Fully Automatic Powder X-ray Diffractometer (Bruker) equipped with a Cu-Kα radiation (λ = 0.15406 nm) and Ni filter. The patterns were recorded for 2θ range from 1^{o} to 70^{o} with a scan speed of 0.05^{o} sec $^{-1}$.

2.2.4.2 FTIR Analysis

The synthesized PMMA nanocomposites were analyzed using Shimadzu (Japan) Fourier transform infrared spectroscopy (FTIR) to confirm the presence of various peaks in the polymer nanocomposites.

2.2.4.3 FESEM Analysis

FESEM analysis was carried out to study dispersion of nanofiller in the fractured surface of the nanocomposites using field emission scanning electron microscope (Make: Zeiss, Germany, Model: Sigma). The samples were mounted on special stubs and coated with gold by sputter coater, prior to examination under the electron beam. The image of the fractured samples were recorded by the use of 2 kV accelerating voltage.

2.2.4.4 TEM Analysis

The TEM image of PMMA nanocomposites was obtained on a transmission electron microscope (Make: JOEL, USA, Model: JEM-2100) with an accelerating voltage of 200 KV.

2.2.4.5 Mechanical Properties

The tensile and flexural tests for the nanocomposite samples were carried out in accordance with ASTM D638 and D790, respectively using INSTRON (M 3382, U.K.), Universal Testing Machine. The tensile strength and Young's modulus for the sample (165.1×19.0×3.0 mm) were measured at a cross-head speed of 5 mm/min. For the measurement of flexural strength and modulus of the composites, a rectangular bar (127×12.7×3mm) was placed on the three point bending configuration at 1.42 mm/min deformation rate. The tensile and flexural tests were carried out for five samples of each composition and the average value was reported. All the tests were performed at 23 ± 2 ^{o}C and at a relative humidity of 50 ±5%. Charpy impact measurement was done using an Impactometer (M/s Tinius Olsen, U.S.A.) as per ASTM D256. The hardness (Shore D) values of various nanocomposites were measured according to ASTM D2240. The hardness test was carried out on each sample with 15 readings, and the average value was reported.

2.2.4.6 DSC Analysis

Differential scanning calorimetry (DSC) was performed on a Metler Toledo-1 series to evaluate the glass transition temperature (T_g) of the PMMA nanocomposites. Samples were

heated from 25 to 250 ^{o}C at a rate of 10 ^{o}C min^{-1} under nitrogen atmosphere (N_2 flow rate of 50 mL/min). Around 6 mg of extruded pellets were used for DSC analysis.

2.2.4.7 Thermogravimetric analysis

Thermogravimetric analyses (TGA) of the nanocomposites and nanoclay were carried out on Mettler Toledo thermo gravimetric analyzer, (TGA/SDTA 851® model, Switzerland). Samples were placed in 900 µl crucible. The samples were heated from room temperature to 700 ^{o}C at a heating rate of 10 ^{o}C/min under nitrogen flow of 60 mL/min.

2.2.4.8 Dynamic mechanical analysis

Dynamic mechanical properties of the nanocomposites (sample size: 35 mm × 12 mm × 3 mm) were determined on a TA Instrument (Q-800) New Castle, DE, USA. The temperature dependence frequency was taken as 1 Hz in the temperature range of 25-150 ^{o}C with a heating rate of 3 ^{o}C/min.

2.2.4.9 Atomic Force Microscope (AFM)

The surface morphology was analyzed in non-contact mode using Atomic Force Microscope (AFM) instrument, Model No. 5500 series, Agilent Technologies, U.S.A. The images were recorded at ambient conditions (25 ^{o}C and 30% relative humidity). The scan angle was perpendicular to the surface of specimen. All offline image flattening and analyses of the images were conducted using software, WSxM v5.0.

2.2.4.10 Optical Test

The optical test for nanocomposite samples was performed according to ASTM D1003 on spherical haze-meter instrument (Make: Diffusion Systems Ltd., U.K., Model: EEL 057D).

2.2.4.11 Flammability Test

The PMMA nanocomposite specimen with dimension of 127 × 12.7 × 3 mm was employed for flammability test in accordance with ASTM D635 method. The gauge length was maintained constant (25 mm). The samples were kept horizontally to perform test and average rate of burning was reported in mm/min.

2.2.4.12 Rheological Analysis

The rheological properties of neat PMMA and PMMA/nanoclay nanocomposites were measured by Anton Paar rheometer (Model: MCR 101, Make: Austria) in an oscillation mode

with parallel plate geometry using 25 mm diameter disc at 200 ^{o}C. Samples with 1 mm thickness were prepared by compression molding at 220 ^{o}C and 40 kg/cm^2 pressure.

2.3 RESULTS AND DISCUSSION

2.3.1 XRD Analysis

XRD is utilized as a valuable tool to characterize the types of the layered structure, i.e. intercalated and/or exfoliated polymer/clay nanocomposites, because the peak position changes with the gallery height of the nanoclay. In the case of intercalated nanocomposites, the XRD peak is seen at a larger *d*-spacing value than in the clay, whereas in the case of exfoliated structure, no peak is seen. The d_{001} spacing is calculated from the peak position using Bragg's law: $n\lambda = 2d \sin \theta$, where λ is the X-ray wave length (1.5406 Å) and $n = 1$. Figure 2.1 depicts the XRD patterns of nanoclay and various PMMA nanocomposites. The basal spacing (d_{001}) of (001) peak that appears at 2θ value of 4.15^{o} for the nanoclay is determined to be 2.13 nm. For neat PMMA, the diffraction peak appears at $2\theta = 13.34^{o}$ and the large broad hump originates from the PMMA matrix. It is evident from Figure 2.1 that for the PMMA-5 sample, the basal spacing (d_{001}) of (001) peak of the clay layers increases to 3.67 nm from 2.13 nm of the pure nanoclay. A similar range of basal spacing (3.54 nm) is also found for PMMA-5-G sample. It is noticed that nanoclay layers in the nanocomposites have been intercalated because single extended polymer chains can penetrate between the silicate layers, and a well-ordered multilayer morphology results with alternating polymeric and inorganic layers. These results are in agreement with the studies reported by Morgan and Gilman, (2003) for polymer-layered silicate nanocomposites**.**

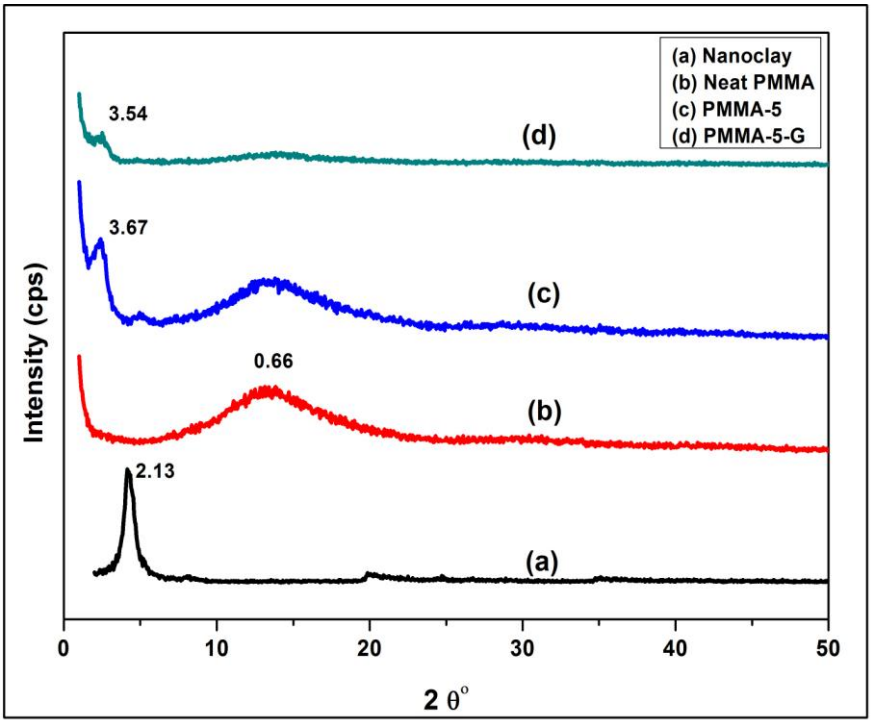

Figure 2.1 XRD patterns of nanoclay, neat PMMA, PMMA-5 and PMMA-5-G nanocomposites

2.3.2 FTIR Analysis

FTIR technique has been used to study the chemical interaction between the nanoclay and PMMA. Figure 2.2 displays the FTIR spectra of nanoclay, neat PMMA, PMMA-5, and PMMA-5-G samples prepared by melt intercalation method. The FTIR spectrum of nanoclay demonstrates that the band appears at 1046 cm^{-1} is attributed to the Si-O stretching vibration of clay. Two peaks are noticed between 3300 and 3700 cm^{-1}, which correspond to –OH stretching vibration. The first peak appeared at 3630 cm^{-1} is assigned to the isolated OH groups, and the other groups, which are involved in hydrogen bonding, are observed at 3246 cm^{-1}. Three subsequent peaks are recorded at 2922, 2849 and 1465 cm^{-1} which denotes CH_2 asymmetric stretching, symmetric stretching, and in-plane scissoring vibrations, respectively. The peaks exhibited at 917, 750, 530, and 458 cm^{-1} correspond to AlAlOH, AlMgOH, Al-O and Mg-O bending vibrations, respectively (Madejová, 2003). The absorption band at 1612 cm^{-1} resembles the bending vibration mode of hydrated water molecules and weakly bonded water molecules (Manoratne et al., 2006).

The FTIR of PMMA and its nanocomposites shows a characteristic peak at 1731 cm^{-1}, which denotes the >C=O group present in the polymer. The peak at 986 represents the –C-H

bending of the polymer chain. The band observed at 1436 cm^{-1} corresponds to -O-CH_3 deformation of PMMA. The band observed at 2994 cm^{-1} is due to the ester methyl stretching vibrations. The band that occurs at 2950 cm^{-1} shows the asymmetric stretching vibration of –CH_3 group, which is broadening in the PMMA-5-G nanocomposite. A very clear and sharp peak is noticed in the range of 3438-3442 cm^{-1} that shows the intra-molecular hydrogen bonding between the nanoclay and PMMA. As the neat polymer and compatibilizer mainly consists of PMMA, it is observed that there is not much difference among samples (b), (c), and (d). Mohanty et al.,(2010) also reported a similar type of result with PMMA-g-MA and Closite 30B clay.

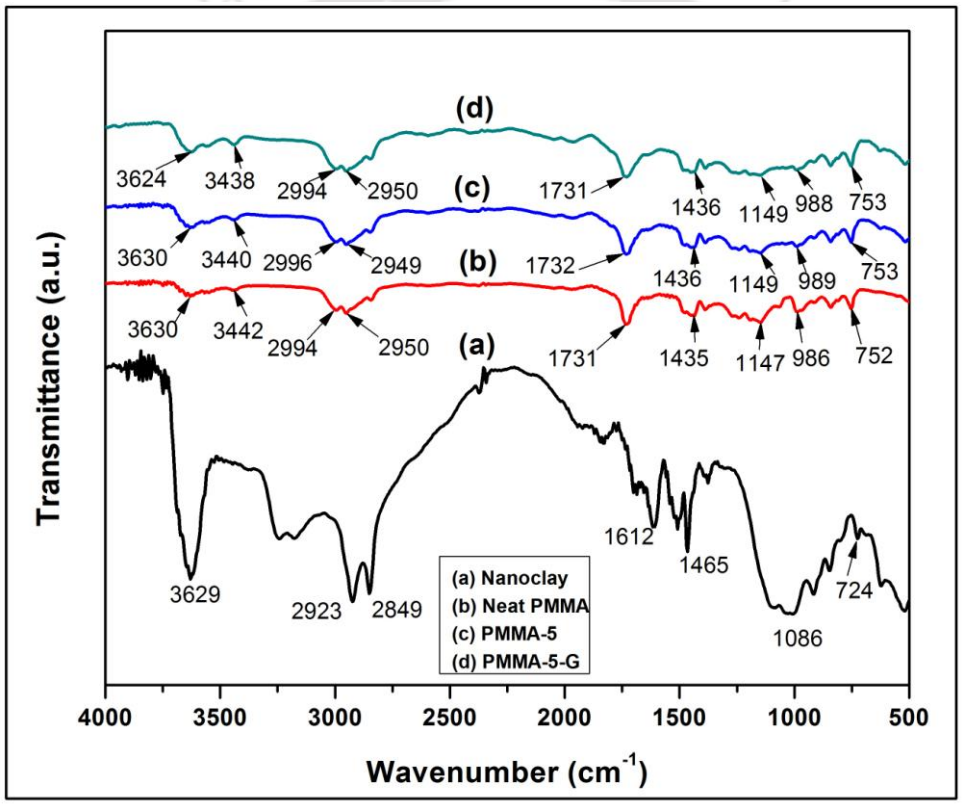

Figure 2.2 FTIR spectra of nanoclay, neat PMMA, PMMA-5 and PMMA-5-G nanocomposites

2.3.3 FESEM Analysis

FESEM studies were carried out to examine the state of clay dispersion in the polymer matrix, fracture surface, nanoclay-polymer interactions at the interface and the load transfer mechanism. Figures 2.3 shows the FESEM micrographs of fractured PMMA-5-G nanocomposite after tensile test. In the case of PMMA-5-G nanocomposite sample, it is seen

that the distribution of nanofiller is more uniform with 5 wt.% of nanoclay loading. It is believed that the compatibilizer i.e. PMMA-g-MA located in the interphase may act as a bridge between the polymer matrix and nanoclay and thus enhances the load ability of the nanocomposite, which results in improved mechanical strength. On the other hand, fractured nanocomposite (Figure 2.3c) reveals that clay platelets are intact with some pullouts as represented by holes.

At higher magnification (Figure 2.3d), filler particles detach themselves from the polymer matrix during fracture as shown by the clean surface of the particle and the hole left around it. Since FESEM magnification is not able to show intercalated or exfoliated clay platelets, the morphological characterization of nanocomposites prepared are further carried out using TEM instrument.

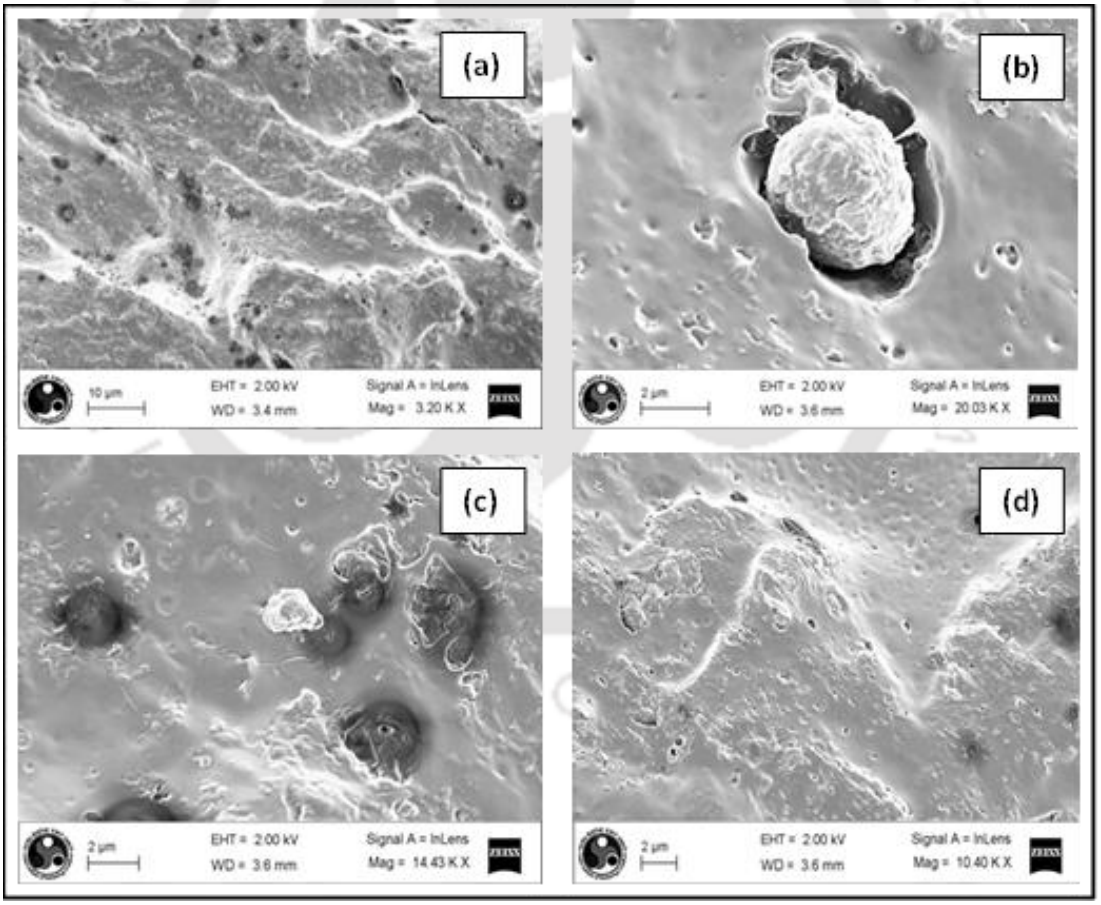

Figure 2.3 FESEM images of PMMA-5-G nanocomposite

2.3.4 TEM Analysis

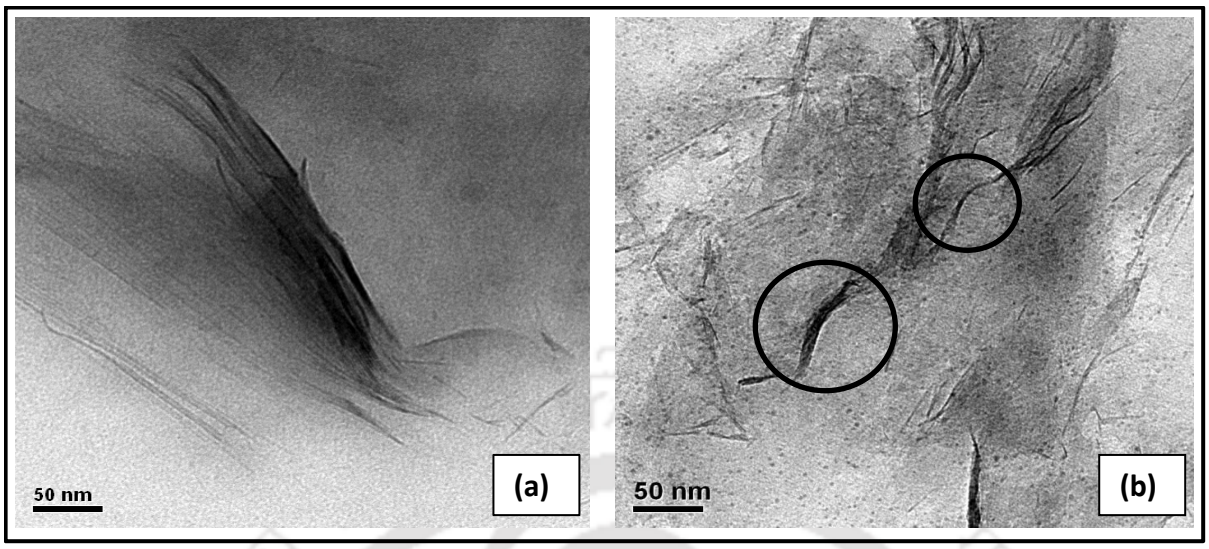

Figure 2.4 TEM images of PMMA-5 (a) and PMMA-5-G (b) nanocomposites

XRD analysis provides the information about gallery spacing of the clay. However, stronger evidence is needed for the judgment about an intercalated or exfoliated structure as well as to explain the dispersion of clay in polymer matrix. Cross-referencing XRD results with the TEM study would provide a basis for more objective analysis. The morphological structure of the nanocomposites was studied by the TEM analysis. Figure 2.4(a) shows the TEM image of PMMA-5 nanocomposites, signifying the formation of intercalated structure. The clay platelets are arranged in parallel manner that leads to tactoid structure. It is also found from the XRD analysis that *d*-spacing of PMMA-5 sample increases to 3.67 nm compared with nanoclay (2.13 nm). This confirms that nanoclay layers are intercalated in the polymer matrix.

Figure 2.4(b) represents the TEM image of PMMA-5-G nanocomposite (prepared with 5 wt.% nanoclay and compatibilizer). This image gives an idea about the nanolevel dispersion of the clay and confirms the partially exfoliated and intercalated morphology of the nanocomposite. From the TEM image, dark lines represent nanoclay layers, whereas the bright areas represent PMMA matrix. In comparison with the PMMA-5 sample, the distribution of clay layers is better in the PMMA-5-G sample, which clearly demonstrates the role of compatibilizer (PMMA-g-MA).

2.3.5 Tensile Properties

One of the main aims of incorporating nanoclay into polymer matrix is the reinforcement provided by clay platelets with polymer matrix that leads to an improvement in mechanical properties. Figure 2.5 depicts the tensile strength and modulus of the PMMA nanocomposites and neat PMMA. It is clear that the PMMA nanocomposites (PMMA-5 and PMMA-5-G) offer an enhanced tensile modulus in comparison with neat PMMA. The PMMA-5 sample displays a marginal increase in tensile modulus compared to neat PMMA, which is probably due to insufficient interaction of the filler to polymer matrix. On the other hand, PMMA-5-G sample demonstrates drastic improvement in tensile modulus with respect to PMMM-5 and neat PMMA. The obtained results indicate that there is effective stress transfer from filler to the matrix in the presence of high aspect ratio nanoclay. The increase in tensile modulus of the PMMA-5-G sample over other nanocomposites is due to the formation of strong interfacial bonds between the anhydride groups of maleic anhydride with -OH groups in nanoclay, which results in good dispersion of the nanoclay in the polymer matrix. A similar observation was also reported by Pavlidou et al., (2008) for PP/PP-MA nanocomposites.

As expected, the introduction of nanofiller into the polymer matrix alters the tensile strength of the polymer. Also, the strength is sensitive to the degree of dispersion of the clay and its interaction with the polymer matrix. It is observed from Figure 2.5 that the tensile strength of the nanocomposite prepared without compatibilizer (PMMA-5) decreases with the addition of nanoclay, while the PMMA-5-G sample displays a slightly higher tensile strength as compared to PMMA-5 and neat PMMA. A decrease in the tensile strength for the PMMA-5 sample is possibly caused by the poor interaction between nanoclay and polymer matrix. This creates stress concentration in the polymer matrix and therefore decreases the tensile strength of PMMA-5 sample (without compatibilizer). However, the addition of compatibilizer, PMMA-g-MA, increases the interaction between nanoclay and maleic anhydride group present in the compatibilizer that results in improved tensile properties of the PMMA-5-G sample over other samples (PMMA-5 and neat PMMA). These results clearly reveal that the incorporation of nanoclay and PMMA-g-MA into the nanocomposite system increases the stiffness and rigidity of the polymer nanocomposites due to increasing the compatibility between PMMA and nanoclay, due to the presence of PMMA-g-MA. PMMA-5-G sample shows an increment of 8% and 98% in tensile strength and modulus, respectively, compared with neat PMMA. While the tensile strength of the PMMA-5-G

sample is slightly increased, the tensile modulus is about doubled by the addition of 5 wt.% compatibilizer. Recently, Unnikrishnan et al., (2011) have also reported the reduction in tensile strength for PMMA nanocomposites prepared with various clays.

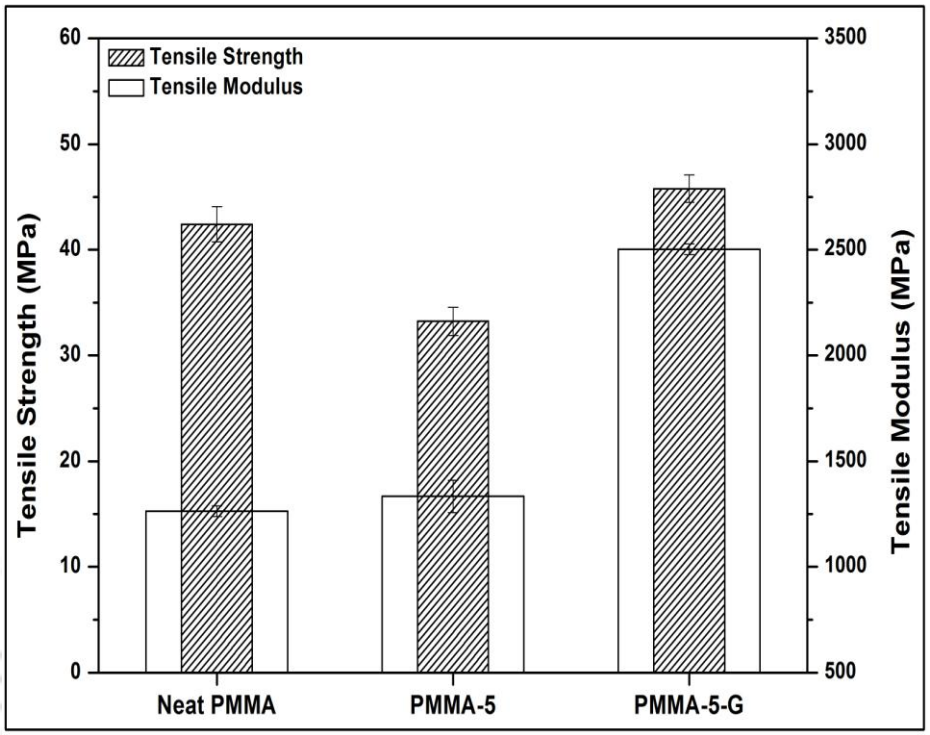

Figure 2.5 Tensile properties of neat PMMA, PMMA-5 and PMMA-5-G nanocomposites

2.3.6 Flexural Properties

The effect of clay as well as compatibilizer on the flexural properties of PMMA nanocomposites is illustrated in Figure 2.6. An addition of 5 wt.% nanoclay in the PMMA (PMMA-5 sample) displays slight improvement (3%) in modulus over neat PMMA. However, a remarkable enhancement in the modulus of PMMA-5-G sample is observed by the addition of PMMA-g-MA. This improvement is about 17 and 21% higher than that of PMMA-5 sample (without compatibilizer) and neat PMMA, respectively. This is due to better dispersion of nanoclay in the PMMA matrix and a strong interfacial adhesion between the nanofiller and polymer matrix. A similar result was also reported by Chow et al., (2005) for the organoclay reinforced polyamide-6/polypropylene nanocomposites.

It is noteworthy to mention that the flexural strength of the nanocomposites can be either increased or decreased, which depends upon various factors, such as dispersion of the nanoclay, interaction of polymer matrix with the filler, organic modifier in the clay, and filler-filler interaction of the clay (Lim et al., 2006). The flexural strength of PMMA-5 sample (see Figure 2.6) decreases when compared to neat PMMA, which is probably due to agglomeration of nanoclay or filler-filler interaction. On the other hand, addition of 5 wt.% compatibilizer (PMMA-g-MA) increases the flexural strength of the nanocomposite (PMMA-5-G) in comparison with neat PMMA and PMMA-5 sample. Comparing with neat PMMA, the presence of nanoclay and PP-g-MA has better enhancement effect on the nanocomposite matrix. This indicates that the interfacial bonding facilitates an effective transfer of load between the polymer and nanofiller. It is also understood that the presence of compatibilizer and nanoclay can boost the fracture energy and offer a strong interfacial shear stress. As a result, crack propagation can be blunted. PMMA-5-G sample shows an increment of 15 and 21% in flexural strength and flexural modulus, respectively, compared with neat PMMA. The enhancement of the mechanical properties of the nanocomposite is considered to be associated with increasing the compatibility of PMMA with nanoclay by the presence of PMMA-g-MA. A similar result was also reported by Lim et al., (2006) for PP nanocomposites.

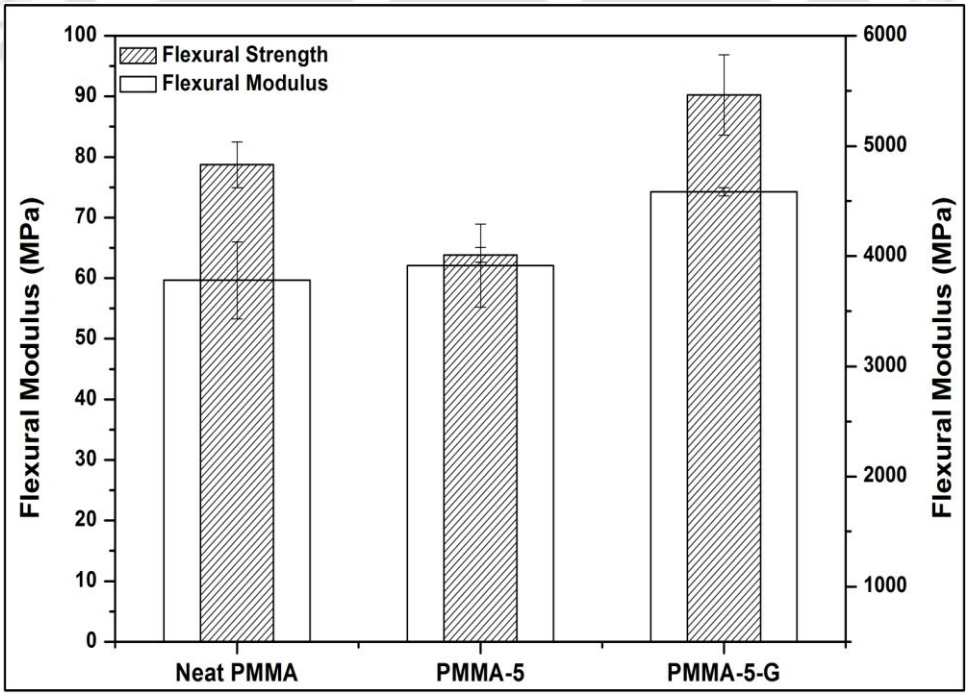

Figure 2.6 Flexural properties of neat PMMA, PMMA-5 and PMMA-5-G nanocomposites

2.3.7 Hardness

Shore D hardness (ASTM D2240) of neat PMMA and its nanocomposites is shown in Figure 2.7. The hardness of PMMA nanocomposite enhances with the addition of nanoclay. The average value of the Shore D Hardness is found to be 81.57, 91.16, and 92.28 for neat PMMA, PMMA-5 and PMMA-5-G sample, respectively. The increase in the hardness of PMMA nanocomposites is due to presence of clay platelets in the polymer matrix. The clay platelets effectively restrict indentation and thus increase the hardness of the nanocomposites. It is noticed that the enhancement of hardness of PMMA-5-G sample over PMMA-5 is less significant. This demonstrates that compatibilizer, PMMA-g-MA, has very little effect on the hardness of PMMA nanocomposite. PMMA-5-G sample exhibits a maximum improvement of Shore D hardness of about 11% over neat PMMA.

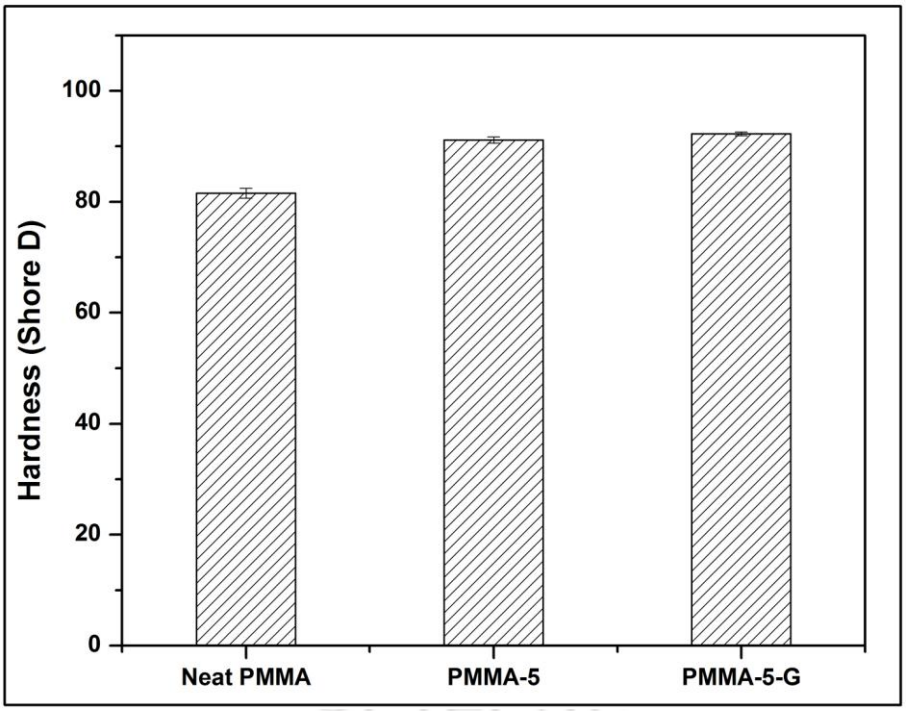

Figure 2.7 Hardness of neat PMMA, PMMA-5 and PMMA-5-G nanocomposites

2.3.8 Differential Scanning Calorimetry

To investigate the mobility of PMMA chains in terms of its T_g (glass transition temperature) in the clay layers, DSC study of neat PMMA and the nanocomposites has been carried out and the results are illustrated in Figure 2.8. The glass transition temperature is determined at

the inflection point between the onset and the end-set temperatures. DSC thermograms represent the presence of second order transition corresponding to the T_g of neat PMMA matrix around 109.31 ^oC. However, there is no first order transition, which indicates the absence of melting temperature, thus confirming amorphous characteristics of the matrix polymer. DSC isotherm of PMMA-5 nanocomposite reveals T_g around 110.36 ^oC. The grafted sample i.e. PMMA-5-G also demonstrates glass transition temperature around 109.58 ^oC indicating no appreciable effect of grafting agent (PMMA-g-MA) on the segmental mobility of the matrix polymer. The results are in agreement with studies reported by Unnikrishnan et al., (2011). The T_g of intercalated polymer nanocomposites is a complicated function of the nature of organic modifier, weight loading of clay, the mean dominant d_{001} spacing of the interlayer gallery space and dispersion and arrangement of the clay stacks in the polymer matrix.

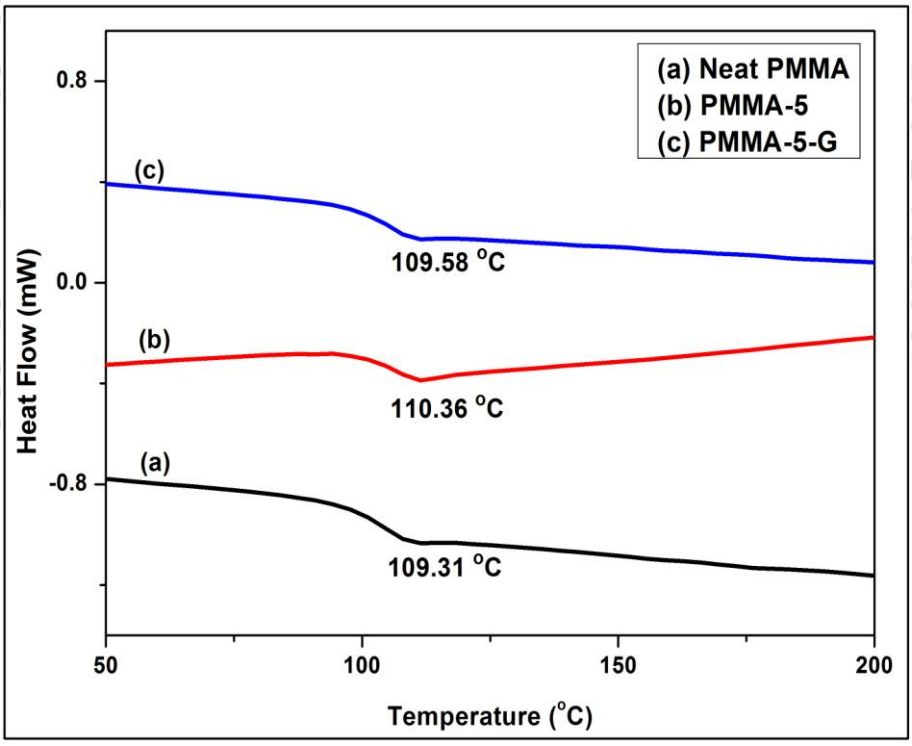

Figure 2.8 DSC curves of neat PMMA, PMMA-5 and PMMA-5-G nanocomposites

2.3.9 Thermogravimetric Analysis

TGA is used to characterize the degradation and thermal stability of the polymer. The dispersion of clay is known to improve the thermal stability of the polymers. Figure 2.9 represents the TGA curves for nanoclay, neat PMMA and PMMA nanocomposites (PMMA-5 and PMMA-5-G). The TGA graph of nanoclay exhibits that total weight loss of about 30% occurs between 50 to 800 ^{o}C. A small weight loss at temperature <300 ^{o}C corresponds to the removal of adsorbed water present in the nanoclay. The weight loss between 300 and 450 ^{o}C is due to the degradation of the organic modifier present in the clay. There is also decomposition at above 450 ^{o}C, which is correlated with dehydroxylation of aluminosilicate.

The parameters that are important from TGA curves are the onset of degradation, which is usually taken as the temperature at which 10% degradation occurs, $T_{10\%}$, and the midpoint temperature of degradation, $T_{50\%}$. From the TGA curves, it is clear that the thermal stability of both PMMA-5 and PMMA-5-G samples is higher, which is confirmed by shifting of the TGA curve of PMMA nanocomposites towards right of the TGA curve of neat PMMA. When 10% weight loss is selected as a point of comparison, the decomposition temperature of neat PMMA, PMMA-5, and PMMA-5-G is found to be 343.6, 351.0 and 350.6 ^{o}C, respectively. The results demonstrate that the degradation of the nanocomposites takes place at a higher temperature than that of neat PMMA (7-8 ^{o}C higher than that of neat PMMA) in the presence of nanoclay. When 50% weight loss is chosen as a point of reference, the decomposition temperature of the nanocomposites is found to be 10-11 ^{o}C higher than that of neat PMMA. This behavior could be explained by the presence of barrier effect of nanoclay lamellar layers, which limit the emission of the produced degradation gases and transmission of heat, therefore resulting in the improvement in thermal stability of the nanocomposites. These results disclose that the PMMA nanocomposites exhibit better thermal stability than that of neat PMMA. The increase in the onset temperature signifies delayed degradation of PMMA nanocomposites. These results are in agreement with the results reported by Sahu et al., (2011) on the thermal degradation of PS/OLDH nanocomposites. The first TGA derivative curve for neat PMMA and PMMA nanocomposites is shown in Figure 2.10. The peak indicates the maximum degradation temperature. All the first TGA derivative curves of PMMA nanocomposites shift towards right side of neat PMMA indicating higher thermal stability of the nanocomposites that will lead to better service performance of the nanocomposites at an elevated temperature. Table 2.1 summarizes the TGA results of the nanocomposites.

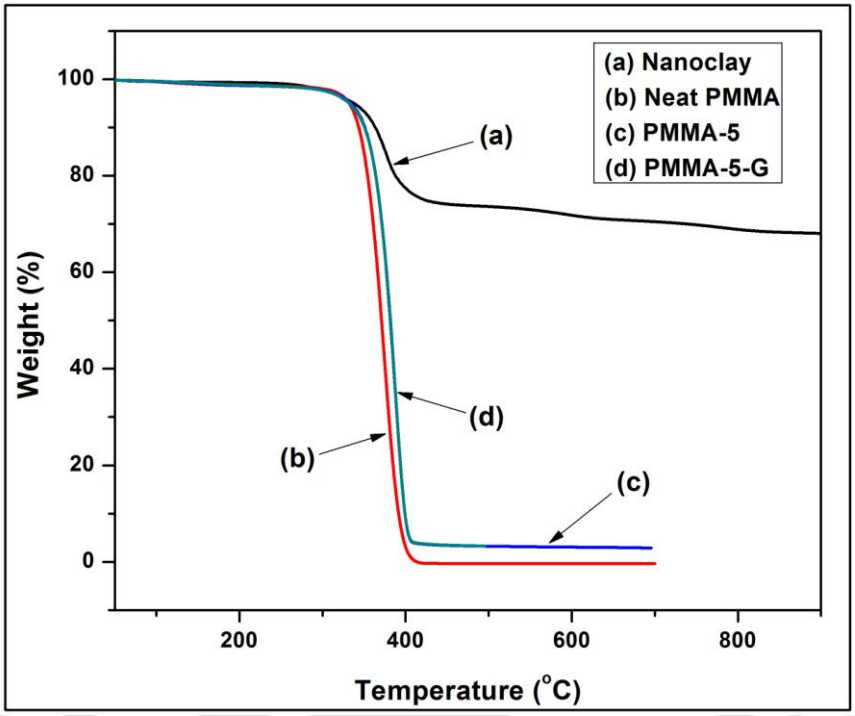

Figure 2.9 TGA curves of nanoclay, neat PMMA, PMMA-5 and PMMA-5-G nanocomposites

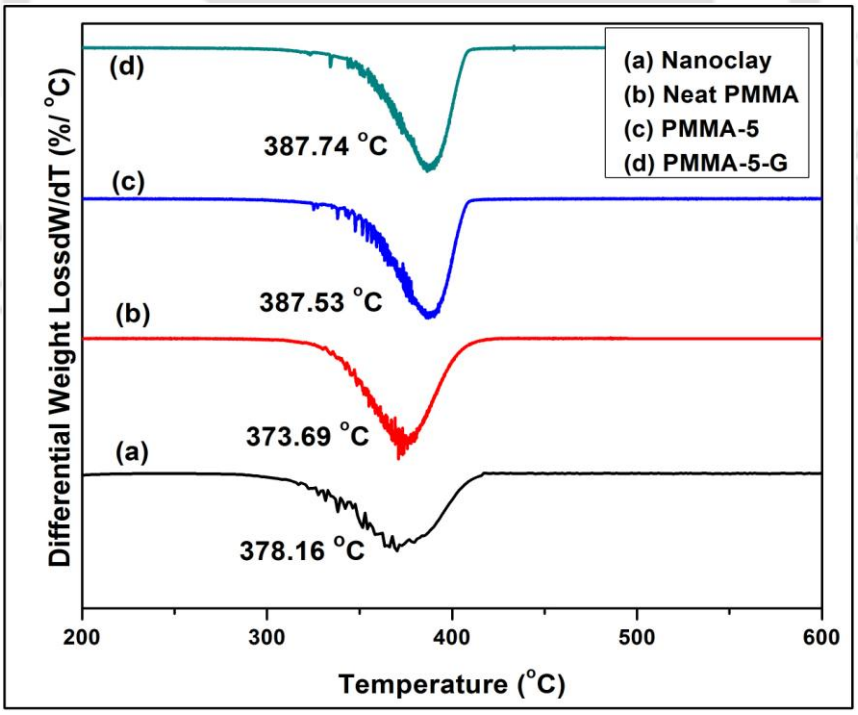

Figure 2.10 TGA derivative of nanoclay, neat PMMA, PMMA-5 and PMMA-5-G nanocomposites

2.3.10 Dynamic Mechanical Analysis

The investigation of storage modulus (E'), loss modulus (E") and tan δ by DMA are very beneficial in determining the performance of a sample under stress at various temperatures. The storage modulus (E') and tan δ, versus temperature for PMMA and its nanocomposites measured from 25 to 150 ^{o}C are illustrated in Figure 2.11(a) and (b). For all the samples, a decrease in storage modulus (E') is observed as the temperature increases. It is seen that at above 70 ^{o}C, the storage modulus decreases sharply with an increase in the temperature. This indicates that the material undergoes a glass/rubber transition state. It is also noticed that the incorporation of nanoclay into the polymer matrix leads to a considerable increase in the storage modulus of PMMA nanocomposites over neat PMMA. This improvement is in agreement with the modulus data obtained from the static mechanical test, as discussed in earlier sections (2.3.5 and 2.3.6). The raise in the storage modulus is due to reinforcing effect of nanoclay, interfacial interaction between clay and polymer that restricts the mobility of polymer chains at polymer-clay interface and high modulus of clay.

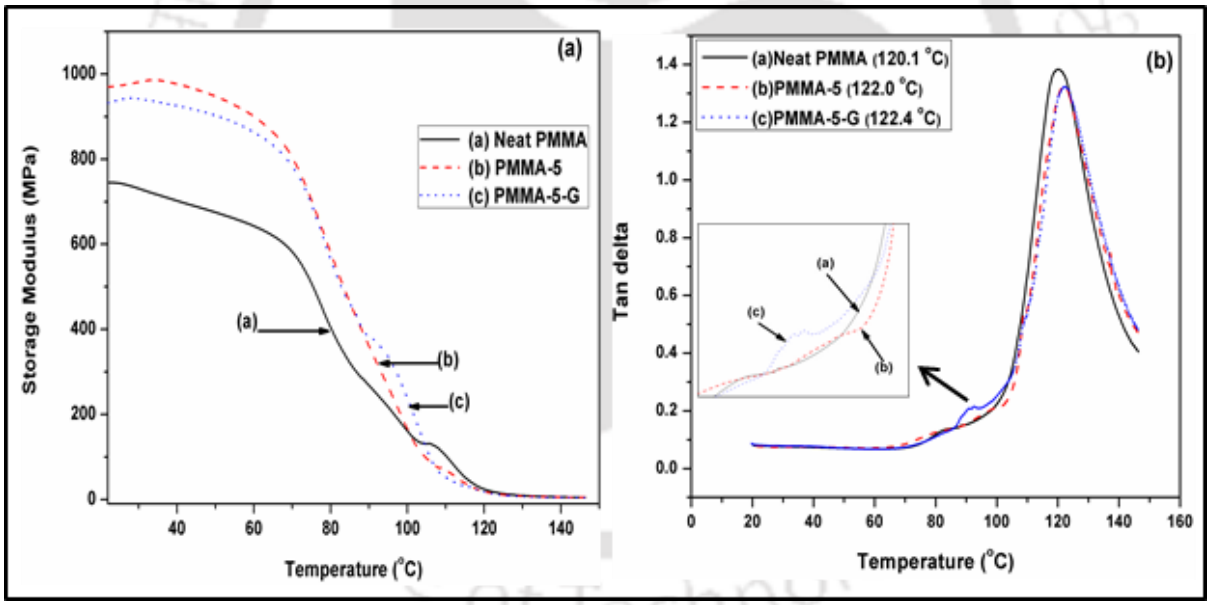

Figure 2.11 (a) Storage modulus and (b) tan δ of neat PMMA, PMMA-5 and PMMA-5-G nanocomposites

The effect of PMMA-g-MA and nanoclay on the damping factor (tan δ) for the PMMA nanocomposites is displayed in Figure 2.11(b). The tan δ graph exhibits the presence of a single glass transition peak around 120 ^{o}C. According to Chow et al., (2005), the T_g is associated with the breakage of hydrogen bonds between the polymer chains that induces long range segmental motion in amorphous region. A hump is appeared in the PMMA-5-G

sample (see inset Figure 2.11(b)), which is related to those segmental anhydride groups that do not contribute in hydrogen bonding. It is observed from the figure that for PMMA-5, tan δ peak shifts towards higher transition temperature due to restricted segmental motions of PMMA in the clay-polymer interface. As the change in T_g of nanocomposites is narrow, the DMA analysis was repeated twice and found similar results. The compatibilizer, PMMA-g-MA provides enhanced interfacial bonding between clay and polymer; as a result, further increase in T_g is observed for PMMA-5-G sample that is confirmed by the rightward shift of tan δ peak.

2.3.11 AFM Analysis

High resolution AFM images (3D) of neat PMMA and its nanocomposites are illustrated in Figure 2.12. It is observed that pits are present in all the images. It is apparent from these images that the thickness of PMMA-5 sample increases to 376.3 nm as compared to 157.7 nm for neat PMMA. In comparison with neat PMMA, the depth of the pits is slightly deeper for PMMA-5 nanocomposite. However, no valid tendency can be proved due to small analyzed area. Further investigations need to be carried out for determining the number and depth of pits. For PMMA-5-G nanocomposite, it is noticed that depth of pits is reduced to 271.5 nm with respect to PMMA-5 nanocomposite (376.3 nm). This suggests that compatibilizer plays an effective role for reducing the thickness (depth of pits) and the same time improves the interaction between the PMMA and nanoclay, as evident from the surface feature of Figure 2.12(c) with respect to Figure 2.12(b). The 2D images of different nanocomposites are given in appendix.

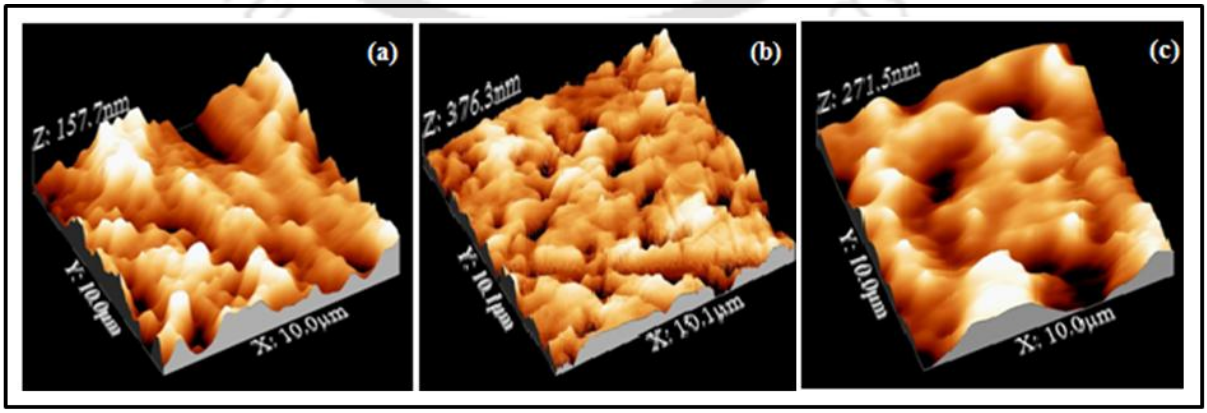

Figure 2.12 AFM images of (a) neat PMMA, (b) PMMA-5 and (c) PMMA-5-G nanocomposites

2.3.12 Optical test

The optical test was carried out in order to study transmission of light through the sample. The effect of nanoclay and compatibilizer (PMMA-g-MA) on the transmittance of PMMA nanocomposites are examined and obtained results are reported in Table 2.2. It is found that neat PMMA shows the transmittance around 67.3%. The PMMA-5 nanocomposite exhibits 35% lower transmittance of light with respect to neat PMMA. This indicates that addition of nanoclay in the PMMA matrix is strong enough to interfere with transmitted light. In addition, staged layers of nanoclay may also occur, which reduces the emitting of light. However, in the PMMA-5-G nanocomposite, the compatibilizer (PMMA-g-MA) improves the bonding between nanoclay and polymer matrix that results in better dispersion of clay particles. As a result, the transparency is more as compared to PMMA-5 sample.

Table 2.2 Optical clarity and rate of burning of neat PMMA, PMMA-5 and PMMA-5-G nanocomposites

Sample	Transmittance (%)	Rate of burning (mm/min)
Neat PMMA	67.6	65
PMMA-5	43.82	41
PMMA-5-G	47.22	44

2.3.13 Flammability Test

The horizontal flammability analysis was performed to characterize the rate of burning of PMMA with the addition of organically modified nanoclay and the results are presented in Table 2.2. The neat PMMA demonstrates a rate of burning of 65 mm/min with melting and dripping characteristics. However, in the PMMA nanocomposite samples, the rate of burning is decreased considerably demonstrating that nanoclay acts as a barrier in protecting the polymer matrix. The PMMA-5 nanocomposite shows lowest rate of burning (41 mm/min) in comparison with PMMA-5-G and neat PMMA, which is probably due to the formation of silica-rich char that inhibits the out dispersion of the volatile decomposition products. This reduction is often observed in intercalated or partly exfoliated clay platelets in

polymer/nanoclay systems (Mohanty and Nayak, 2010). The PMMA-5-G nanocomposite also displays almost similar rate of burning as PMMA-5 sample suggesting that compatibilizer has no effect on the flammability. Zhu et al., (2001) reported that development of char acts as barrier to the degradation products and as a heat insulation layer, a catalytic charring action of the strongly acidic proton sites created in the silicate by the thermal degradation of the organic modifier, and radical trapping by paramagnetic iron within the clay. The intercalation of PMMA matrix into clay galleries results in decreased rate of burning. The other mechanism proposed by Zannetti et al., (2001) indicates that the clay serves as a char promoter by slowing down the degradation and providing a transient protective barrier to the nanocomposites.

2.3.14 Rheological Properties

Rheological analysis of polymer composites is an efficient method to predict the processing behavior and microstructure of composites. Many polymer composites showed transition in rheological behavior from liquid-like to pseudo-solid-like or solid-like with increasing filler concentration (Ray et al., 2002; Krishnamoorty et al., 1996). This transition concentration is called the rheological percolation threshold. The frequency dependence of the storage modulus (G') and loss modulus (G"), measured at 200 ^{o}C for PMMA and its nanocomposites are shown in Figure 2.13 (a, b). The frequency dependence of storage modulus (G') for the PMMA nanocomposites containing nanoclay demonstrates the normal response of a conventional thermoplastic polymer with a liquid-like behavior at lowest frequency i.e. below 0.1. It is clear from the graph (Figure 2.13 (a)) that neat PMMA along with PMMA-5 and PMMA-5-G show similar trend at lower frequency region. As the frequency increases, the storage modulus is also enhanced and is less dependent on the shear rate. This entire phenomenon indicates the behavior from a liquid-like to a solid-like viscoelastic i.e. rheological percolation threshold and the formation of nanoclay-polymer chain network. The appearance of rheological percolation threshold of PMMA-5 can be attributed to the formation of continuous network of nanoclay and polymer chains. However, in the case of PMMA-5-G sample, formation of interfacial bond between the anhydride groups of PMMA-g-MA and amino groups in nanoclay can entangle with polymer chains of matrix to form a continuous polymer-nanofiller network. From the loss modulus graph (Figure 2.13 (b)), it is observed that at lower frequency, PMMA nanocomposites show higher loss modulus with

respect to neat PMMA. This indicates that nanoclay has pronounced effect on it. At higher frequency, it is noticed that long-time relaxation for all the samples has perturbed. Nanoclay and PMMA-g-MA have less effect. A similar type of results is also reported by Zhang et al., (2012) for graphene based PMMA composites.

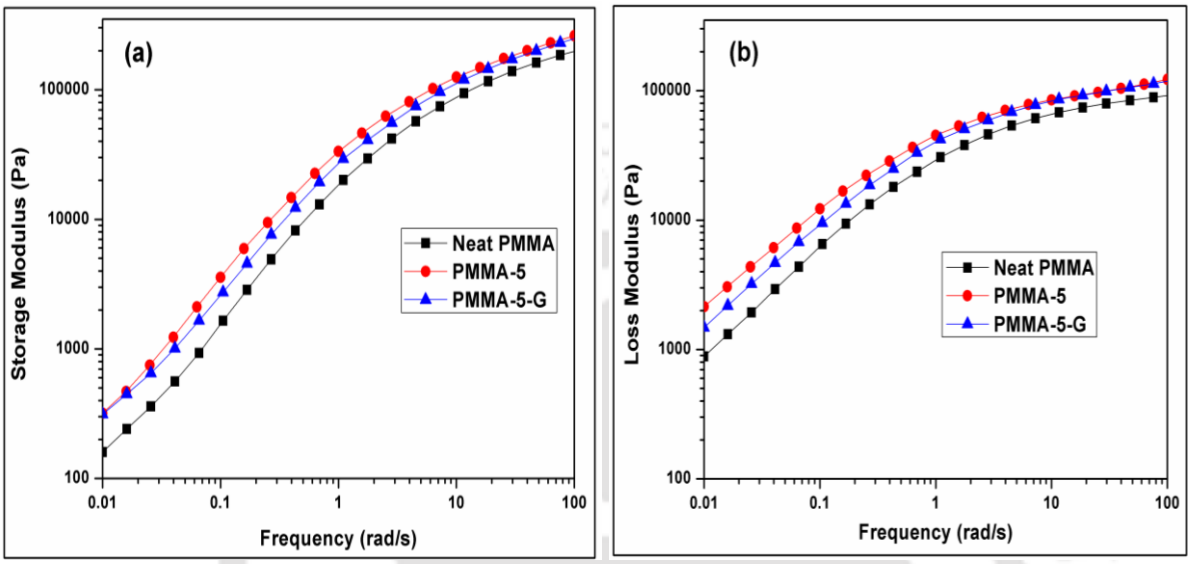

Figure 2.13 (a) Storage modulus and (b) loss modulus of neat PMMA, PMMA-5 and PMMA-5-G nanocomposites at 200 ^{o}C

The complex viscosity of the polymer melts can be easily understood by the shear thinning phenomenon. This states that polymer melts are non-Newtonian fluids and their viscosity decreases with increasing shear rate and this behaviour is considered the most important property in polymer processing. The complex viscosity versus angular frequency (ω) of neat PMMA, PMMA-5 and PMMA-5-G analyzed at 200 ^{o}C is displayed in Figure 2.14(a). The graph shows that PMMA nanocomposites (PMMA-5 and PMMA-5-G) have a higher viscosity at lower frequency in comparison with neat PMMA. At lower frequency, the entanglement of polymer chains hinders shear flow and therefore, viscosity is high. As the frequency increases, the chains begin to orient in the flow direction and disentangle from one another, the viscosity reduces. Finally, the molecules become fully oriented in the flow direction at very high frequency. At this point, stable entanglements are no longer possible and the viscosity reaches a low-level that is again independent of shear-strain rate.

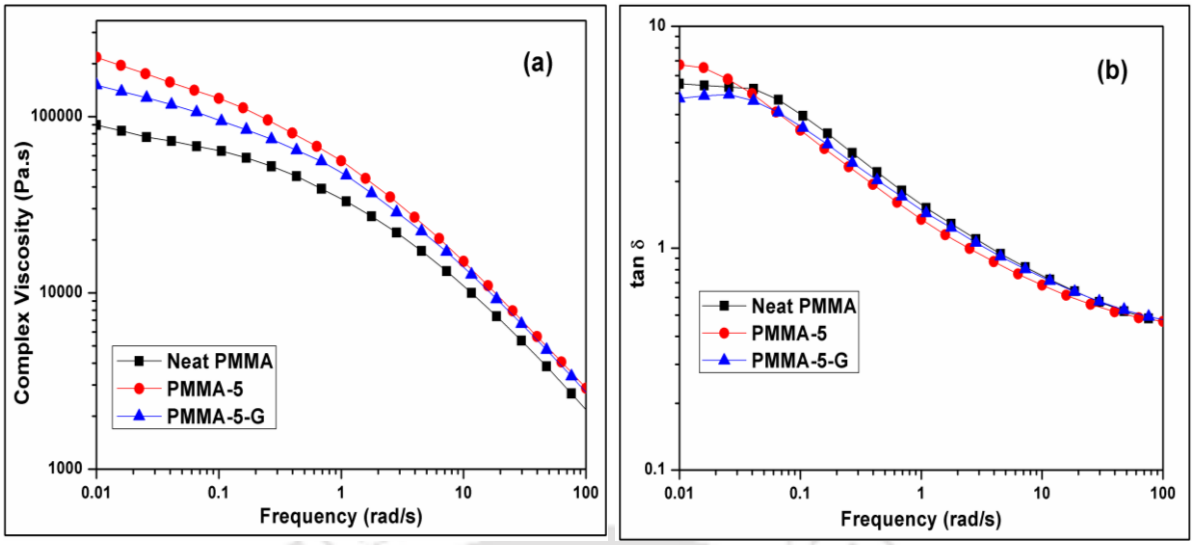

Figure 2.14 (a) Complex viscosity and (b) tan δ of neat PMMA, PMMA-5 and PMMA-5-G nanocomposites at 200 ^{o}C

The tan δ of PMMA and its nanocomposites is shown in Figure 2.14(b). The ratio of loss modulus to storage modulus is defined as tan δ. The plot shows a slight increase in tan δ and then a major drop as the frequency increases. The physical entanglements of polymer chains with the addition of nanoclay particles cause the formation of some network structures among the nanoclay particles and polymer chains and also among nanoclay particles themselves. The rigid structure of nanoclay particles inhibits the viscous behaviour and facilitates the transition from viscous to elastic behaviour. Once the network is formed, no further change in loss factor is observed with increasing frequency. The decrease of loss factor values in the high frequency region is attributed to the partial orientation of polymer chains and nanoclays as result of deformation. Majid et al., (2011) also found similar type of reduction in the loss factor for PP/ZnO nanocomposites.

2.4 SUMMARY

PMMA nanocomposites have been successfully fabricated by melt-blending technique. This work demonstrates the role of the compatibilizer, PMMA-g-MA, and nanoclay on the mechanical, thermal, and morphological properties of PMMA nanocomposites. TEM images show that the lamellar structure of nanoclay is intercalated by polymer chains. The TGA result displays that the thermal stability of PMMA nanocomposites is enhanced relatively to

the neat PMMA. When 50% weight loss is selected as comparison point, the thermal stability of PMMA nanocomposites is 11 ^{o}C higher than that of neat PMMA. The results of the mechanical properties of the PMMA-5-G sample elucidate that the compatibilizer (PMMA-g-MA) endorses adequate interface adhesion between clay and polymer, resulting in better mechanical properties over the neat PMMA and PMMA-5 samples. The addition of clay and PMMA-g-MA into the nanocomposites elevates the stiffness and rigidity of the polymer nanocomposites. The improvement of tensile strength, Young's modulus, flexural strength, flexural modulus, and impact strength for the PMMA nanocomposite prepared with PMMA-g-MA (PMMA-5-G) is found to be 40, 87, 41, 17, and 19%, respectively over PMMA-5. It can be concluded that the grafting contributes to the mechanical properties of PMMA nanocomposites.

The rheological properties of PMMA nanocomposites (PMMA-g-MA) are also successfully examined. It is found that storage and loss modulus increase as the frequency increases and it is less dependent at high frequency for a fixed temperature. The shear-thinning behaviour is also noticed for nanocomposites at 200 ^{o}C. The optical clarity of PMMA-5-G nanocomposite is 7% higher as compared to PMMA-5 nanocomposite. From the flammability analysis, it is confirmed that PMMA-5 nanocomposites have ~36% higher fire retardancy in comparison with neat PMMA. Since there is not much difference between the thermal stability of PMMA-5 and PMMA-5-G sample, kinetic analysis of the different compositions is not performed.

Chapter 3

Synthesis and Properties of PMMA/clay nanocomposites containing different compatibilizers

In the previous chapter, it was noticed that the addition of compatibilizer (PMMA-g-MA) altered the mechanical properties of the nanocomposites. Hence, in order to identify the best suitable compatibilizer for PMMA/clay system, the role of three commercially available compatibilizers were examined in this chapter. The present work primarily deals with the development of poly(methyl methacrylate) (PMMA)/clay nanocomposites containing different compatibilizers (PP-g-MA, PE-g-MA and PS-g-MA) with 5 wt.% nanoclay by melt intercalation method using co-rotating twin screw extruder. The mechanical, thermal and morphological properties of nanocomposites were evaluated by tensile test, impact, hardness, thermogravimetric analysis (TGA), differential scanning calorimetry (DSC), X-Ray diffraction (XRD) and transmission electron microscopy (TEM). The rheological properties of the PMMA nanocomposites were analyzed by dynamic mechanical analysis (DMA) and parallel-plate rheometer. The results suggest that PMMA nanocomposite prepared with PS-g-MA compatibilizer promotes adequate interface adhesion between the nanoclay and polymer matrix. As a result, PMMA-5-PS sample displays improved mechanical properties over PMMA-5-PP and PMMA-5-PE samples.

The part of this work has been published in **International Journal of Mechanical and Materials Engineering, 10 (2015) 7.

3.1 INTRODUCTION

The effect of various compatibilizers on polymer matrix or blends has been studied by numerous authors (Shanks and Cerezo, 2012; Dayma et al., 2011; Jiang et al., 2003; Lu et al., 2004, Zhu et al., 2008). The HDPE and nitrile copolymer nanocomposites with organoclay were synthesized by solution blending method and found that greater dispersion was obtained in nitrile copolymer matrix (Jeon et al., 1998). Kim et al., (2007) developed PP/clay nanocomposites and reported that the aspect ratio of clay decreased when the clay content increased and the aspect ratio increased with an increase in the PP-g-MA content. Kitayama and co-workers, (1991) prepared triblock copolymer of PMMA and polyisobutylene by anionic polymerization and reported that block copolymer formed was rigid spherical particles, which can be used as elastomer. Kouini et al., (2012) found that the impact property increased with the incorporation of PP-g-MA in PP/PA66 nanocomposites. TPO/PP-g-MA/MMT nanocomposites prepared by Kim et al., (2007) revealed that the modulus and yield strength enhanced by increasing PP-g-MA/organoclay ratios. Zhou et al., (2007) prepared the PMMA/PVC by melt blending method using PB-g-MMA as impact modifier. The result clearly indicated that the sample broke in brittle mode when the matrix was PMMA rich, while in PVC-rich system, ductile fracture occurred. Lai et al., (2009) fabricated PP/nanocomposites with two different compatibilizers (POE-g-MA and PP-g-MA) by melt mixing method. They found that PP-g-MA compatibilized system conferred higher tensile strength, modulus and optical properties as compared to POE-g-MA compatibilized system. Wang et al., (2013) reported the development of PP nanocomposites using PP-g-MA by compression method. The results suggested that MCM-41 and SBA-15 exhibited favourable effect on flammability and tensile properties of PP nanocomposites. Lin and co-workers, (2013) studied β-PP/PA6 blends and the results indicated that the addition of PP-g-MA resulted in PP-g-MA graft copolymer, which improved the interfacial adhesion and reduced the sizes of PA6 domains. Lee et al., (2005) synthesized the PE/clay nanocomposites containing PP-g-MA by melt-intercalation method. They found that tensile and gas barrier properties were improved at 7% clay loading. Zhao et al., (2008) reported that the T_g and thermal decomposition temperature of PMMA nanocomposite were enhanced by 23 and 93 ^oC, respectively in the presence of octavinyl-polyhedral oligomeric silseoquioxane (OV-POSS). In the study of Wang et al., (2011), the addition of PMMA/MCM-41 filler and PP-g-MA in PP nanocomposites showed better tensile and impact properties. Quintanilla et al., (2006) prepared PP/MMT nanocomposites with different grafting efficiency of PP-g-MA.

The result clearly indicated that PP/Cloisite 20A nanocomposites with higher efficiency PP-g-MA (2.0), exhibited better tensile and impact properties as compared to Cloisite 30B and neat clay. The incorporation of POE-g-MA in PET/PP blends considerably improved mechanical properties such as elongation at break and impact strength (Chiu and Hsiao, 2006). It is very clear from the literature review that the compatibilizer plays a major role in improving the properties of nanocomposite systems. Hence, it is essential to examine the role of various compatibilizers on the properties of PMMA nanocomposites.

The aim of the present work is to investigate the role of various compatibilizers (PP-g-MA, PE-g-MA, PS-g-MA) on the properties of PMMA/clay nanocomposites developed by melt blending method. The morphological, thermal and mechanical properties of the nanocomposites are evaluated using various techniques.

3.2 EXPERIMENTAL

3.2.1 Materials

Details of PMMA and nanoclay are given in chapter 2 (Section 2.2.1). Polypropylene-grafted maleic anhydride (PP-g-MA), polyethylene-grafted maleic anhydride (PE-g-MA) and polystyrene-block-poly(ethylene-ran-butylene)-block-polystyrene-graft-maleic-anhydride (PS-g-MA) were purchased from Sigma-Aldrich, USA. Figure 3.1 illustrates the structure of these compatibilizers used in this work.

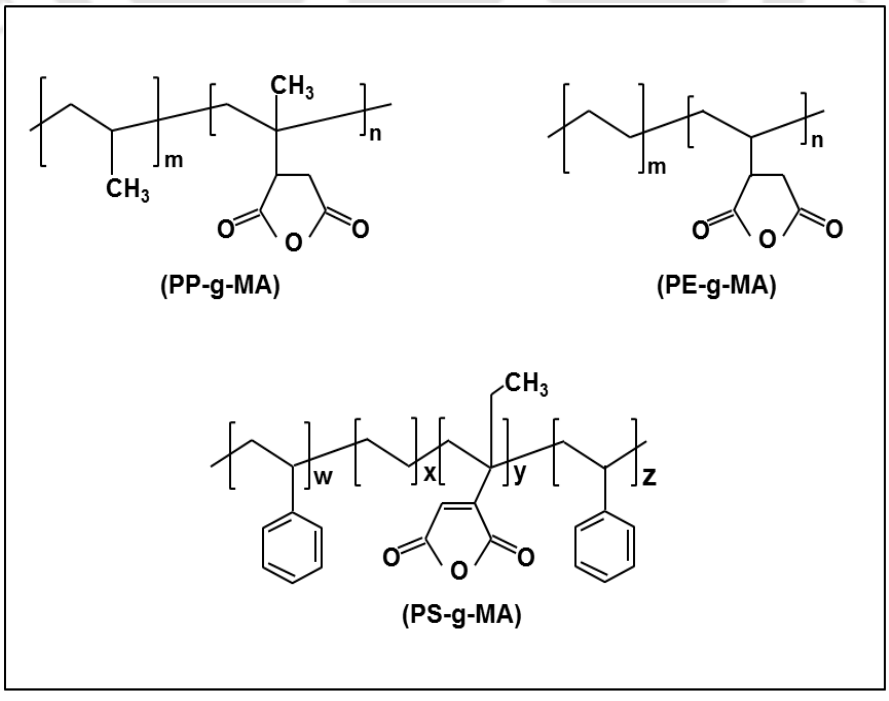

Figure 3.1 Structure of different compatibilizers

3.2.2 Preparation of PMMA/clay nanocomposites

Prior to melt intercalation, PMMA pellets and nanoclay were dried in a vacuum oven at 80 ^{o}C and 65 ^{o}C, respectively for 12 h. PMMA nanocomposites containing 5 wt.% of nanoclay and 5 wt.% of compatibilizer were prepared by melt intercalation technique in a counter-rotating twin screw extruder (Make: Specifiq Engineering and Automats, Vadodara, India; Model-ZV-20 HI TORQUE). In a typical experiment, PMMA, nanoclay and different compatibilizers were fed into the extruder and the obtained extrudate was quenched in water at room temperature. A schematic representation of twin screw extruder is given in Figure 3.2. Subsequently, the extrudate was cut into pellets and then dried before being injection moulded (JSW, Japan; Model-180 High Pressure) at 180-250 ^{o}C to make specimens for mechanical testing. Hereafter, the nanocomposites prepared using PP-g-MA, PE-g-MA and PS-g-MA along with 5 wt.% nanoclay are referred as PMMA-5-PP, PMMA-5-PE and PMMA-5-PS (see Table 3.1). Neat PMMA sample was also prepared by a similar method in the absence of compatibilizer and clay.

Table 3.1 Composition of PMMA nanocomposites

Sample Name	PMMA (wt%)	Nanoclay (wt %)	Compatibilizer (wt%)
Neat PMMA	100	-	-
PMMA-5-PP	90	5	5
PMMA-5-PE	90	5	5
PMMA-5-PS	90	5	5

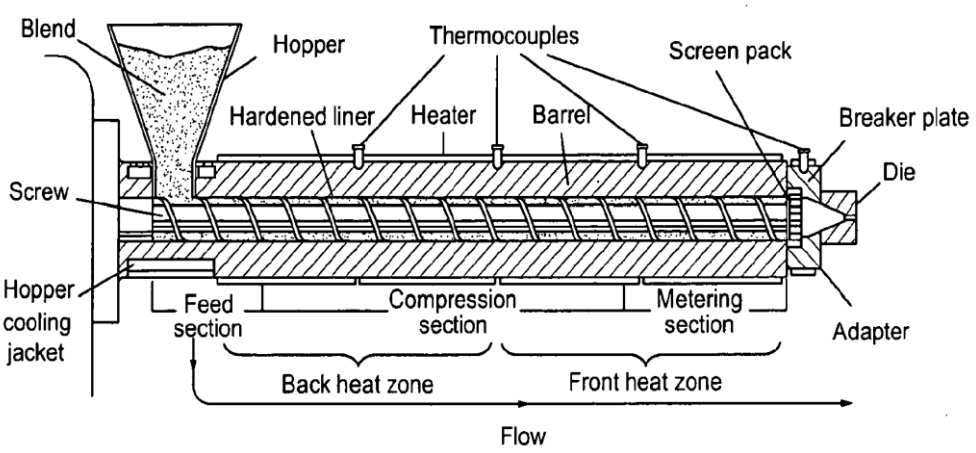

Figure 3.2 Twin Screw Extruder

3.2.3 Characterization Techniques

The polymer nanocomposites were characterized under the same conditions as already reported in Chapter 2 (section 2.2.4).

3.2.4 Thermal Degradation Kinetics

Nanoclay was added in the polymer to increase the thermal stability of the polymer nanocomposite mainly due to the barrier effect of the clay platelets distributed throughout the matrix. The effect of the clay and compatibilizer loading was observed by calculating the activation energy of neat polymer and polymer nanocomposites using kinetic models. The calculation involves determination of the kinetic parameters such as activation energy, pre-exponential factor, and order of the reactions of different polymer nanocomposites using Coats-Redfern method. Thermal decomposition reaction mechanism of nanocomposites was done using Criado method.

Kinetic Methods

Isothermal rate of conversion is a linear function of rate constant (k) and fractional weight loss (α).

$$\frac{d\alpha}{dt} = kf(\alpha) \tag{3.1}$$

Arrhenius equation is given by following expression:

$$k = Ae^{\frac{-E_a}{RT}} \tag{3.2}$$

Combination of equation 3.1 and 3.2 yields,

$$\frac{d\alpha}{dt} = kf(\alpha) = Ae^{\left(\frac{-E_a}{RT}\right)} f(\alpha) \tag{3.3}$$

where, t is the reaction time, T is the temperature, R is the gas constant, A is the pre-exponential factor, E_a is the apparent activation energy, $f(\alpha)$ is the reaction model and α is conversion degree or fractional weight loss.

$$\alpha = (w_0 - w_t)/(w_0 - w_\infty) \tag{3.4}$$

where, w_0, w_t and w_α are the initial, actual and final weight of the samples during TGA analysis.

$$\frac{d\alpha}{dt} = \frac{d\alpha}{dT}\frac{dT}{dt} = \beta\frac{d\alpha}{dT} \tag{3.5}$$

where, $\beta = \frac{d\alpha}{dT}$ = heating rate. Now by combining equation 3.3 and 3.5, we get:

$$\frac{d\alpha}{dT} = \frac{A}{\beta}e^{\frac{-E_a}{RT}} f(\alpha) \tag{3.6}$$

Taking integration on both sides and rearranging:

$$g(\alpha) = \int_0^\alpha \frac{d\alpha}{f(\alpha)} = \frac{A}{\beta}\int_0^T e^{\frac{-E_a}{RT}} dT \tag{3.7}$$

where, $g(\alpha)$ is the integral function of conversion degree α. The polymer degradation processes, mainly obey the sigmoidal or deceleration functions. For the different solid reaction mechanism, $g(\alpha)$ has different expressions, which is presented in Table 3.2.

(i) Coats-Redfern Method (Coats and Redfern, 1964)

Using equation 3.7 and putting $f(\alpha) = (1-\alpha)^n$ and $x = E_a / RT$ rearranging, we get:

$$g(\alpha) = \frac{ART^2}{\beta E_a}\left(1 - \frac{2RT}{E_a}\right)\exp\left(-\frac{E_a}{RT}\right) \tag{3.8}$$

g(α) can be written in different ways for different *n* values:

when n = 1, $g(\alpha) = -\ln(1-\alpha)$ (3.9a)

when n≠1, $g(\alpha) = \frac{1}{n-1}[(1-\alpha)^{1-n} - 1]$ (3.9b)

The combination of equation 3.8 and 3.9 and by the rearrangement, we get:

n=1, $\ln\left(-\frac{\ln(1-\alpha)}{T^2}\right) = \ln\left[\frac{AR}{\beta E_a}\left(1-\frac{2RT}{E_a}\right)\right] - \frac{E_a}{RT}$ (3.10a)

n≠1, $\ln\left(\frac{1-(1-\alpha)^{1-n}}{(1-n)T^2}\right) = \ln\left[\frac{AR}{\beta E_a}\left(1-\frac{2RT}{E_a}\right)\right] - \frac{E_a}{RT}$ (3.10b)

Plotting the left hand side term versus *-1/T* gives the straight line and the slope gives the activation energy. The constant value gives the value of pre-exponential factor (A), by taking the expression $\left(1-\frac{2RT}{E_a}\right)$ inside the parenthesis as 1. Analysis can be done using only single heating data which is different from other kinetic methods where multiple heating data are required for analysis.

(ii) Criado Method

Criado et al., (1989) proposed a method which can accurately determine the reaction mechanism in the solid phase reaction process using the activation energy value obtained from Coats Redfern method. This method is used to study the mechanism of thermal degradation at a particular heating rate. The values of activation energy, pre-exponential factor and the apparent order of the reaction are calculated by Coats-Redfern method.

Criado introduced a new function, Z(α)

$$Z(\alpha) = \frac{\frac{d\alpha}{dt}}{\beta}\pi(x)\mathrm{T} \quad (3.11)$$

where, $x = E_a / RT$ and *π(x)* is an estimated expression acquired by integration against temperature, which cannot be articulated by simple analysis formula. Paterson (1971) proposed a reasonable relationship between *π(x)* and *P(x)*

$$\pi(x) = xe^{x}P(x) \tag{3.12}$$

Senum and Yang, (1977) and Flynn, (1997) projected an estimated biquadratic rational expression for *P(x)*:

$$P(x) = \frac{e^{-x}}{x}\frac{x^3 + 18x^2 + 86x + 96}{x^4 + 20x^3 + 120x^2 + 240x + 120} \tag{3.13}$$

when $x > 20$, Eq.(3.13) can give negligible error, which is the basis for analysing the TG data. Combining equation (3.5), (3.11) and (3.12), the following relationship is obtained:

$$Z(\alpha) = f(\alpha)g(\alpha) \tag{3.14}$$

The combination of equations, (3.6) and (3.14) results in the following equation:

$$Z(\alpha) = \frac{\beta}{A}g(\alpha)\frac{d\alpha}{dt}e^{\frac{E_a}{RT}} \tag{3.15}$$

From the equations. (3.5), (3.11) and (3.12) the following relationship can also be obtained:

$$Z(\alpha) = \frac{d\alpha}{dt}\frac{E_a}{R}e^{\frac{E_a}{RT}}P(x) \tag{3.16}$$

Using equation (3.16), *Z(α)* versus *α* experimental plots are obtained and then compared with the master plot between *Z(α)* versus *α* using the equation (3.15) for different mechanism function, *g(α)* and accurately predict the reaction mechanism of the thermal degradation reaction.

Table 3.2 The expressions of *g(α)* for the commonly used reaction mechanism of solid state process

Mechanism	g(α)	Solid state process
Sigmoidal function		
A2	$-[\ln(1-\alpha)]^{1/2}$	Nucleation and growth
A4	$-[\ln(1-\alpha)]^{1/3}$	Nucleation and growth
A3	$-[\ln(1-\alpha)]^{1/4}$	Nucleation and growth
Deceleration Functions		
R2	$[1-(1-\alpha)^{1/2}]$	Phase boundary controlled reaction: contraction area
R3	$[1-(1-\alpha)^{1/3}]$	Phase boundary controlled reaction: contraction volume
D1	α^{2}	One-D diffusion
D2	$(1-\alpha)\times\ln(1-\alpha)+\alpha$	Two-D diffusion
D3	$[1-(1-\alpha)^{1/3}]^{2}$	Three-D diffusion, Jander equation
D4	$(1-2/3\alpha)-(1-\alpha)^{2/3}$	Three-D diffusion, Ginstlinge Brounshtein equation
F1	$-\ln(1-\alpha)$	Random nucleation having one nucleus on individual particle
F2	$1/(1-\alpha)$	Random nucleation having two nucleus on individual particle
F3	$1/(1-\alpha)^{2}$	Random nucleation having two nucleus on individual particle

3.3 RESULTS AND DISCUSSION

3.3.1 XRD Analysis

XRD is a most useful technique for the measurement of d-spacing of ordered intercalated and exfoliated nanocomposites. The intercalated nanocomposite with increased d-spacing denotes that polymer has entered the clay gallery. In exfoliated nanocomposites, no peak is noticed recommending that a considerable amount of polymer has inserted in the gallery space and expanding the clay layers so far (Morgan and Gilman, 2003). The XRD pattern of nanoclay, neat PMMA and its nanocomposites in the 2θ range of 1-60^{o} is shown in Figure 3.3.

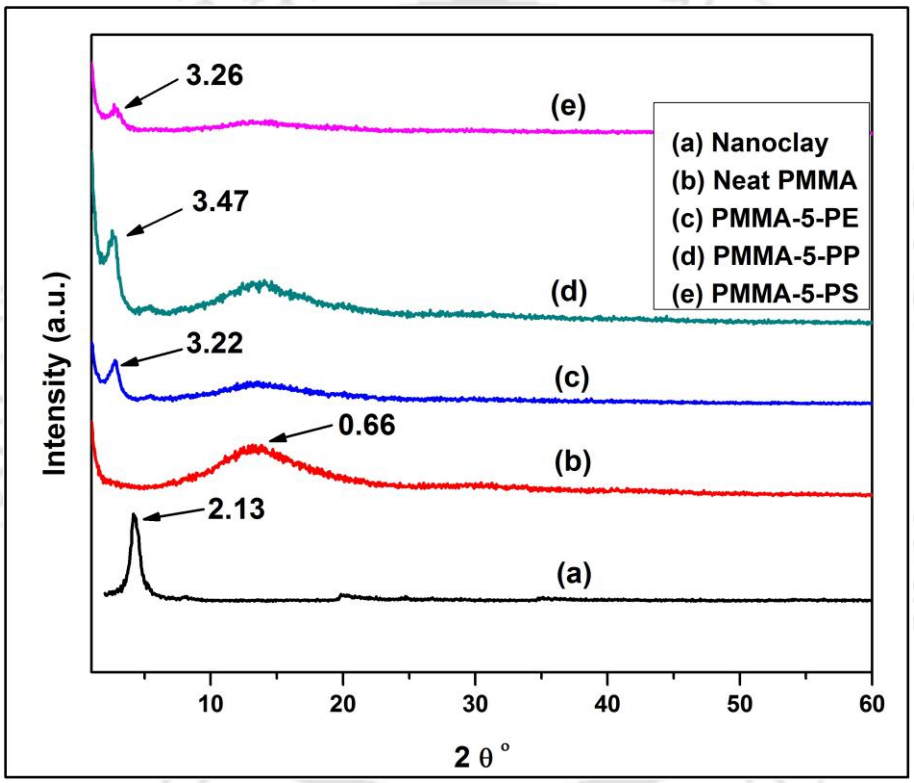

Figure 3.3 XRD pattern of nanoclay, neat PMMA, PMMA-5-PE, PMMA-5-PP and PMMA-5-PS nanocomposites

The main diffraction peak for nanoclay, neat PMMA, PMMA-5-PE, PMMA-5-PP and PMMA-5-PS sample are obtained at 2θ value of 4.15^{o}, 13.34^{o}, 2.74^{o}, 2.54^{o} and 2.70^{o}, respectively. The d_{001} spacing is calculated from peak positions using Bragg's law: $n\lambda=2d\sin\theta$, where λ is the X-ray wave length (1.5406 Å). The basal spacing of the d_{001} peak of organically modified nanoclay is estimated as 2.13 nm. In the nanocomposites, a large broad hump is originated from the PMMA matrix. The d-spacing (d_{001}) value of PMMA-5-PE, PMMA-5-PP and PMMA-5-PS is found to be 3.22, 3.47, 3.26 nm, respectively. This clearly

reveals that nanoclay layers have been introduced in the nanocomposites as a single polymer chain enters between the silicate layers, and a tactoid morphology results with alternating polymeric and inorganic layers. The diverse d-spacing value obtained for the PMMA nanocomposite with different compatibilizer materials is probably due to the amount of polymer penetrated between the clay platelets and the interaction between a particular compatibilizer with PMMA matrix.

3.3.2 FTIR Analysis

Figure 3.4 represents the FTIR spectra of different compatibilizers (PE-g-MA, PP-g-MA and PS-g-MA) used in this study. The CH- asymmetric (2930-2970 cm^{-1}) and symmetric stretching (2840-2860 cm^{-1}) are clearly seen in polyolefin based compatibilizers. The characteristic peak of grafted anhydride, which is too small to observe, is found at 1843 cm^{-1} (Kouini and Serier, 2012; Wang et al., 1999). In PS-g-MA compatibilizer, the band present at 671 cm^{-1} is the $\delta_{c=c}$ of the phenyl group (Li et al., 2002).

In Figure 3.5, the FTIR spectrum of nanoclay displays that the peak exhibited at 1046 cm^{-1} is attributed to the Si-O stretching vibration of clay. For nanoclay, two peaks were observed between 3300 and 3700 cm^{-1}, which corresponds to –OH stretching vibration. The first peak at 3630 cm^{-1} is assigned to isolated -OH groups, while the other found at 3246 cm^{-1} is assigned to isolated hydrogen bonding. Three subsequent peaks were recorded at 2922, 2849 and 1465 cm^{-1}, which denote CH_2 asymmetric stretching, symmetric stretching and in-plane scissoring vibrations, respectively. The peaks appeared at 917, 750, 530 and 458 cm^{-1} correspond to AlAlOH, AlMgOH, Al-O and Mg-O bending vibration, respectively (Madejová, 2003). The absorption band at 1612 cm^{-1} resembles to the bending vibration mode of hydrated water molecules and weakly bonded water molecules (Manoratne et al., 2006).

The FTIR of neat PMMA and its nanocomposites show a characteristic peak at 1731 cm^{-1}, which denotes the >C=O group present in the polymer. The band at 986 denotes the –C-H bending of polymer chain. The peak observed at 1436 cm^{-1} corresponds to -O-CH_3 deformation of PMMA. The band exhibited at 2994 cm^{-1} is due to the ester methyl stretching vibrations. The peak appeared at 2950 cm^{-1} corresponding to the asymmetric stretching vibration of –CH_3 group. A very clear and sharp peak is noticed in the range of 3438-3442 cm^{-1} that shows the intra-molecular hydrogen bonding between nanoclay and PMMA

(Mohanty and Nayak, 2010). As the neat polymer and different composite samples mainly consist of PMMA, it is observed that there is no much difference among composites prepared with various compatibilizers (Figure 3.5c-e). Mohanty and Nayak, (2010) also reported similar type of result with PMMA-g-MA and Closite 30B clay.

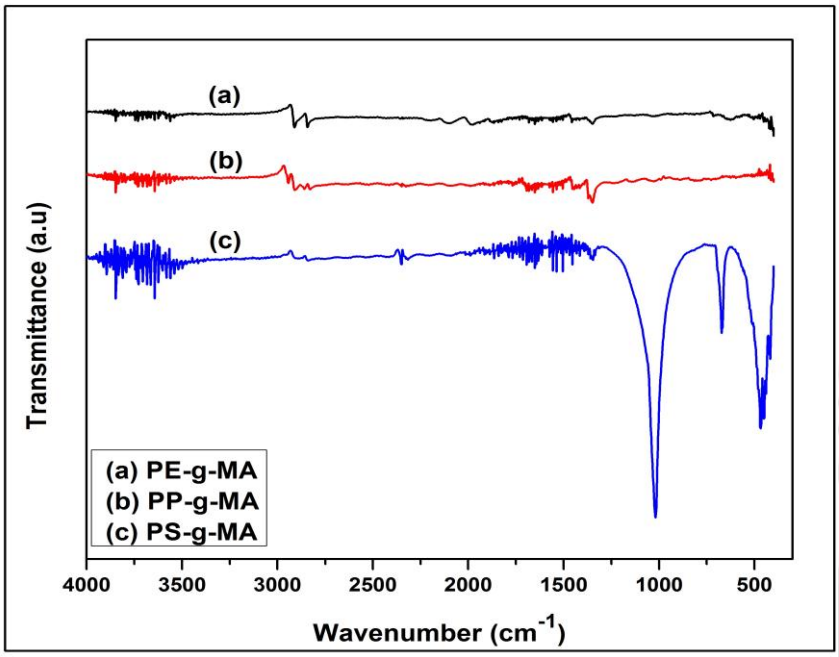

Figure 3.4 FTIR spectra of various compatibilizers

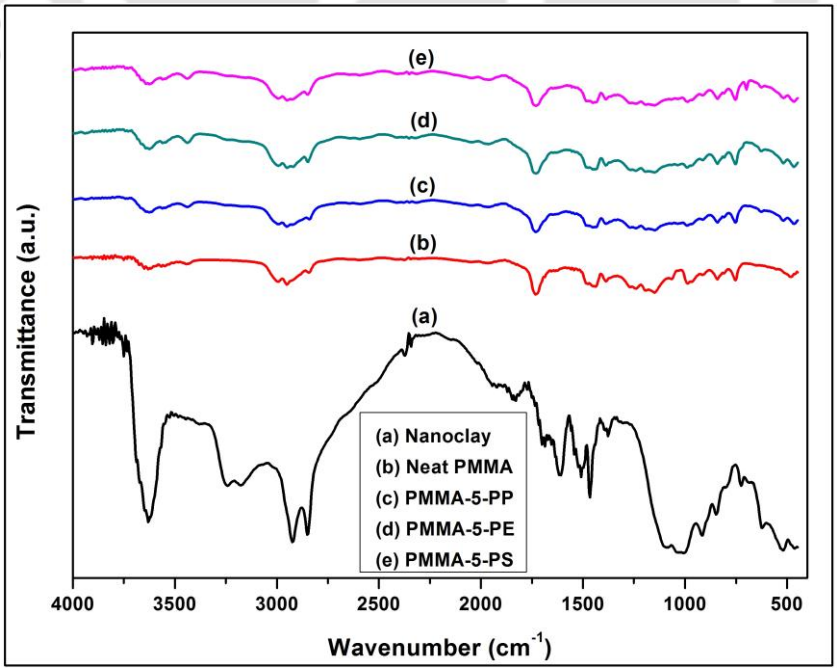

Figure 3.5 FTIR spectra of nanoclay, neat PMMA, PMMA-5-PP, PMMA-5-PE and PMMA-5-PS nanocomposites

3.3.3 FESEM Analysis

The field emission scanning electron microscopy (FESEM) is an appropriate method to directly reveal the state of clay dispersion in the polymer matrix. FESEM images of PMMA-5-PP, PMMA-5-PE and PMMA-5-PS nanocomposites prepared by melt-blending technique are provided in Figure 3.6. From the image of PMMA-5-PP nanocomposite, it can be seen that nanoclay is thoroughly present in web like manner and some places, agglomerated particles are also observed. In the case of PMMA-5-PE, it is found that nanoclay is homogenously dispersed, however few pin holes are also seen. Relatively, better distribution is observed in PMMA-5-PS nanocomposite; meanwhile, accumulated particles are noticed in the matrix.

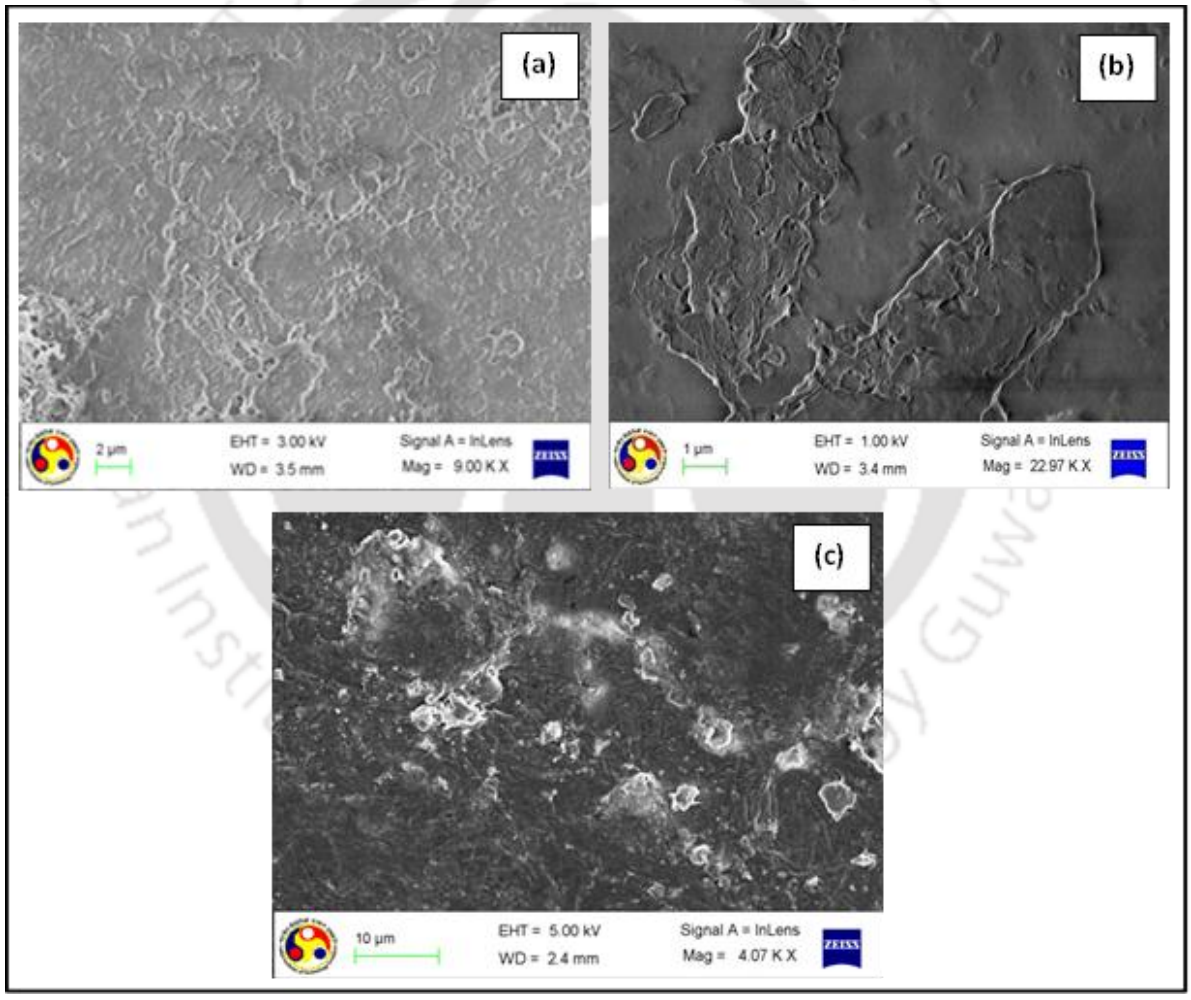

Figure 3.6 FESEM images of (a) PMMA-5-PP, (b) PMMA-5-PE and (c) PMMA-5-PS nanocomposites

3.3.4 TEM Analysis

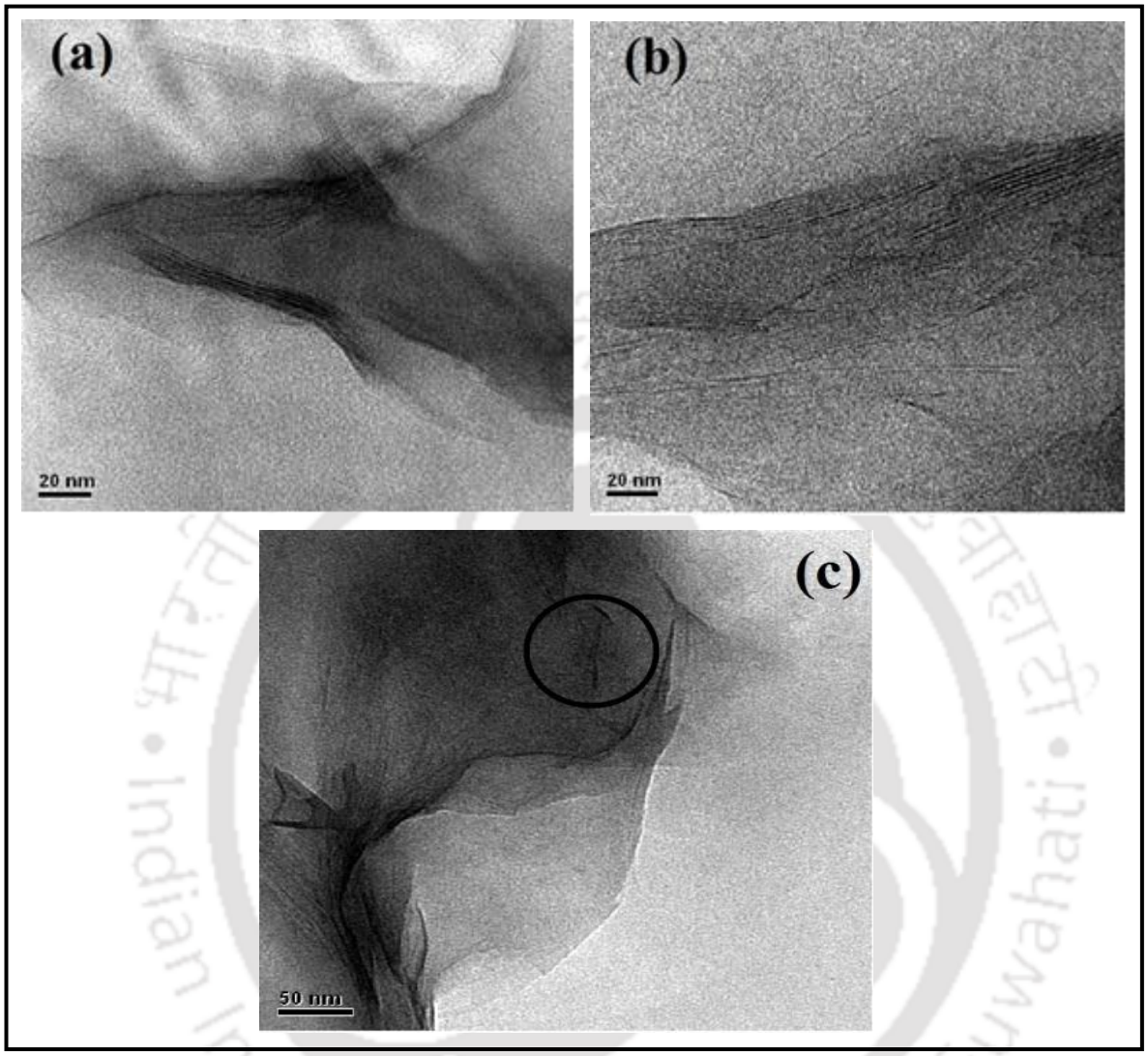

Figure 3.7 TEM images of (a) PMMA-5-PP, (b) PMMA-5-PE and (c) PMMA-5-PS nanocomposites

In addition to XRD investigations, TEM analysis of the PMMA nanocomposites was performed to delineate the dispersion status of nanoclay in the PMMA matrix. The TEM images of PMMA nanocomposites with different compatibilizer are depicted in Figure 3.7. The dark lines (stacked silicate platelets) denote clay tactoids and the rest of the area represents organic matrix. The extent of exfoliation and intercalation completely depends on the hydrophilicity of the compatibilizer and the chain length of the organic modifier in the clay (Wang et al., 2001). All the images exhibit intercalated structure, which is in agreement with XRD results as shown in Figure 3.3. In the PMMA-5-PP sample, four to five layers of

nanoclay are stacked together, which leads to tactoid structure. However, it is clearly visible from the image of PMMA-5-PE sample (Figure 3.6b) that a small amount of PMMA enters into the gallery spacing between the clay platelets resulting in an intercalated structure. The PMMA-5-PS nanocomposite has mixed morphological structure, i.e. a combination of tactoids and exfoliated particles.

3.3.5 Tensile Properties

Figure 3.8 shows the role of different compatibilizer on the tensile properties of PMMA. In general, an addition of clay increases the reinforcement of polymer matrix that results in enhanced mechanical properties. It is observed from Figure 3.8 that the PMMA nanocomposites prepared with different compatibilizers display enhanced tensile modulus with respect to neat PMMA. In comparison with neat PMMA, the enhancement of modulus is found to be 16, 17, and 20% for PMMA-5-PP, PMMA-5-PE, PMMA-5-PS, respectively. This clearly indicates that there is an effective stress transfer from nanoclay to polymer matrix in the presence of high aspect ratio nanoscale platelets. It is also observed that polystyrene based compatibilizer demonstrates higher modulus when compared with PE-g-MA compatibilizer. It is presumed that both polystyrene and PMMA are amorphous in nature and hence, there may be good miscibility between two polymers that results in increased modulus over PMMA-5-PE and PMMA-5-PP nanocomposites. Similar observations were obtained by Mohanty and Nayak, (2010) for PMMA-g-MA nanocomposites based on Cloisite 30B clay. It is noteworthy to mention that even though tensile strength reduced slightly after incorporation of nanoclay, modulus is constantly increased. Similar findings were also obtained for polystyrene (Lee et al., 2009) and polyurethane (Chung et al., 2008) containing organoclay.

It is clear from Figure 3.8 that PMMA nanocomposites demonstrate slightly lower tensile strength as compared to neat PMMA. It is known that PMMA is brittle in nature to some extent, and the addition of nanoclay particles provides further brittleness characteristics in the amorphous polymer, thus leading to a slight decrease in tensile strength. It is also observed that tactoids structure present in the polymer matrix (see Figure.3.7) leads to lower tensile strength. The PMMA-5-PS nanocomposite shows the tensile strength of 55.5 MPa by the incorporation of PS-g-MA compatibilizer, which is higher than that of PMMA-5-PP and PMMA-5-PE samples. One of the main reasons is that both polystyrene and PMMA are

amorphous in nature. Hence, there may be a possibility that PS makes good compatibility with PMMA resulting in enhanced tensile strength over other composites.

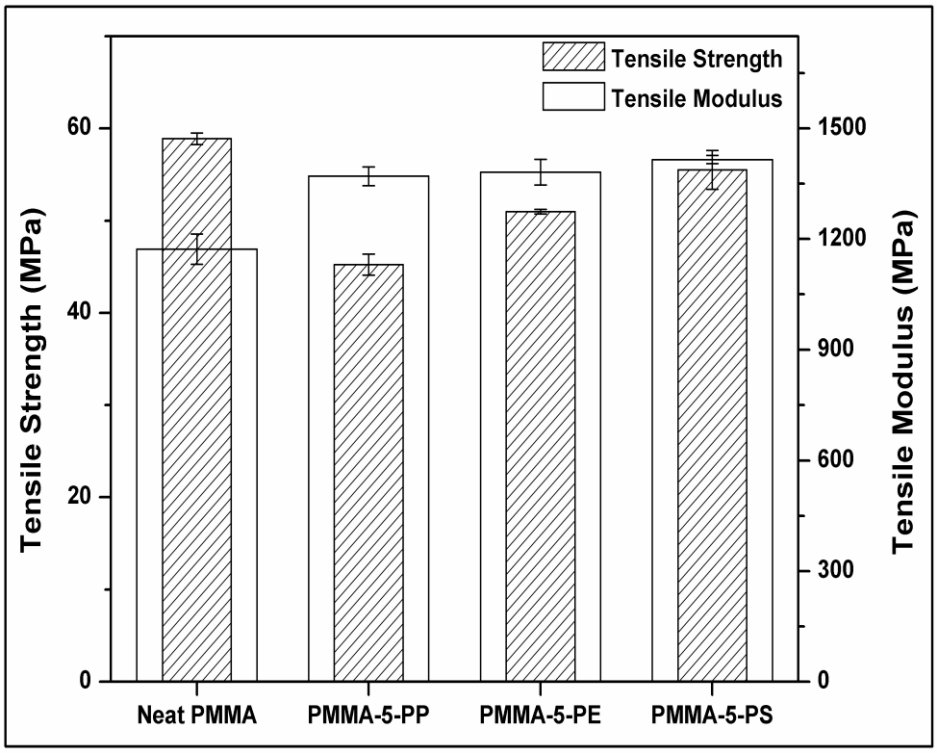

Figure 3.8 Tensile Properties of neat PMMA, PMMA-5-PP, PMMA-5-PE and PMMA-5-PS nanocomposites

3.3.6 Flexural Properties

The influence of different compatibilizers on the flexural properties is depicted in Figure 3.9. The PMMA-5-PP, PMMA-5-PE and PMMA-5-PS samples have the flexural modulus of 4064, 3092 and 3561 MPa, respectively, whereas the neat PMMA sample possesses the flexural modulus of 3688 MPa. The PMMA-5-PP nanocomposite shows 10% enhanced modulus when compared with pristine PMMA. This elucidates that PP-g-MA provides better distribution of silicate platelets of nanoclay in the polymer matrix and as a result, stiffness of the PMMA-5-PP nanocomposite is improved. The reduced modulus in the nanocomposite may be due to the stacked layers of nanoclay in the PMMA matrix. The degree of intercalation/exfoliation, distribution and orientation of nanoclay platelets in the direction of flow in PMMA nanocomposites also play a major role in ascertaining the flexural modulus (Shah, 2007). Nevertheless, the flexural modulus of the PMMA-5-PS sample is almost same

as neat PMMA indicating that PS-g-MA compatibilizer makes good bonding with PMMA matrix when compared with PE-g-MA. The obtained results are in good agreement with polypropylene based nanocomposites using PP-g-MA as a compatibilizer (Kim et al., 2007). Similarly, the flexural strength of the PMMA-5-PE sample is lower with respect to neat PMMA, which is assumed due to the aggregation of nanoclay arises by filler-filler interaction. On the other hand, the addition of PS-g-MA compatiblizer improves the flexural strength of the PMMA-5-PS nanocomposite in comparison with PMMA-5-PE sample. It is believed that the presence of compatibilizer and nanoclay increases the fracture energy and provides a strong interfacial shear stress. Therefore, the applied stress is expected to be easily transferred from the polymer matrix onto the nanoclay particles resulting in an enhancement of the mechanical properties. The PMMA-5-PS sample exhibits ~53% improvement in flexural strength with respect to PMMA-5-PE nanocomposite.

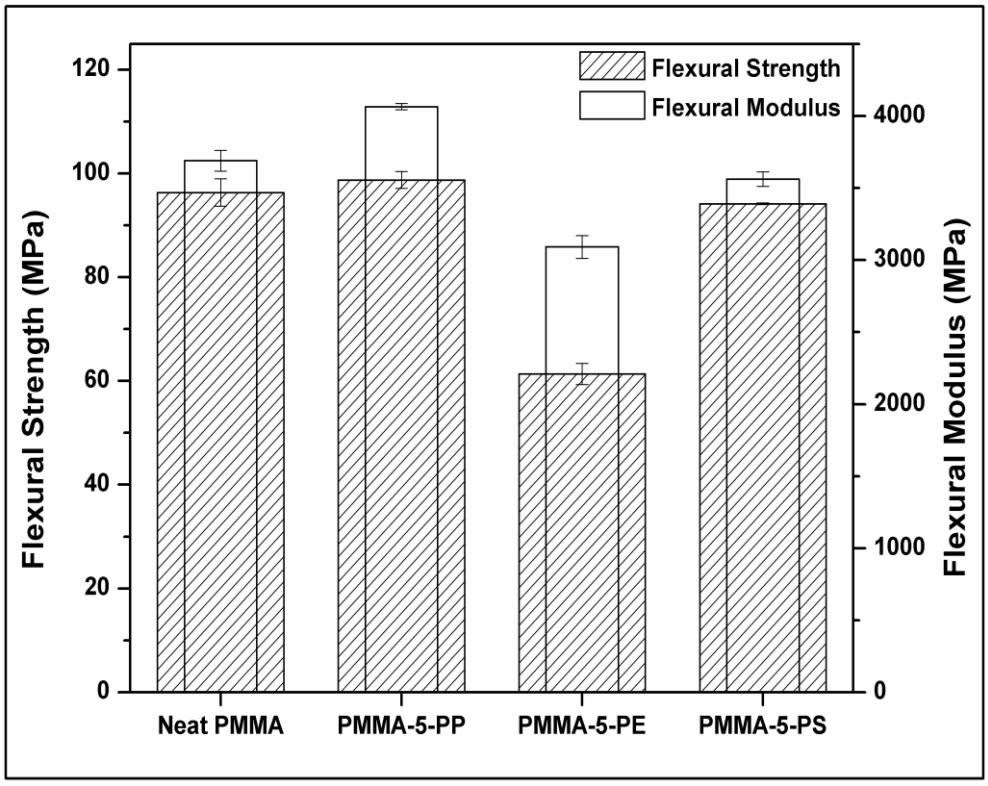

Figure 3.9 Flexural Properties of neat PMMA, PMMA-5-PP, PMMA-5-PE and PMMA-5-PS nanocomposites

3.3.7 Impact Strength

The impact strength of PMMA nanocomposites with nanoclay and different compatibilizer are shown in Figure 3.10. It can be seen from the graph that impact energy of different PMMA nanocomposites reduces as compared to neat PMMA. The reduction in impact strength is presumably due to the partially exfoliated nanoclay platelets in polymer matrix. The PMMA-5-PE and PMMA-5-PP nanocomposite exhibit 44 and 56% lower impact energy with respect to neat PMMA, respectively. It is observed from these results that polyolefin-based compatibilizers are not much efficient to improve the reinforcing properties of the polymer nanocomposites. It is found that immobilization of macromolecular chains is increased by the addition of nanoclay in polymer matrix. Therefore the brittleness property of PMMA is further increased, which might be one of the main reasons for reduced impact strength. It is also noticed that the movement of nanoparticles in polymer nanocomposites is constrained, as a result unable to provide additional energy dissipating mechanism. Thus, during impact test, the nanocomposites absorb a smaller amount of energy through deformation, and breaks easily (Mohanty and Nayak, 2010). The PMMA-5-PS sample has impact energy of 54.15 J/m and it is about 4.31% lower than the neat PMMA. It is also noticed from the mechanical properties that PMMA-5-PS shows very close property to neat PMMA. As discussed earlier, polystyrene is amorphous in nature and may have good compatibility with PMMA matrix, which is also amorphous. As a result of good blending, the impact strength of PMMA-5-PS is close to virgin PMMA.

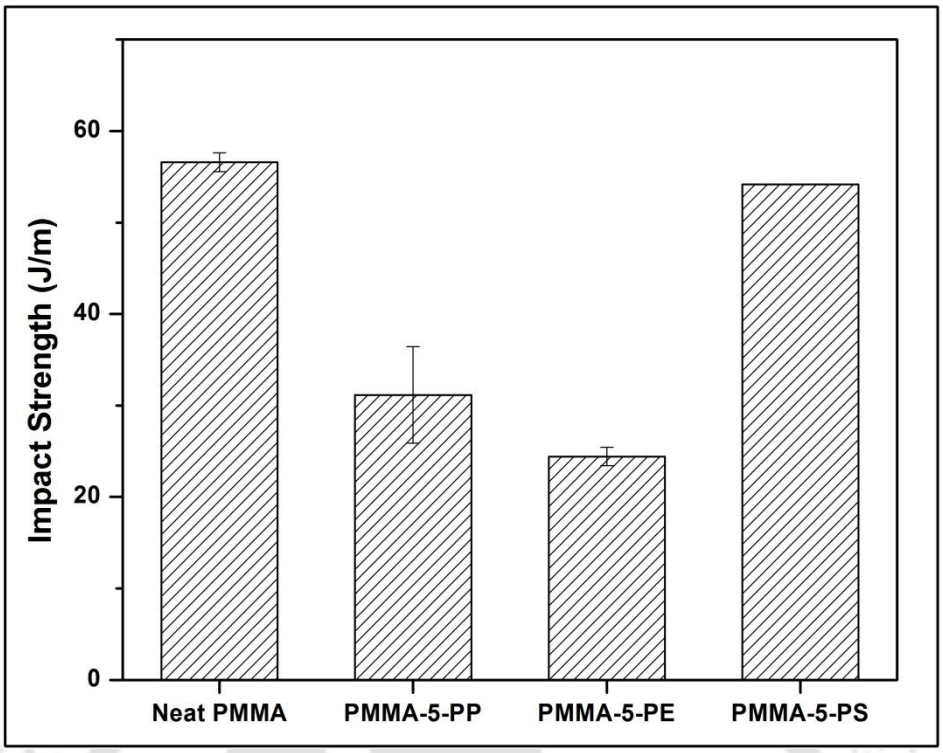

Figure 3.10 Impact Strength of neat PMMA, PMMA-5-PP, PMMA-5-PE and PMMA-5-PS nanocomposites

3.3.8 Hardness

Figure 3.11 represents the Shore D hardness (ASTM D2240) of neat PMMA and its nanocomposites. The hardness of PMMA nanocomposites increases with incorporation of nanoclay and compatibilizer. The average value of the Shore D hardness is observed to be 58, 70, 62 and 78 for neat PMMA, PMMA-5-PP, PMMA-5-PE and PMMA-5-PS nanocomposites, respectively. All the nanocomposites exhibit better hardness over neat PMMA. The increase in the hardness is due to the presence of clay platelets in the polymer matrix. The clay platelets adequately restrict the indentation and thus enhance the hardness of the nanocomposites. It is noteworthy to mention that improvement of hardness for PMMA-5-PS sample is significant in comparison with PMMA-5-PP, and PMMA-5-PE. PMMA-5-PS nanocomposite demonstrates a maximum improvement of Shore D hardness of 34% over neat PMMA.

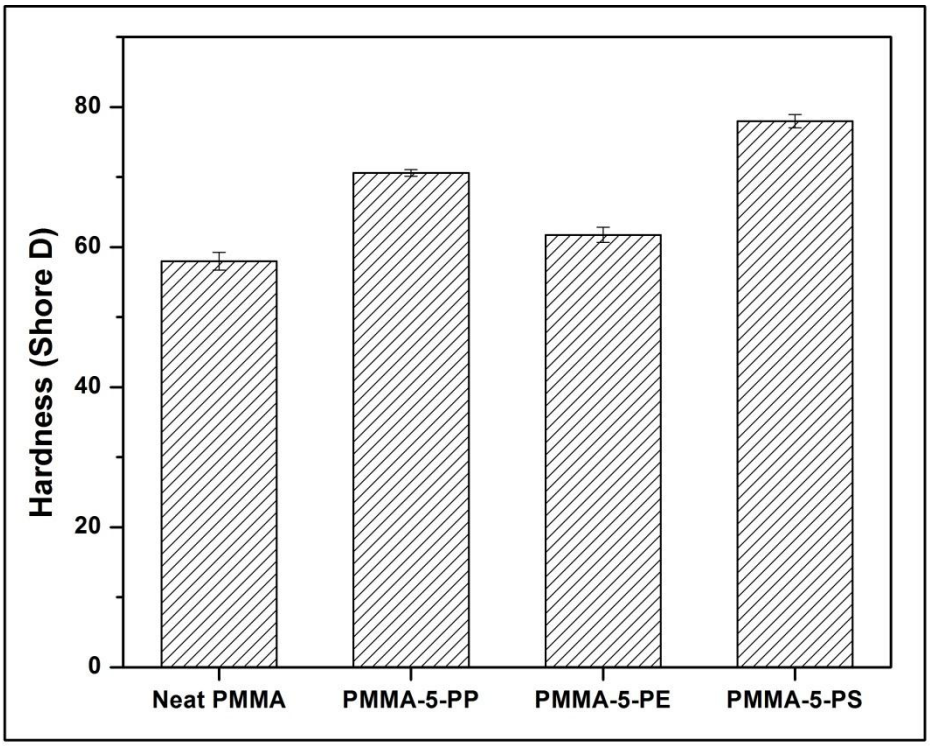

Figure 3.11 Hardness of neat PMMA, PMMA-5-PP, PMMA-5-PE and PMMA-5-PS nanocomposites

3.3.9 Differential Scanning Calorimetry

The DSC study of neat PMMA and its nanocomposites has been carried out in order to examine the mobility of PMMA chains in terms of its T_g (glass transition temperature) in the clay layers, and the results are displayed in Figure 3.12. The glass transition temperature is determined at the inflection point between the onset and the end-set temperatures. The DSC graph exhibits the presence of second order transition corresponding to the T_g of neat PMMA matrix around 109.3 ^oC. However, there is no first order transition, which indicates the absence of melting temperature, thus confirming amorphous characteristics of the matrix polymer. The T_g of PMMA-5-PP, PMMA-5-PE and PMMA-5-PS nanocomposite is found to be 111.4, 111.5 and 111.4 ^oC, respectively. This demonstrates that nanocomposites exhibit marginal improvement in T_g of about 2 ^oC as compared to neat PMMA. The DSC isotherm also shows that compatibilizers improved the bonding between the nanoclay and polymer matrix, which results in enhanced glass transition temperature. The segmental motions of the polymer chains are restricted at the organic-inorganic interface; as a result, T_g has improved for nanocomposites. The confinement of polymer chains between the nanoclay layers and nanoclay surface-polymer interaction are other reasons for enhanced glass transition

temperature. Unnikrishnan et al., (2011) also reported improvement in thermal stability for PMMA/clay nanocomposites prepared by melt intercalation method.

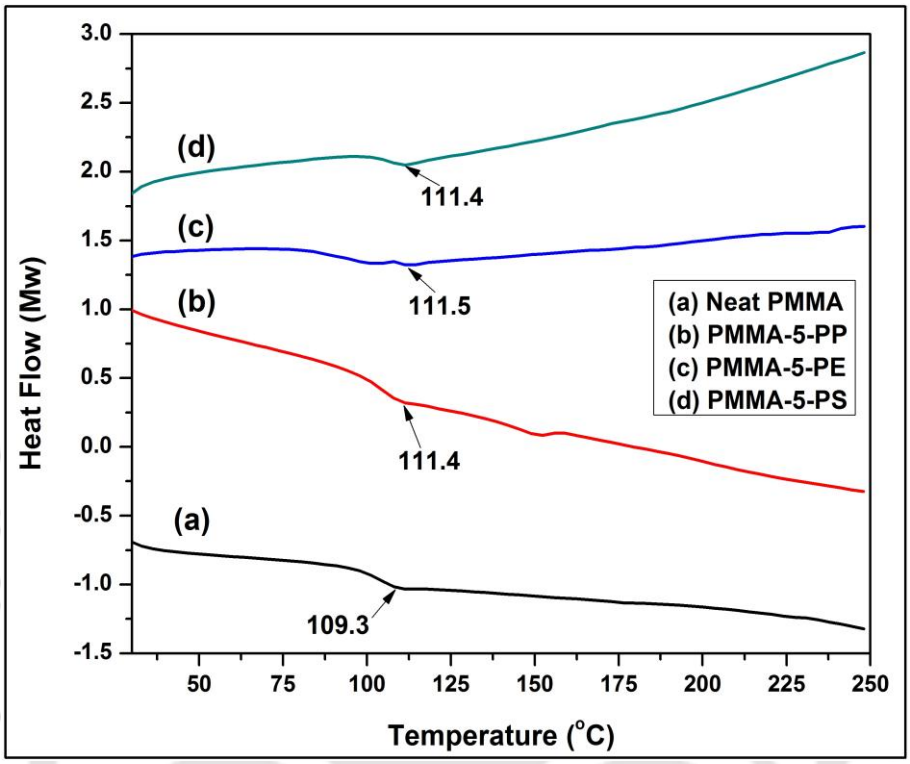

Figure 3.12 DSC curves of neat PMMA, PMMA-5-PP, PMMA-5-PE and PMMA-5-PS nanocomposites

3.3.10 Thermogravimetric Analysis

TGA is used to study the thermal degradation and stability of the polymer. The incorporation of clay is known to augment the thermal stability of polymers. The TGA results of nanoclay, neat PMMA and its nanocomposites are represented in Figure 3.13. The TGA graph of nanoclay shows that the total weight loss of about 30% occurs between 50 to 800 ^{o}C. The weight loss between 300 and 450 ^{o}C is due to the degradation of organic modifier present in the clay. The parameters that are important from TGA curves are the onset of degradation, which is usually taken as the temperature at which 10% degradation occurs ($T_{10\%}$) and the midpoint temperature of degradation ($T_{50\%}$). When 10% weight loss is selected as a point of comparison, the decomposition temperature of neat PMMA, PMMA-5-PP, PMMA-5-PE and PMMA-5-PS is found to be 343.6, 341.3, 361.2 and 358.7 ^{o}C, respectively. The result clearly explains that the degradation of the nanocomposites takes place at higher temperatures than

that of neat PMMA in the presence of nanoclay and compatibilizer. When 50% weight loss is chosen as a point of reference, the decomposition temperature of neat PMMA, PMMA-5-PP, PMMA-5-PE, PMMA-5-PS is 371.1, 393.4, 407.7 and 403.8 ^{o}C, respectively, which is 32 to 36 ^{o}C higher than that of neat PMMA. The enhancement in the thermal stability of PMMA nanocomposites is due to the formation of char that inhibits the out dispersion of the volatile decomposition products as a direct result of the decrease in permeability. This reduction is commonly noticed in the intercalated or exfoliated clay platelets in polymer/organoclay nanocomposites (Unnikrishnan et al., 2011). The PMMA-5-PS nanocomposite shows 27 ^{o}C higher thermal stability as compared to PMMA-g-MA/C30B sample (Mohanty and Nayak, 2010) at 50% weight loss. It can be concluded that all the compatibilizers improve the thermal stability of the PMMA significantly.

The TGA derivative of PMMA nanocomposites is demonstrated in Figure 3.14. The peak indicates the temperature (T_{max}) at a maximum rate of degradation. The entire first TGA derivative curves for PMMA nanocomposites are shifted towards the right side of neat PMMA, indicating enhanced thermal stability. The maximum degradation temperature for neat PMMA is 373.69 ^{o}C whereas of PMMA-5-PS nanocomposite is 414.59 ^{o}C. This indicates 40 ^{o}C improvement in thermal stability that will lead to better service performance of the nanocomposites at an elevated temperature. Similar observations were also reported for polystyrene nanocomposites (Sahu and Pugazhenthi, 2011).

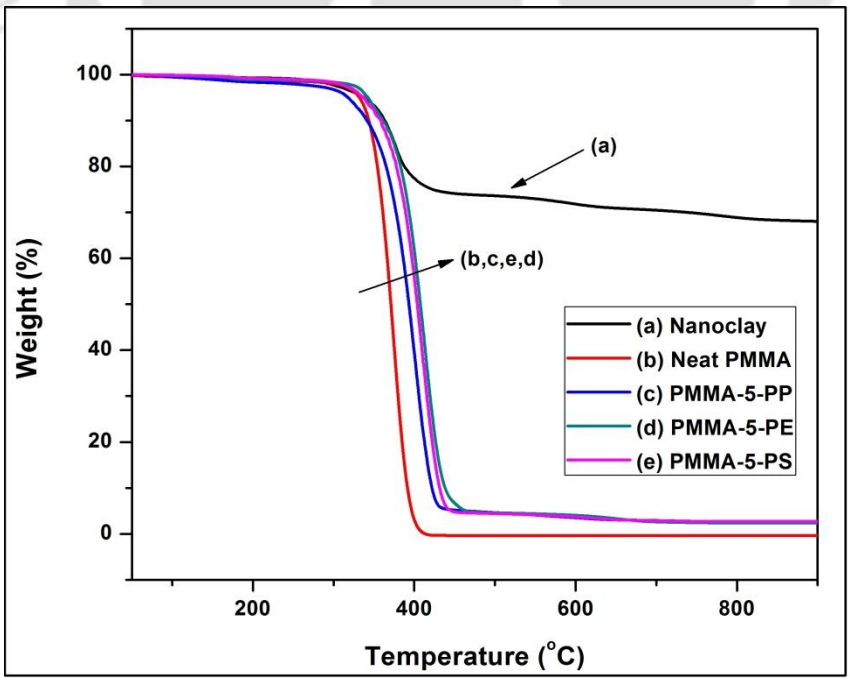

Figure 3.13 TGA curves of nanoclay, neat PMMA, PMMA-5-PP, PMMA-5-PE and PMMA-5-PS nanocomposites

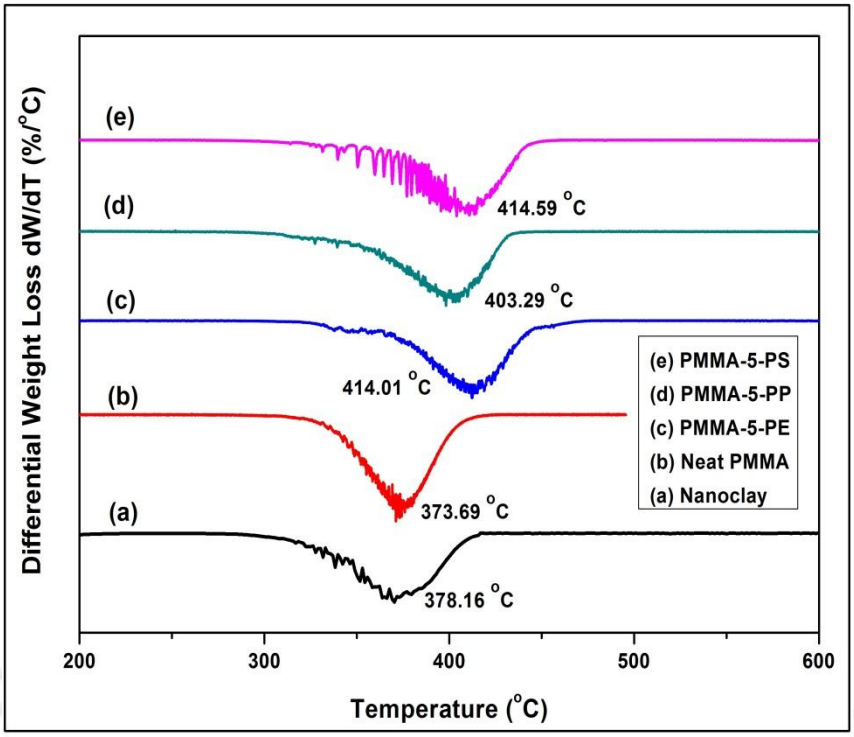

Figure 3.14 TGA derivative of nanoclay, neat PMMA, PMMA-5-PP, PMMA-5-PE and PMMA-5-PS nanocomposites

3.3.11 Dynamic Mechanical Analysis

DMA is an effective method to study storage modulus (E'), loss modulus (E") and tan δ of a sample under stress at varies temperatures. Figure 3.15 illustrates the storage modulus (E') and tan δ versus temperature for PMMA and its nanocomposites measured from 25 to 140 ^{o}C. From the graph, it is noticed that at 25 ^{o}C, the storage modulus (E') increases from ~ 820 MPa for neat PMMA to ~ 1280 MPa for PMMA-5-PS nanocomposite. It is considered that addition of nanoclay into the PMMA matrix significantly enhance the storage modulus of polymer nanocomposites over the neat PMMA. The improvement of stiffness at room temperature is in the resemblance with the modulus, which is already discussed in the mechanical analysis. Various factors such as high modulus of clay, interfacial interaction between clay and polymer, reinforcing effect of filler and restrained chain mobility of polymer chains are directly related to the altering in storage modulus. A gradual decrease in storage modulus (E') is noticed as the temperature increases. It is also observed that above 60 ^{o}C, the storage modulus declines sharply, which is due to the reduction of stiffness of polymer nanocomposites. These findings are in good agreement with the PMMA/OMMT nanocomposites (Krajnc et al., 2009).

The effect of different compatibilizers on the loss factor (tan δ) for the PMMA nanocomposites is displayed in Figure 3.15(b). The graph indicates a shift in the loss-tangent peaks towards higher temperatures, which corresponds to the glass transition temperature (T_g). The T_g of the nanocomposites increases to ~ 2-4 ^oC with respect to neat PMMA. This evidently indicates that the incorporation of organically modified nanoclay has certainly caused restriction of mobility of the polymer chains since the glass transition shifted to higher temperatures. Dyama et al., (2011) have also reported a similar type of increment in T_g for PA-6/PP-g-MA/nanoclay ternary nanocomposites.

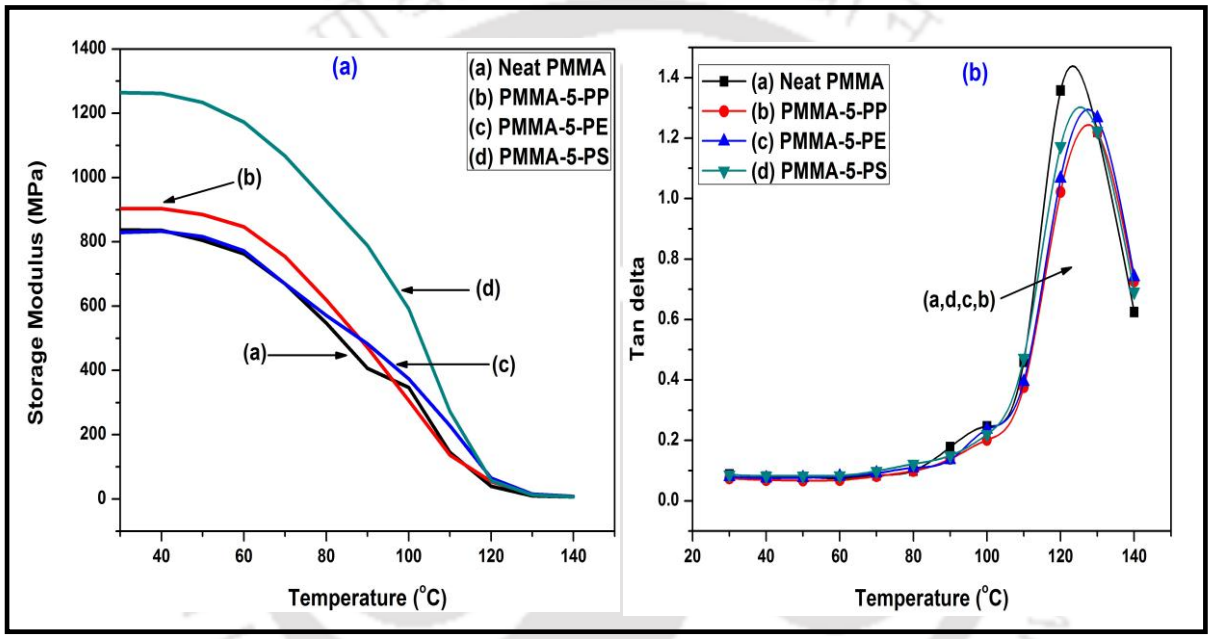

Figure 3.15 Storage modulus (a) and tan δ (b) of neat PMMA, PMMA-5-PP, PMMA-5-PE and PMMA-5-PS nanocomposites

3.3.12 AFM analysis

High resolution AFM images of neat PMMA and its nanocomposites prepared by compression moulding machine are displayed in Figure 3.16. It is observed that pits are present in all the images. The height of the pit is increased (except for PMMA-g-PE) from 157.7 nm (neat PMMA) to 305 nm, after the incorporation of nanoclay in nanocomposites. In comparison with neat PMMA, the depth of the pits is slightly deeper for PMMA-5-PP nanocomposite. However, no valid tendency can be proved due to small analyzed area. Further investigations are required for determining the depth of pits. For PMMA-5-PS nanocomposites, it is noticed that depth of pits are reduced to 210 nm with respect to

PMMA-5-PP nanocomposites. This suggests that compatibilizer played an effective role for reducing the thickness and the same time improving the interaction between the PMMA and nanoclay.

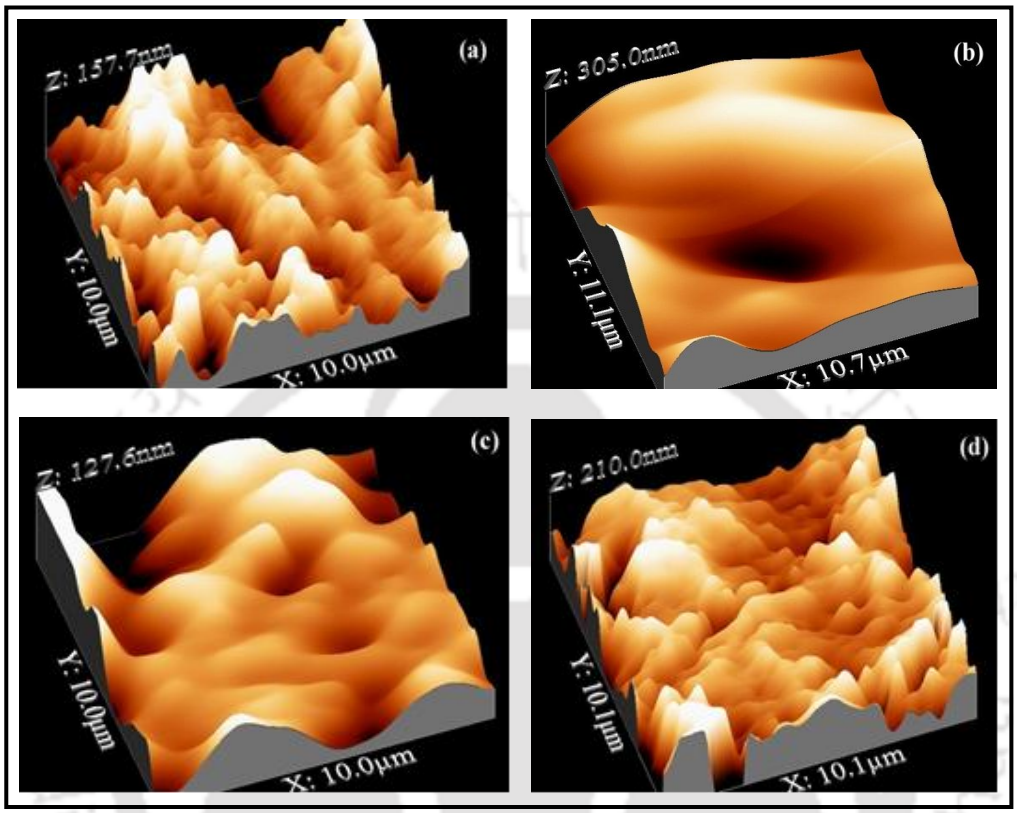

Figure 3.16 AFM images of (a) Neat PMMA, (b) PMMA-5-PP, (c) PMMA-5-PE and (d) PMMA-5-PS nanocomposites

3.3.13 Optical Test

The effect of different compatibilizer on the optical clarity has been examined and it is termed as transmittance of light (%) passing through the sample, when it is exposed to light source. It is clear from the Table 3.3 that neat PMMA shows maximum transmittance of 77.0%. PMMA-g-PP nanocomposite displays only 11.3% transmittance of light, which is very less with respect to neat PMMA. The PMMA-g-PE nanocomposites exhibits 74.5% lower transmittance of light when compared to neat PMMA. This indicates that polyolefin based compatibilizer interfere with optical property of polymer matrix and make it almost opaque. It is also observed from the Table 3.3 that PMMA-g-PS nanocomposite exhibits 33.5% transmittance of light through it and is superior as compared to other polymer nanocomposites. This again proves that compatibilizer, PS-g-MA contains polystyrene,

which makes good blending with PMMA, as both are amorphous in nature and transparent, thus, improves the optical clarity of PMMA-g-PS.

Table 3.3 Optical clarity and rate of burning of neat PMMA, PMMA-5-PP, PMMA-5-PE and PMMA-5-PS nanocomposites

Sample	Transmittance (%)	Rate of burning (mm/min)
Neat PMMA	77.0	65
PMMA-g-PP	11.3	51
PMMA-g-PE	19.6	46
PMMA-g-PS	33.5	41

3.3.14 Flammability Test

The flammability test was carried out to examine the influence of nanoclay and various compatibilizers on the PMMA nanocomposites. It is observed that fire retardancy is improved by the incorporation of nanofiller in the polymer matrix (see Table 3.3). The neat PMMA exhibits the flame propagation rate of 65 mm/min. In the PMMA nanocomposites, flame retardancy is enhanced by the presence of nanofiller and compatibilizer, which acts an interfacial agent to make a strong bonding between the nanoclay and PMMA. The network structure formed by the nanoclay, acts as a barrier in the polymer matrix. As a result, the rate of flame propagation is decreased in PMMA nanocomposites samples. It is noticed that PMMA-5-PS sample demonstrates the maximum flame retardancy of 41 mm/min. This may be due to the presence of benzene ring in PS-g-MA compatibilizer, which acts as flame-retardant. Zhu et al., (2001) stated that the formation of char acts as barrier and heat insulation layer that reduced the flammability of different nanocomposites. Zannetti et al., (2001) proposes that the clay serves as a char promoter by slowing down the degradation and providing a temporary protective barrier to the nanocomposites.

3.3.15 Rheological Properties

Rheology study was performed to analyze the viscoelastic characteristic of any polymer nanocomposites. It is an important factor in extrusion or injection processing condition. The different parameters are discussed as follows:

Storage Modulus (*G'*) denotes the elastic or solid like behaviour and it is related to the energy stored in the material. Figure 3.17(a) represents the frequency dependence storage modulus graph of neat PMMA and its different nanocomposites at 200 ^{o}C. The graph clearly indicates that modulus is increased with the addition of nanoclay in different samples and it is found to be maximum for PMMA-5-PS nanocomposite. It is well documented that the polymer nanocomposites exhibits the transition from liquid-like to pseudo-solid like or solid like when the filler loading increases (Krishnamoorty et al., 1997). This transition concentration is known as rheological percolation threshold. It is observed from the storage modulus graph that all the samples show similar trend of liquid-like behaviour at lower frequency (< 0.1 s^{-1}). The storage modulus increases with an increase in frequency and it is less reliant on the shear rate. This whole phenomenon demonstrates the liquid-like to solid-like viscoelastic, i.e. the formation of strong nanoclay-polymer chain network in the presence of compatibilizer.

Loss modulus (*G''*) signifies the viscous (liquid-like) behaviour of the polymer melt. The loss modulus of neat PMMA and other different nanocomposities is depicted in Figure 3.17(b). The loss modulus also shows a similar trend of storage modulus. However, at lower frequency, PMMA nanocomposites display higher loss modulus with respect to storage modulus. It is found that long-time relaxation has perturbed for all the samples at higher frequency. Nanoclay layers and compatibilizer have less effect. Zhang et al., (2012) also reported similar behaviour for PMMA/graphene composites.

Loss factor (tan δ) is ratio of loss modulus to storage modulus and it arises due to the discrepancy between strain and stress in the polymer when exhibits to an external force, which is strongly related to applied frequency. The loss factor of neat PMMA and its nanocomposites containing different compatibilizer are depicted in Figure 3.18(a). The loss factor (tan δ) of polymer nanocomposites is nearly unconstrained at lower frequency, which develops due to the material elasticity. This material elasticity is altered with an addition of nanoclay at lower frequency or it is higher for neat polymer. The decrease of tan δ at higher frequency is due to partial orientation of nanofiller and polymer chains as a result of deformation.

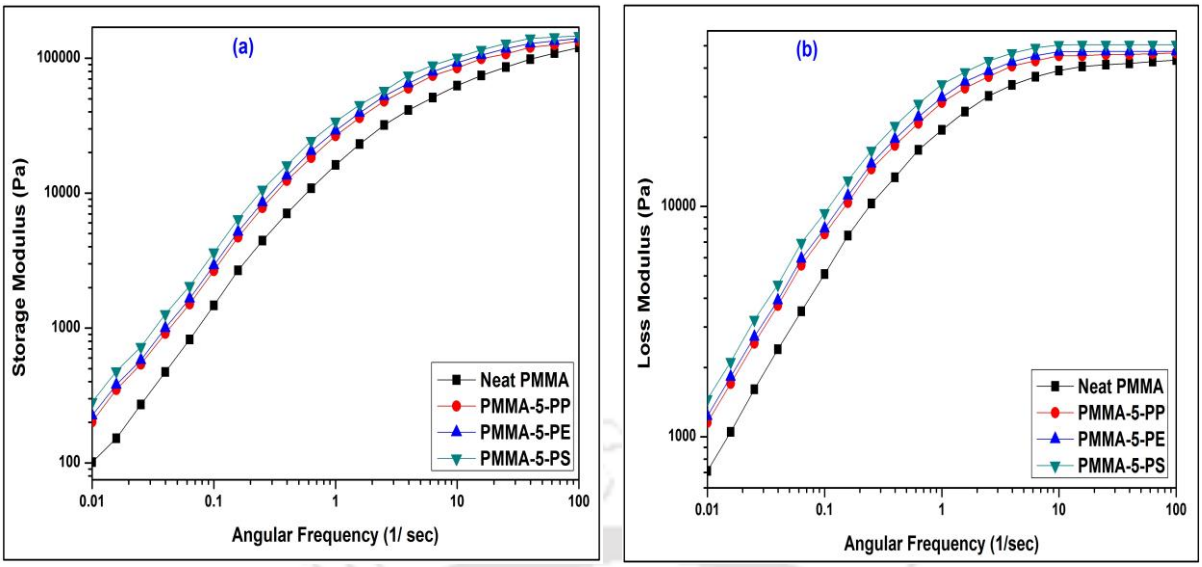

Figure 3.17 (a) Storage modulus and (b) loss modulus of (a) Neat PMMA, (b) PMMA-5-PP, (c) PMMA-5-PE and (d) PMMA-5-PS nanocomposites at 200 ^{o}C

The complex viscosity of neat PMMA, PMMA-5-PP, PMMA-5-PE and PMMA-5-PS nanocomposites at different angular frequency is shown in Figure 3.18(b). At lower frequency, complex viscosity increases with the addition of nanofiller. Similar behaviour is also observed for both moduli. The polymer melts follows the shear thinning phenomenon which representing that polymer melts are non-Newtonian fluids and their viscosity decreases with increasing shear rate. Therefore, when the frequency increases, the polymer chains begin to orient in the flow direction and disentangle from each other, as a result viscosity reduces.

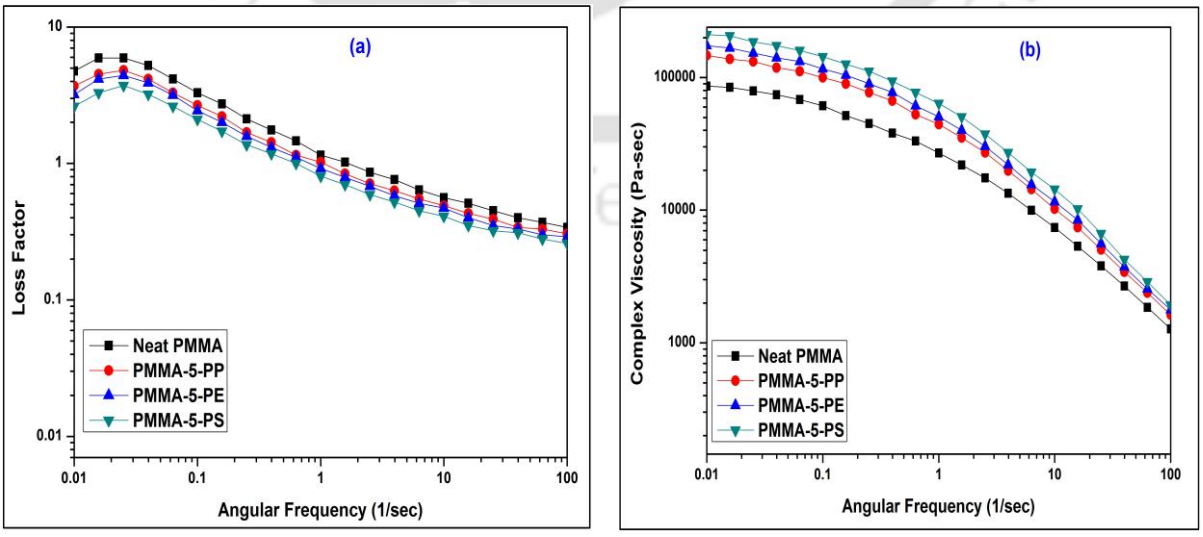

Figure 3.18 (a) Loss factor and (b) complex viscosity of (a) Neat PMMA, (b) PMMA-5-PP, (c) PMMA-5-PE and (d) PMMA-5-PS nanocomposites at 200 ^{o}C

3.3.16 Kinetics Analysis

Figure 3.19 (a-d) shows all the linear fitted graph of PMMA and its nanocomposites with different compatibilizers. The calculated reaction order at the best *R* value is considered as the reaction order for that sample. Afterwards, the activation energy and the pre-exponential factor are estimated from the slope and intercept of fitted straight line. The activation energy of neat PMMA, PMMA-5-PP, PMMA-5-PE, PMMA-5-PS sample is 99.4, 101.76, 139.37 and 137.77 kJ/mol, respectively. It is evident from the Table 3.4 that activation energy (E_a) of different PMMA nanocomposite is 2-39 kJ/mol higher than that of pristine PMMA. The PMMA-5-PE sample has the highest activation energy value among all other samples. Chen and Wang, (2007) also reported the improvement in activation energy of nanocomposites as compared to neat polymer, which is in accordance with this work.

The kinetic parameters obtained from Coats-Redfern method are utilized to estimate the different reaction mechanism in Criado method. Figure 3.20 (a-d) displays the Z(α)-α master and experimental curve of neat PMMA and its nanocomposites with different compatibilizers. It is noticed that for the neat PMMA, experimental Z(α)-α curve initially follows A2 reaction mechanism (nucleation and growth) with lower α value (α=0.1-0.2) then it deviates from A2 to F1 mechanism (random nucleation having one nucleus on individual particle) at medium α value (α=0.3-0.5) and then again deviates from F1 to A4 mechanism (nucleation and growth) for higher α value (α=0.7-0.9). In case of PMMA-5-PP nanocomposites, Z(α)-α experimental curve initially follows the F1 reaction mechanism and then it deviates from it and then follows the A4 reaction mechanism at higher α value (0.9). While for PMMA-5-PE and PMMA-5-PS nanocomposite, Z(α)-α experimental curve primarily follows the F1 reaction mechanism and at higher conversion follows the A2 reaction mechanism at higher value of α (0.7-0.9).

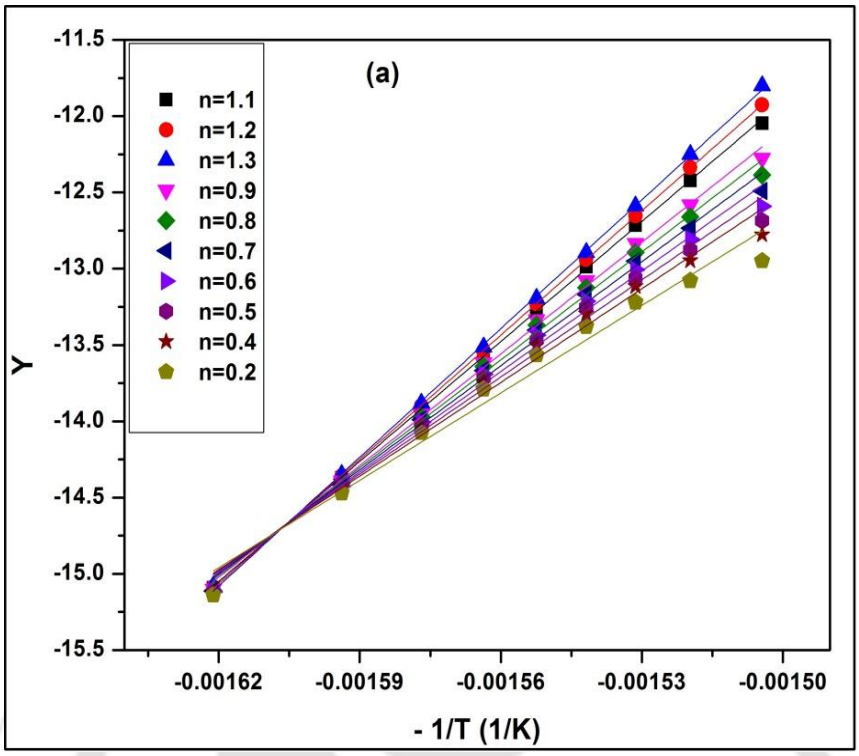
(a)
n=1.1
n=1.2
n=1.3
n=0.9
n=0.8
n=0.7
n=0.6
n=0.5
n=0.4
n=0.2
Y
-11.5
-12.0
-12.5
-13.0
-13.5
-14.0
-14.5
-15.0
-15.5
-0.00162
-0.00159
-0.00156
-0.00153
-0.00150
- 1/T (1/K)

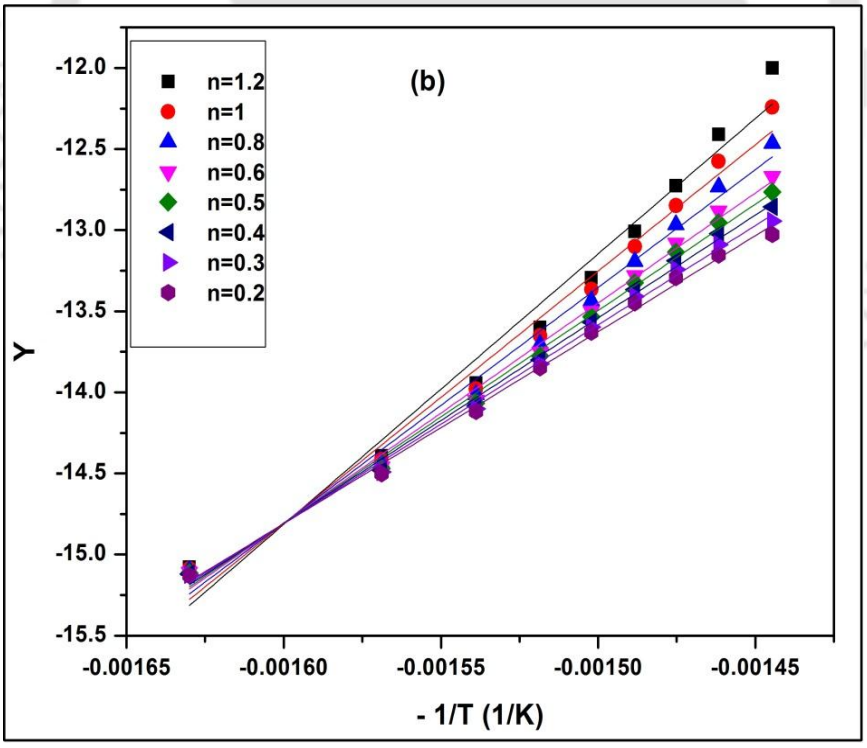
(b)
n=1.2
n=1
n=0.8
n=0.6
n=0.5
n=0.4
n=0.3
n=0.2
Y
-12.0
-12.5
-13.0
-13.5
-14.0
-14.5
-15.0
-15.5
-0.00165
-0.00160
-0.00155
-0.00150
-0.00145
- 1/T (1/K)

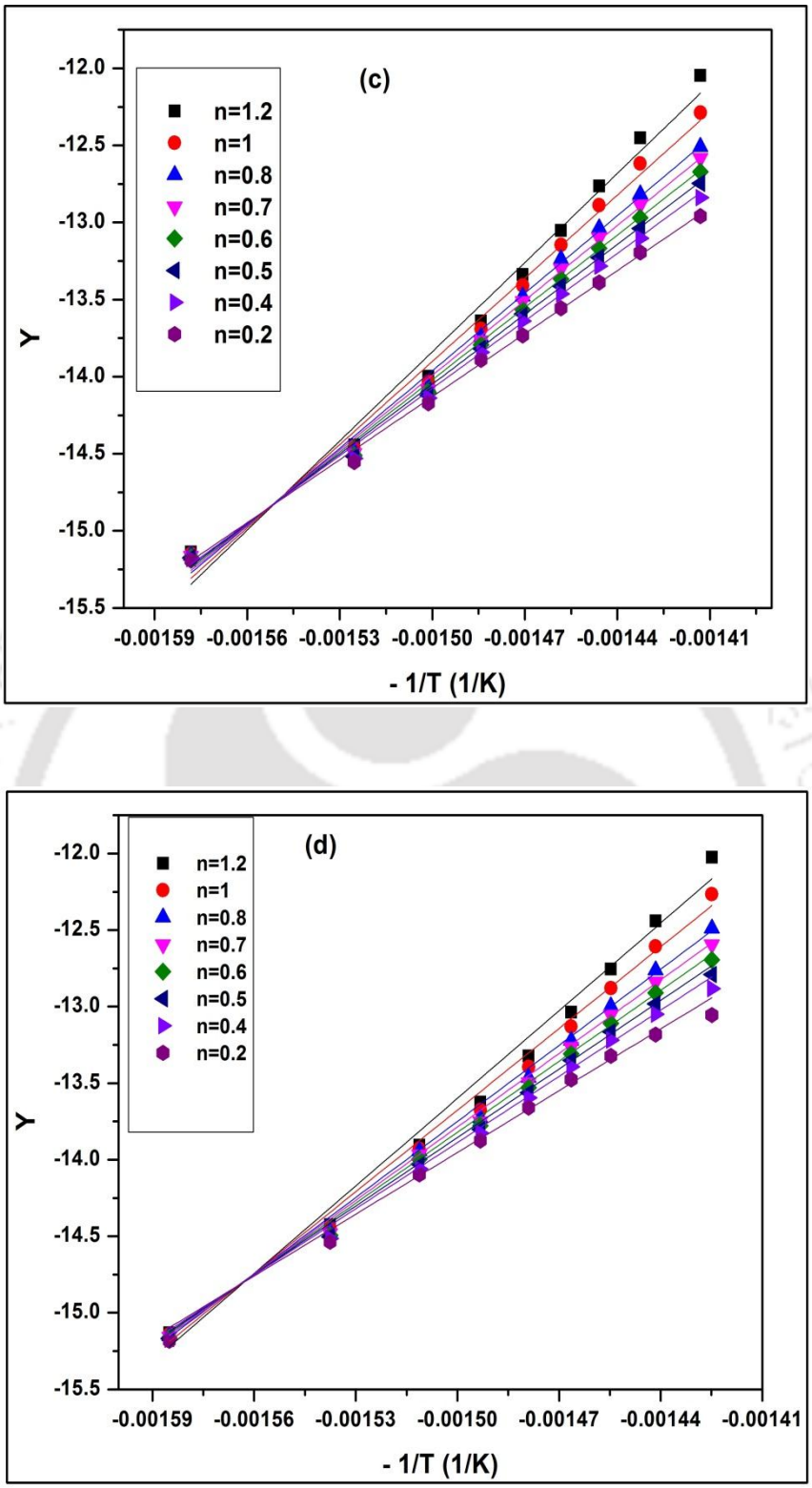

Figure 3.19 Determination of kinetic parameters by plots of the left part in equation 3.10 against -1/T using Coats-Redfern method: (a) Neat PMMA, (b) PMMA-5-PP, (c) PMMA-5-PE and (d) PMMA-5-PS nanocomposites

Table 3.4 Kinetic parameters of different samples at the better correlation coefficient obtained from Coats-Redfern method

Sample	E_a(kJ/mol)	A	n	R
Neat PMMA	99.2	24.36×10^6	0.6	0.997
PMMA-5-PP	101.76	145.05×10^6	0.3	0.996
PMMA-5-PE	139.37	120.17×10^8	0.5	0.992
PMMA-5-PS	137.77	110.42×10^8	0.5	0.984

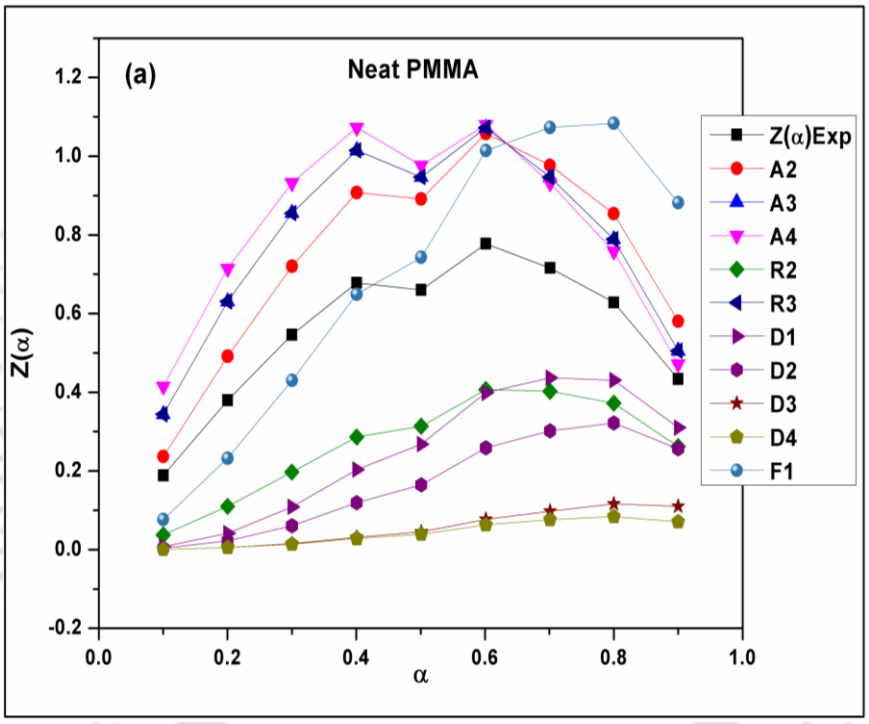

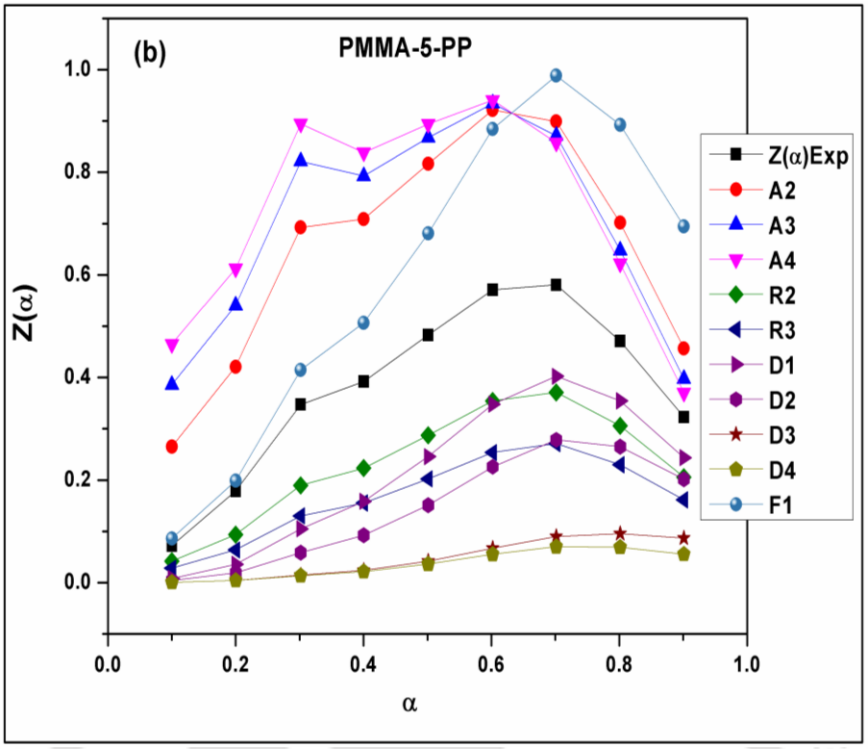
(b)
PMMA-5-PP
Z(α)
α
Z(α)Exp
A2
A3
A4
R2
R3
D1
D2
D3
D4
F1

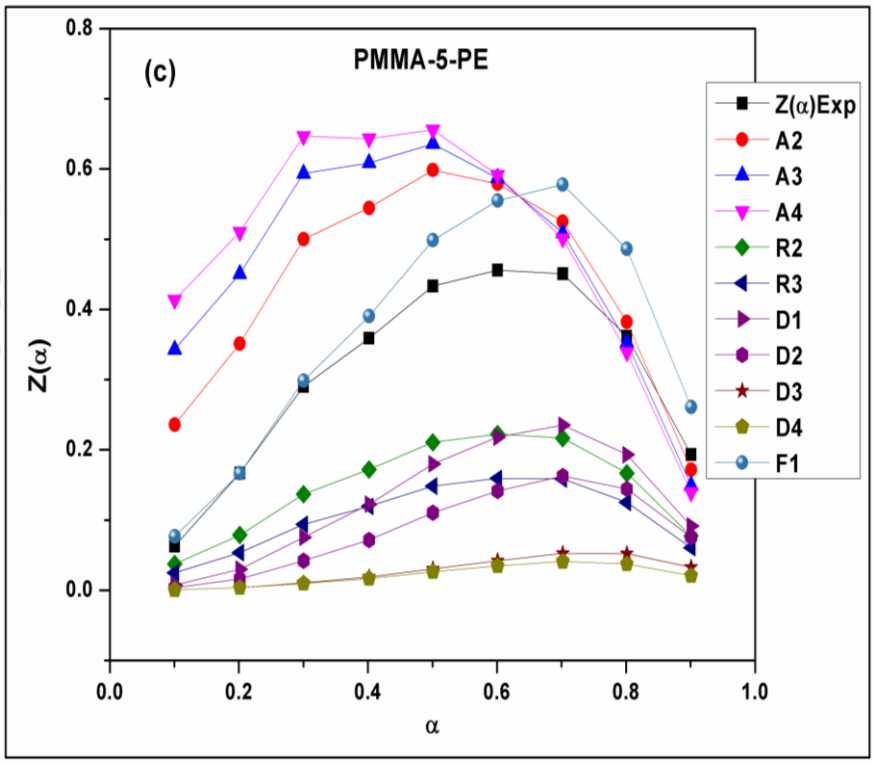
(c)
PMMA-5-PE
Z(α)
α
Z(α)Exp
A2
A3
A4
R2
R3
D1
D2
D3
D4
F1

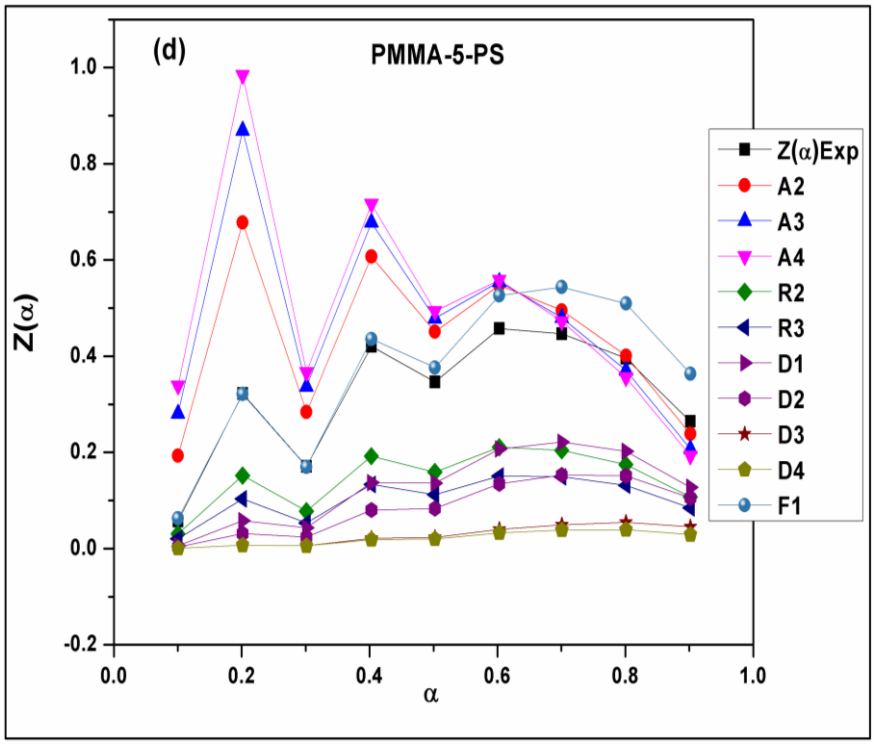

Figure 3.20 Determination of the thermal degradation mechanism by plotting Z(α) versus α using Criado model

3.4 SUMMARY

PMMA nanocomposites with different compatibilizer have been successfully prepared by melt compounding technique. It is found from the XRD analysis that PMMA-5-PS sample shows a d-spacing of 3.26 nm. The TEM image also demonstrates that PMMA-5-PS nanocomposite possesses partially exfoliated structure. The tensile modulus of nanocomposites increases by the incorporation of compatibilizers and it is found to be 16, 17 and 20% higher over neat PMMA for PMMA-5-PP, PMMA-5-PE, PMMA-5-PS, respectively. The hardness (Shore D) is also improved by 34% for PMMA-5-PS as compared to neat PMMA. TGA study reveals that all the nanocomposites exhibit enhanced thermal stability when compared with pristine PMMA. The DSC results show that glass transition temperature (T_g) is marginally improved by 2^{o}C. DMA suggests that storage modulus is enhanced by the strong bonding between clay and polymer matrix induced by comaptibilizers. It is clearly found that optical clarity and flammability are reduced with addition of clay. As suggested by Coats-Redfern method, the activation energy of PMMA-5-PP nanocomposite is 39 kJ/mol higher compared to neat PMMA, which primarily follows the

F1 mechanism and deviates to A2 reaction mechanism at higher conversion rate. From the rheological studies, it is found that both storage and loss modulus increase with an increase in frequency. The complex viscosity follows the shear-thinning behavior. As a whole, PMMA-5-PS sample displays better properties over other samples.

Chapter 4

Influence of Co-Al LDH and Cu-Cr LDH content on the properties of PMMA nanocomposites prepared via Melt Intercalation Technique

In this present work, two different layered double hydroxides (LDHs), cobalt aluminium (Co-Al) and copper chromium (Cu-Cr) LDHs have been synthesized by co-precipitation method. PMMA nanocomposites containing LDH's content of 1-7 wt.% were fabricated by melt intercalation method using twin screw extruder. As suggested from the previous chapter, PS-g-MA was used as a compatibilizer. The structural properties of the PMMA nanocomposites were evaluated by X-Ray diffraction (XRD), field emission scanning electron microscopy (FESEM), transmission electron microscopy (TEM) and atomic force microscopy (AFM). The mechanical properties of different nanocomposites were evaluated by tensile, flexural, impact and hardness tests. The thermal stability investigation was done by thermogravimetric analysis (TGA) and differential scanning calorimetry (DSC). The thermal degradation activation energy of the nanocomposites was determined by Coats-Redfern method and the obtained results were compared with the neat PMMA. Criado method was employed to determine the degradation reaction mechanism of different samples. The improvement of thermal stability was also confirmed by integral procedural decomposition temperature (IPDT). Finally, the measurement of rheological properties of PMMA nanocomposites was done under molten state.

The part of this work has been communicated to* ***Composites Science and Technology.

4.1 INTRODUCTION

It is observed from the previous chapter that twin-screw extruder and compatibilizer had significantly improved the properties of the nanocomposites. In this chapter, we have made an attempt to investigate the effect of different layered double hydroxides (LDHs) on the properties of PMMA nanocomposites. LDHs can be easily synthesized by co-precipitation method in laboratory with high purity and tunable chemical compositions. Organic modification of LDH is essential prior to its application for preparing polymer nanocomposites, as it provides the intercalated or exfoliated structure. The LDH exhibits potential advantage in flame retardants (Hong et al., 2014), medical field (Li et al., 2011) and capacitors (Wimalasiri et al., 2014; Zhu et al., 2015). Based on melt-intercalation method, a very limited number of literatures are available on the fabrication of LDH based polymer nanocomposites. Realinho et al., (2009) prepared the polystyrene and poly(styrene-*co*-acrylonitrile) nanocomposites by melt-extrusion process and studied the influence of modified Mg-Al LDH on the properties of the nanocomposites. They found that LDH particles to poly(styrene-*co*-acrylonitrile) caused an improvement in fracture toughness and fracture energy by 50 and 200%, respectively over pure polymer. While for polystyrene matrix, both tensile properties and elastic fracture were remain unaffected. Coiai et al., (2010) examined the effect of PP-g-MAH compatibilizer on the polypropylene (PP) nanocomposites synthesized using modified and unmodified Mg-Al LDH. They observed that only modified LDH exhibited intercalated and partial delaminated structure of the nanocomposites. It was also found that thermal decomposition temperature was enhanced by 19 ^{o}C for compatibilized PP nanocomposites containing modified LDH at $T_{10\%}$. In another study, the influence of MMT and Zn-Al LDH on the PP nanocomposites was investigated by Ding and Qu, (2006). They reported that PP/LDH nanocomposites exhibited 17 ^{o}C higher thermal decomposition temperature than PP/MMT nanocomposites when 80% weight was considered as point of comparison.

4.2 EXPERIMENTAL

4.2.1 Materials

PMMA (IG 840) used in this study was a commercial product from LG Polymers, South Korea. The melt flow index (MFI at 230 ^{o}C and 3.8 kg load) and specific gravity of PMMA were 5.8 g/10 min and 1.18, respectively. The compatibilizer, polystyrene-block-

poly(ethylene-ran-butylene)-block-polystyrene-graft-maleic-anhydride (PS-g-MA) was obtained from Sigma-Aldrich, USA. Copper nitrate ($Cu(NO_3)_2.3H_2O$), chromium nitrate ($Cr(NO_3)_3.7H_2O$), cobalt nitrate ($Co(NO_3)_2.6H_2O$), nickel nitrate ($Ni(NO_3)_2.6H_2O$), aluminium nitrate ($Al(NO_3)_3.9H_2O$), sodium nitrate ($NaNO_3$), sodium dodecyl sulfate ($NaC_{12}H_{25}SO_4$) and sodium hydroxide (NaOH) were purchased from Merck India Ltd, Mumbai. Millipore water was used throughout the study.

4.2.2 Preparation of Co-Al, Cu-Cr and Ni-Al LDHs

The method adopted for the preparation of modified Co-Al LDH was reported elsewhere (Du et al., 2009). The modified Co-Al LDH was prepared by instinctive self-assembly approach. In a typical process, $Co(NO_3)_2.6H_2O$, $Al(NO_3)_3.9H_2O$ and sodium dodecyl sulfate (as a modifier) were dissolved in Millipore water (200 ml) to obtain solution (A) with Co^{2+}/Al^{3+}/SDS molar ratio of 2:1:1.5. Then an aqueous solution (B) containing NaOH was prepared. After that, the solution (B) was added drop wise into solution (A) and the resultant solution was continuously stirred to maintain the pH of mixture at 8.3. Then the slurry was kept at an ambient temperature for 16 h. The resultant precipitate was filtered, thoroughly washed with Millipore water and dried at 70 ^oC to remove water content.

The Cu-Cr LDH was prepared by co-precipitation method (Sahu and Pugazhenthi, 2011). First, an aqueous solution of nitrate salts, $Cu(NO_3)_2.3H_2O$ (0.12 mol), $Cr(NO_3)_3.7H_2O$ (0.06 mol) and $NaNO_3$ (0.12 mol) was prepared. M^{2+}/M^{3+} ratio of 2:1 was maintained for the synthesis. To this, an aqueous solution of NaOH (2M) was added drop wise with vigorous stirring until the required pH of 10.2 was obtained. The resultant slurry was aged at room temperature for 16 h. Then the precipitate was filtered, washed thoroughly with Millipore water until pH of filtrate was neutral, and subsequently dried at 80 ^oC for 12 h.

In the next stage, Cu-Cr LDH sample (2.5 g) was calcined at 500 ^oC for 5 h in a muffle furnace (air atmosphere) with a heating rate of 2 $^oC\ min^{-1}$ to obtain the oxide form. Then the calcined LDH was dispersed into a 120 mL of aqueous solution containing 2.5 g of SDS. This dispersion was refluxed for 12 h to ensure complete regeneration of the host LDH structure. Finally the residues were separated by centrifuging and washed with Millipore water several times to remove of unreacted SDS molecules. The solids were dried at 80 ^oC to produce organically modified Cu-Cr LDH.

A co-precipitation method was adopted for the synthesis of pristine Ni-Al LDH. An aqueous solution of $Ni(NO_3)_2.6H_2O$, $Al(NO_3)_3.9H_2O$ and $NaNO_3$ was prepared using the mole ratio of the nitrate salts as 2:1:2, respectively. After which, NaOH solution (2N) was added drop wise and the solution was stirred until the pH level reached 10. The resulting solution was stirred for 16 hr at room temperature. The obtained final solution was filtered and precipitate was washed with Millipore water until the filtrate was neutral. Then the precipitate was dried at room temperature for 24 h and 65 ^oC for 6 h in an oven to get pristine LDH. Figure 1 depicts the schematic of modification of Ni-Al LDH with SDS by rehydration method. For this 2.5 gm of dried pristine LDH was calcined at 500 ^oC for 5 h in muffle furnace with a heating rate of 10 ^oC/min. After calcination, the LDH was modified with SDS for better dispersion of LDH in the polymer matrix. For this, the calcined LDH was dispersed into 120 ml of aqueous solution containing 2.5 gm of SDS and was refluxed at 80 ^oC for 12 h to yield organomodified LDH. Finally it was filtered and dried at 50 ^oC in an oven. The dried modified Ni-Al LDH sample was then grinded into finer particles.

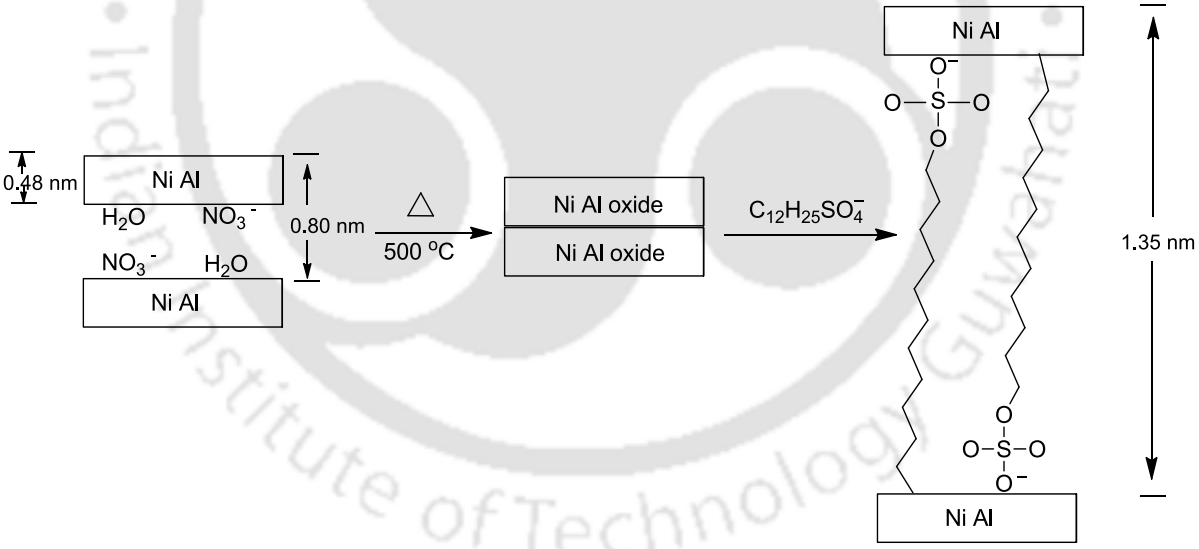

Figure 4.1 Schematic representation of modification of Ni-Al LDH with SDS

4.2.3 Preparation of PMMA/LDHs nanocomposites

Prior to melt intercalation, PMMA pellets and LDHs were dried in a vacuum oven at 80 ^oC and 65 ^oC, respectively for 12 h. PMMA nanocomposites containing different loading (1-7

wt.%) of LDH's were prepared by melt intercalation technique in a counter rotating twin screw extruder (Make: Specifiq Engineering and Automats, Vadodara, India; Model-ZV-20 HI TORQUE). In a typical experiment, PMMA, LDH's and PS-g-MA compatibilizer were fed into the extruder and the obtained extrudate was quenched in water at room temperature. Subsequently, the extrudate was cut into pellets and then dried before being injection moulded (JSW, Japan; Model-180 High Pressure) at 180-250 ^{o}C to make specimens for mechanical testing. Hereafter, the nanocomposites prepared using 1, 3, 5 and 7 wt.% Co-Al LDH is referred as PMMA/Co-Al 1%, PMMA/Co-Al 3%, PMMA/Co-Al 5% and PMMA/Co-Al 7%, respectively (see Table 4.1). Neat PMMA sample was also prepared by a similar method in the absence of compatibilizer and LDH. Similarly, a series of PMMA/Cu-Cr LDH nanocomposites containing 1-5 wt.% of LDH is also prepared and compared with PMMA/Ni-Al LDH having 5 wt.% LDH.

Table 4.1 Composition used for the fabrication of PMMA/Co-Al LDH nanocomposites

Sample Name	PMMA (wt.%)	LDH concentration (wt.%)	Compatibilizer (wt.%)
Neat PMMA	100	-	-
PMMA/Co-Al 1%	94	1	5
PMMA/Co-Al 3%	92	3	5
PMMA/Co-Al 5%	90	5	5
PMMA/Co-Al 7%	88	7	5

4.2.4 Characterization Techniques

The polymer nanocomposites were characterized under the same conditions as already reported in Chapter 2 (section 2.2.4).

4.3 RESULTS AND DISCUSSION

4.3.1 XRD Analysis

XRD is an effective method to characterize the structure of nanocomposites. Nanocomposites can be described as immiscible, intercalated or exfoliated depending upon the type of dispersion of the polymer matrix in between the layers of nanomaterial. In an immiscible system, also known as microcomposite, the polymer does not enter into the gallery space of the nanomaterial; this is a conventional composite. An intercalated nanocomposite is obtained when the polymer enters the gallery space and the registry between the layers is maintained. In an exfoliated system, also known as delaminated system, excellent nano-dispersion of the layered material into the polymer material is accompanied with a loss of the registry between the layers (Manzi-Nshuti et al., 2009). The d-spacing is calculated from peak position using Bragg's law: $n\lambda = 2d\sin\theta$, where λ is the X-ray wave length (1.5406Å) and n=1. The XRD patterns of Co-Al LDH and various PMMA nanocomposites are shown in Figure 4.2(i). The basal spacing (d_{003}) of (003) peak appeared at 2θ value of 3.10^{o} for Co-Al LDH is calculated to be 2.84 nm.

For neat PMMA, the diffraction peak is appeared at $2\theta = 13.34^{o}$ and the large broad is originated due to amorphous nature of PMMA matrix. The diffraction peak of PMMA/Co-Al LDH nanocomposites containing different loading (1-7 wt.%) of LDHs is disappeared. Similarly, it is also noticed that (003) diffraction peak is absent in PMMA/Cu-Cr LDH nanocomposites [see Figure 4.2(ii)]. Wang et al., (2005) also reported similar kind of pattern for PMMA/Mg-Al LDH nanocomposites. Two extreme cases can explain the disappearance of the diffraction peaks in XRD: (a) complete exfoliation of the LDH layers in the polymer matrix, and/or (b) disordering of the LDH layers within the polymer matrix with no change in the d-spacing. Morphological study will be more useful in this regard.

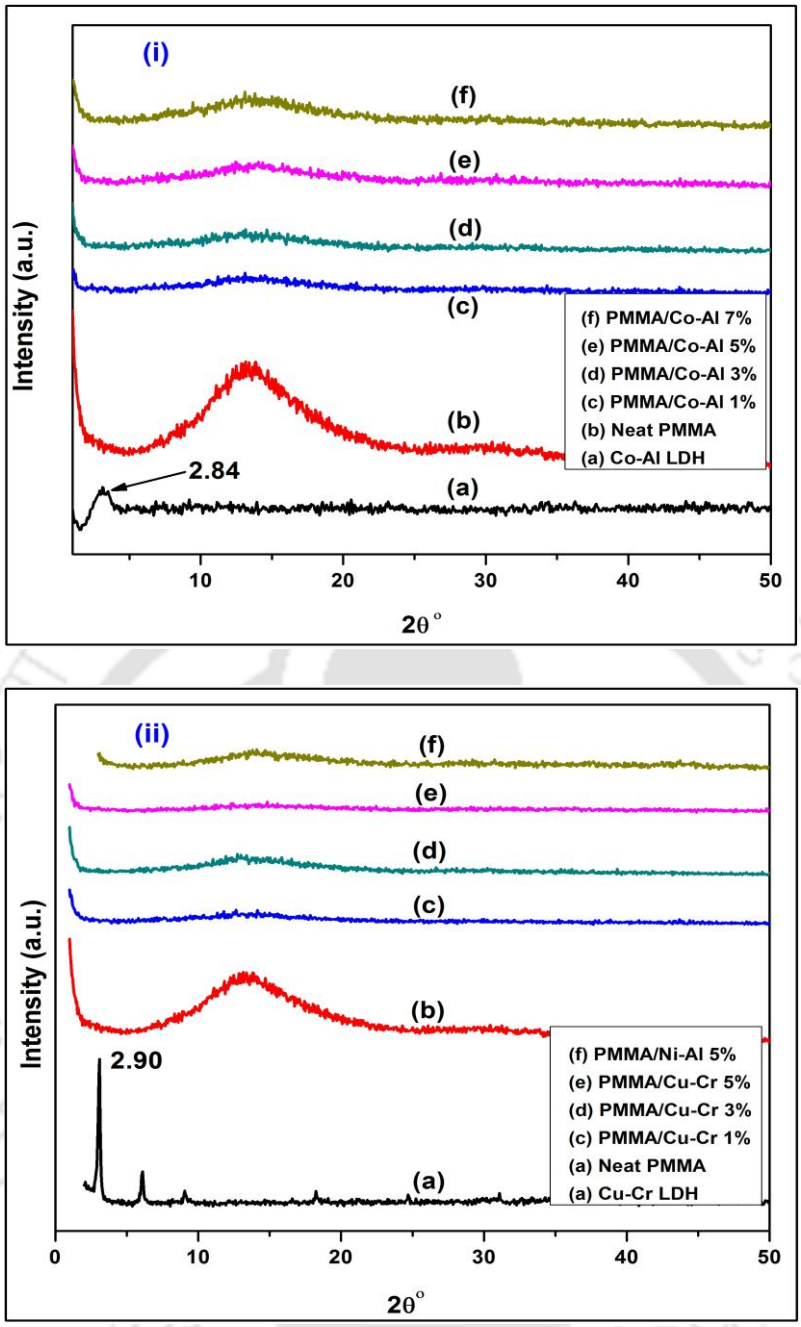

Figure 4.2 XRD patterns of (i) PMMA/Co-Al LDH and (ii) PMMA/Cu-Cr LDH nanocomposites

4.3.2 FTIR Analysis

The FTIR spectra for neat PMMA and its different nanocomposites recorded for the frequency range 500 to 4000 cm^{-1} are presented in Figure 4.3. The FTIR analysis has been performed to identify the various functional groups present in the Co-Al LDH, Cu-Cr LDH and polymer nanocomposites.

In Figure 4.3(i), the nitrate anions which are observed in the Co-Al LDH, exhibit three different characteristics peaks, i.e., the nitrate absorption peak found at 1370 cm^{-1}, two other nitrate vibration band at 1470 and 822 cm^{-1}. The aliphatic band ($–CH_2$) of the long chain of SDS molecules is observed between 2840-2965 cm^{-1}. The small bands appeared at 1218 and 1063 cm^{-1} relate to the symmetric (v_s=o) and asymmetric vibration (v_{os}=o) of sulfate from dodecyl sulfate, respectively. The broad band in the range of 3400-3530 is due to the O-H stretching vibration of water molecules. The peaks observed at lower frequency (400-700 cm^{-1}) correspond to the vibration of metal-oxygen bond in the brucite-like lattice, which is particular of this kind of layered solids. The Cu-Cr LDH is also demonstrated similar kind of functional groups [see Figure 4.3(ii)].

For neat PMMA and its nanocomposites, the characteristic peak is observed around 1730 cm^{-1} which is assigned to the carbonyl group (>C=O) present in the polymer. The band found at 2995 is assigned to the ester-methyl stretching vibrations. The peak exhibits at 2949 cm^{-1} is due the asymmetric stretching vibration of $–CH_3$ group. The small peaks appeared at 1218 and 1063 cm^{-1} correspond to the symmetric (v_s=o) and asymmetric vibration (v_{os}=o) of sulfate from dodecyl sulfate, respectively. It is found that the spectra of all nanocomposites have similar bands with those of neat PMMA, as well as some additional small peaks coming from the LDH (i.e., the metal-oxide bonds of Si–O and Mg–O). From these results, it is confirmed the presence of LDH in the PMMA matrix.

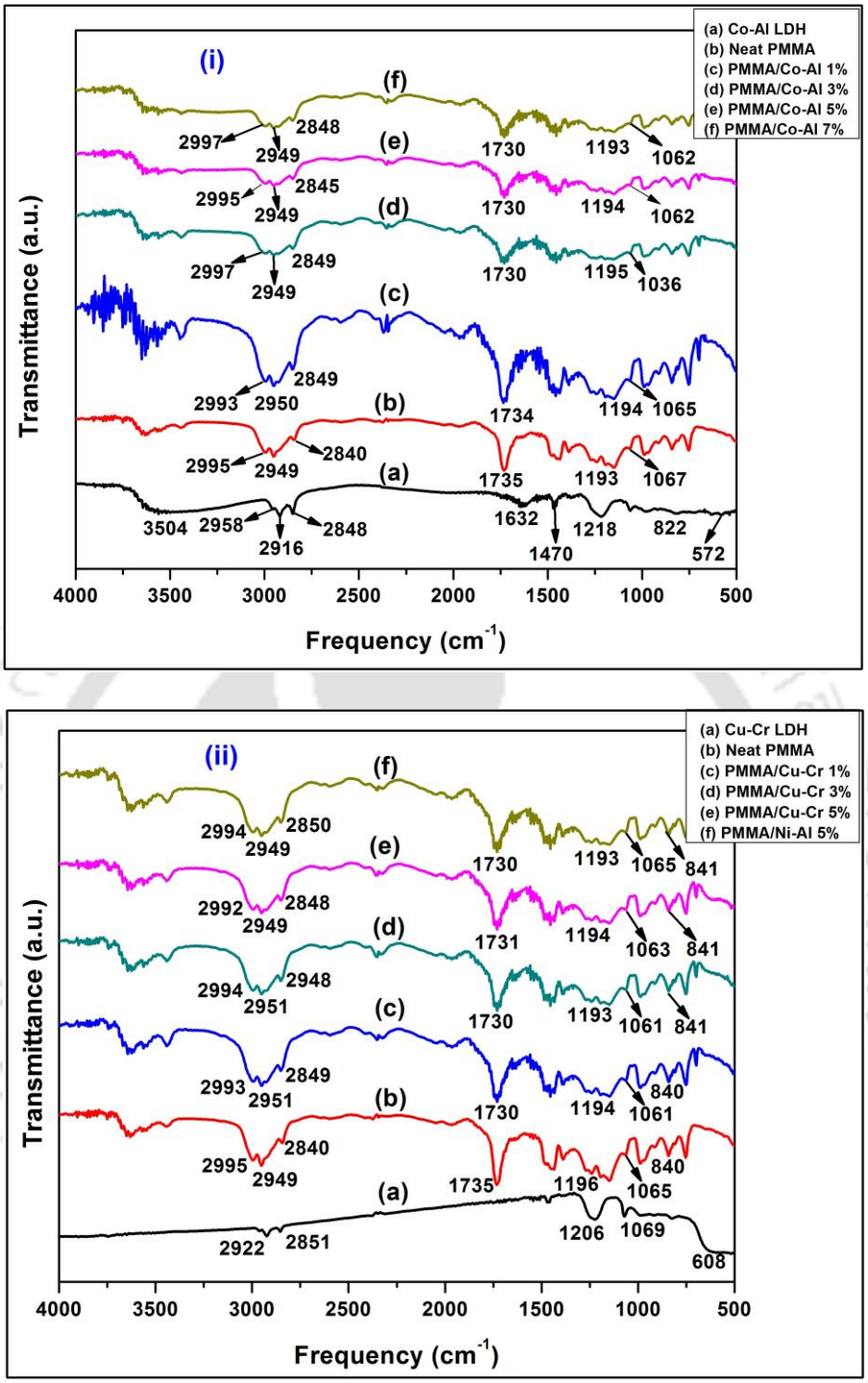

Figure 4.3 FTIR spectra of (i) PMMA/Co-Al LDH and (ii) PMMA/Cu-Cr LDH nanocomposites

4.3.3 FESEM Analysis

The distribution of LDH layers in the polymer matrix and their interfacial bonding are important features that influence the mechanical and thermal properties of the nanocomposite materials. The most direct measurement of the dispersion of LDH particles in the PMMA matrix is made by FESEM. Figure 4.4 displays the FESEM micrographs of the tensile fractured specimen of PMMA nanocomposites containing Co-Al and Cu-Cr LDHs. The figure 4.4 (i, a-d) represents the PMMA/Co-Al 1%, PMMA/Co-Al 3%, PMMA/Co-Al 5% and PMMA/Co-Al 7% nanocomposites while the figure 4.4(ii a-d) denotes the PMMA/Cu-Cr 1%, PMMA/Cu-Cr 3%, PMMA/Cu-Cr 5% and PMMA/Ni-Al 5% nanocomposites. It is observed from all the images of PMMA nanocomposites that LDH particles are arbitrarily dispersed in the PMMA matrix. Although on careful inspection, a regular pattern of LDH particles, showing wave-like wrinkles is detected. On further addition of nanofiller, it is observed that the LDH particle organize themselves in the form of aggregates around which the polymer is wrapped. As shown in figure 4.4 (i, d) and (ii, c), poor distribution is noticed in the images of higher loading of LDH. Because the LDH particles are aggregated together, and many holes are left behind after particles are pulled out from the PMMA matrix when stress applied. Maiti and Das, (2005) also found similar type of morphology for isotactic polypropylene (iPP)/chlorosulfonated polyethylene (CSM) rubber blends.

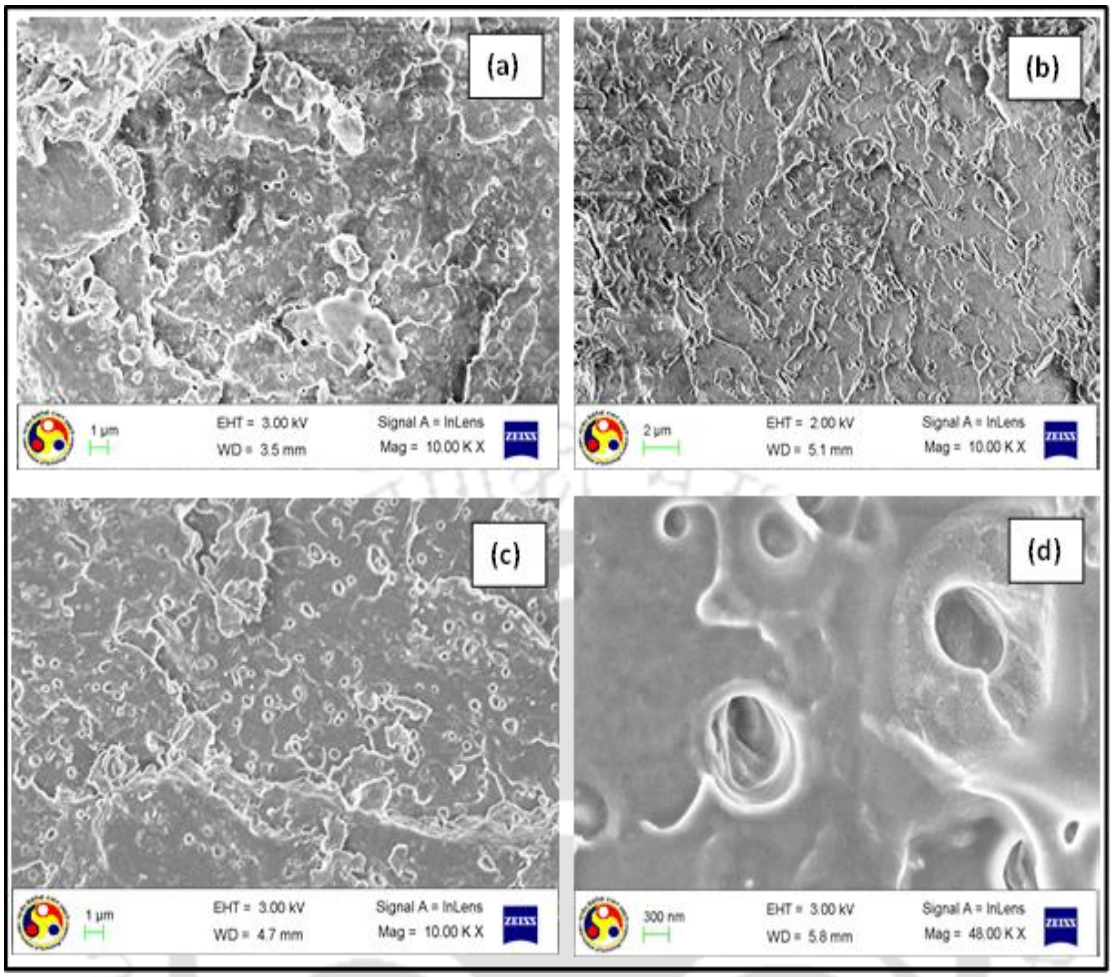

Figure 4.4 (i) FESEM images of (a) PMMA/Co-Al 1%, (b) PMMA/Co-Al 3%, (c) PMMA/Co-Al 5% and (d) PMMA/Co-Al 7% nanocomposites

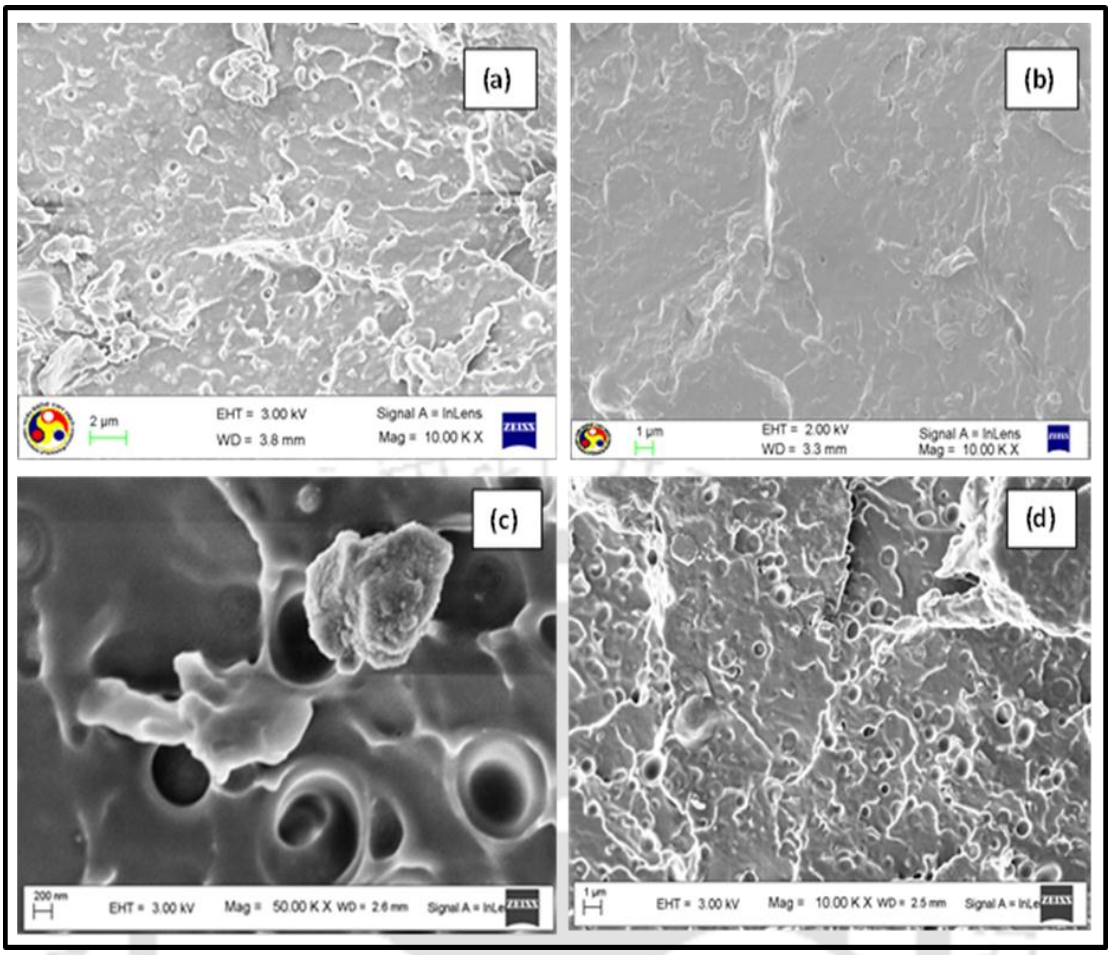

Figure 4.4 (ii) FESEM images of (a) PMMA/Cu-Cr 1%, (b) PMMA/Cu-Cr 3%, (c) PMMA/Cu-Cr 5% and (d) PMMA/Ni-Al 5% nanocomposites

4.3.4 TEM Analysis

TEM observations are used to further verify XRD analysis of the nanocomposites. Figure 4.5 exhibits the micrographs of different PMMA/Co-Al LDH nanocomposites where the brighter region represents the polymer matrix and the dark narrow stripes represent the LDH nanolayers. The higher magnification images are required in order to distinguish between intercalated and exfoliated structures. Figure 4.5(a) and 4.5(b) reveals that individual layers of Co-Al LDH are well dispersed in the PMMA matrix and separated one from the other. This suggests that LDH layers are exfoliated into the secondary particles with a length of 20 nm. This also suggested that PS-g-MA compatibilizer plays an effective role for dispersion of Co-Al LDH in matrix. At higher loading of Co-Al LDH content (5-7 wt.%), it is noticed from the Figure 4.5 (c-d) that the nanocomposites appear to contain oriented collections of 4-5 parallel LDH layers exhibiting an intercalated structure.

For PMMA/Cu-Cr LDH nanocomposites, the micrograph evidently illustrates the lamellar structure of Cu-Cr LDH, which is exfoliated by the PMMA macromolecular chain; the lines of the layers are well shown using the aero marks and the exfoliated Cu-Cr LDH sheets are dispersed in the PMMA matrix, being consistent with the XRD results presented in Figure 4.2(ii). The modified Cu-Cr LDH platelets might be broken into smaller ones when they are exfoliated during the extrusion probably due to the occurrence of layer breakage. In Figure 4.5(ii,b), it is observed that as the loading increases, the nanocomposites having 4-5 parallel layers of LDH layers, which leads to intercalated structures. Above 5 wt.% loading, it is clearly seen that the Cu-Cr LDH layers are dispersed in lamellar form and randomly distributed in polymer matrix [see, Figure 4.5 ii (c)]. The PMMA/Ni-Al 5% nanocomposite exhibits partially exfoliated Ni-Al LDH layers in the PMMA matrix.

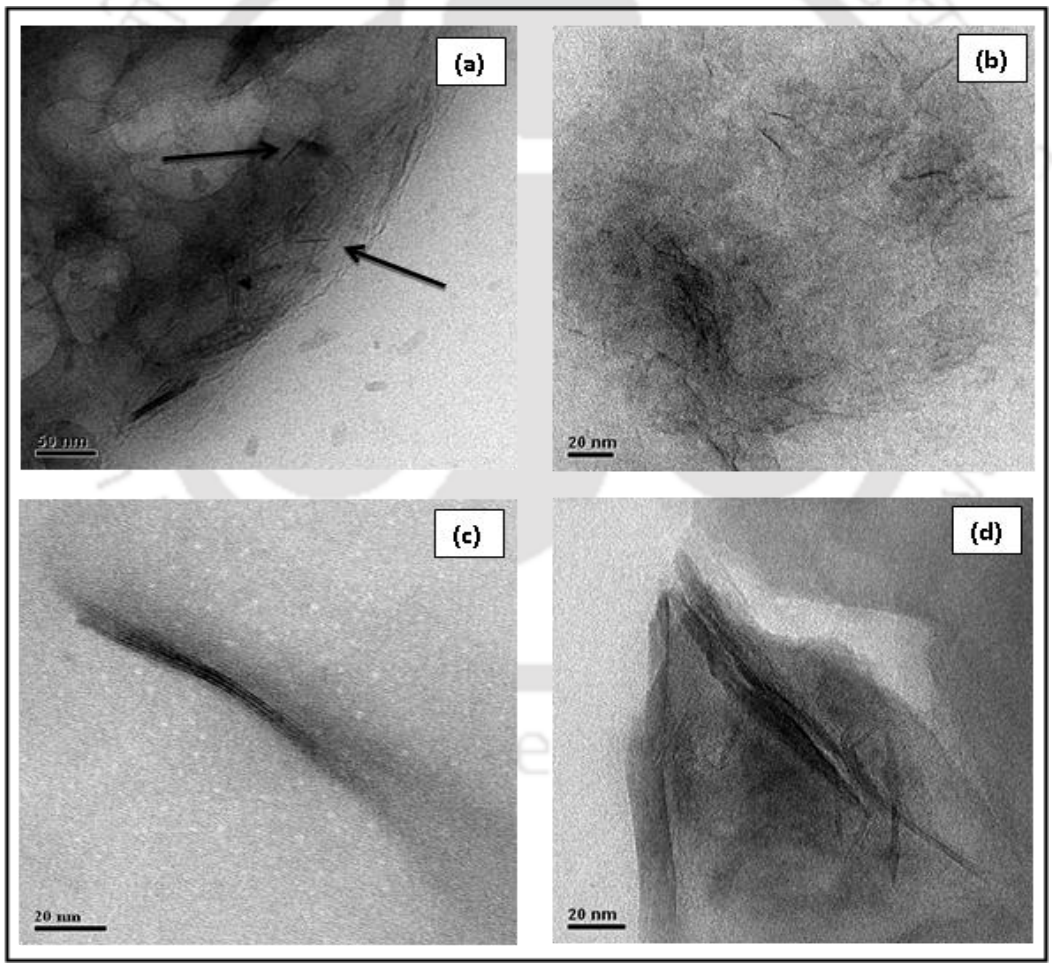

Figure 4.5 (i) TEM images of (a) PMMA/Co-Al 1%, (b) PMMA/Co-Al 3%, (c) PMMA/Co-Al 5% and (d) PMMA/Co-Al 7% nanocomposites

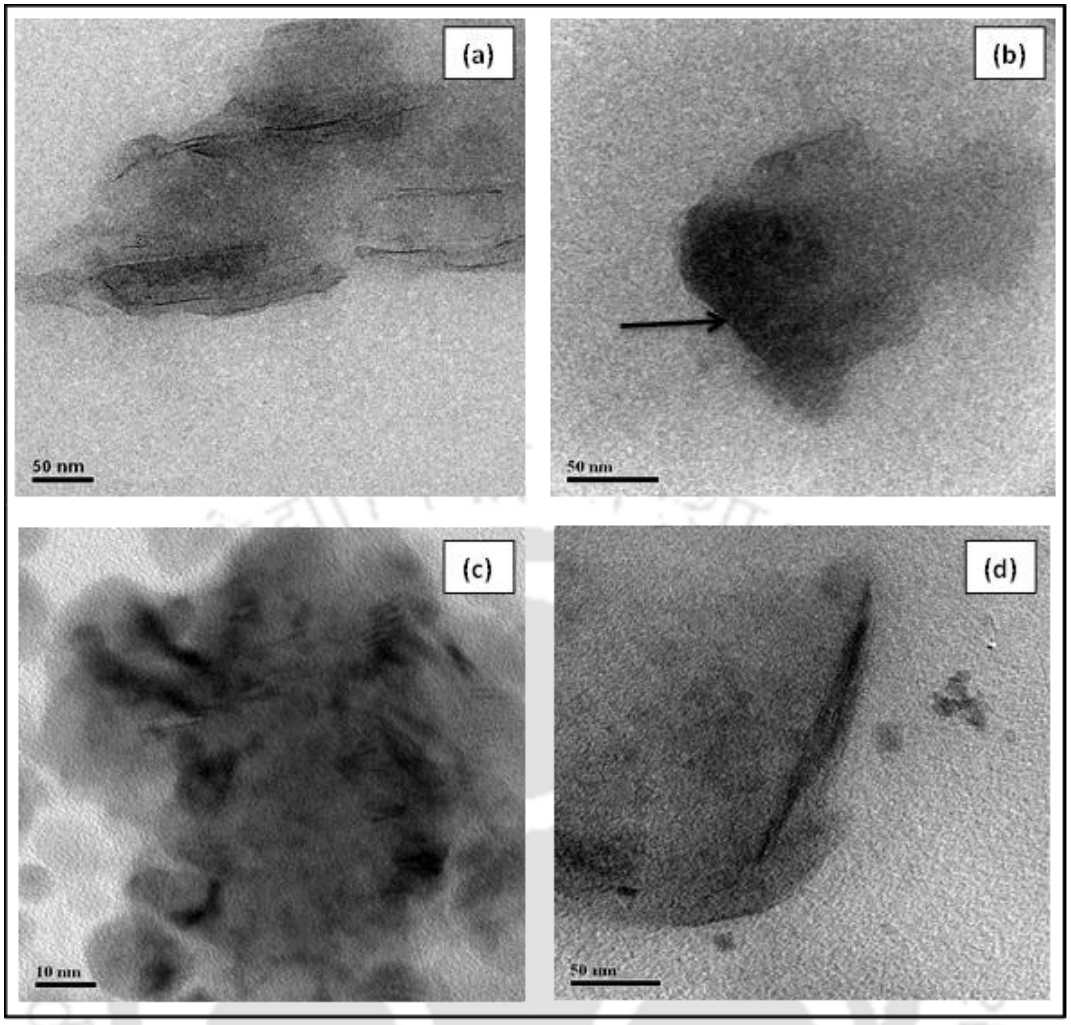

Figure 4.5 (ii) TEM images of (a) PMMA/Cu-Cr 1%, (b) PMMA/Cu-Cr 3%, (c) PMMA/Cu-Cr 5% and (d) PMMA/Ni-Al 5% nanocomposites

4.3.5 Tensile Properties

The tensile strength and modulus of neat PMMA and its nanocomposites with respect to Co-Al and Cu-Cr LDH content are shown in Figure 4.6. The tensile strength of both the nanocomposites is found to be higher at 1 wt.% loading of LDH when compared with neat PMMA. However, the PMMA/Co-Al LDH nanocomposites demonstrate higher tensile properties as compared to PMMA/Cu-Cr LDH nanocomposites. The PMMA/Co-Al 1% nanocomposite exhibits the highest tensile strength of 72 MPa as compared to PMMA/Co-Al 3% (64 MPa), PMMA/Co-Al 5% (58 MPa) and PMMA/Co-Al 7% (54 MPa) and neat PMMA (58 MPa). PMMA/Cu-Cr LDH nanocomposites also demonstrate a similar trend. It is also noticed that PMMA/Co-Al 7% sample exhibits lower tensile strength with respect to neat PMMA. This reduction is might be due to the uneven dispersion of Co-Al LDH in

polymer matrix. Therefore, in the case of Cu-Cr LDH based nanocomposites, the tensile properties is evaluated up to 5 wt.% loading and also compared with PMMA/Ni-Al 5% sample (see Figure 4.6). The enhanced property demonstrated by PMMA/Ni-Al 5% nanocomposite is due to strong bonding between Ni-Al LDH and polymer matrix. The gradual decline in the tensile strength values for further loadings explicates that addition as well as dispersion of LDH in the PMMA matrix are the dominant factors to enhance the mechanical properties. Therefore, it is clear that noticeable aggregation and the quality of dispersion become poor at higher loading of LDH (>1%). Therefore, a slight reduction in tensile strength is observed for PMMA nanocomposites. The enhanced strength for PMMA/Co-Al 1% and PMMA/Cu-Cr 1% samples is an indication of good adhesion between the PMMA and the nanofiller. Fu and Naguib, (2006) also found that maximum strength was obtained at 0.5 wt.% loading of clay for PMMA nanocomposites.

Figure 4.6 represents the tensile modulus of neat PMMA and its nanocomposites. The incorporation of nanofiller directly alters the reinforcement of polymer nanocomposites. It is clearly shown by the graph that there is a slight decrease in tensile modulus for both PMMA/Co-Al LDH and PMMA/Cu-Cr LDH nanocomposites. The tensile modulus is also directly related to the reinforcement of polymer nanocomposites. It is observed that intercalated morphology makes little contribution to the tensile modulus (Zhang et al., 2003). So there may be possibility that as the loading of nanofiller increases, more intercalated structures may occur, which reduces the tensile modulus of PMMA nanocomposites. Eng et al., (2013) also reported similar enhancement in tensile properties at 1 wt.% for PLA/PCL/clay nanocomposites.

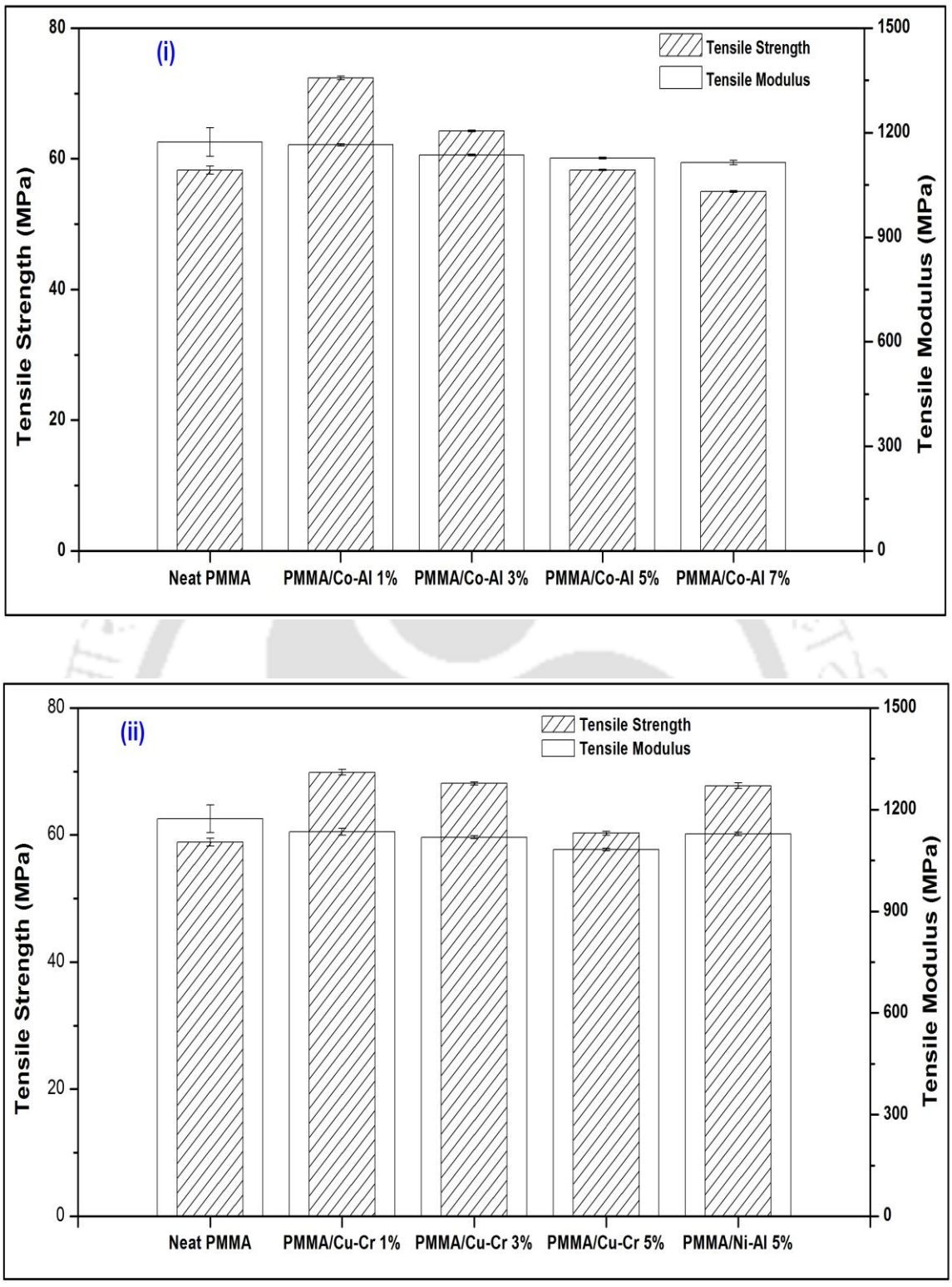

Figure 4.6 Tensile properties of (i) PMMA/Co-Al LDH and (ii) PMMA/Cu-Cr LDH nanocomposites

4.3.6 Flexural Properties

The influence of Co-Al LDH and Cu-Cr LDH on the flexural properties of PMMA nanocomposites is depicted in Figure 4.7. The neat PMMA exhibits flexural strength of 96 MPa. The different nanocomposites i.e. PMMA/Co-Al 1%, PMMA/Co-Al 3%, PMMA/Co-Al 5% and PMMA/Co-Al 7% nanocomposites have flexural strength of 120, 110, 101 and 99 MPa, respectively. Similarly, the PMMA/Cu-Cr 1%, PMMA/Cu-Cr 3%, PMMA/Cu-Cr 5%, PMMA/Ni-Al 5% nanocomposites show the flexural strength of 116, 113, 109 and 120 MPa, respectively. The flexural strength of both nanocomposites display a maximum value at 1 wt.% loading of LDHs when compared to other nanocomposites and neat PMMA. It is apparent that the flexural strength of the nanocomposites is higher than that of neat PMMA. This enhancement of flexural strength might be due to good adhesion between the LDH nanofiller and polymer matrix as PS-g-MA compatibilizer acts as a bridge between them. However, flexural strength reduces when the LDH concentration increases beyond 1 wt.%. Various factors including degree of intercalation/exfoliation, distribution and orientation of LDH platelets in the direction of flow also play a major role in ascertaining the flexural properties of the nanocomposites (Lim et al., 2006).

The flexural modulus of neat PMMA and different nanocomposites is illustrated in Figure 4.7. It is found that there is a marginal decrease in the flexural modulus as the loading of LDH increases in the PMMA nanocomposites. This result can be correlated with FESEM images of corresponding nanocomposites (see Figure 4.4). From the FESEM images, it is clear that at a higher loading, the nanofiller are pulled out from the matrix surface and leaving behind a large cavity. This suggests that aggregation of LDH particles takes place in polymer matrix; as a result flexural modulus reduces. However, the PMMA/Ni-Al 5% sample exhibits an enhanced modulus over PMMA/Cu-Cr 5% nanocomposites due to the strong interaction between matrix and nanofiller. More research is needed in this region as no literature has found for the reduction on modulus.

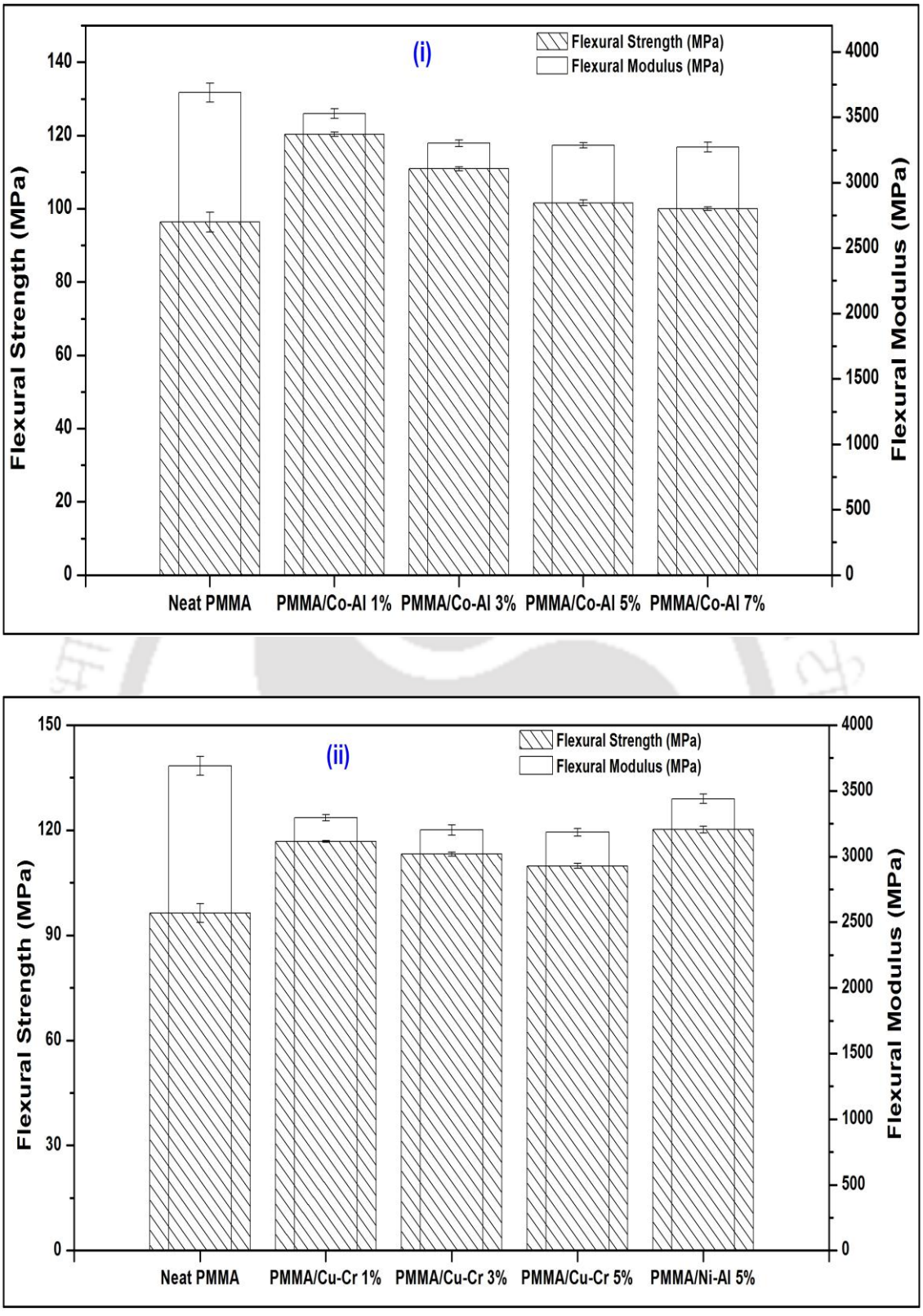

Figure 4.7 Flexural properties of (i) PMMA/Co-Al LDH and (ii) PMMA/Cu-Cr LDH nanocomposites

4.3.7 Impact Strength

The impact strength of neat PMMA and various nanocomposites is displayed in Figure 4.8. The PMMA/Co-Al LDH nanocomposites demonstrate higher impact strength over Cu-Cr LDH based nanocomposites. It is clearly seen from the graph that PMMA/Co-Al 1% nanocomposite shows the highest impact strength (62 J/m) over neat PMMA (56 J/m) and other compositions. It is also noticed that there is a linear decrease in impact strength with an increase of nanofiller loading (1-7 wt.%). The reduction in impact strength is probably due to agglomeration of LDH particles in the PMMA matrix, which results in less absorption in impact energy. It is known that impact energy of nanofiller is less than the impact strength of thermoplastic amorphous polymers. The restricted mobility of the nanoparticles in the nanocomposites can initiate crack formation and ultimately lead to brittle behaviour (Unnikrishnan et al., 2011). Additionally, LDH particles cause immobilization of macromolecular chains, as a result of which, their ability to deform freely is limited rendering the material less ductile. However, the impact strength of PMMA/Co-Al 1% nanocomposite is found to be higher among all the other compositions. This is attributed to the fact that exfoliated layers of Co-Al LDH are homogenously distributed at lower loading in the PMMA matrix. It is also noticed that Ni-Al layers are more effectively dispersed in PMMA/Ni-Al 5% sample and therefore it exhibits higher impact strength as compared to PMMA/Co-Al 5% and PMMA/Cu-Cr 5% nanocomposites.

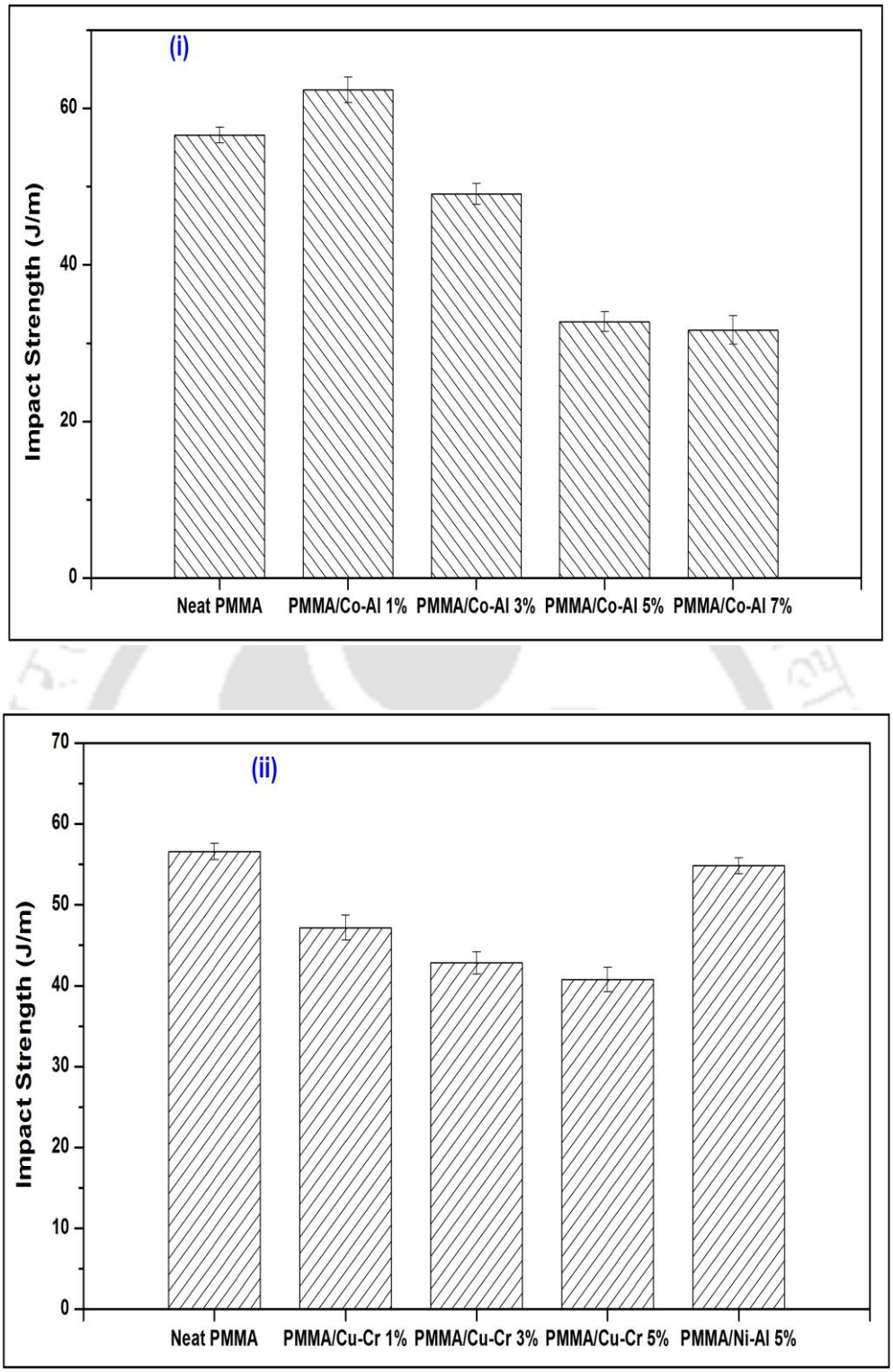

Figure 4.8 Impact strength of (i) PMMA/Co-Al LDH and (ii) PMMA/Cu-Cr LDH nanocomposites

4.3.8 Hardness

Figure 4.9 represents Shore D hardness (ASTM D2240) of neat PMMA, PMMA/Co-Al LDH and PMMA/Cu-Cr LDH nanocomposites. The hardness of PMMA nanocomposites increases with increasing LDH loading in the PMMA matrix. The average value of Shore D hardness is observed to be 58, 75.2, 80.8, 84.6, 87.8 for neat PMMA, PMMA/Co-Al 1%, PMMA/Co-Al 3%, PMMA/Co-Al 5%, and PMMA/Co-Al 7% nanocomposites, respectively. Similarly, the PMMA/Cu-Cr 1%, PMMA/Cu-Cr 3%, PMMA/Cu-Cr 5% and PMMA/Ni-Al 5% exhibit the hardness of 81, 84, 88 and 85, respectively. The hardness of the sample was taken from eight different region of each sample and average value was reported. All the nanocomposites exhibit enhanced hardness over neat PMMA. The increase in the hardness is due to presence of LDH layers in the polymer matrix. The LDH layers adequately restrict indentation and thus enhance the hardness of the nanocomposites. The PMMA/Co-Al 7% nanocomposite demonstrates a maximum improvement of Shore D hardness of 51% over neat PMMA.

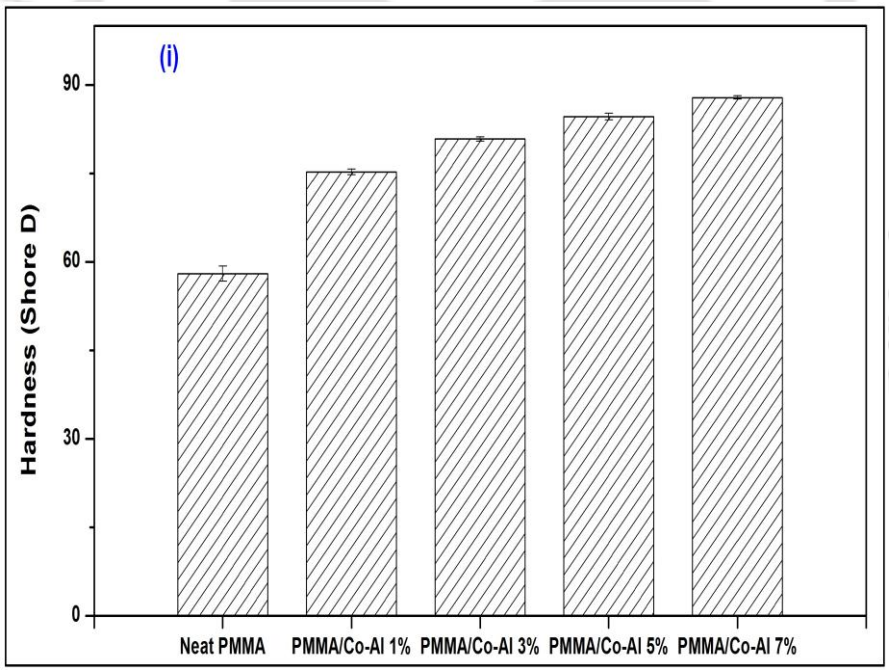

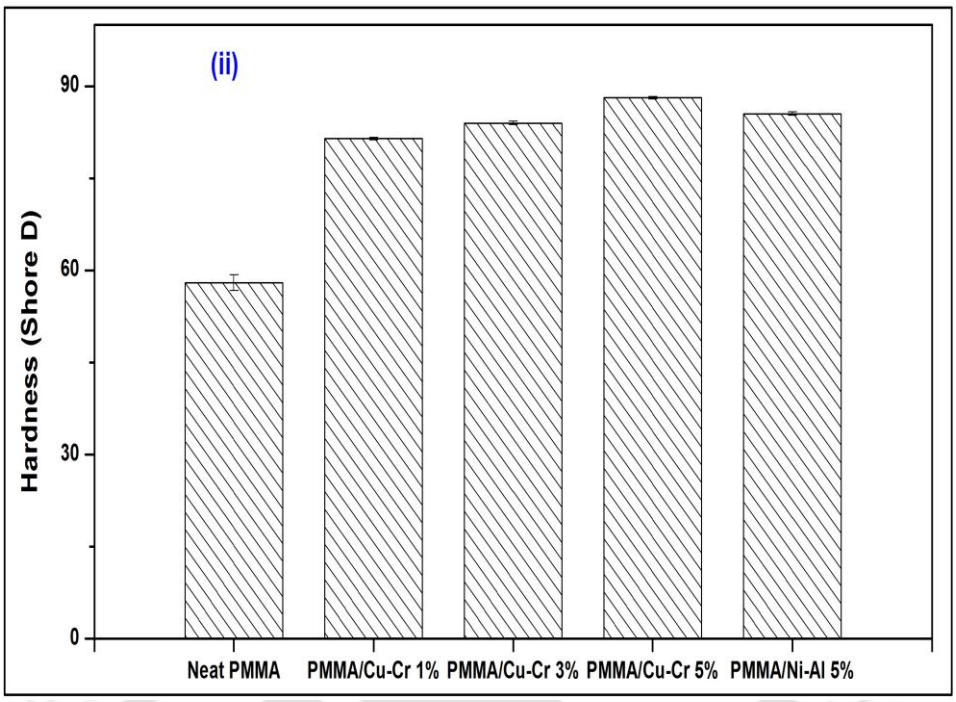

Figure 4.9 Hardness of (i) PMMA/Co-Al LDH and (ii) PMMA/Cu-Cr LDH nanocomposites

4.3.9 Differential Scanning Calorimetry

DSC is most commonly used to evaluate transition temperature such as glass transition temperature, melting and crystallization temperature. However, it only measures the total heat flow and the sum of all thermal transition in the sample and the rate of crystallization temperature, in addition to the associated enthalpy for each process. The DSC study of neat PMMA and its different nanocomposites has been carried out in order to examine the mobility of PMMA chains in terms of its T_g in the LDH layers and the results are enumerated in Figure 4.10. The glass transition temperature (T_g) is recorded at the inflection point between the outset and the end-set temperatures. DSC thermograms display the second order transition, which is related to the T_g of the neat PMMA matrix at 109.3 ^oC.

The T_g of PMMA/Co-Al 1%, PMMA/Co-Al 3%, PMMA/Co-Al 5%, PMMA/Co-Al 7% nanocomposites is found to be 114.6, 114.7, 114.8 and 114.6 ^oC, respectively (see Figure 4.10(i)). This demonstrates that nanocomposites exhibit around 5 ^oC higher glass temperature as compare to neat PMMA. Similarly, the PMMA/Cu-Cr LDH nanocomposites display the T_g enhancement of 2-3 ^oC over PMMA, while PMMA/Ni-Al 5 exhibits a marginal increment

in T_g over neat PMMA (see Figure 4.10(ii)). It is also noticed that higher loading of nanofiller does not have substantial influence on the mobility of PMMA chains. A possible explanation for the increase in T_g of the polymer nanocomposites might be due to confinement of PMMA chains within the LDH layers that prevents the segmental motion of the polymer chains (Gao et al., 2001). The intercalation could limit the mobility of the molecules that extend into the bulk region outside the LDH. Even if a chain is only constrained at one end because of intercalation, the immobility may still result in an increase in T_g of external chains. A further possibility is that intercalation leads to a reduction in the polymeric free volume because the chain ends become located in LDH galleries and this would lead to increase in T_g (Shen et al., 2004). In the work of Kuila et al., (2011), around 2 ^oC enhancement in T_g was observed for PMMA/graphene nanocomposites with 0.1 wt.% graphene loading. The PMMA/Co-Al LDH nanocomposites show improvement of 4 ^oC over PMMA/ZnS nanocomposites at 1 wt.% loading (Wang et al., 2014).

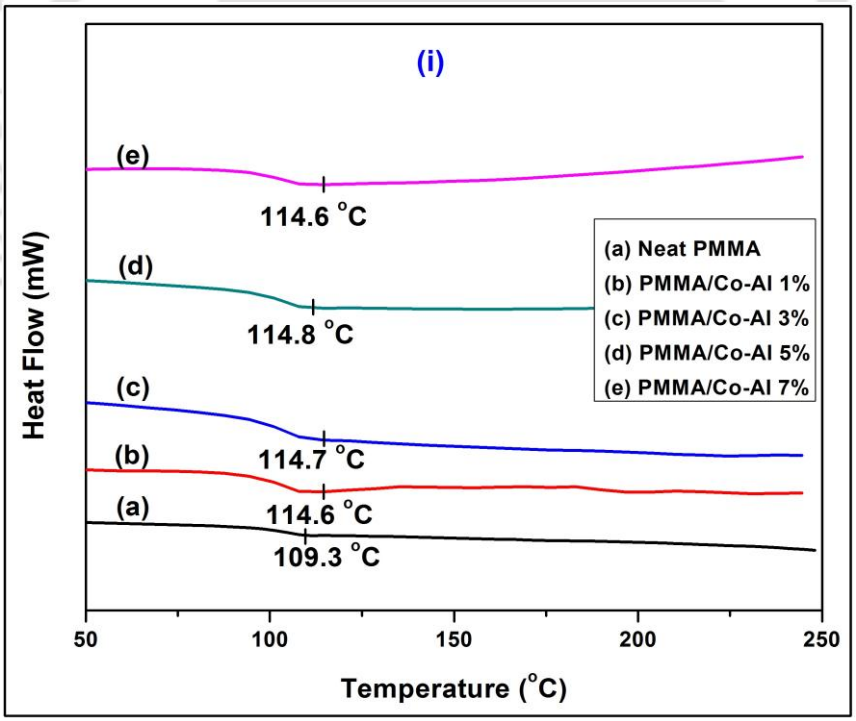

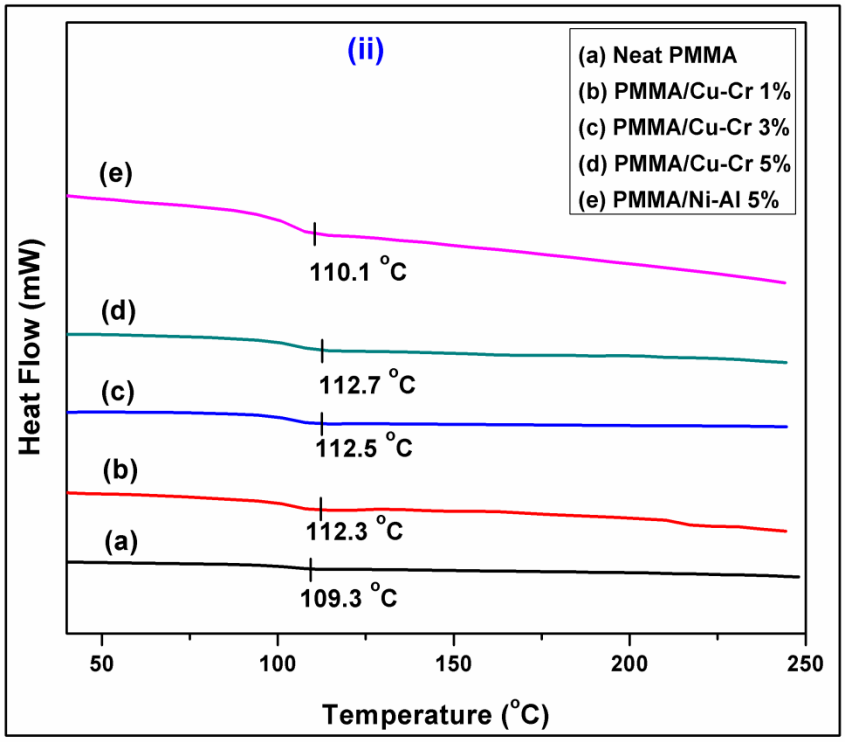

Figure 4.10 DSC curves of (i) PMMA/Co-Al LDH and (ii) PMMA/Cu-Cr LDH nanocomposites

4.3.10 Thermogravimetric Analysis

TGA analysis is generally carried out to assimilate the effect of LDH content on the thermal stability of the polymer. The dispersion of clay is known to modify the thermal stability of polymers. Figure 4.11(i) shows the TGA curves for neat PMMA and PMMA/Co-Al LDH nanocomposites. The parameters that are important from TGA curves are the onset of degradation, which is usually taken as the temperature at which 10% degradation occurs, $T_{10\%}$ and the midpoint temperature of degradation, $T_{50\%}$. From the TGA curves, it is observed that thermal stability of the PMMA/Co-Al LDH nanocomposites increase, which is confirmed by shifting of the TGA curve of PMMA/LDH nanocomposites towards right of the TGA curve of the neat PMMA. When 10% weight loss is selected as a point of comparison, the decomposition temperature of neat PMMA, PMMA/Co-Al 1%, PMMA/Co-Al 3%, PMMA/Co-Al 5%, PMMA/Co-Al 7% LDH nanocomposite is found to be 343.6, 375.5, 377.3, 375.7 and 369.5 ^{o}C respectively. The result suggests that the degradation of the nanocomposites takes place at higher temperatures than that of neat PMMA (26-34 ^{o}C) higher than that of neat PMMA) in the presence of Co-Al LDH. When 50% weight loss is

considered as a point of reference, the decomposition temperature of the nanocomposites is found to be 31-35 ^{o}C higher than that of neat PMMA (see Table 4.2). The Cu-Cr based nanocomposites also display a higher thermal stability over neat PMMA (see Figure 4.11(ii)). The decomposition temperature of the PMMA/Cu-Cr LDH nanocomposites is found to be 26-32 ^{o}C higher than that of neat PMMA at $T_{50\%}$ as a reference point. This behaviour could be explained by the presence of barrier effect of LDH lamellar layers, which limits the emission of the produced degradation gases and transmission of heat. Therefore, it results in the improvement of the thermal stability of the nanocomposite material. It is noticed that at higher loading (>5%) the nanocomposite exhibits lower thermal stability. The most probable reason is that the relatively large amount of organic surfactant present in the nanocomposites produced less stable charred layers during the decomposition (Chen and Qu, 2005; Krishna and Pugazhenthi, 2011). Similar kind of behavior was also observed by Qiu et al., (2005) for polystyrene/Zn-Al LDH nanocomposites. The research findings suggest that the PMMA/Co-Al LDH nanocomposites exhibit better thermal stability than that of neat PMMA. The increase in the onset temperature signifies delayed degradation of PMMA nanocomposites. Laachachi et al., (2009) reported that PMMA/AlOOH 5% sample showed around 19 ^{o}C higher thermal stability over neat PMMA, which was lower than the PMMA/Co-Al LDH and PMMA/Cu-Cr LDH nanocomposites at the same loading.

The temperature which corresponds to the maximum degradation (T_{max}) is considered as another significant thermal property for the polymer nanocomposites. The T_{max} is defined as the peak value that is obtained from the first derivative curve of TGA thermograph. The TGA derivative of neat PMMA and its nanocomposites is illustrated in Figure 4.11. The peak indicates that the maximum degradation temperature (T_{max}) of different nanocomposites is shifted towards right side of neat PMMA, demonstrating enhanced thermal stability of the nanocomposites. The improved thermal stability is attributed to the 'tortuous path' effect of LDH layers, which deferments the diffusion pathway of the degradation by-products and hinders the diffusion of the volatile decomposition products. Table 4.2 summarizes the TGA results of nanocomposites.

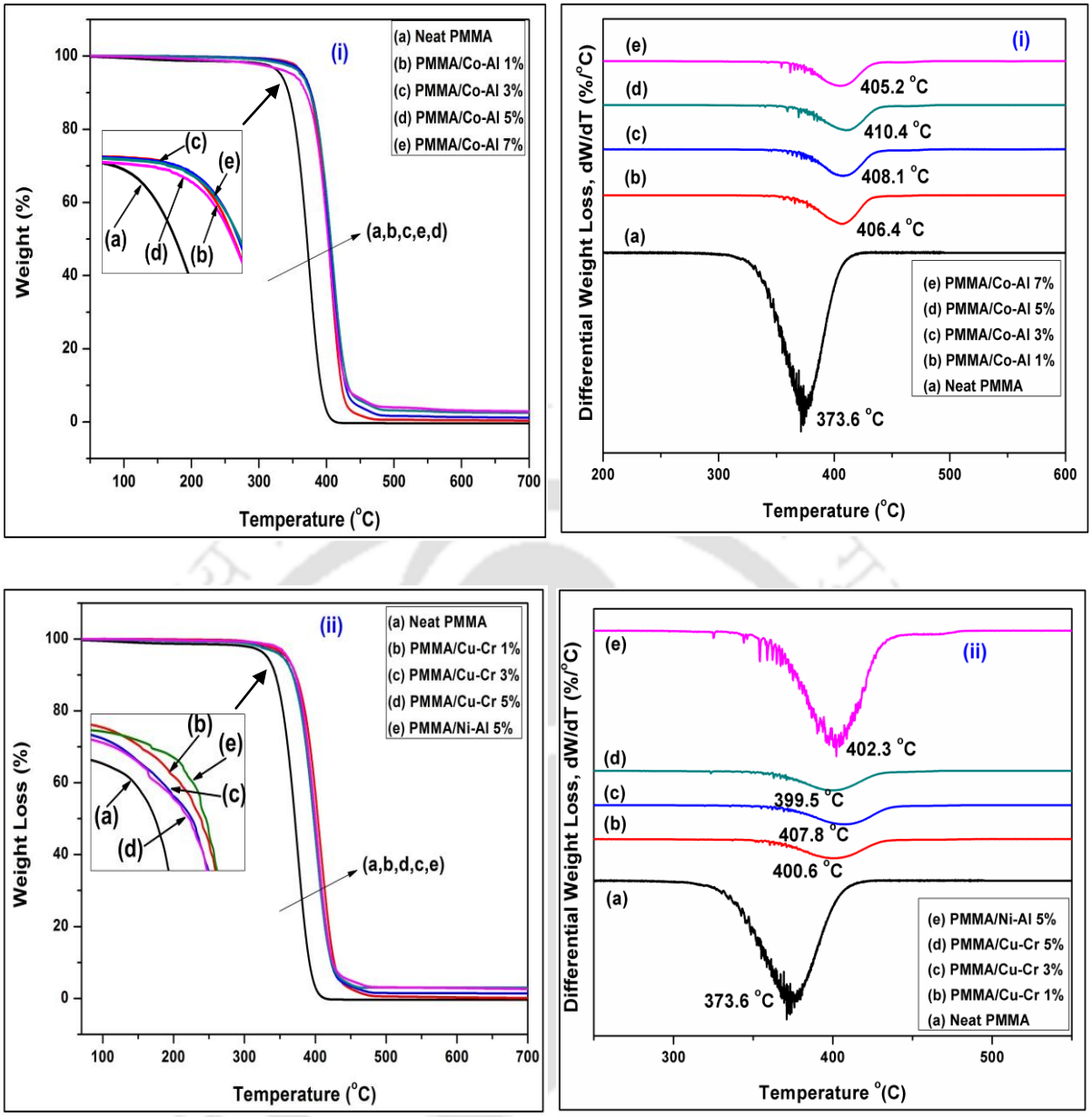

Figure 4.11 TGA and DTG curves of (i) PMMA/Co-Al LDH and (ii) PMMA/Cu-Cr LDH nanocomposites

Table 4.2 TGA results for neat PMMA and PMMA/LDH nanocomposites

Sample	Temperature ($T_{10\%}$) at 10% weight loss (^oC)	Temperature ($T_{50\%}$) at 50% weight loss (^oC)
Neat PMMA	343.6	371.1
PMMA/Co-Al 1%	375.5	402.3
PMMA/Co-Al 3%	377.7	405.0
PMMA/Co-Al 5%	375.7	406.3
PMMA/Co-Al 7%	369.5	402.4
PMMA/Cu-Cr 1%	368.3	397.9
PMMA/Cu-Cr 3%	372.6	403.6
PMMA/Cu-Cr 5%	367.7	397.6
PMMA/Ni-Al 5%	372.0	399.9

4.3.11 Kinetic Analysis

The Coats-Redfern method can deal with the main degradation region of TGA curve of sample and requires the TGA data at just one heating rate to calculate the related reaction order (n), reaction activation energy (E_a) and pre-exponential factor (A). In this work, the TGA data of PMMA/Co-Al LDH samples with 1, 3, 5 and 7 wt.% LDH at heating rate of 10 ^oC/min were processed to evaluate the kinetic parameters. Similar procedure was also repeated for PMMA/Cu-Cr LDH nanocomposites. For this, a reaction order (n) value was assumed and then substituted the assumed n value into equation (3.10) [discussed in chapter 3, section 3.2.4]. The plot of the left part of equation against -1/T was fitted to determine the correlation coefficient R. Above procedure was repeated till the best R value was obtained. The calculated reaction order at the best R value is just required one. Subsequently, the activation energy and the pre-exponential factor can be calculated from the slope and intercept of the fitted straight line, respectively (see Figures 4.12 and 4.13). The activation energy (E_a) for neat PMMA and PMMA/Co-Al LDH nanocomposites containing 1, 3, 5 and 7% of LDH is found to be 99.2, 256.1, 253.6, 224.7 and 227.4 kJ/mol, respectively. Similarly the E_a values of PMMA/Cu-Cr 1%, PMMA/Cu-Cr 3%, PMMA/Cu-Cr 5%, PMMA/Ni-Al 5%

nanocomposites are 222.0, 230.7, 225.2 and 245.2 kJ/mol, respectively. It can be observed from the Table 4.3 that the E_a of PMMA/Co-Al LDH nanocomposites is 124-156 kJ/mol higher than that of neat PMMA. Table 4.3 also clearly indicates that the higher loading of LDH can make the nanocomposites to decrease the E_a value because relatively large quantity of organic modifier present in the nanocomposites produces less stable charred layers during the decomposition. The obtained results are in good agreement with TGA data. Krishna and Pugazhenthi, (2011) also reported similar kind of results for PS/organoclay nanocomposites prepared by solvent blending method.

Table 4.3 Kinetic parameters of different samples at the better correlation coefficient obtained from Coats-Redfern method

Sample	E_a(kJ/mol)	A	n	R
Neat PMMA	99.2	24.63×10^{6}	0.6	0.997
PMMA/Co-Al 1%	256.1	3.304×10^{19}	1.2	0.999
PMMA/Co-Al 3%	224.1	1.800×10^{19}	1.3	0.999
PMMA/Co-Al 5%	227.4	8.550×10^{16}	0.2	0.999
PMMA/Co-Al 7%	224.7	1.984×10^{17}	1.5	0.995
PMMA/Cu-Cr 1%	222.0	6.021×10^{14}	1.2	0.999
PMMA/Cu-Cr 3%	230.7	4.478×10^{16}	1.3	0.999
PMMA/Cu-Cr 5%	225.2	1.650×10^{15}	1.2	0.999
PMMA/Ni-Al 5%	245.2	5.724×10^{16}	1.3	0.999

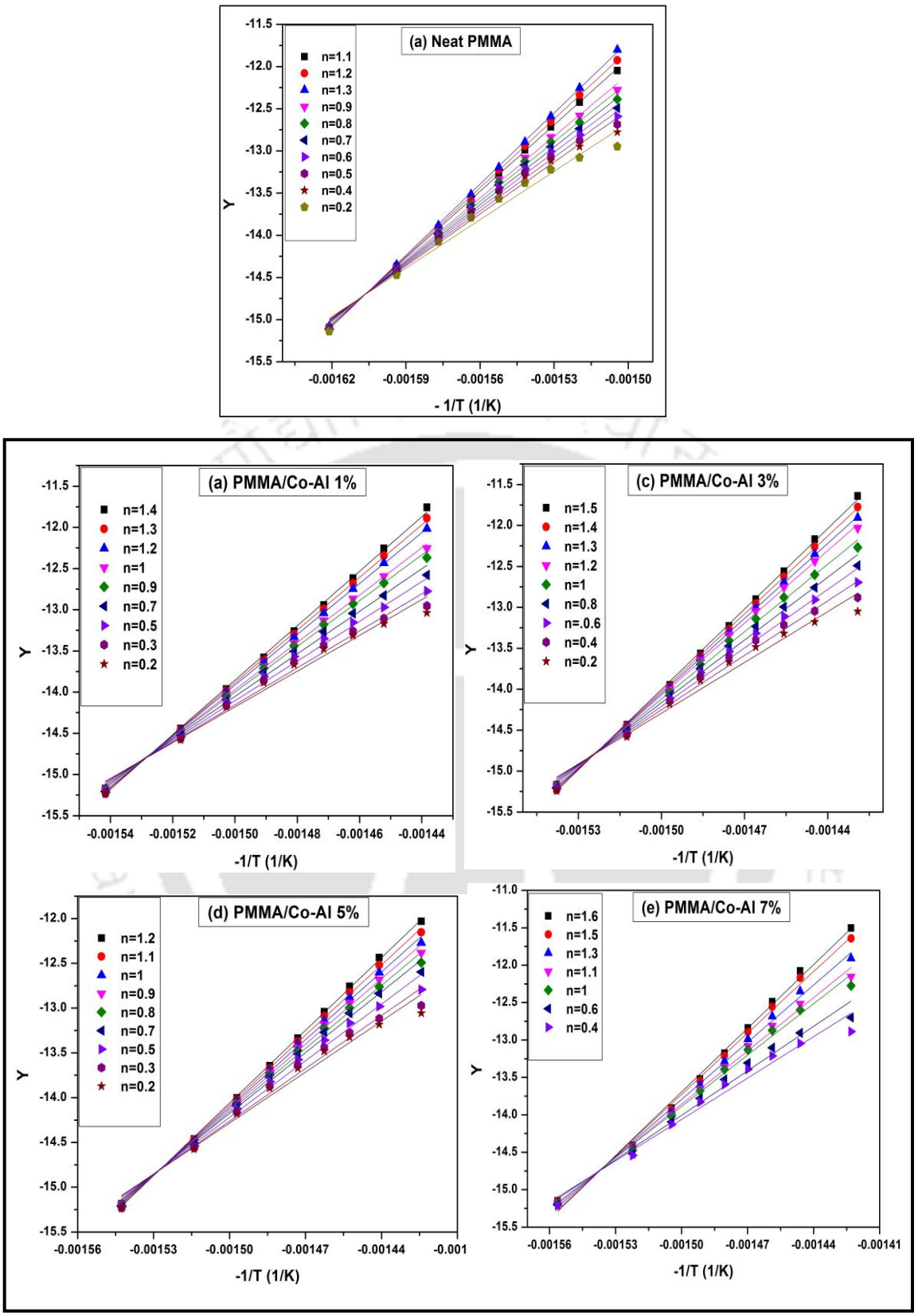

Figure 4.12 Determination of kinetic parameters by plots of the left part in equation 3.10 against -1/T using Coats-Redfern methods: (a) Neat PMMA, (b) PMMA/Co-Al 1%, (c) PMMA/Co-Al 3%, (d) PMMA/Co-Al 5% and (e) PMMA/Co-Al 7% nanocomposites

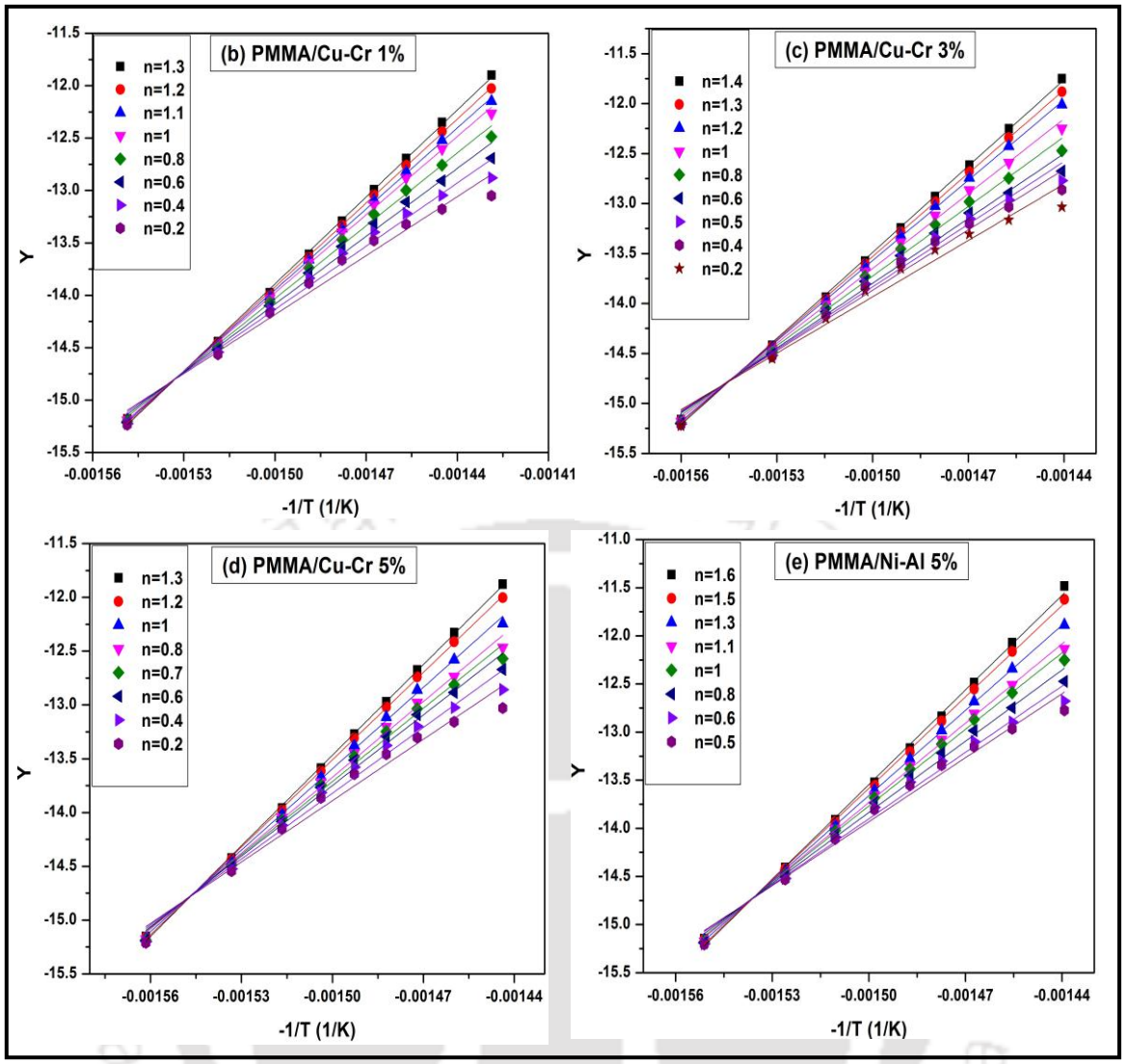

Figure 4.13 Determination of kinetic parameters by plots of the left part in equation 3.10 against -1/T using Coats-Redfern methods: (b) PMMA/Cu-Cr 1%, (c) PMMA/Cu-Cr 3%, (d) PMMA/Cu-Cr 5% and (e) PMMA/Ni-Al 5% nanocomposites

The kinetic parameters obtained from Coats-Redfern method were utilized to estimate the different reaction mechanism in Criado method. Figure 4.14 (i) displays the Z(α)-α master and experimental curve of neat PMMA and PMMA nanocomposites having Co-Al LDH with 1, 3, 5 and 7 wt.% concentration. The same has considered for PMMA/Cu-Cr LDH nanocomposites (see Figure 4.14 (ii)). It is observed that for neat PMMA, experimental Z(α)-α curve initially follows A2 reaction mechanism (Nucleation and growth) with lower α value (α=0.1-0.2) then it deviates from A2 reaction mechanism to F1 mechanism at medium α value (α=0.3-0.5) and then again deviates from F1 to A4 mechanism for higher α value (α=0.7-0.9). In case of PMMA/Co-Al LDH and PMM/Cu-Cr LDH nanocomposites, Z(α)-α experimental curve initially follows the F1 reaction mechanism. However, with the evolution

of thermal decomposition reaction, the involved system gradually transits toward A4 mechanism (nucleation and growth).

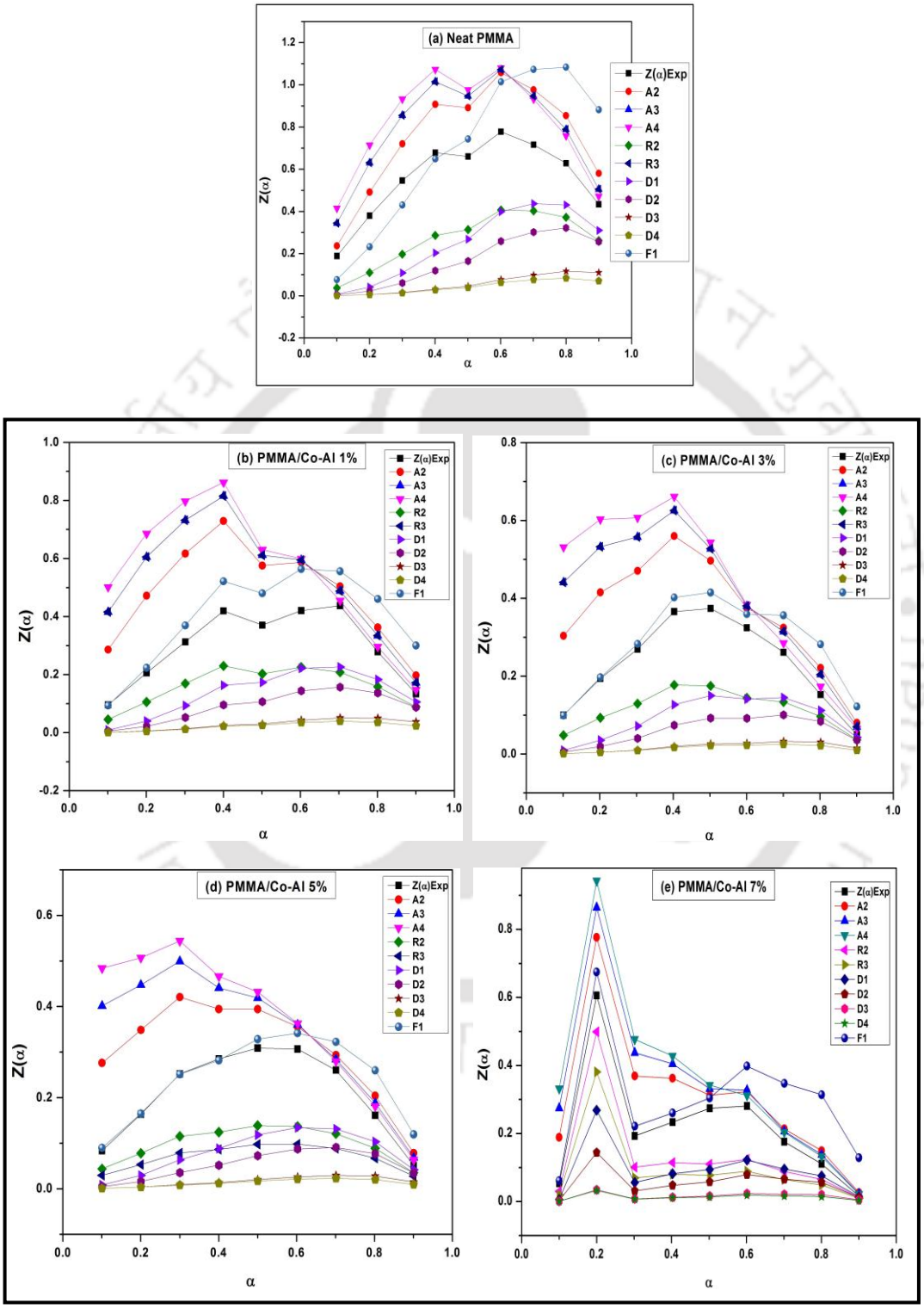

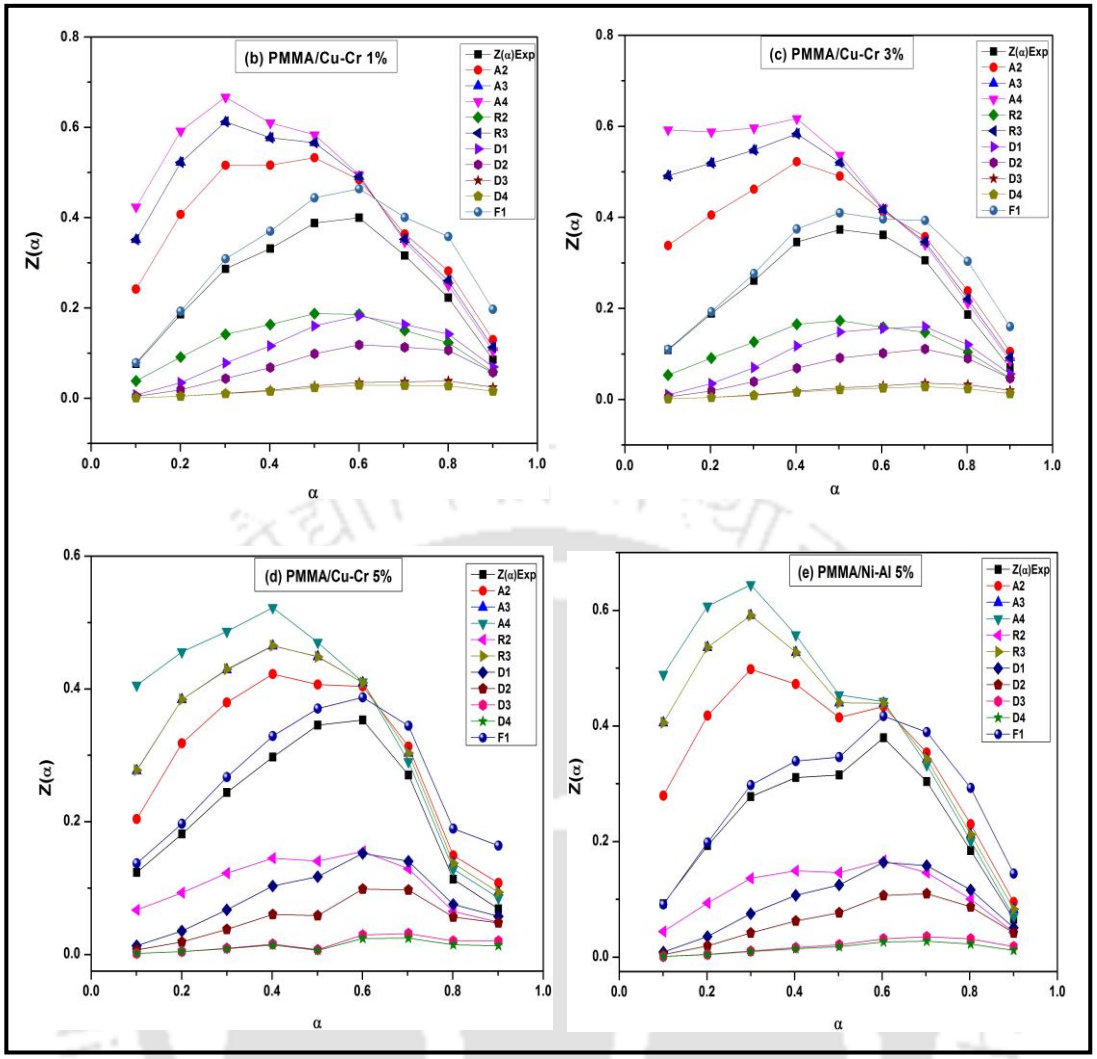

Figure 4.14 Determination of the thermal degradation mechanism by plotting Z(α) versus α using Criado model (i) PMMA/Co-Al LDH nanocomposites and (ii) PMMA/Cu-Cr LDH nanocomposites

The integral procedure decomposition temperature (IPDT) method was employed for the estimation of thermal stability of the nanocomposites as follows:

$$IPDT\ (^{\circ}C) = A \times K \times (T_f - T_i) + T_i \qquad (4.1)$$

Where, $A = (S_1+S_2)/(S_1+S_2+S_3)$

$K = (S_1+S_2)/(S_1)$

Where, A is the area ratio of total experimental curve specified by the total TGA thermogram, T_i is the initial experimental temperature (^{o}C), T_f is the final experimental temperature (^{o}C). A graphical representation of a typical TGA thermogram divided into three areas of S_1, S_2, and S_3 is depicted in Figure 4.15.

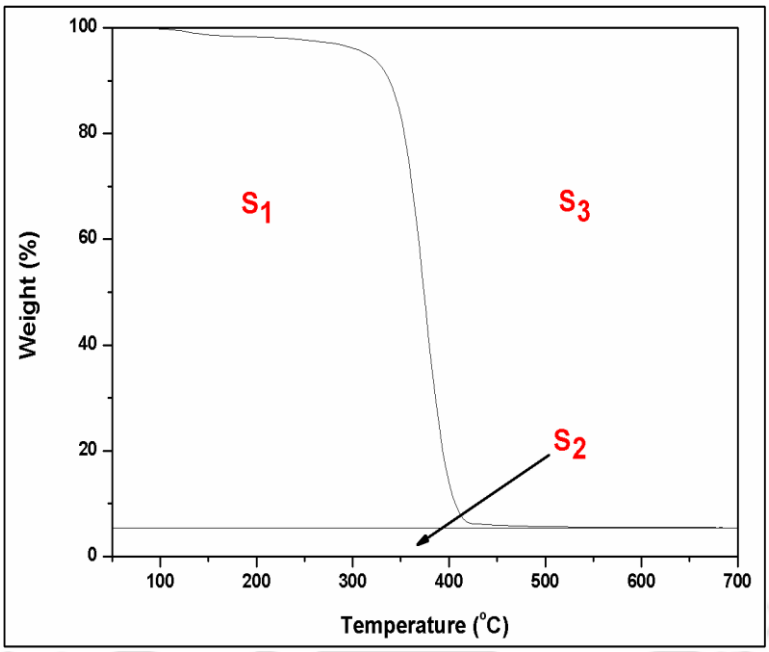

Figure 4.15 Schematic diagram for determining IPDT

Table 4.4 IPDT results of different PMMA nanocomposite samples

Samples	Initial Temperature (T_i) ^oC	Final Temperature (T_f) ^oC	IPDT (^oC)
Neat PMMA	50	700	385.4
PMMA/Co-Al 1%	50	700	404.5
PMMA/Co-Al 3%	50	700	418.2
PMMA/Co-Al 5%	50	700	432.2
PMMA/Co-Al 7%	50	700	428.9
PMMA/Cu-Cr 1%	50	700	394.8
PMMA/Cu-Cr 3%	50	700	435.3
PMMA/Cu-Cr 5%	50	700	407.5
PMMA/Ni-Al 5%	50	700	428.5

IPDT values of all the samples are calculated using the equation (4.1) at a constant heating rate of 10 ^oC/min. All the nanocomposites exhibit higher IPDT value as compared to the neat PMMA, which indicates the enhanced thermal stability of the nanocomposites. The IPDT values of neat PMMA and PMMA nanocomposites with 1, 3, 5 and 7 wt.% Co-Al LDH

loading are 385.4, 404.5, 418.2, 432.2 and 428.9 ^{o}C (see, Table 4.4). The PMMA/Cu-Cr LDH nanocomposites exhibit 394.8, 435.3 and 407.5 ^{o}C for various compositions (1-5 wt.% of LDH loading). However, for Ni-Al LDH based nanocomposites, the IPDT value is 428.5 ^{o}C. The IPDT value of PMMA/Co-Al LDH nanocomposite with 5 wt% loading is highest among their respective samples, which is also reflected in the TGA analysis. IPDT results are also consistent with activation energy calculation.

4.3.12 Dynamic Mechanical Analysis

To analyze the influence of Co-Al LDH and Cu-Cr LDH on the mechanical behaviour of PMMA, DMA test was performed. The temperature dependence of storage modulus and loss factor (tan δ) for PMMA nanocomposites containing different loading of Co-Al LDH and Cu-Cr LDH nanofiller is shown in Figure 4.16(i) and 4.16(ii), respectively. It is clearly observed from the figure that the storage modulus (E') increases from ~ 254 MPa for neat PMMA to ~ 348 MPa for PMMA nanocomposites having 7 wt.% Co-Al LDH at 40 ^{o}C. Similarly, PMMA/Cu-Cr LDH nanocomposites also demonstrate a higher storage modulus at 40 ^{o}C. The increase of LDH content in the PMMA nanocomposite leads to higher values of storage modulus up to 90 ^{o}C, proving that the addition of LDH into the polymer matrix increases the rigidity of the nanocomposites. This effect is more pronounced for the nanocomposites containing higher loadings of the nanofiller. As the temperature increases, a sharp decrease in the E' value is observed in the temperature from 70 to 105 ^{o}C. This corresponds to the primary relaxation process (α) of the PMMA, where tan δ goes through a maximum. Then the modulus reaches a linear region, corresponding to the rubbery state of the polymer. Similar to the neat PMMA, both the nanocomposites i.e. PMMA/Co-Al LDH and PMMA/Cu-Cr LDH nanocomposites exhibit a drastic drop in the E' value.

The tan δ (loss factor) versus temperature curves for neat PMMA and PMMA nanocomposites containing various weight percent of different LDH are also represented in Figure 4.16. A stiffening of the structure of different PMMA nanocomposites as compared to neat PMMA is also reflected by a slight shift of tan δ peak connected with the α relaxation process, which involves energy dissipation and cooperative chain motions (Lu and Larock, 2006). Generally, strong interactions between the LDH layers and the PMMA matrix can restrict the movement of polymer segments near to the filler surface, thus resulting in an enhancement of T_g of the matrix. It is clearly seen from the graph that tan δ curve of nanocomposites has broadened and shifted to higher temperature. As a result, PMMA/Co-Al

LDH and PMMA/Cu-Cr LDH nanocomposites exhibit higher T_g over neat PMMA. **Logakis et al., (2011)** also found similar results for PMMA/CNT composites.

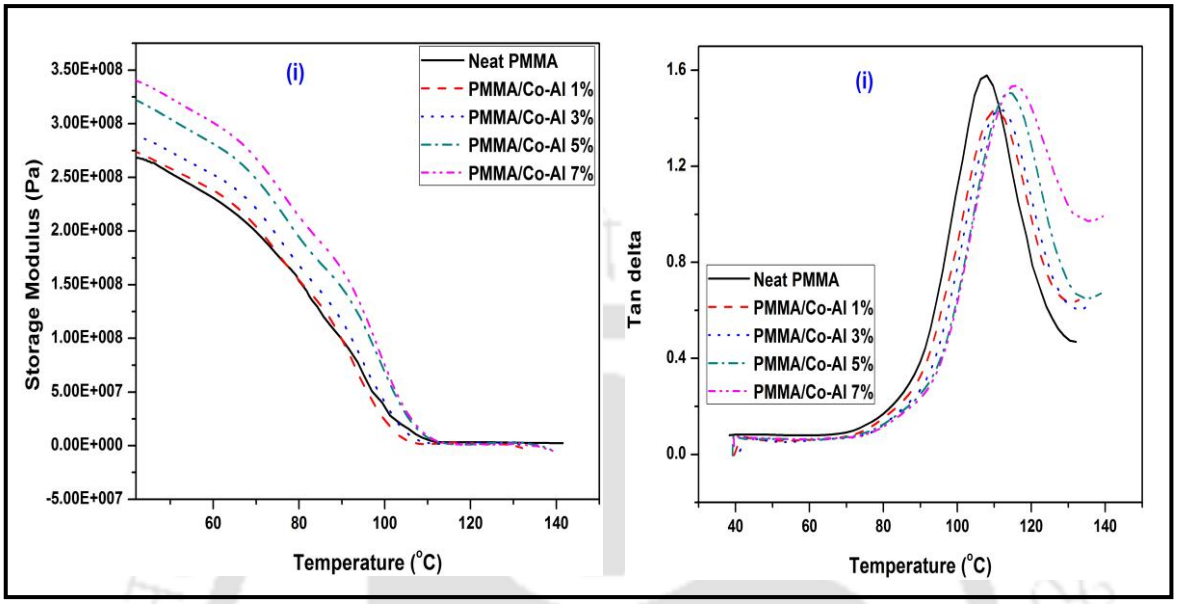

Figure 4.16(i) Storage modulus and loss factor curves of PMMA/Co-Al LDH nanocomposites

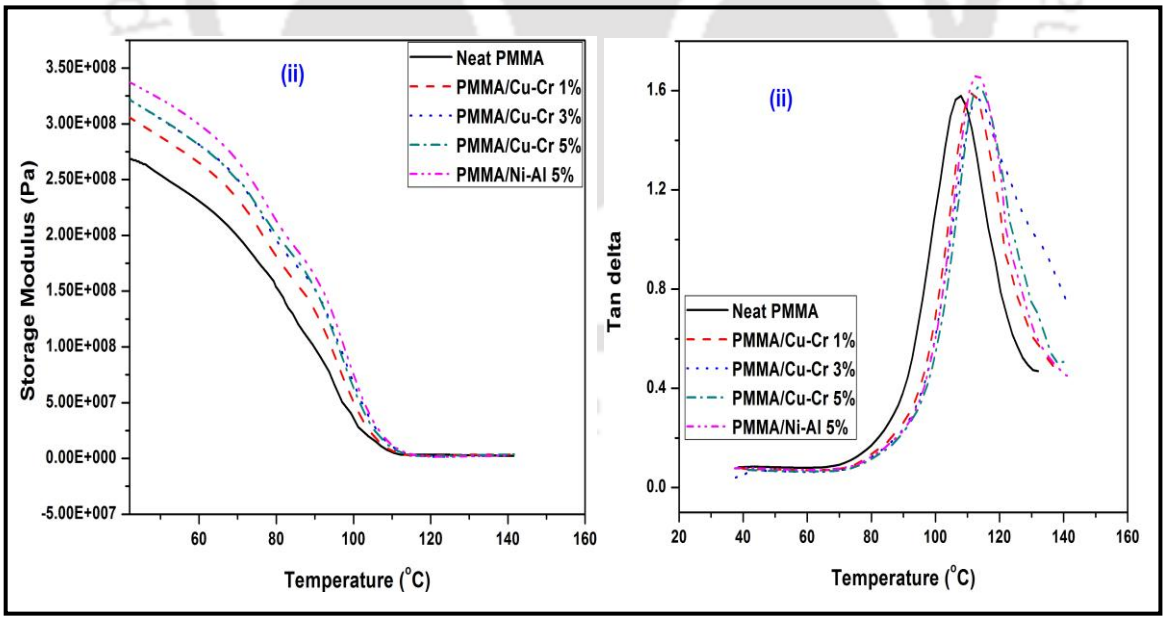

Figure 4.16(ii) Storage modulus and loss factor curves of PMMA/Cu-Cr LDH nanocomposites

4.3.13 AFM Analysis

Atomic force microscopy (AFM) has been used for surface characterization i.e. imaging topography and phase morphology of polymer nanocomposites. The AFM images of PMMA/Co-Al LDH and PMMA/Cu-Cr LDH nanocomposites are depicted in Figure 4.17. From the AFM images, it is clearly seen that LDH loading has pronounced influence on the roughness of the polymer nanocomposites. It is also observed that pits are also present on the surfaces. The roughness of the PMMA nanocomposites increases with an increase in the LDH content in the polymer matrix. The minimum surface roughness is noticed at 1 wt.% LDH loading and maximum at 7 wt.% loading of LDH in PMMA/Co-Al LDH nanocomposites. The 2D images of different PMMA nanocomposites are given in appendix.

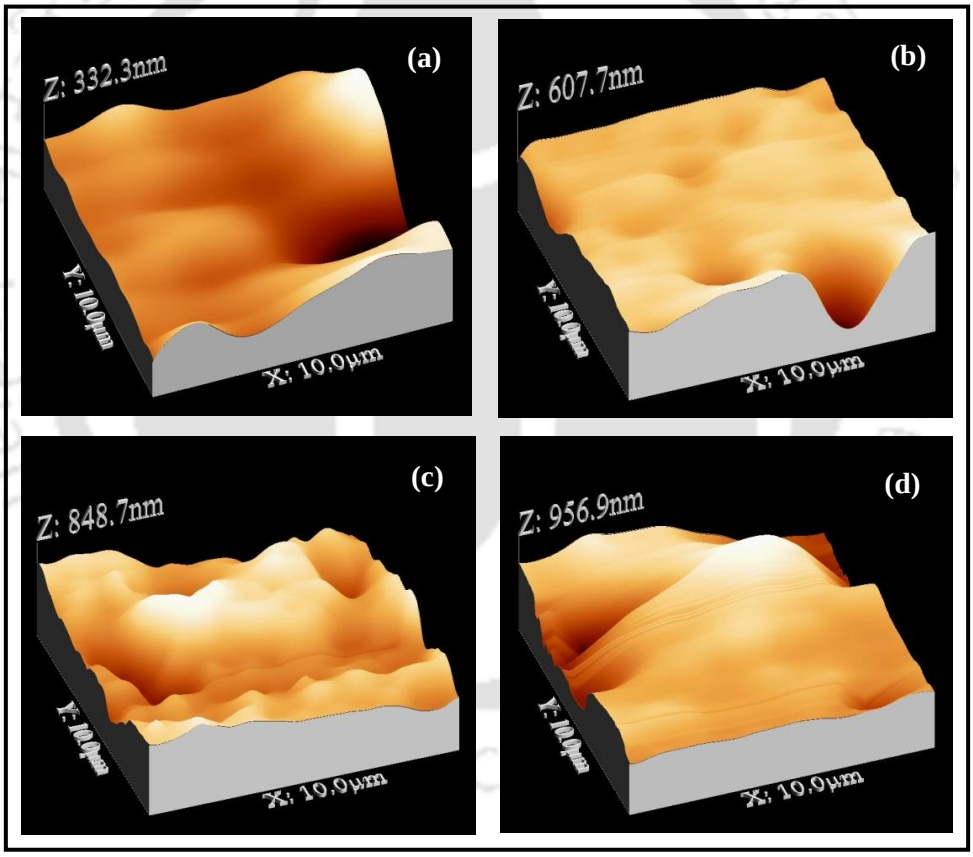

Figure 4.17 (i) AFM images of (a) PMMA/Co-Al 1%, (b) PMMA/Co-Al 3%, (a) PMMA/Co-Al 5% and (d) PMMA/Co-Al 7% nanocomposites

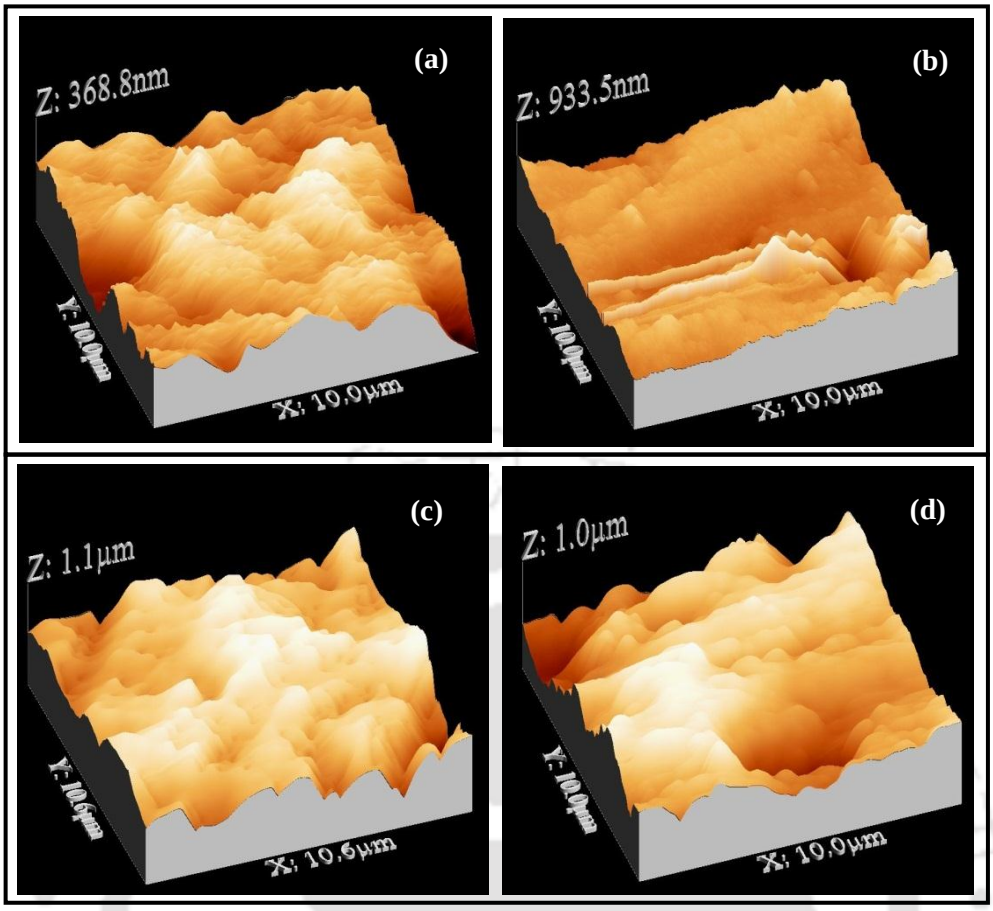

Figure 4.17 (ii) AFM images of (a) PMMA/Cu-Cr 1%, (b) PMMA/Cu-Cr 3%, (c) PMMA/Cu-Cr 5% and (d) PMMA/Ni-Al 5% nanocomposites

4.3.14 Optical Test

The optical transmittance value of the PMMA/Co-Al LDH nanocomposites is presented in Table 4.5. In general, matrix properties, the interfacial refractive index difference between matrix and nanofiller, and the size of dispersed nanofiller govern the optical properties of the polymer nanocomposites. The optical transmittance for the nanocomposite without nanofiller is generally higher than that of the nanocomposites. It is apparent from the Table 4.5 that the neat PMMA shows a maximum transmittance of 77%. This specifies that most of the light pass through PMMA sample. After reinforcement of LDH in the PMMA matrix, the transparency of PMMA reduces with an increase in the concentration of LDH (wt.%). The possible reason is that the formation of intercalated morphology at higher LDH loading that restricts the light transmittance through the nanocomposites. For the PMMA/Co-Al 7% sample, maximum reduction in the transparency of 91% is noticed in comparison with neat PMMA. The translucent PMMA nanocomposite results from the Co-Al LDH filler, can find

application for the light sensitive materials such as lipids, vitamins and pigments. The optical transmittance test of PMMA/Cu-Cr LDH samples was also analyzed and found opaque except for PMMA/Ni-Al 5% sample.

Table 4.5 Optical clarity and rate of burning of PMMA/LDH nanocomposites

Sample	Transmittance (%)	Rate of burning (mm/min)
Neat PMMA	77.0	65
PMMA/Co-Al 1%	55.7	56
PMMA/Co-Al 3%	27.2	52
PMMA/Co-Al 5%	14.2	49
PMMA/Co-Al 7%	6.7	44
PMMA/Cu-Cr 1%	-	37
PMMA/Cu-Cr 3%	-	35
PMMA/Cu-Cr 5%	-	33
PMMA/Ni-Al 5%	6.3	34

4.3.15 Flammability Test

The flammability analysis of PMMA/Co-Al LDH and PMMA/Cu-Cr LDH nanocomposites was performed to investigate the effect of different LDHs on PMMA and the average value was reported in Table 4.5. It is clearly seen that PMMA nanocomposites have higher flame retardancy with respect to neat PMMA. This suggests that LDH's have substantial influence on the flame retardancy of the polymer nanocomposites. It is noticed that as the concentration of LDH increases, the amount of char that can be formed increases and the rate at which heat is released decreases. It is also found that intercalated structures are more effective as the path is intervened by LDH platelet structures. It is evident from the Table 4.5 that PMMA/Cu-Cr LDH nanocomposites are more flame retardant than Co-Al LDH based nanocomposites. According to Xu et al., (2012), the layered double hydroxides have lost their hydroxyl groups and interlayer anions and converted to a mixed metal oxide, which can

promote a charring on the surface of the nanocomposites. The charring layer can create a physical protective barrier surface and slow the volatilization rate of polymer.

4.3.16 Rheological Properties

It is believed that rheology offers an effective way to assess the state of nanofiller dispersion and to detect the state of presence of interconnecting microstructure of the nanocomposites in molten state directly (Kashiwagi et al., 2008). The nanofiller loading of the particles as well as other factors, such as the shape and size of the particles and state of dispersion of particles (well-dispersed state or agglomerated state), are known to influence the rheology of polymer melts. The rheological properties of two different PMMA nanocomposites are discussed herein.

Figure 4.18 and 4.19 demonstrate the frequency dependence of storage and loss modulus of the PMMA/Co-Al LDH and PMMA/Cu-Cr LDH nanocomposites at 200 ^{o}C. The storage modulus characterizes the elastic property (G') of the material, while the loss modulus suggests the viscous property. It is clearly observed from the graph that both the moduli are influenced by the addition of LDH in the PMMA matrix. At lower frequency, the storage and loss modulus gradually increases with increasing the concentration of the LDH and are found maximum for the PMMA/Co-Al 7% nanocomposite. The increase at lower frequency is the characteristic of pseudo-solid like behaviour due to the formation of network percolating LDH lamellae. The addition of LDH to the PMMA matrix increases the storage modulus significantly and indicates a transition from liquid like to pseudo solid like or solid-like rheological behaviour. It is generally believed that the extent of these changes reflects the state of dispersion of LDH nanofiller (Song et al., 2015). This has been attributed to the formation of percolated network of the exfoliated layers or stacks of intercalated layers (Ray et al., 2002). At higher frequency region, the viscoelastic behaviour of all PMMA nanocomposites is quite the same, indicating that the observed chain relaxation modes are almost unaffected by the presence of LDH layers. Similar behaviour was also reported by Du et al., (2004) for PMMA/SWCNT nanocomposites. It is also noticed that PMMA nanocomposites display higher loss modulus with respect to storage modulus at lower frequency region (see Figure 4.19). The storage and loss modulus behaviour of PMMA/Cu-Cr 5% and PMMA/Ni-Al 5% sample are almost identical.

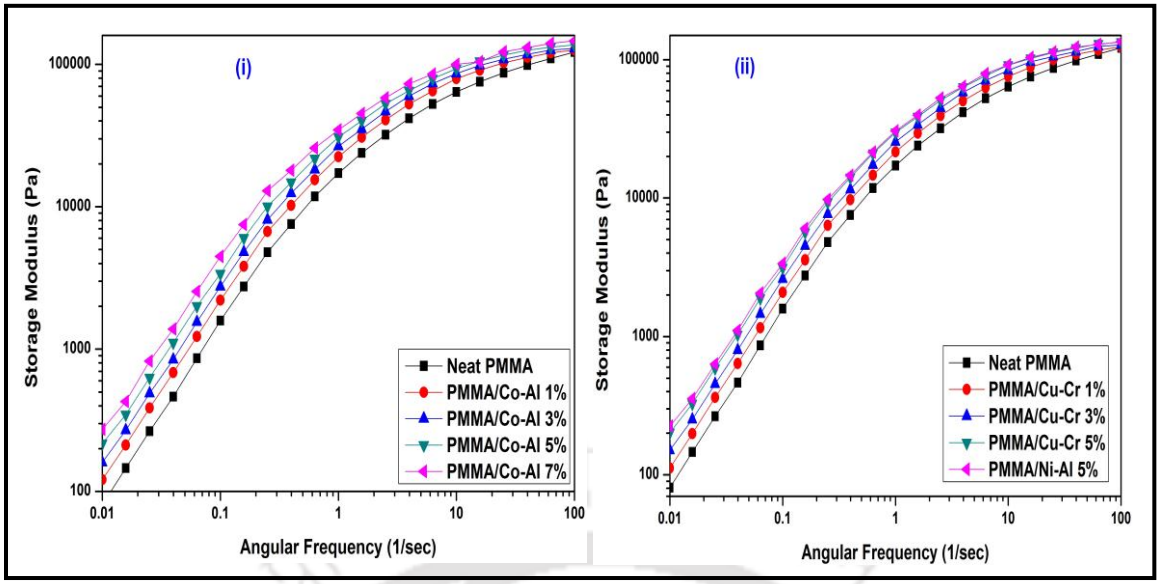

Figure 4.18 Storage modulus of (i) PMMA/Co-Al LDH and (ii) PMMA/Cu-Cr LDH nanocomposites at 200 ^{o}C

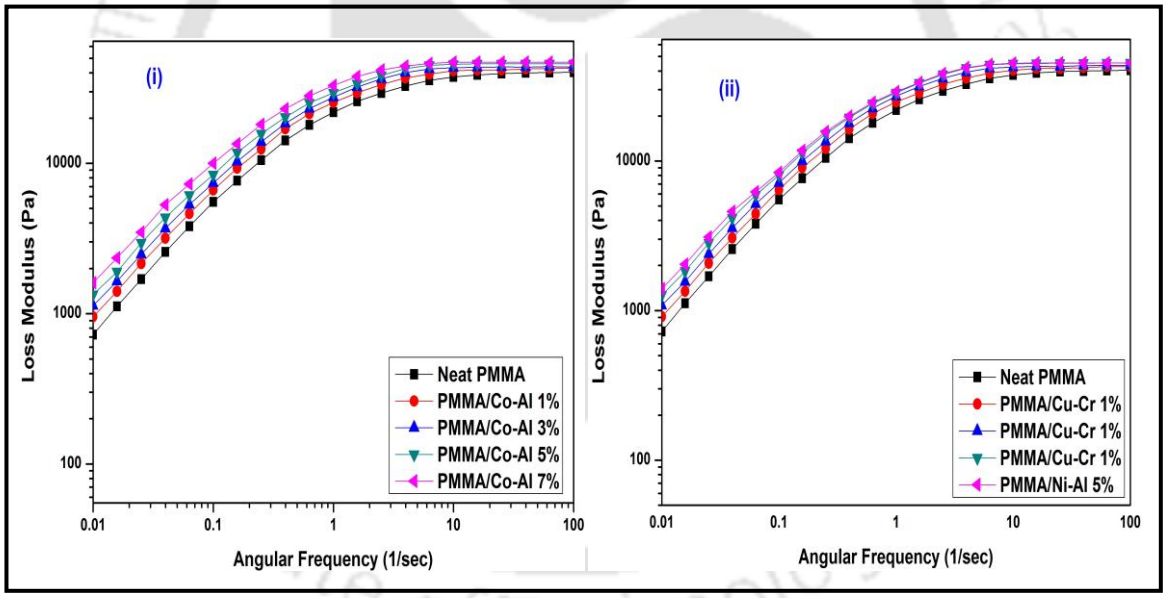

Figure 4.19 Loss modulus of (i) PMMA/Co-Al LDH and (ii) PMMA/Cu-Cr LDH nanocomposites at 200 ^{o}C

Loss factor **(**tan δ) is the ratio of loss modulus (G'') to storage modulus (G'). It is a useful parameter to measure the extent of elasticity in a given sample**.** Figure 4.20 exhibits the loss factor of PMMA/Co-Al LDH and PMMA/Cu-Cr LDH. The graphs demonstrate a drop in tan δ as the frequency increases. The physical entanglements of the PMMA chains in addition to the presence of LDH layers cause the formation of some network structures among LDH

particles and polymer chains and also LDH particles themselves. The rigid structure of LDH nanoparticles hinders the viscous behaviour and facilities the transition from viscous to elastic behaviour (He et al., 2006; Zhou et al., 2007). In comparison with neat PMMA, the decrease of maximum values of tan δ for both type of nanocomposites indicate an improved elastic behaviour upon incorporation of nanofiller into the nanocomposites, as the loss factor is inversely proportional to storage modulus (elastic). The reduction of loss factor in the high frequency region is attributed to partial orientation of polymer chains and LDH layers as a result of shear deformation (Motahari et al., 2012).

Similar to storage modulus and loss modulus, the complex viscosity of Co-Al LDH and Cu-Cr LDH based nanocomposites increase upon the introduction of different nanofiller and shear thinning behaviour is intensified (see Figure 4.21). Higher viscosity of nanocomposites arises from the three-dimensional structure of LDH nanoparticles, leading to formation of aggregates, which are stable under high stress conditions. Another possible reason for enhanced viscosity of nanocomposites is the higher flow resistance of macromolecules due to the interaction between the nanofillers and polymer matrix (Galgali et al., 2001). As the frequency increases, the viscosity of both type of nanocomposites decrease, which might be due to partial disruption of three-dimensional structure or the alignment of the LDH layers under shear, the microstructure changes from a random oriented to a shear induced ordered orientation. Zhang et al., (2012) showed similar trend of reduced complex viscosity for PMMA/graphene composites at higher angular frequency.

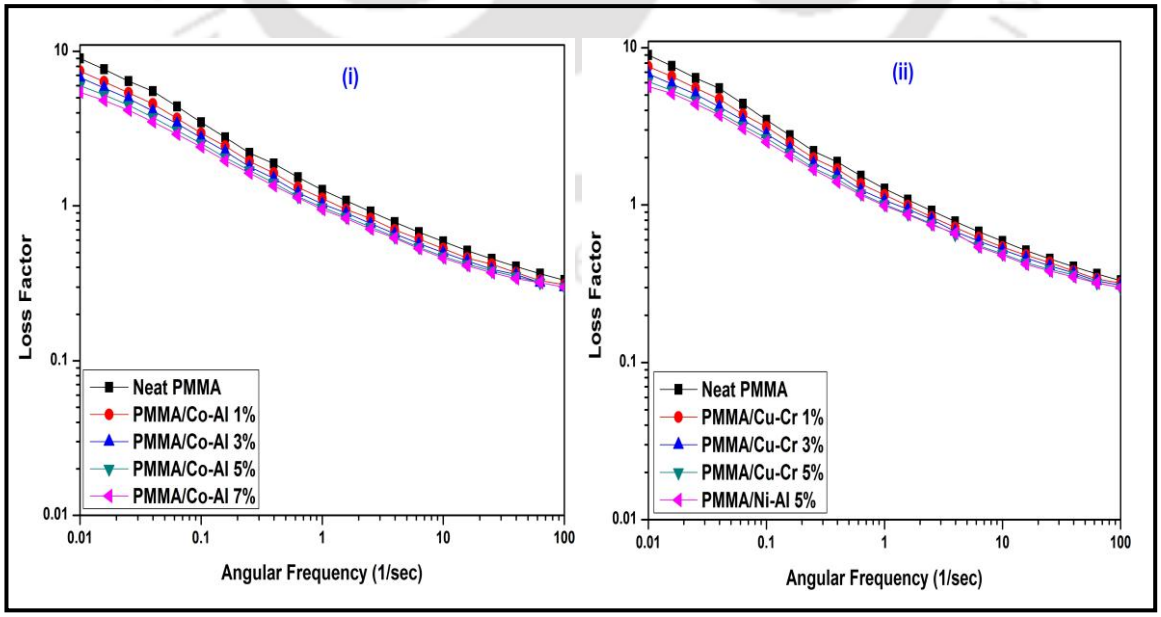

Figure 4.20 Loss factor of (i) PMMA/Co-Al LDH and (ii) PMMA/Cu-Cr LDH nanocomposites at 200 ^{o}C

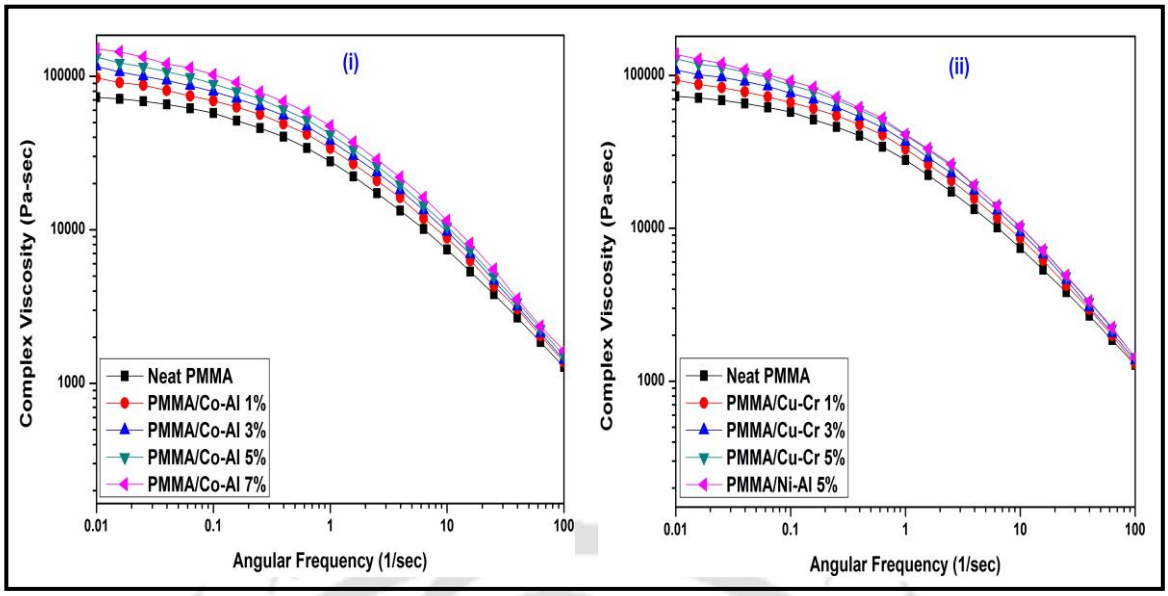

Figure 4.21 Complex viscosity of (i) PMMA/Co-Al LDH and (ii) PMMA/Cu-Cr LDH nanocomposites at 200 ^{o}C

4.4 SUMMARY

It can be concluded that Co-Al LDH based nanocomposites demonstrates better properties over Cu-Cr LDH based nanocomposites. The Co-Al LDH was synthesized in single step while the Cu-Cr LDH was prepared in two step process, which reflects that a single step has pronounced effect. The tensile, flexural and impact properties of the nanocomposites are found to be maximum at 1 wt.% loading of LDH nanofiller. The improvement in tensile strength, flexural strength, impact strength for the PMMA/Co-Al 1% sample over neat PMMA is found to be 24, 25 and 10%, respectively. The PMMA/Cu-Cr 1% nanocomposite displays 18, 21% increment for tensile and flexural strength, respectively. It is also found that PMMA/Ni-Al 5% nanocomposite shows enhanced properties over PMMA/Cu-Cr 5% sample. The hardness is found to be maximum for PMMA/Co-Al 7% nanocomposites. At 50% weight loss, the PMMA/Co-Al LDH nanocomposites demonstrate 31-35 ^{o}C higher improvement over neat PMMA, while PMMA/Cu-Cr LDH nanocomposites display 26-32 ^{o}C increment over neat PMMA. The T_g is enhanced by 5 and 3 ^{o}C for PMMA/Co-Al LDH and PMMA/Cu-Cr LDH nanocomposites, respectively.

It is confirmed from the Coats-Redfern and IPDT method that thermal stability of PMMA nanocomposites is increased, which is higher for PMMA/Co-Al LDH nanocomposites over Cu-Cr LDH based samples. The rheological studies also indicate that the storage and loss modulus increase as the frequency increases, however complex viscosity

reduces. It can also be concluded that the nature of LDH also plays a vital role in addition to the concentration of LDH.

Chapter 5

Fabrication and Characterization of PMMA/Clay, PMMA/Ni-Al LDH and PMMA/Co-Al LDH Nanocomposites via Solvent Blending Method

From the earlier chapter, it was found that the melt-intercalation method produced primarily intercalated morphology at higher loadings (>1 wt.%) and exfoliated structure with only 1 wt.% loading. It is also well known that the solvent blending process gives exfoliated structure. Therefore, an attempt has been made to check whether exfoliated morphology of nanocomposites is achievable with three different fillers (OMMT (Nanomer 1.31 PS), Co-Al LDH, Ni-Al LDH) by solvent blending method. This chapter deals with the preparation and characterization of various PMMA nanocomposites. PMMA nanocomposites based on nanoclay, Ni-Al LDH and Co-Al LDH were prepared by solvent blending technique using dichloromethane as a solvent. Various characterization techniques such as Fourier Transform Infra-red spectroscopy (FTIR), X-ray diffraction analysis (XRD), transmission electron microscopy (TEM), atomic force microscopy (AFM), field emission scanning microscopy (FESEM), thermogravimetric analysis (TGA) and differential scanning calorimetry (DSC) were carried out to characterize the different PMMA nanocomposites. Hardness, water uptake test, optical properties were also evaluated for the nanocomposite films. Finally, water vapor transmission rate (WVTR) and rheological analysis were conducted to examine the water vapor permeability and processing properties, respectively.

*** The part of this work has been published in **International Journal of Nano and Biomaterials,** 2014, 5, 27-44, **RSC Advances,** 2015, 5, 39810-39820, **Chinese Journal of Polymer Science,** 2016. **Macromolecular Symposia,** 2016, 365, 104-111.

5.1 INTRODUCTION

A series of nanocomposites consisting of PMMA polymer and different clays have been appeared in the literatures (Blumstein, 1965; Wang et al., 2002; Shen et al., 1999; Jiang et al., 2000; Sahoo et al., 2007; Liqiang et al., 2008; Liaw et al., 2007; Kuila et al., 2009; Ramaraj et al., 2010; Pradhan et al., 2011). Jiang and Tsai, (2000) have shown an improvement in properties of PMMA/clay nanocomposites synthesized by in-situ polymerization over neat PMMA. Sahoo et al., (2007) have reported that the strong interactions between PMMA and dispersed clay layers in emulsion polymerized PMMA/clay nanocomposite significantly improved the thermal stability of PMMA. Shen et al., (1999) have reported that the thermal stability of PMMA was increased in melt-intercalated PMMA/clay nanocomposite compared to that of the neat PMMA. The effect of clay modification and clay loading on the morphology and mechanical properties of in-situ polymerized PMMA/clay nanocomposites was studied by Liqiang et al., (2008). Liaw et al., (2007) have investigated the thermal properties of melt-intercalated PMMA/clay nanocomposites. They revealed that higher clay loading could improve thermal stability significantly. Qiu et al., (2006) have investigated the thermal properties of the exfoliated PS/Mg-Al LDH nanocomposites prepared via emulsion polymerization method. Du et al., (2007) have prepared nylon 6/Mg-Al LDH nanocomposites by melt intercalation of nylon 6 into the part of organo modified Mg-Al LDH interlayers. XRD results demonstrated that too high LDH loading makes the LDH layer difficult to exfoliate. Wang et al., (2006) have developed disorderly exfoliated PMMA nanocomposites by in-situ bulk polymerization of MMA in presence of various amount of LDH-U content. The glass transition temperature (T_g) was significantly higher for disorderly exfoliated PMMA/LDH (127 ^oC) nanocomposites than that of pure PMMA (105 ^oC). An exfoliation/adsorption process was used by Li et al., (2003) to synthesis exfoliated nanocomposites based on Mg-Al LDH and PMMA. The decomposition temperature of PMMA/LDH nanocomposites at 5 wt.% loss was about 288.5 ^oC, which was higher than that of pure PMMA (140 ^oC). Wang et al., (2011) have fabricated polypropylene (PP)/Co-Al LDH nanocomposites via melt compounding method and performed the thermal degradation study using different kinetic models.

Liu et al., (2006) prepared Co-Al LDH with different anions (nitrate, chlorate, acetate, oleate, lactate) and reported that nitrate-LDH provided better exfoliation degree as compared to other modifiers. Manzi-Nshuti et al., (2009) examined the thermal stability of PMMA nanocomposites using two different LDH's (Ca_3Al and Ca_3Fe LDH). The enhancement in the

fire retardant property of PMMA nanocomposites with Ca_3Al LDH is better as compared to Ca_3Fe LDH. Wang et al., (2006) synthesized PMMA nanocomposites by melt blending method using MMT, MgAl LDH and kaolinite as fillers. Among the studied fillers, nanocomposites prepared with MMT and LDH exhibited better thermal stability than kaolinite. In another study (Matusinović et al., 2009), PS-PMMA/CoAl LDH nanocomposites (7.5phr) fabricated by in-situ polymerization technique displayed a maximum thermal stability of 26 ^{o}C over neat polymer. Huang et al., (2011) reported that modified LDH reduced the peak Heat Release Rate (pHRR) by 35% in PMMA/MgAl nanocomposites at 5 wt.% loading. Acharya et al., (2007) reported that thermal stability was improved by 40 ^{o}C in EPDM/Mg-Al LDH nanocomposites prepared via in-situ polymerization method. In the study of Li et al., (2003), it was observed that Mg-Al LDH layers were dispersed individually in the PMMA matrix that was prepared by exfoliation-adsorption process. Organo-modified Zn-Al LDH incorporated in the syndiotactic polystyrene proceeded as a nucleating agent and also accelerated the overall non-isothermal crystallization process (He et al., 2006).

The aim of this study is to examine the influence of clay, Co-Al LDH and Ni-Al LDH on the properties of PMMA nanocomposites synthesized by solvent blending method. The morphological, thermal and rheological properties of the nanocomposites are assessed using various techniques. Thermal degradation kinetics of the nanocomposites is also analyzed using different models.

5.2 EXPERIMENTAL

5.2.1 Materials

All the materials are same as mentioned in Chapter 4 (section 4.2.1)

5.2.2 Synthesis and modification of Ni-Al LDH and Co-Al LDH

The synthesis and modification of Ni-Al LDH and Co-Al LDH are already discussed in Chapter 4 (section 4.2.2).

Table 5.1 Preparation chart for different PMMA nanocomposites

Sample Name	LDH concentration (wt.%)	LDH (g)	Solvent (mL)	PMMA (g)
Neat PMMA	0	0	72	5
PMMA/clay 3	3	0.15	72	4.85
PMMA/clay 5	5	0.25	72	4.75
PMMA/clay 7	7	0.35	72	4.65
PMMA/Co-Al 3	3	0.15	72	4.85
PMMA/Co-Al 5	5	0.25	72	4.75
PMMA/Co-Al 7	7	0.35	72	4.65
PMMA/Ni-Al 3	3	0.15	72	4.85
PMMA/Ni-Al 5	5	0.25	72	4.75
PMMA/Ni-Al 7	7	0.35	72	4.65

5.2.3 Preparation of PMMA nanocomposites

The properties of the nanocomposites increase with even small amount of nanofiller addition. Therefore, to study the effect of clay/LDH content on the properties of PMMA nanocomposites, various PMMA nanocomposites were prepared with 3, 5, and 7 wt% of nanofiller (relative to PMMA) by solvent blending method. For this, PMMA and nanofiller were first dried at 120 ^{o}C to remove any moisture, so as to ensure less hindrance on solubility because of presence of water molecules. The schematic diagram for the preparation of PMMA nanocomposite is represented in Figure 5.1. After that, a desired quantity of nanoclay was dispersed in 30 ml of methylene chloride and stirred for 24 h at room temperature (25^{o}C) and then sonicated (Sonics and Materials, Model VCX 500) for 30 min (referred as Solution A). Clay dispersion was checked after 24 h by keeping the Solution A undisturbed for 1 h. If any settling of clay was noticed, the sample was again sonicated. An estimated amount of PMMA was mixed with 42 ml of methylene chloride and stirred at room temperature till the entire PMMA completely dissolves (Solution B). Then these above prepared two solutions (Solution A and B) were mixed and stirred for 12 h at room temperature. The resulting PMMA/nanoclay or LDH solution was spread over a Petri dish and left for 24 h in ambient

condition yielding a viscous gel layer. Finally, the nanocomposite films were dried in an oven at 65 ^{o}C for 6 h. The neat PMMA film was also prepared by an identical procedure in the absence of clay. Table 5.1 shows the composition of different PMMA nanocomposites. All the experiments were conducted in duplicate and the average value was reported.

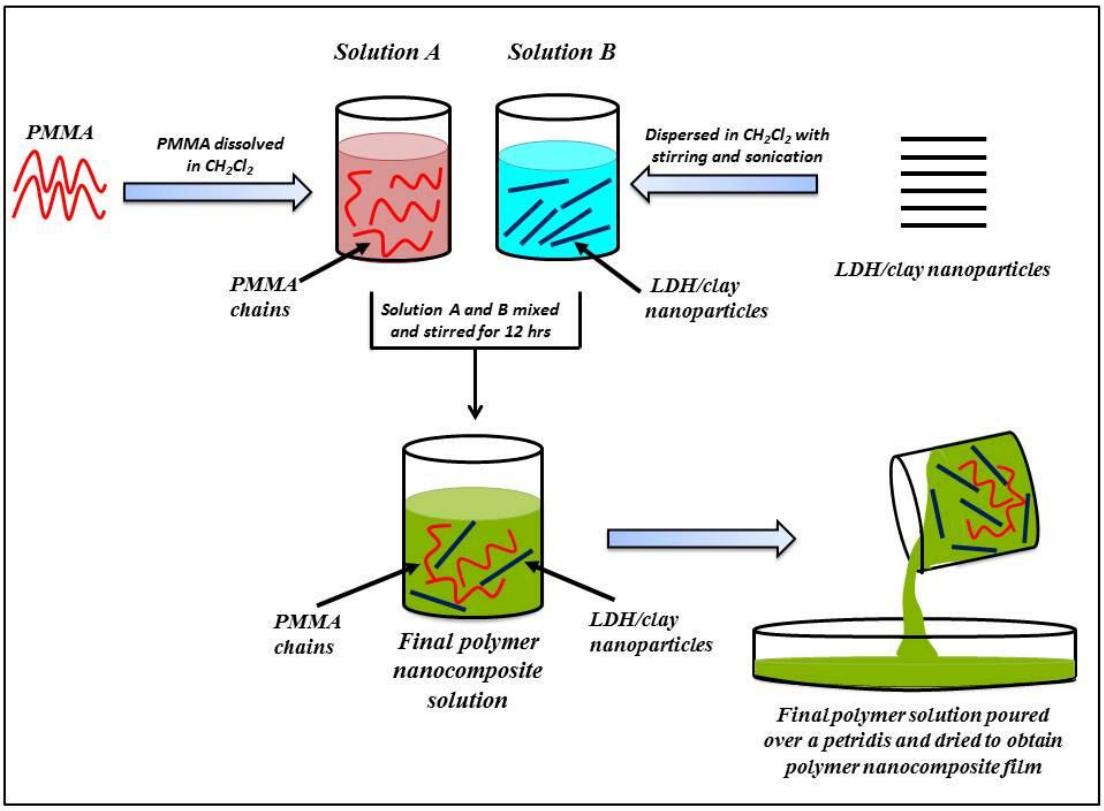

Figure 5.1 Schematic of the preparation of PMMA nanocomposites

5.2.4 Characterization Techniques

FTIR spectra of the prepared PMMA nanocomposites were performed using Shimadzu Fourier transform infrared spectroscopy to identify the different peaks in polymer nanocomposites. The X-ray diffraction (XRD) profile of different nanoclays and PMMA nanocomposites were recorded using AXS D8 ADVANCE Fully Automatic Powder X-ray Diffractometer (Bruker) fitted with Cu-Kα radiation (λ = 0.15406 nm) and Ni filter. The patterns were acquired for 2θ range from 1-50^{o} with 0.05^{o} s^{-1} scan speed. TEM micrographs of PMMA nanocomposite was attained on a JOEL JEM-2100 transmission electron micro analyser with an accelerating voltage of 200 KV. The morphological study of polymer nanocomposites samples were analysed by scanning electron microscopy (model LEO 1430 VP) operating at an accelerating voltage of 15 KV. In order to predict the glass transition

temperature (T_g) of the PMMA nanocomposites, Differential scanning calorimetry (DSC) analysis was carried out using Metler Toledo-1 series instrument. Samples were heated from 25 to 250 ^{o}C at a heating rate of 10 ^{o}C/min under a flowing nitrogen atmosphere. Thermo gravimetric analysis of various nanocomposites was characterized on TGA/SDTA/851e/LF/1100 (Mettler Toledo) at a heating rate of 10 ^{o}C/min under the nitrogen atmosphere. The surface morphology was analysed by Atomic Force Microscope (AFM) instrument (Model No. 5500 series, Agilent Technologies, USA) in non-contact mode. The scan angle was perpendicular to the surface of specimen. All offline image flattening and analyses of the images were conducted using software, WSxM v5.0. Hardness (Shore D) values of nanocomposite films were measured using durometer according to ASTM D2240. The water vapor transmission rate (WVTR) analysis was performed at according to ASTM E 398 using PERMATRAN-W instrument (Model: 1/50, Mocon USA). The WVTR test was executed at 37.8^{o}C temperature and 90% relative humidity. The optical transmittance of different compositions was analyzed using Canon 550D digital camera.

The rheological properties of pristine PMMA and its nanocomposites were measured by Anton Paar MCR 301 in an oscillation mode with parallel plate geometry using 50 mm diameter disc at 190 ^{o}C. Samples with ~1 mm thickness were used for rheological study. Water uptake test is considered as a standard method to measure the water resistance nature of the nanocomposite films. Water uptake capacity of the nanocomposite film was measured by taking weight before and after hydration. The nanocomposite films having dimensions of 2×2 cm were taken and dried at 70 ^{o}C for 4 h to bring all the samples to a similar state. After which, the dry weight of the samples was measured. Each of the dried samples was then dipped into individual conical flasks containing 100 ml of Millipore water for 48 h. Then these samples were taken out, wiped the surface with tissue paper, and weighed immediately. The water uptake capacity of the nanocomposite films was calculated using the following equation.

$$\text{Water uptake (\%)} = \left(\frac{W_w - W_d}{W_d}\right)100 \qquad (5.1)$$

where, W_w and W_d are the wet and dry weight of nanocomposite films, respectively.

5.3 RESULTS AND DISCUSSION

5.3.1 FTIR Analysis

The FTIR analysis has been carried out to study the different functional groups present in the clay, LDH and polymer nanocomposites. To make sure that the nanoclay is dispersed in the PMMA matrix, FTIR analysis was performed for PMMA nanocomposites and the results were compared with neat PMMA and clay. The FTIR results are shown in Figure 5.2(i) for all the samples. Nanoclay (Figure 5.2(i)e) shows its characteristic peaks at 3630, 3246, 2922, 2849, 1612, 1465, 1048, 918, 750, 530, 458 cm^{-1}. Clear broad band in the region 3300-3700 cm^{-1} is observed, which corresponds to the –OH stretching vibration. This band has two features at 3630 cm^{-1} and at 3246 cm^{-1} showing the presence of two types of O-H groups: isolated OH groups and those involved in hydrogen bonding. The peaks at 2922, 2849, and 1465 cm^{-1} are for CH_2 asymmetric stretching, symmetric stretching, and in-plane scissoring vibrations, respectively. The peak at 1612 cm^{-1} corresponds to the bending vibration mode of hydrated water molecules and weakly bonded water molecules (Manoratne et al., 2006). A peak at 1046 cm^{-1} is attributed to Si-O stretching vibration. The bands observed at 917, 750, 530 and 458 cm^{-1} corresponds to AlAlOH, AlMgOH, Al-O stretching and Mg-O bending vibration, respectively (Madejova, 2003). For neat PMMA, the absorbance band in the region 2650-3000 cm^{-1}, namely at 2996 and 2950 cm^{-1} are due to C-H stretching vibrations of CH_3 and methylene (CH_2) groups and a peak in the region 1870-1540 cm^{-1} at 1731 cm^{-1} is due to the C=O stretching (see Figure 5.2 (i)d). It is observed that the spectra of all nanocomposites have same peaks with those of neat PMMA, as well as some additional small peaks coming from the nanoclay (i.e., the bonds of Si–O and Mg–O). From these results, it is confirmed the presence of nanoclay in the PMMA matrix.

FTIR spectra of Co-Al LDH and nanocomposites are shown in Figure 5.2(ii). The nitrate anions which are present in LDH have three different characteristics peaks, i.e., the nitrate absorption peak observed at 1370 cm^{-1}, two other nitrate vibration band at 1470 and 822 cm^{-1}. The stretching band for aliphatic CH_3 or $–CH_2$ of the long chain of SDS molecules is observed around 2840-2965 cm^{-1}. The small peaks appeared at 1218 and 1063 cm^{-1} correspond to the symmetric (v_s=o) and asymmetric vibration (v_{os}=o) of sulfate from dodecyl sulfate, respectively. The broad peak in the vicinity of 3300-3700 cm^{-1} is assigned to O-H stretching vibration of hydrogen bonded interlayer water molecules and metal hydroxide layer (Du et al., 2009).The peaks observed at lower frequency (400-700 cm^{-1}) correspond to the vibration of metal-oxygen bond in the brucite like lattice that is particular of this kind of

layered solids. The Ni-Al LDH and its nanocomposites also exhibits similar functional groups (see, Figure 5.2(iii)).

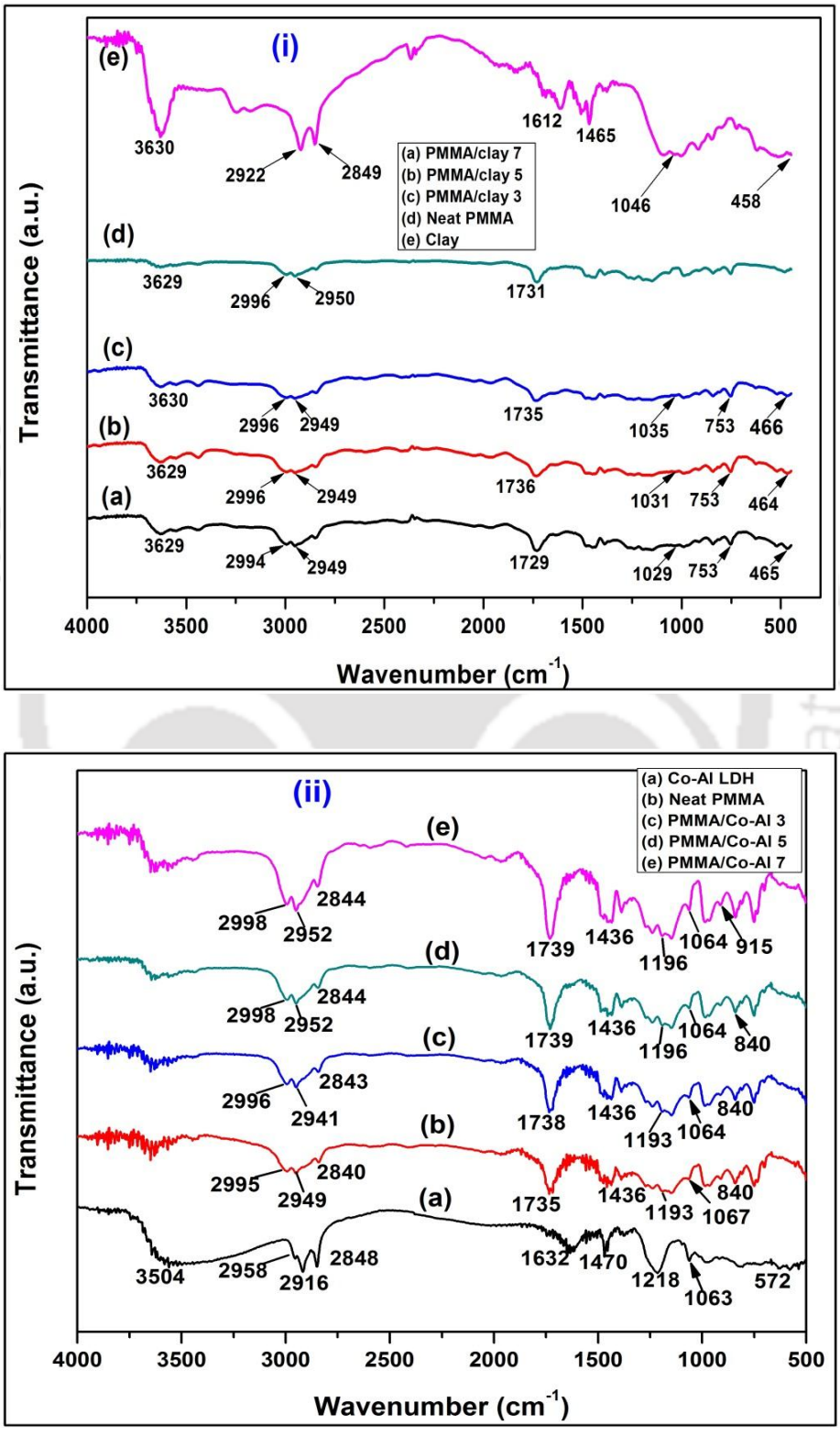

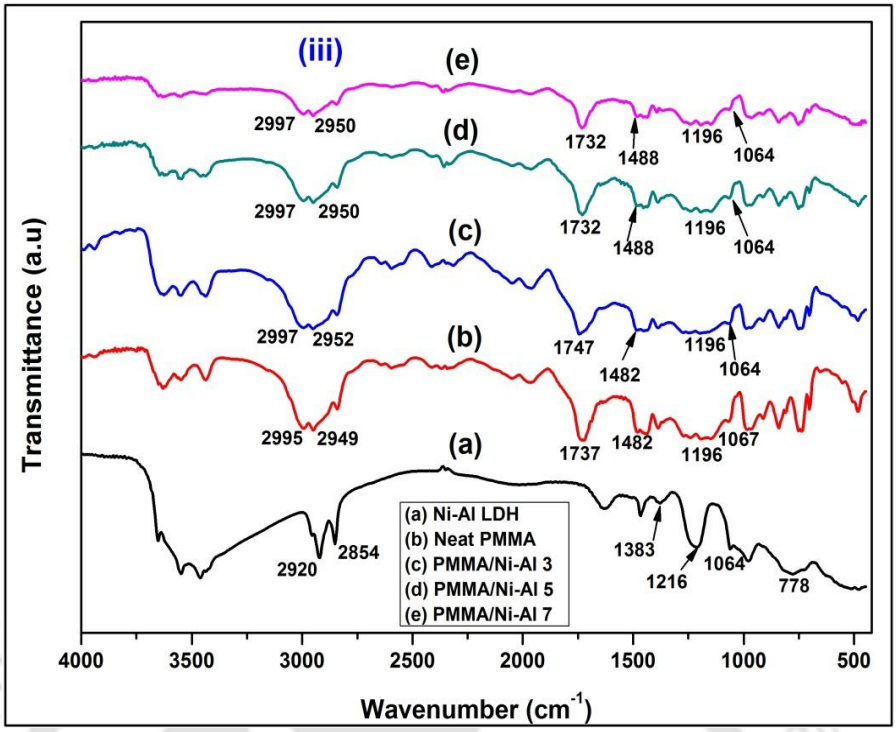

Figure 5.2 FTIR spectra of (i) PMMA/clay, (ii) PMMA/Co-Al LDH, (iii) PMMA/Ni-Al LDH nanocomposites

5.3.2 XRD Analysis

The nanocomposites can be characterized according to the degree of dispersion of the nanofiller in the polymeric matrix as intercalated and exfoliated nanocomposites. The particular form depends on the clay content, the chemical nature of the organic modifier, and the synthetic method. XRD is one of the most widely used tools to characterize the structure of the polymer/clay nanocomposites, i.e. intercalated or exfoliated. In the case of intercalated nanocomposite, there is an increase in the *d*-spacing (d_{001}) (i.e. 001 peak is shifted to lower angle) as compared to the original clay *d*-spacing and for completely exfoliated structures, no (001) peak is given by the XRD. The intercalation capability of the PMMA into the clay galleries is evaluated by monitoring the clay interlayer spacing using XRD analysis as follows: The gallery height (d_{001} spacing) is calculated from peak positions using Bragg's law: $n\lambda = 2d\sin\theta$, where λ is the X-ray wave length ($\lambda = 0.15406$ nm) and n = 1 (Hwu et al., 2004). Figure 5.3(i) shows the XRD pattern of the nanoclay, neat PMMA and their corresponding PMMA/clay nanocomposites. It is observed that the nanoclay shows a peak (d_{001}) at about 4.15°, corresponding to a basal spacing about 2.13 nm. However, the XRD patterns (Figure 5.3(i) c-e) of all the PMMA nanocomposites exhibit the appearance of two

peaks at lower angles. One is shifted to lower angle with respect to nanoclay (at 2θ value of 2.75^o and corresponding d_{001} value is 3.21 nm), while other appears at a greater angle (about 5.5^o). This indicates that there is presence of a mixed morphology in the nanocomposites. The peak that is shifted to lower angle compared to clay indicates the increased interlayer spacing of the clay. Accordingly, intercalated nanocomposite morphology is obtained. However, the d_{001} spacing for the PMMA nanocomposites is independent of the clay loading and these results are consistent with the results reported by Krajnc and Sebenik, (2009) and Kim et al., (2003) for PMMA/OMMT, PS/clay nanocomposites, respectively. The possible coalescence of clay platelets can be inferred from the position of the second peak. The collapse of the platelets is certainly due to the relatively lower interaction energy between the PMMA and the modifiers used in the nanoclay. The intercalants/modifiers used for clay modification probably possess higher polarity. In general, stronger interaction energy of clay and modifiers/intercalants produces relatively less organophilic clays. Another possible reason is the change of organization of the intercalant molecules in the interlayer spacing during processing. These results are in agreement with the results published in literatures (Park et al., 2008; Rohlmann et al., 2008). Based on the work reported by Ho and Glinka, (2003), the dispersion force of the solvent is the major factor determining whether the nanoclay layers remain suspended in the solvent, while the forces of polarity and hydrogen bond induce the tactoid formation (intercalated structure) of the clay in solution. In all the nanocomposites, the higher order peak (at 2θ value of 20^o) of the nanoclay disappears that strongly suggests the increased disordering of the tactoid stacking. On the whole, these results demonstrate the successful formation of partially intercalated PMMA nanocomposites via simple solvent blending method.

Figure 5.3 (ii) and (iii) represents the XRD graphs of organomodified Co-Al and Ni-Al LDH respectively, along with their corresponding PMMA nanocomposites. The basal spacing (d_{003}) of (003) peak appeared at 2θ value of 3.14^o for Co-Al LDH is estimated to be 2.8 nm. This value represents the thickness of the brucite like layer as well as the size of anions existing in the interlayer. The basal spacing (d_{003}) of (003) peak for SDS modified Ni-Al LDH at 2θ value of 6.54^o is 1.35 nm. The diffraction peak corresponding to (003) is not seen in the PMMA nanocomposites with different concentration (3-7 wt.%) of LDH. Two major affirmations can be suggested for the absence of diffraction peaks in XRD: (a) either complete delamination of LDH layers in the PMMA/LDH nanocomposites, and/or (b) disarrangement of the LDH layers within the PMMA matrix without altering the d-spacing.

Krishna et al., (2013) were also obtained the exfoliated structure of PS/Co-Al LDH nanocomposites with up to 5 wt.% of LDH content, and higher LDH content yielded intercalated structure. Table 5.2 represents the complete XRD results of different PMMA nanocomposites.

Table 5.2 XRD results of nanoclay, Co-Al LDH, Ni-Al LDH and their corresponding PMMA nanocomposites

Sample Name	LDH concentration (wt.%)	$2\theta^0$	d-spacing (nm)	Structure
Nanoclay	-	4.15	2.13	Intercalated
PMMA/clay 3	3	2.75	3.21	Intercalated
PMMA/clay 5	5	2.75	3.21	Intercalated
PMMA/clay 7	7	2.75	3.21	Intercalated
Co-Al LDH	-	3.14	2.8	Intercalated
PMMA/Co-Al 3	3	-	-	Exfoliated
PMMA/Co-Al 5	5	-	-	Exfoliated
PMMA/Co-Al 7	7	-	-	Exfoliated
Ni-Al LDH	-	6.54	1.35	Intercalated
PMMA/Ni-Al 3	3	-	-	Exfoliated
PMMA/Ni-Al 5	5	-	-	Exfoliated
PMMA/Ni-Al 7	7	-	-	Exfoliated

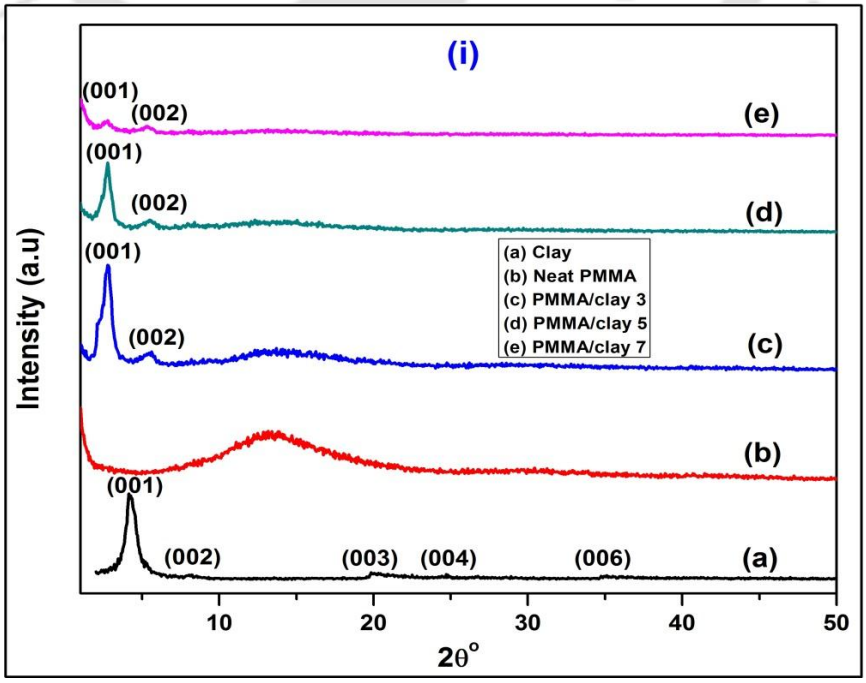

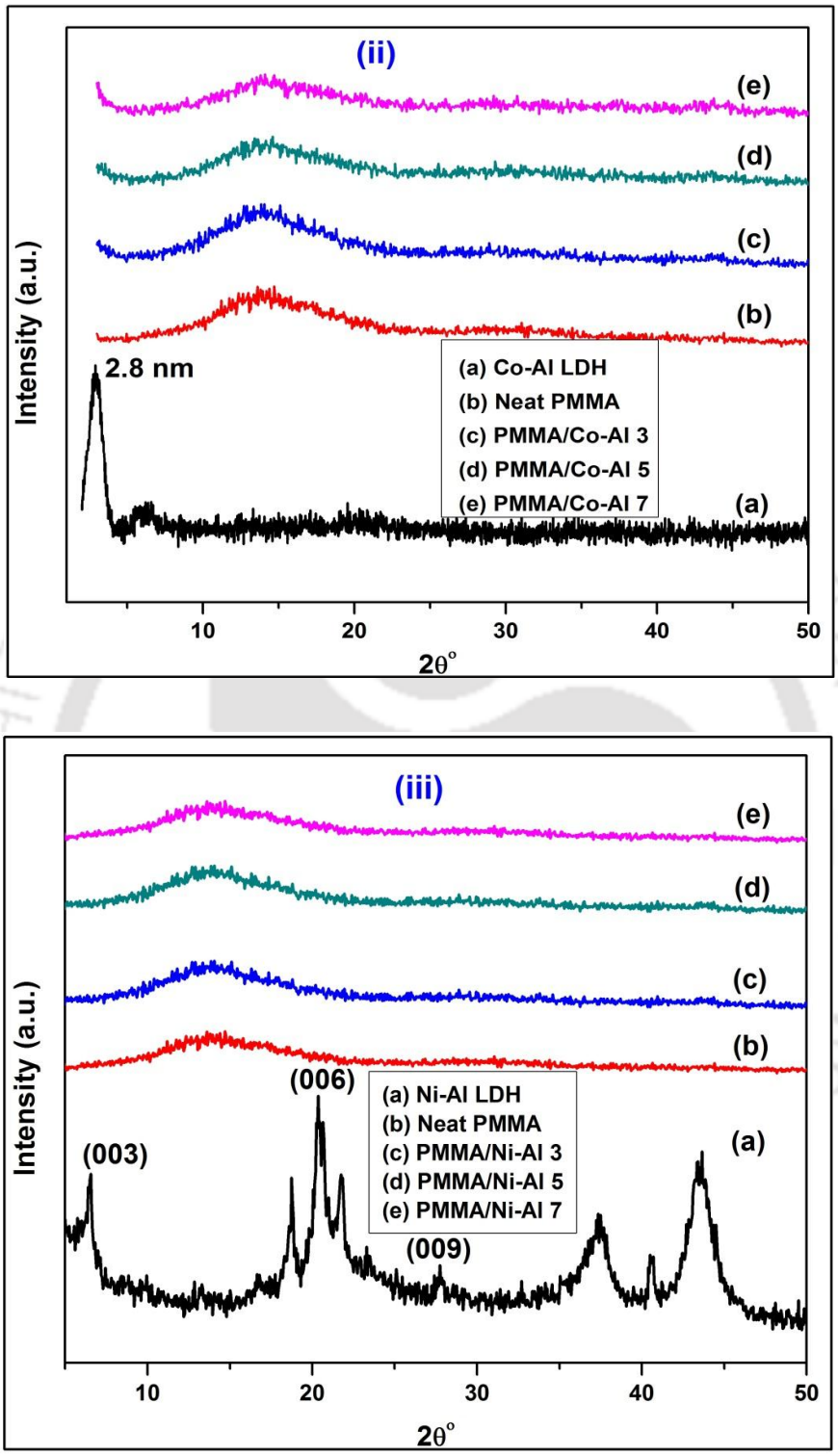

Figure 5.3 XRD pattern of (i) PMMA/clay, (ii) PMMA/Co-Al LDH, (iii) PMMA/Ni-Al LDH nanocomposites

5.3.3 TEM Analysis

XRD alone is not adequate to describe the morphology of the nanocomposites as it gives the information about the interlayer distance of the LDH or clay. TEM analysis is more useful for investigating the detail structure (intercalated or exfoliated) of nanocomposites as well as to illustrate the distribution of LDH or clay layers in the polymer matrix. Figure 5.4(i) presents the TEM image of PMMA/clay nanocomposite sample prepared with 3 wt.% loading. It is seen from the image that the clay layers (dark lines) are dispersed in the PMMA matrix (bright area). The photograph shows the intercalated clay layers by the PMMA macromolecular chain and some small tactoids are present in this intercalated material. From this result, it is reasonable to suggest that the prepared PMMA/clay nanocomposite is intercalated in structure.

Figure 5.4(ii) represents the TEM images of PMMA/Co-Al LDH nanocomposites at different magnifications. The black lines represent the LDH platelets, whereas the light region represents the polymer matrix. From the Figure 5.4 ii (a,b), it is observed that the segregated layers of Co-Al LDH are dispersed in polymer matrix for PMMA/Co-Al LDH 3 nanocomposite. This implies that the LDH layers lose their tactoids morphology, and are completely exfoliated in the PMMA matrix (Krishna and Pugazhenthi, 2013). The arrow marks represent the exfoliated structure; however, circle denotes the intercalated state. In the case of PMMA/Co-Al LDH 5 nanocomposite, exfoliated structure is seen in Figure 5.4 ii(c), while in other region (Figure 5.4 (ii) d) it is found that intercalated arrangements are also exist in the nanocomposite (marked in circle). This suggests that PMMA/Co-Al LDH 5 possesses partially exfoliated structure. The LDH platelets might be fragmented into smaller parts when they are exfoliated due to the occurrence of layer deterioration. The TEM micrographs of PMMA/Co-Al LDH 7 nanocomposite shown in Figure 5.4 ii (e, f) demonstrate that lamellar structures of Co-Al LDH are distributed in the PMMA matrix and this recommends that the intercalated morphology is obtained at higher loading of Co-Al LDH. These tactoids contain 4-5 layers of Co-Al LDH. It is generally observed that when layer spacing goes beyond 6-7 nm in the intercalated structure, the structure becomes disordered (Morgan and Gilman, 2003). In this circumstance, XRD results are not useful to analyze nanocomposite structure. In our previous work (Krishna and Pugazhenthi, 2013), TEM analysis confirmed the formation of exfoliated PS/Co-Al LDH nanocomposites with 3 and 5 wt.% LDH loading.

It is observed from Figure 5.4 iii (a) that the Ni-Al LDH layers are dispersed in intercalated form in polymer matrix for PMMA/Ni-Al LDH 3 sample. While the mixed morphology i.e. partially intercalated and exfoliated, is exhibited in PMMA/Ni-Al LDH 5 sample (see, Figure 5.2.4 (iii) b). The 'E' represents the exfoliated structure however 'I' denotes the intercalated state.TEM images clearly demonstrate the formation of partially exfoliated. The obtained results are in good agreement with the works of Wang et al., (2010) and Nyambo et al., (2009) on PMMA/ Ni-Al LDH nanocomposite.

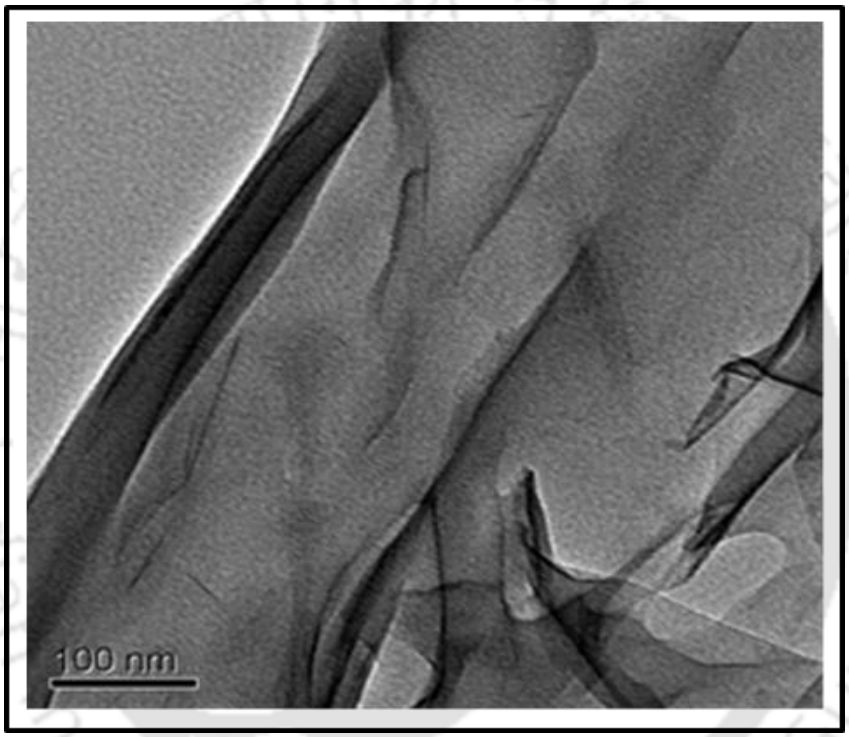

Figure 5.4 (i) TEM image of PMMA/clay 3 nanocomposite sample

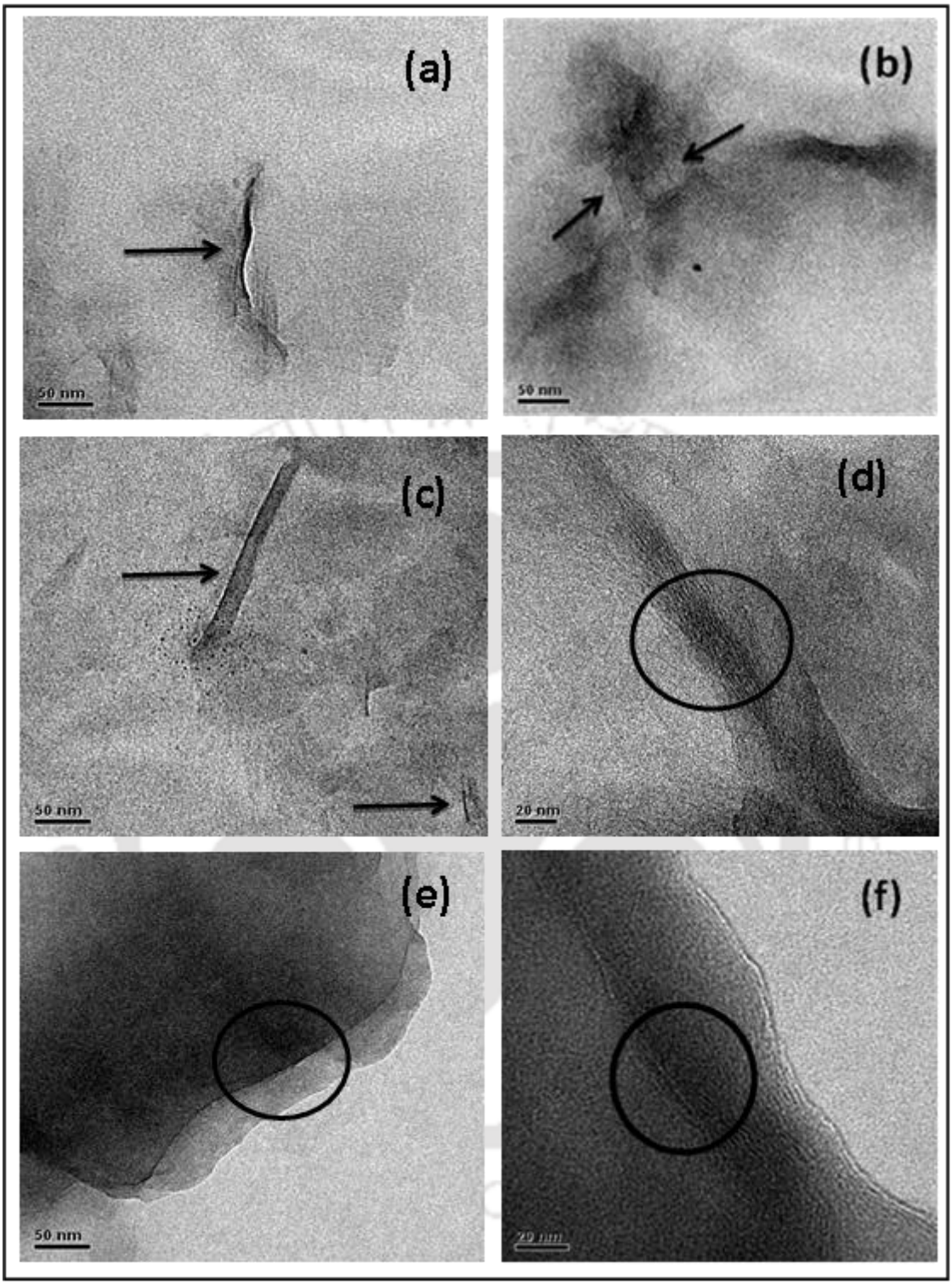

Figure 5.4 (ii) TEM images of PMMA/Co-Al LDH 3 (a, b), PMMA/Co-Al LDH 5 (c, d) and PMMA/Co-Al LDH 7 (e, f) nanocomposites

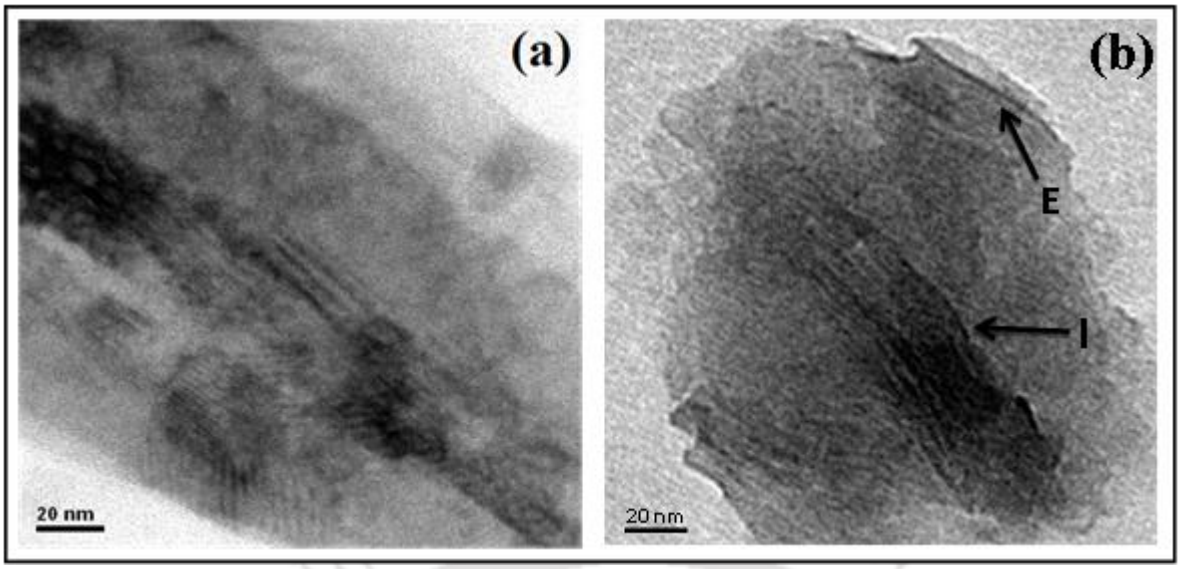

Figure 5.4 (iii) TEM image of (a) PMMA/Ni-Al LDH 3 and (b) PMMA/NI-Al LDH 5 nanocomposite

5.3.4 SEM Analysis

Figure 5.5(i) shows the SEM images of clay in PMMA-3 nanocomposite and it can be seen clearly that clay is uniformly distributed rather than agglomerates. Scanning Electron Microscope is a scientific instrument that uses a beam of highly energetic electrons to examine objects of very fine scale. This examination yields information about the topography (surface features of an object), morphology (shape and size of the particles making up the object), and composition (the elements compounds that the object is composed of and the irrelative amounts). The sample is irradiated by the beam and secondary electrons are produced i.e. the excited electrons in the sample and lose most of its energy in the process. The excited electron moves towards the surface of the sample undergoing elastic and inelastic collisions interactions inside the irradiated sample. These interactions and effects are detected and transformed into an image. SEM image reveals the presence of clay and its distribution in the nanocomposite.

In PMMA/Co-Al LDH nanocomposites, it is observed that LDH is homogenously dispersed in the polymer matrix. The aggregation of Co-Al LDH particles is also noticed at higher loading (see Figure 5.5 ii). The SEM image of PMMA/Ni-Al LDH nanocomposites (Figure 5.5 iii) indicates that with increasing the LDH concentration, the distribution of LDH in the polymer matrix is significantly affected. In lower magnification range, global dispersion of LDH particle in the PMMA matrix can be seen. Higher magnification shows

large agglomerated LDH particle, when PMMA/Ni-Al LDH 7 sample compared with PMMA/Ni-Al LDH 5 and PMMA/Ni-Al LDH 3 sample. SEM image of PMMA/Ni-Al LDH 3 shows relatively uniform LDH distribution in the PMMA matrix (Figure 5.5 (iii) a). As the LDH loading increases from 3 to 7 wt.%, degree of random distribution increases and large agglomerates start to form throughout the PMMA matrix.

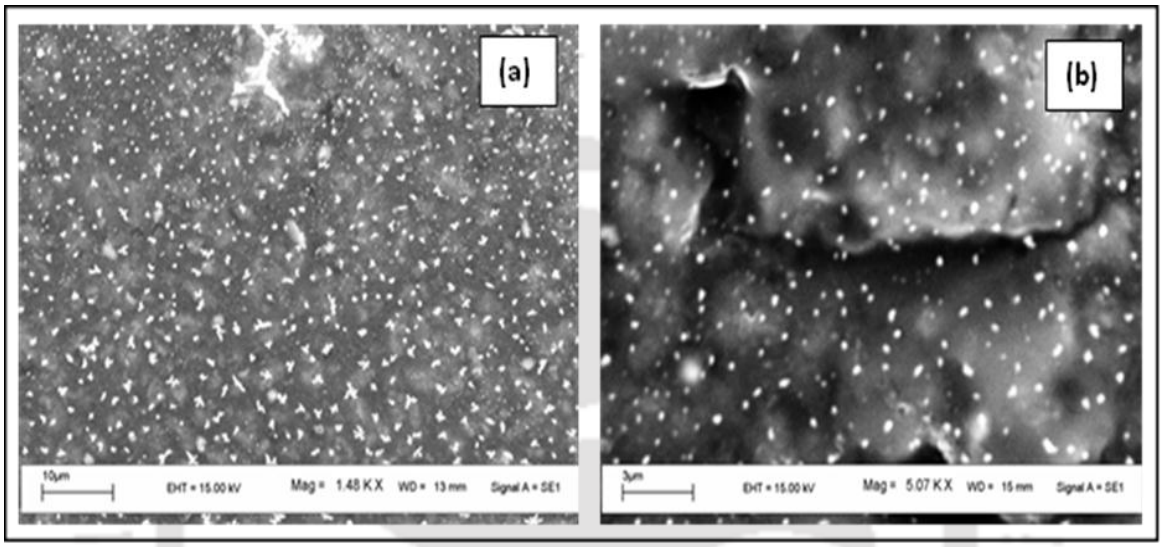

Figure 5.5 (i) SEM image of PMMA/clay 3 nanocomposite

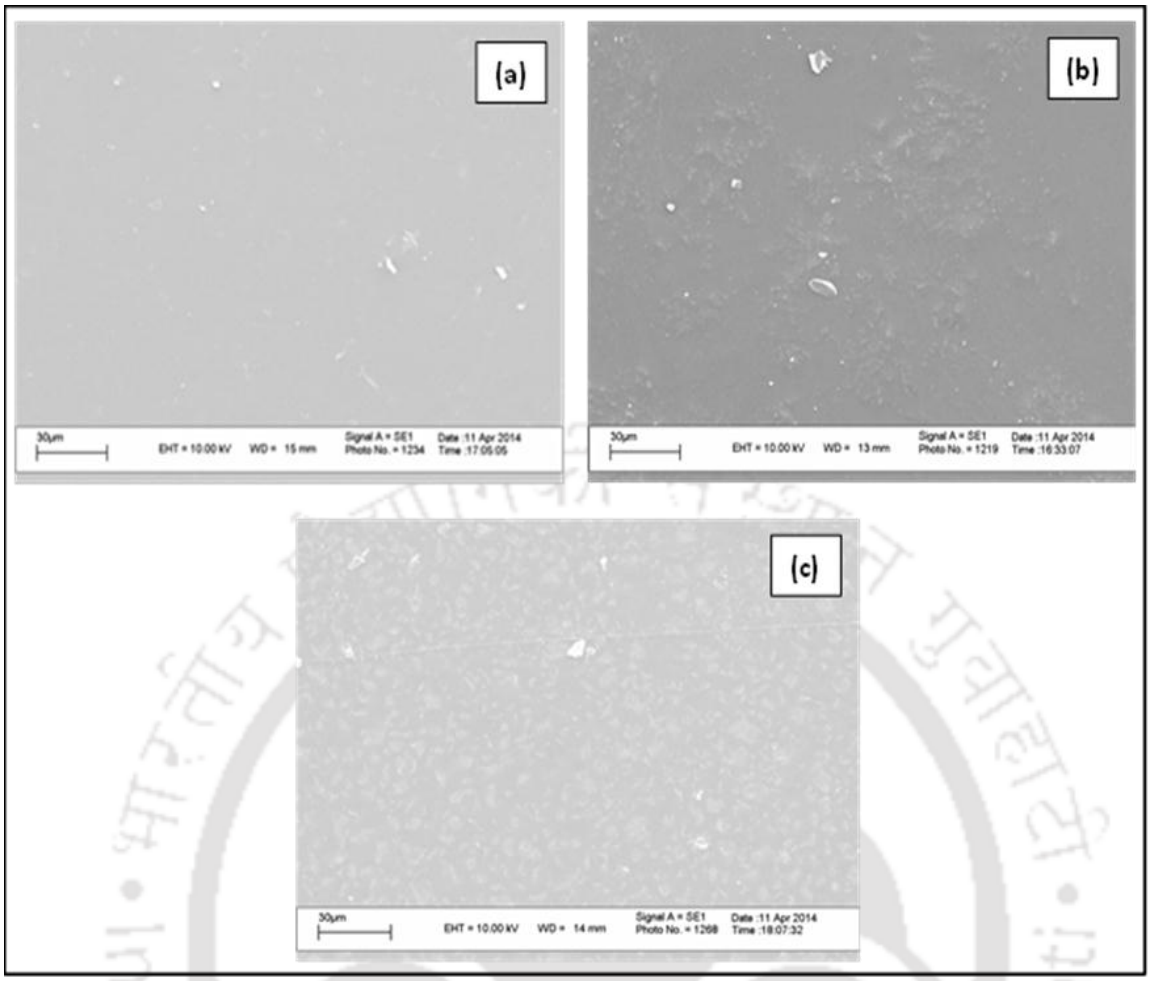

Figure 5.5 (ii) SEM images of (a) PMMA/Co-Al LDH 3, (b) PMMA/Co-Al LDH 5 and (c) PMMA/Co-Al LDH 7 nanocomposites

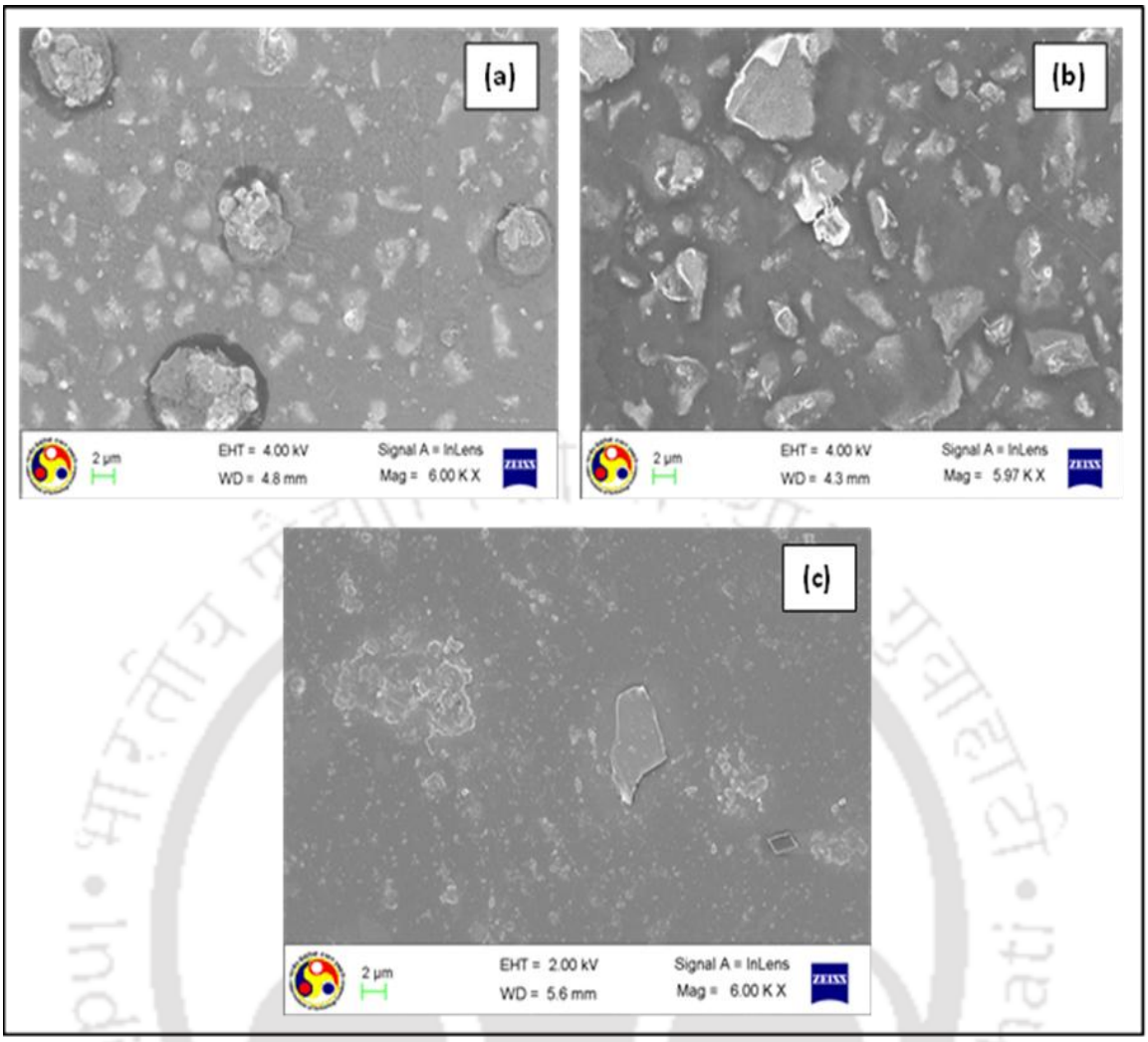

Figure 5.5 (iii) SEM images of (a) PMMA/NI-Al LDH 3, (b) PMMA/Ni-Al LDH 5 and (c) PMMA/Ni-Al LDH 7 nanocomposites

5.3.5 Thermogravimetric Analysis

TGA analysis is mainly employed to examine the thermal stability and degradation temperature of the polymer. Figure 5.6(i) represents the TG curves of the clay, neat PMMA and PMMA nanocomposites with various content of clay (3, 5 and 7 wt.%) at a heating rate of 10 ^{o}C/min. The TGA analysis of nanoclay shows a total weight loss of about 30 wt% between 30-800 ^{o}C. A small weight loss observed below 300 ^{o}C corresponds to the removal of physorbed water present in the clay. The weight loss between 300 and 450 ^{o}C is due to the degradation of the organic fraction introduced as modifier in the clay as well as to the loss of hydration water. There is also decomposition at above 450 ^{o}C, which is associated with dehydoxylation of aluminosilicate.

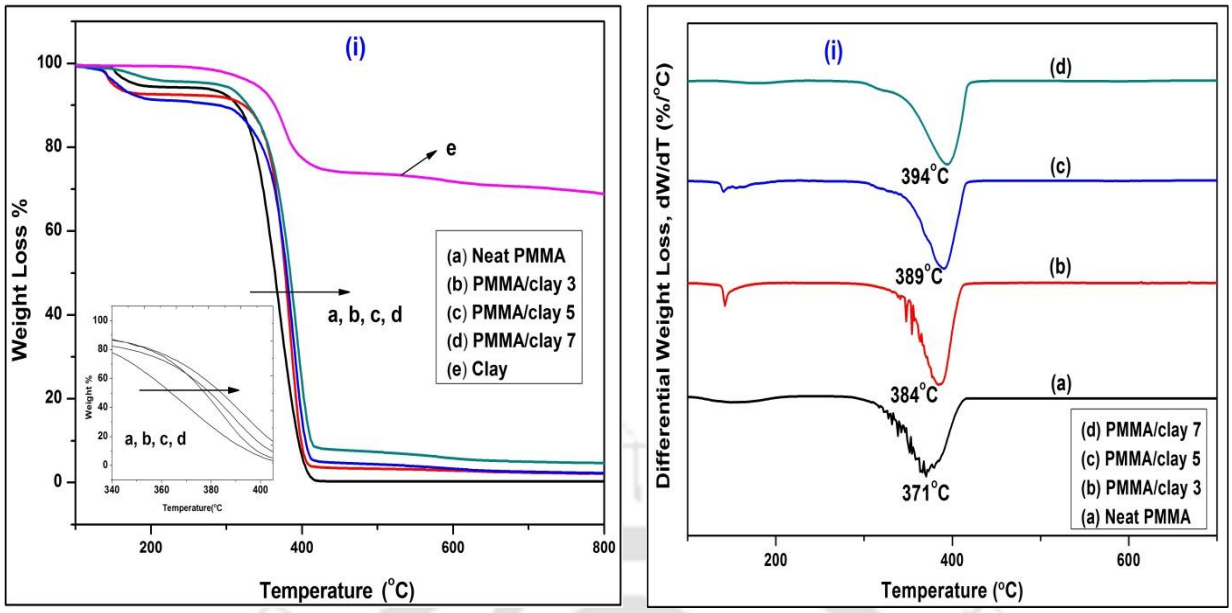

Figure 5.6 (i) TGA and DTG curves of PMMA/clay nanocomposites

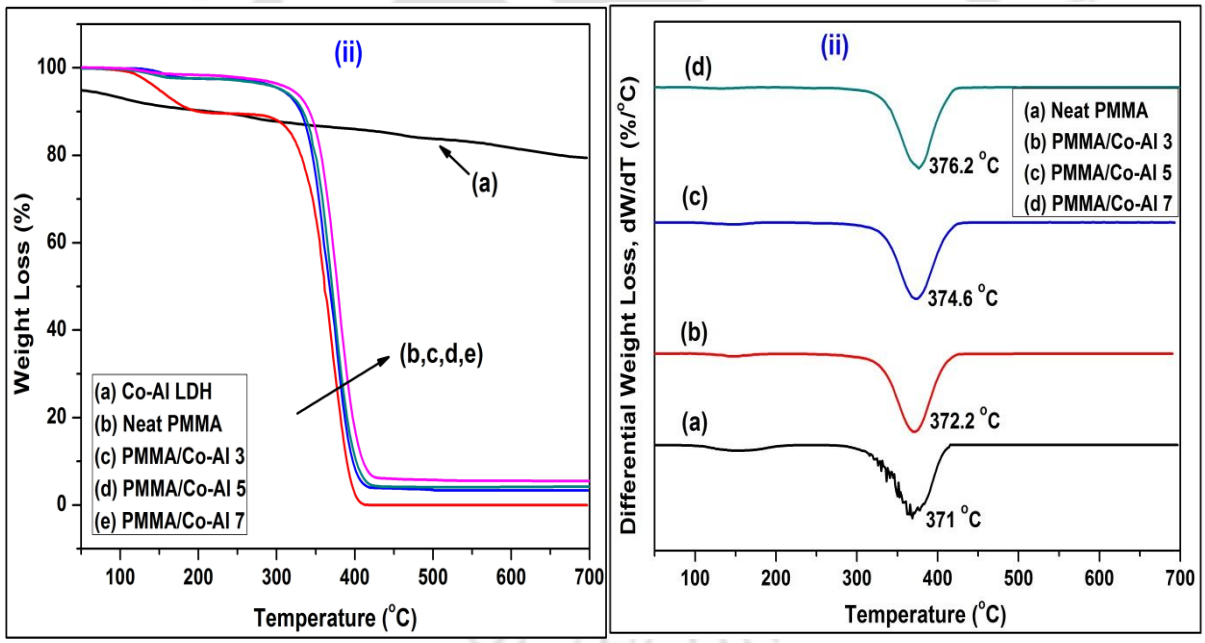

Figure 5.6 (ii) TGA and DTG curves of PMMA/Co-Al LDH nanocomposites

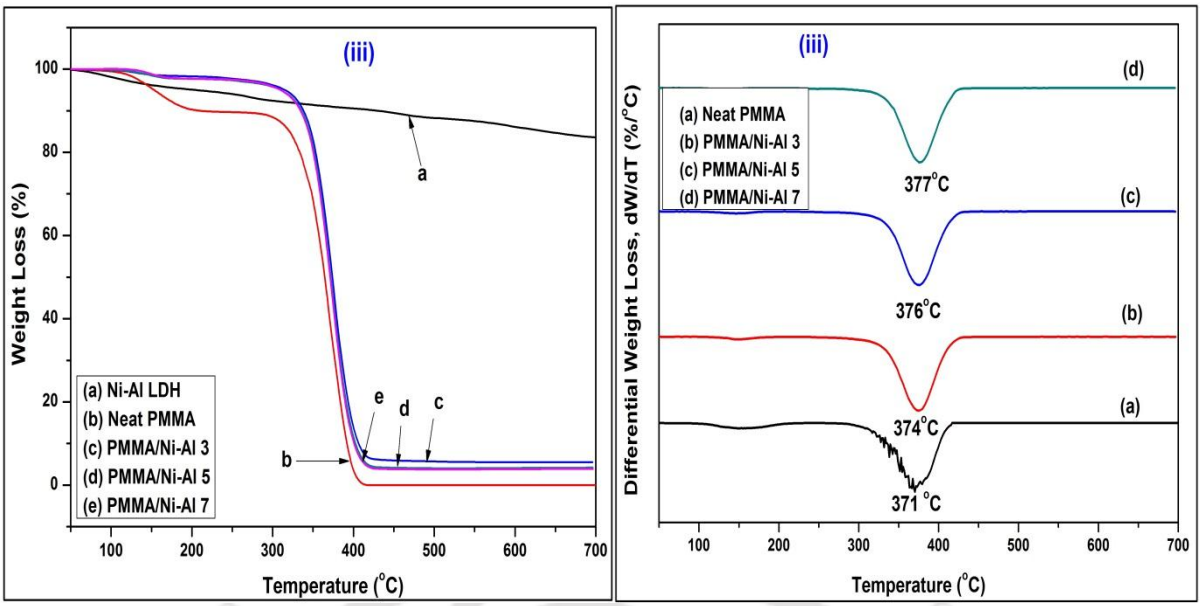

Figure 5.6 (iii) TGA and DTG curves of PMMA/Ni-Al LDH nanocomposites

Figure 5.6 (i) (a-e) shows the characteristic TGA curves of PMMA nanocomposites. The relatively low weight loss in the temperature range 100–200 ^{o}C observed in the TGA curves could be attributed to the evaporation of solvent molecules trapped by the polymer chains or into the organophilic interlayer space of the clay. The main degradation (300-420 ^{o}C) occurs due to the polymer chain degradation with production of the products including solid and gases. The degradation of the nanocomposites differs with organoclay content and the contribution to total apparent activation energy becomes more significant. The PMMA nanocomposites exhibit superior thermal stability compared to neat PMMA, which is confirmed by the shifting of the TGA curve of the nanocomposites towards the right of the TGA curve of neat PMMA. When 50% weight loss ($T_{50\%}$) is selected as a point of comparison, the decomposition temperature of PMMA nanocomposite is found to be 13-20 ^{o}C higher than that of neat PMMA and increases with an increase in the clay content. This beneficial effect is because of the hinder effect of clay platelets for the diffusion of volatile products throughout the composite material. The clay acts as a heat barrier, which enhances the overall thermal stability of the system. Further, these assist in the formation of char after thermal decomposition. The thermal stability of nanocomposites obtained in this study is better than the stability of PMMA nanocomposites prepared with other organoclays (Krajnc and Sebenik, 2009; Oral et al., 2009). Krajnc and Sebenik, (2009) have observed around 7 and 16 ^{o}C improvement in the decomposition temperature ($T_{50\%}$) for PMMA nanocomposite

containing 10 wt.% OMMT content (Cloisite15A) over PMMA, which was prepared by melt compounding, and bulk polymerization method, respectively. In another work reported by Oral et al., (2009), the PMMA nanocomposite with 5 wt.% OMMT content exhibited about 3^{o}C enhancement in the thermal decomposition temperature ($T_{50\%}$) relative to that of pristine PMMA.

The enhanced thermal stability of the nanocomposites can also be obtained from the DTG curve as shown in Figure 5.6(i). The peak indicates the maximum degradation temperature (T_{max}). It is clear from this figure that the maximum degradation temperature shifts towards the higher value with an increase in the clay content. The T_{max} value for neat PMMA is 371 ^{o}C while the T_{max} value for the nanocomposites is found to be 384 ^{o}C, 389 ^{o}C and 394 ^{o}C, respectively, for 3, 5 and 7% clay content. This confirms further that the incorporation of nanoclay into polymer matrix enhances the thermal stability of the nanocomposites. Therefore, an improvement in the thermal stability will lead to the better service performance of the nanocomposites at an elevated temperature. Around 10-30 wt.% of inorganic materials (glass fiber, talk, etc.) are usually utilized to reinforce a polymer. When nanoclay is used as filler, about 1-5 wt.% is enough to improve the properties of a matrix polymer. The reason is supposed to be the molecular level dispersion and high aspect ratio (defined as the ratio between length and thickness of the clay platelets) of the clay. It is well documented that as the aspect ratio of the layered nano fillers increases, the enhancement in the properties of polymer matrix also increases (Yano et al., 1997). Those facts maximize the available surface area of the reinforcing phase between the clay and the polymer matrix, and lead to excellent properties.

The TGA curves of Co-Al LDH, Ni-Al LDH, neat PMMA and PMMA/LDH nanocomposites are represented in Figure 5.6(ii) and (iii). The main weight loss of organically modified Co-Al LDH takes place due to the loss of inter layer water molecules, destruction of alkyl chains of the SDS molecule and loss of hydroxide from LDH layers. The thermal degradation of neat PMMA mainly occurs in the temperature range of 303-420 ^{o}C and no residues are left above 430 ^{o}C. Generally, PMMA nanocomposites exhibit weight loss in two main steps. The initial weight loss occurred majorly in the temperature range of 120-250 ^{o}C is due to vaporization of physically absorbed water molecule in the intercalated layers, thermal decomposition of alkyl chains of the SDS molecule and loss of hydroxide from LDH layers (Du et al., 2009). The second step of weight loss starts from 250-440 ^{o}C due to the thermal degradation of PMMA as well as the generation of black carbonized

residues. The thermal degradation rate of PMMA/LDH nanocomposites is much slower in this step when compared with neat PMMA. A slow degradation rate of PMMA nanocomposites is attributed to the restrained effect of LDH layers for diffusion of volatile outputs throughout the nanocomposite samples. Above ~500 ^{o}C, all the graphs become smooth because only inorganic residues remain at that temperature. When 15% weight loss is selected as a point of consideration, the degradation temperature of neat PMMA, PMMA/Co-Al LDH 3, PMMA/Co-Al LDH 5 and PMMA/Co-Al LDH 7 are 320, 342, 343.4 and 345.5 ^{o}C, respectively. This result clearly shows the enhanced thermal decomposition temperature of PMMA nanocomposites in comparison with neat PMMA. At 15% weight loss, the decomposition temperatures of PMMA/Co-Al LDH nanocomposites is 22-25 ^{o}C higher than that of pristine PMMA. A similar type of result was also reported for PMMA/ZnAl LDH nanocomposites (Chen and Qu, 2005). When 15% weight loss was selected as a point of comparison, PS nanocomposites prepared with 5 wt.% LDH showed 2-7 ^{o}C improvement in thermal stability compared to other PS nanocomposites synthesized with 5 wt.% Cu-Al, Ni-Al and Cu-Fe LDHs (Sahu and Pugazhenthi, 2011). Unnikrishnan et al., (2011) reported about 2-16 ^{o}C enhancement in the thermal degradation temperature for PMMA/organoclay nanocomposites over pristine PMMA at 10% weight loss as a point of reference. In our previous work (Kumar et al., 2014), PMMA/organoclay nanocomposites prepared by melt blending technique demonstrated around ~9 ^{o}C improvement in the thermal decomposition temperature over neat PMMA when 15% weight loss was considered as a point of comparison. The comparison analysis points out that PMMA/Co-Al LDH nanocomposites have better thermal stability compared to other PMMA and PS based nanocomposites. When 50% weight loss is selected as a point of consideration, the degradation temperature of PMMA, PMMA/Co-Al LDH 3, PMMA/Co-Al LDH 5 and PMMA/Co-Al LDH 7 are estimated to be 364.2, 370.5, 371.7 and 374 ^{o}C. The decomposition temperature of PMMA nanocomposites is observed to be 6-9 ^{o}C greater than that of neat PMMA. For PMMA/Ni-Al LDH nanocomposites, the decomposition temperature of neat PMMA, PMMA/Ni-Al LDH 3, PMMA/Ni-Al LDH 5 and PMMA/Ni-Al LDH 7 is 320, 345, 346 and 348 ^{o}C, respectively at 15% weight loss as a reference point. Similar type of results is also observed when 50% weight loss is chosen as a point of comparison. The decomposition temperature of neat PMMA, PMMA/Ni-Al LDH 3, PMMA/Ni-Al LDH 5 and PMMA/Ni-Al LDH 7 are 364.2, 372, 373 and 376 ^{o}C respectively at $T_{50\%}$. An improved thermal resistance may be caused by the inhibition of out-diffusion of the volatile gas from thermally decomposed materials because the exfoliated LDH layers, which are well dispersed in the PMMA matrix, act as a

gas barrier that reduces the permeability of the volatile gas (Wang and Zhang, 2004). The enhanced thermal stability is also supported by the TGA derivative curves displayed in Figure 5.6 (ii) (b-d). The entire TGA derivative curves for PMMA nanocomposites are migrated towards higher side of pristine PMMA, demonstrating the enhanced thermal stability that will promote to superior work performance of the nanocomposites at higher temperature. The complete thermal analysis of nanoclay, Co-Al LDH, Ni-Al LDH and their corresponding PMMA nanocomposites are given in Table 5.3.

Table 5.3 TGA and DSC results of various PMMA nanocomposites

Sample Name	Temperature at 15 wt.% degradation in ^{o}C (T_{15})	Temperature at 50 wt.% degradation in ^{o}C (T_{50})	Temperature at maximum rate of degradation ^{o}C (T_{max})	Glass transition temperature in ^{o}C (T_g)
Neat PMMA	320	364	371	110.5
PMMA/clay 3	345	377	384	111.4
PMMA/clay 5	330	379	389	111.5
PMMA/clay 7	345	384	394	113.1
PMMA/Co-Al 3	342	370.5	372.2	112.6
PMMA/Co-Al 5	343.4	371.7	374.6	113.7
PMMA/Co-Al 7	345.5	374	376.2	114.6
PMMA/Ni-Al 3	345	372	374	112.6
PMMA/Ni-Al 5	346	373	376	112.9
PMMA/Ni-Al 7	348	376	377	113.8

5.3.6 Differential Scanning Calorimetry

Differential scanning calorimetry (DSC) is used to study the phase transitions like fusion, crystallization and glass transition temperature (T_g). To investigate the mobility of polymer chains in term of its T_g in the clay layers, DSC study of neat PMMA and PMMA/clay nanocomposites has been carried out at a heating rate of 5 ^oC/min and the results are reported in Figure 5.7(i). The T_g value for neat PMMA is 110.5 ^oC and the maximum increase of 2.6 ^oC is noticed with the clay loading of 7% (113.1 ^oC). As evidenced, the T_g increases with increasing clay content from 3 to 7 wt.%. These results infer that the prepared PMMA nanocomposites have a larger interfacial area between the polymer matrix and the clay to influence the T_g (Krajnc and Sebenik, 2009). The improvement in the T_g is owing to the clay nano platelets with high aspect ratios in the PMMA matrix, as the segmental motions of the polymer chains are restricted at the organic-inorganic interface, due to the confinement of the PMMA chains between the silicate layers and the silicate surface-polymer interaction in the nanocomposites (Huang et al., 2001; Tsai et al., 2009; Oral et al., 2009). The chemical bonding at the interface of the nanoclay layer and the PMMA matrices reduces the relaxation mobility of the polymer at the interface region.

Figure 5.7 (ii) and (iii) represents the DSC curves of PMMA/Co-Al LDH and PMMA/Ni-Al LDH nanocomposites respectively. The glass transition values of neat PMMA, PMMA/Co-Al LDH 3, PMMA/Co-Al LDH 5 and PMMA/Co-Al LDH 7 are 110.5, 112.6, 113.7 and 114.6 ^oC, respectively. It is noticeable from the DSC analysis that T_g of PMMA/Co-Al LDH 7 is 4 ^oC higher than that of pristine PMMA. The glass transition temperature (T_g) values of neat PMMA, PMMA/Ni-Al LDH 3, PMMA/Ni-Al LDH 5 and PMMA/Ni-Al LDH 7 are 110.5, 112.6, 113 and 114 ^oC, respectively. It can be seen from the DSC analysis that T_g of PMMA/Ni-Al LDH 7 is 3 ^oC higher than the neat PMMA. The increase in T_g value is due to the restricted movements of PMMA chains between the LDH interlayer. Even if only one end of the PMMA chain is constrained by LDH layers, it will still increase the T_g value. It is well documented in the literature (Li et al., 2008; Stretz and Paul, 2005) that T_g of nanocomposite depends on various factors, such as nature of modifier, weight of clay loading, basal spacing and arrangement of clay layers. Unniskrishnan et al., (2011) and Mohanty et al., (2010) also observed marginal improvements in T_g for PMMA/MMT (1.1-1.7 ^oC) and PMMA-g-MA/B109 (0.45 ^oC) nanocomposites.

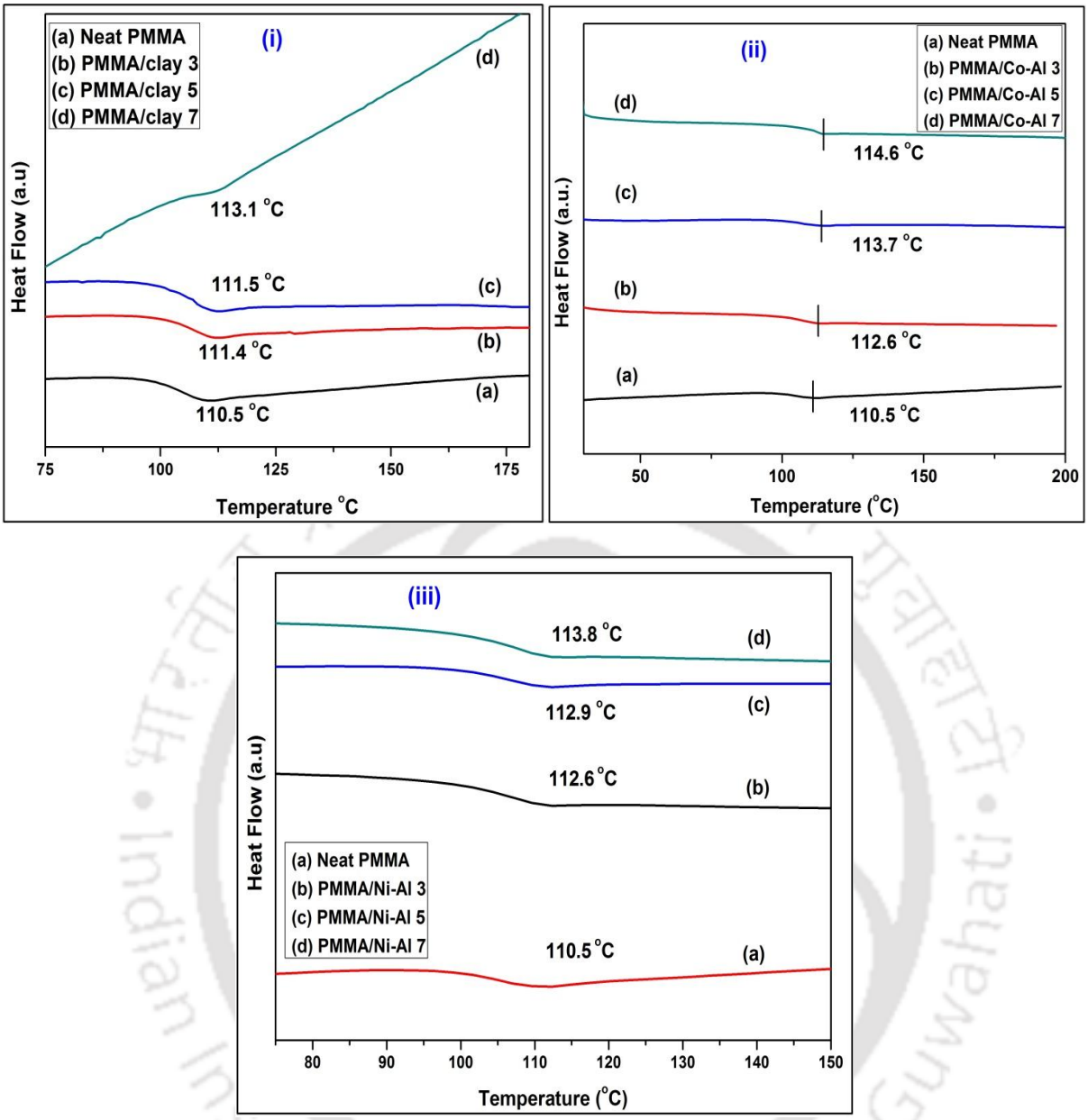

Figure 5.7 DSC curves of (i) PMMA/clay, (ii) PMMA/Co-Al LDH and (iii) PMMA/Ni-Al LDH nanocomposites

5.3.7 AFM Analysis

The AFM analysis of different PMMA nanocomposite was carried out to access the effect of nanoparticle loading on the surface morphology of the nanocomposite film. The incremental addition of the clay or LDH led to increase the surface roughness of all nanocomposite films. The 3D pictorial representation of each sample is displayed in Figure 5.8 (i-iii). It is clearly seen that pits are present in all the images. The minimum surface roughness is observed for

the PMMA/Co-Al LDH nanocomposite with 3 wt.% loading, whereas maximum roughness is seen in case of PMMA/clay nanocomposite with 7 wt.% loading. To confirm measurement repeatability, each nanocomposite (for 3-7 wt.% loading) film is scanned in two separate location. The 2D images of different PMMA nanocomposites are given in appendix.

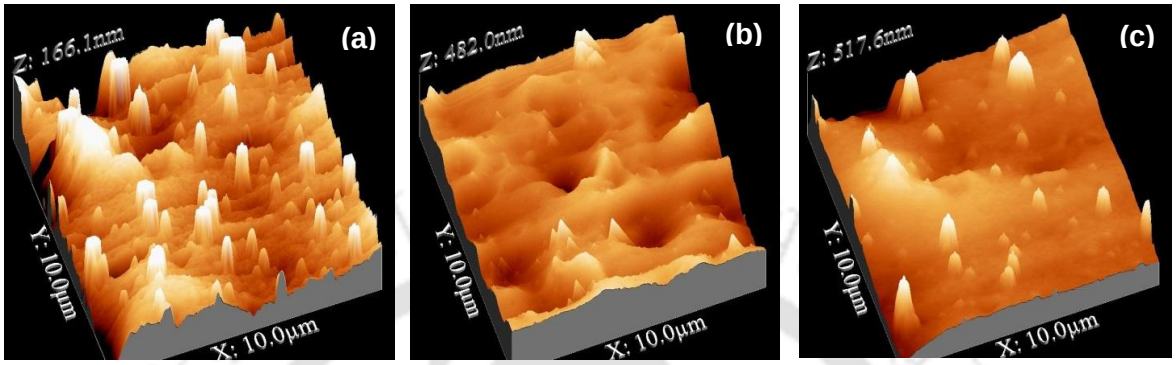

Figure 5.8(i) AFM images of (a) PMMA/clay 3, (b) PMMA/clay 5 and (c) PMMA/clay 7 nanocomposites

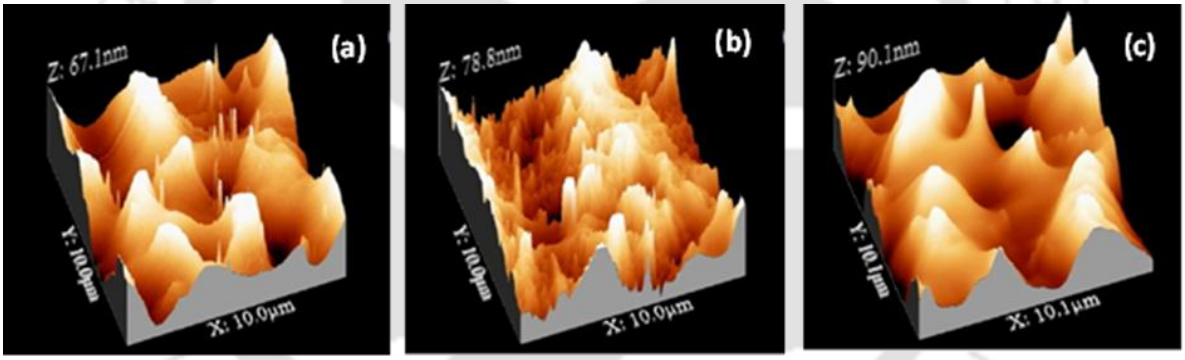

Figure 5.8(ii) AFM images of (a) PMMA/Ni-Al 3, (b) PMMA/Ni-Al 5 and (c) PMMA/Ni-Al 7 nanocomposites

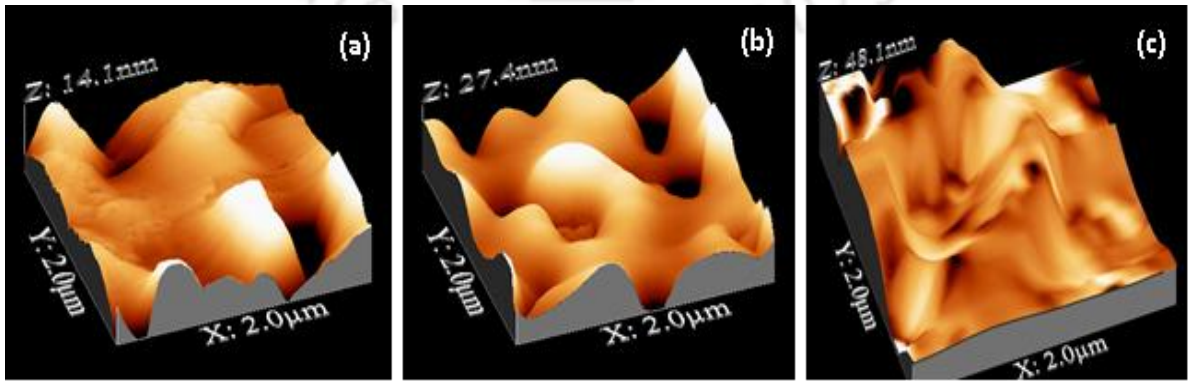

Figure 5.8(iii) AFM images of (a) PMMA/Co-Al 3, (b) PMMA/Co-Al 5 and (c) PMMA/Co-Al 7 nanocomposites

5.3.8 Hardness

Hardness is the resistance of a polymeric material to localized deformation. The deformation can arise either from indentation, scratching, cutting or bending. Hardness of polymeric materials i.e. thermoplastic and thermoset, and other hard elastomers are measured in Shore D scale. The Shore D hardness (ASTM D2240) of neat PMMA (thermoplastic) and its nanocomposites with different nanofiller loading is shown in Figure 5.9. Hardness test shows improved hardness for different PMMA nanocomposites as compared to neat PMMA. With an increase in the clay or LDH content in the PMMA matrix, hardness of PMMA nanocomposites increases gradually. Hardness data is taken from fifteen different part of each film sample and finally average value is shown in the Figure 5.9. The average Shore D values of PMMA/clay nanocomposites are found to be 53, 58, 60, 62 for neat PMMA, PMMA-3, PMMA-5 and PMMA-7, respectively. The hardness of PMMA/Co-Al LDH nanocomposites is 54, 56 and 58 for LDH loading of 3, 5 to 7 wt.%, respectively. Similarly, PMMA/Ni-Al LDH nanocomposites exhibit 55, 56, 58 Shore D hardness for PMMA/Ni-Al LDH 3, PMMA/Ni-Al LDH 5 and PMMA/Ni-Al LDH 7, respectively. The reason behind this improved hardness is due to the presence of exfoliated nanofiller layers in PMMA matrix. The clay or LDH layers are uniformly distributed throughout the PMMA matrix. The clay layers are having higher interfacial/contact area with PMMA matrix, hence effectively restricts indentation. This causes increased hardness of the nanocomposites. The PMMA-7 nanocomposites containing 7 wt.% of clay shows a maximum hardness increase of 16% as compared to pure PMMA.

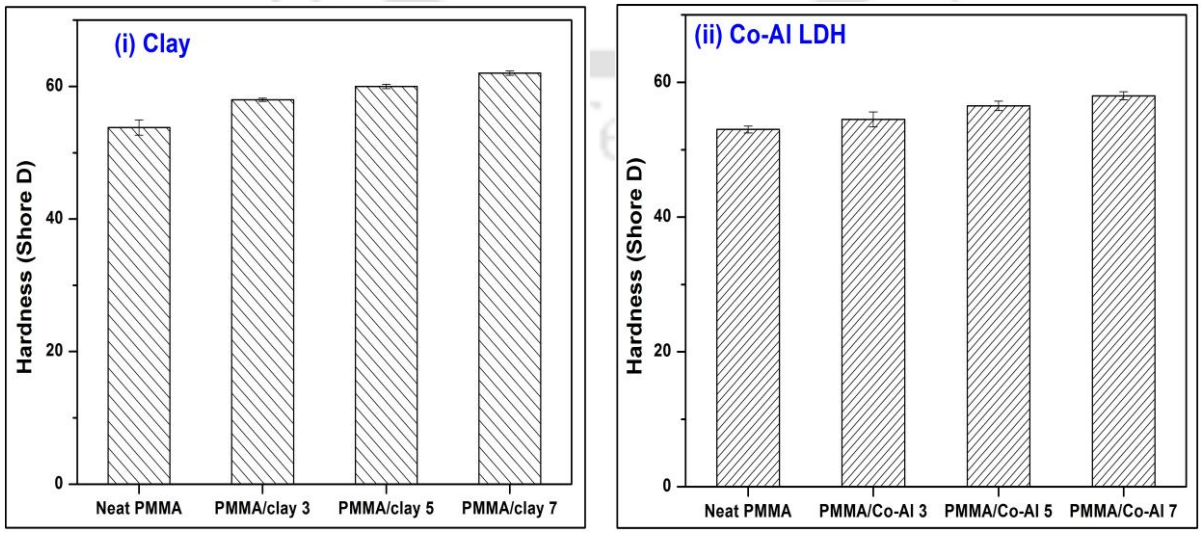

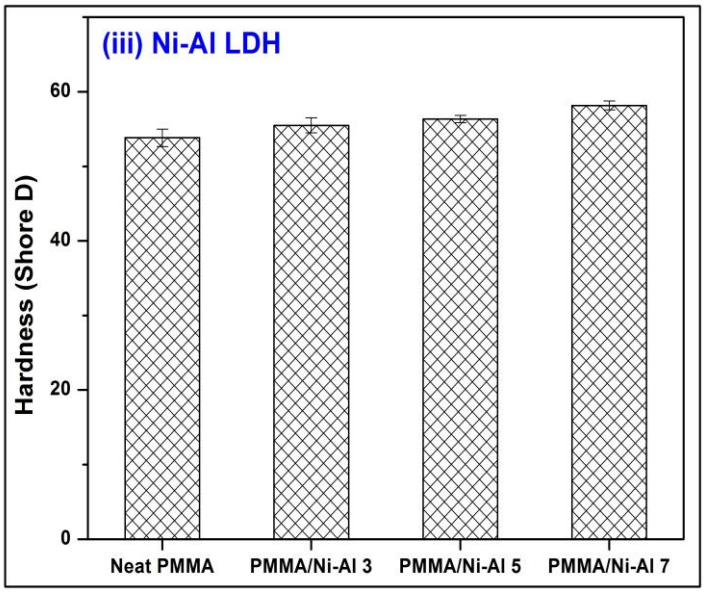

Figure 5.9 Hardness of (i) PMMA/clay, (ii) PMMA/Co-Al LDH, (iii) PMMA/Ni-Al LDH nanocomposites

5.3.9 Water Uptake Test

The films of different PMMA nanocomposite are tested for water intake capacity. The water uptake tests show that, the water uptake capacity of PMMA nanocomposites decreases as the amount of clay or LDH loading increases. The water uptake capacity of neat PMMA is 1.11%, while the water uptake capacities of PMMA/Co-Al LDH nanocomposite with 3, 5 and 7 wt.% LDH loading are 0.86, 0.73 and 0.66%, respectively. Similarly, PMMA/Ni-Al LDH nanocomposites demonstrate 0.86, 0.82 and 0.63% water-uptake capacity for different loading of LDH (3-7 wt.%). The hydrophilic nature of LDH is reduced with organic modification of LDH using SDS as modifier. Even though neat PMMA is hydrophobic in nature, the presence of modified LDH acts as an additional barrier against the water intake capacity of nanocomposite and making it more water resistant.

5.3.10 Optical Test

The optical test of different polymer nanocomposites films has performed using digital camera. It is clearly noticed from the images that transmittance is altered by the presence of different nanofillers and reduced as the loading increases. It is also observed that 3 wt.% loading of nanofiller has little influence on transmittance. The shape, dispersion and loading of nanofiller have prominent effect on the optical properties of nanocomposites films. The

layers of clay or LDH nanofiller is strong enough to reduce the transmittance of polymer films and found to be maximum at 7 wt.% loading of nanofiller (see Figure 5.10).

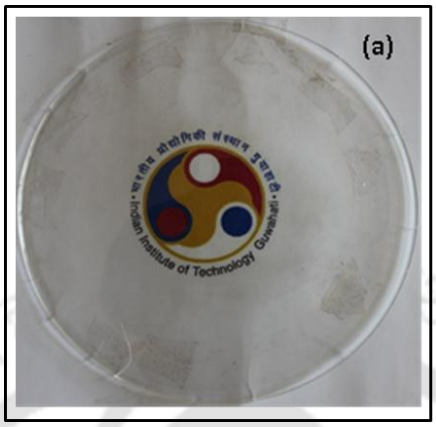

Neat PMMA

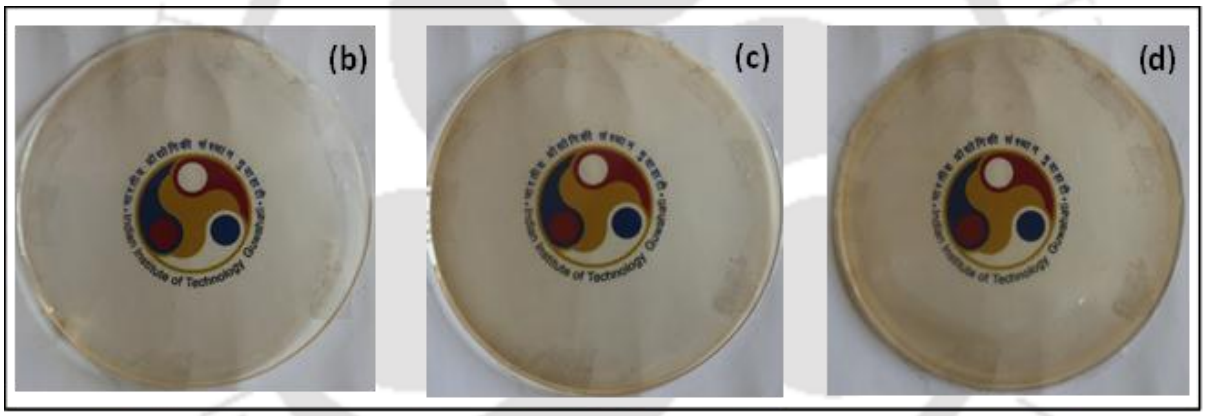

(i) PMMA/clay nanocomposites

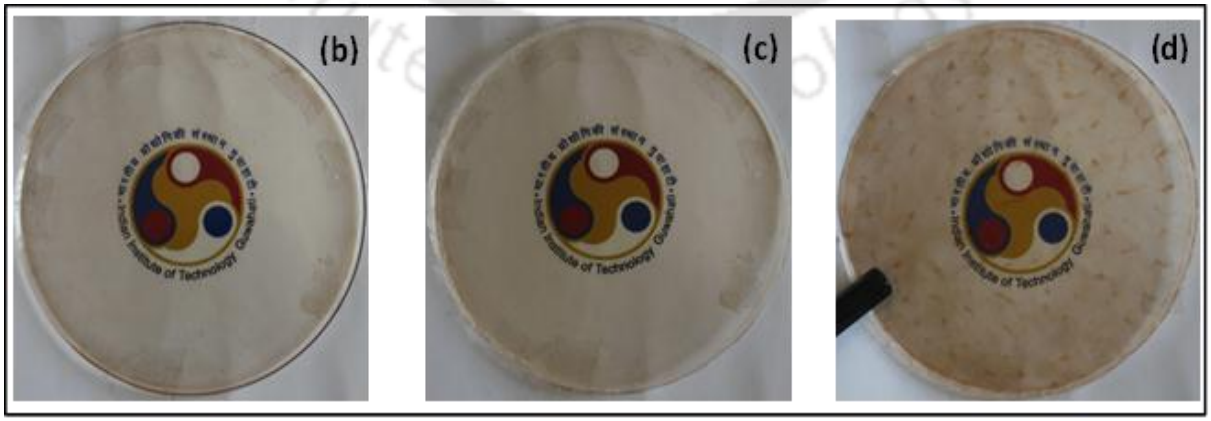

(ii) PMMA/Co-Al LDH nanocomposites

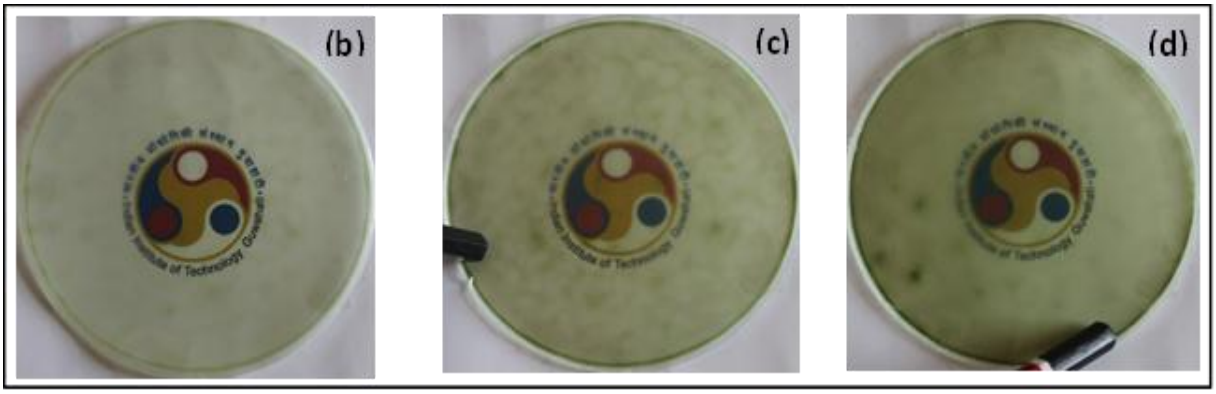

(iii) PMMA/Ni-Al LDH nanocomposites

Figure 5.10 Transparency of neat PMMA, (i) PMMA/clay, (ii) PMMA/Co-Al LDH and (iii) PMMA/Ni-Al LDH nanocomposites with (b) 3, (c) 5 and (d) 7 wt.%

5.3.11 WVTR Analysis

The water vapor transmission rate (WVTR) is also known as moisture vapor transmission rate (MVTR), and is an important parameter for food packaging application. It is quantified by the water vapor permeability coefficient (WVPC), which indicates the amount of water vapor that permeates per unit of area and time in a packing material. From the above thermal characterization results, it is observed that the different polymer nanocomposites exhibit enhanced properties at higher loading. Therefore, the water vapor transmission test was carried out using PMMA nanocomposite sample with 7 wt.% loading of nanofiller. It is well known that LDHs or silicates are able to reduce the transmission rate of packing film. The water vapor transmission rate for neat PMMA, PMMA/clay, PMMA/Co-Al LDH, PMMA/Ni-Al LDH nanocomposites with 7 wt.% loading of nanofiller is found to be 73, 34.2, 46.9 and 15.2 gm/m^2/day, respectively. The results suggest that transmission rate is reduced by the addition of different nanofiller. The reduced transmission rate is related to various factors such as shape and loading of nanofiller, degree of exfoliation and porosity that will influence the tortuous path. It is clearly shown in Figure 5.11 that how layered silicate or LDH nanoplatelets hinder the permeation path of polymer film that results in reduced transmission rate. Similarly, the thermal decomposition temperature of polymer nanocomposite is also enhanced due to the addition of nanoparticles.

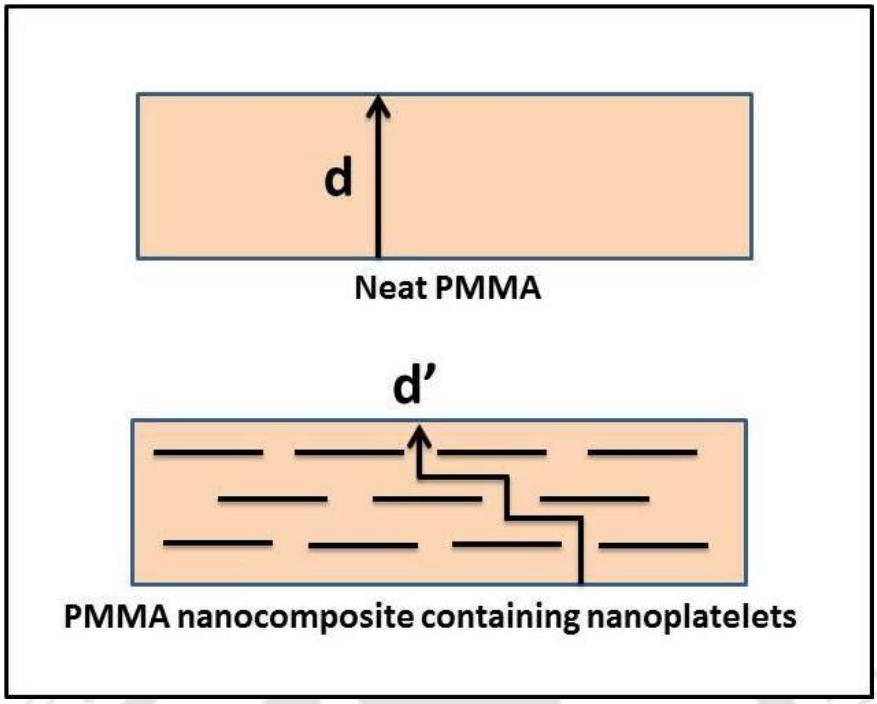

Figure 5.11 Permeation path imposed by nanoparticles imbedded in polymer films

5.3.12 Kinetic Analysis

Figure 5.12 (a-c) shows all the linear fitted graph of PMMA and its nanocomposites with various concentration of clay or LDH. The calculated reaction order at the best *R* value is considered as the reaction order for that sample. Afterwards, the activation energy and the pre-exponential factor are estimated from the slope and intercept of fitted straight line. The activation energy of neat PMMA, PMMA/clay nanocomposites samples having 3, 5, 7 wt.% is 99.4, 130.9, 137.7 and 149.2 kJ/mol, respectively. Similarly, PMMA/Co-Al LDH nanocomposite samples containing 3, 5, 7 wt.% LDH is 158.1, 163.3 and 175.5 kJ/mol, respectively. For PMMA/Ni-Al LDH samples, it is in the range of 167-170 kJ/mol. It is evident from the Table 5.4 that E_a of PMMA/Co-Al LDH nanocomposite is 58-76 kJ/mol higher than that of neat PMMA. The PMMA/Co-Al LDH 7 has the highest activation energy value among all other samples. Chen and Wang, (2007) also reported the improvement in activation energy of nanocomposites as compared to neat polymer, which is in accordance with this work.

Table 5.4 Kinetic parameters of different samples at better correlation coefficient obtained from Coats-Redfern method

Sample	E_a(kJ/mol)	A	n	R
Neat PMMA	99.4	3.862×10^7	0.6	0.996
PMMA/clay-3	130.9	6.980×10^9	0.7	0.991
PMMA/clay-5	137.7	9.915×10^9	0.7	0.996
PMMA/clay-7	149.2	4.413×10^{10}	0.7	0.991
PMMA/Co-Al LDH 3	158.1	2.731×10^{12}	1.1	0.998
PMMA/Co-Al LDH 5	163.3	6.407×10^{12}	1.1	0.998
PMMA/Co-Al LDH 7	175.5	6.274×10^{13}	1.2	0.998
PMMA/Ni-Al LDH 3	167	1.190×10^{13}	1.1	0.998
PMMA/Ni-Al LDH 5	167.1	1.243×10^{13}	1.1	0.998
PMMA/Ni-Al LDH 7	170	1.942×10^{13}	1.1	0.998

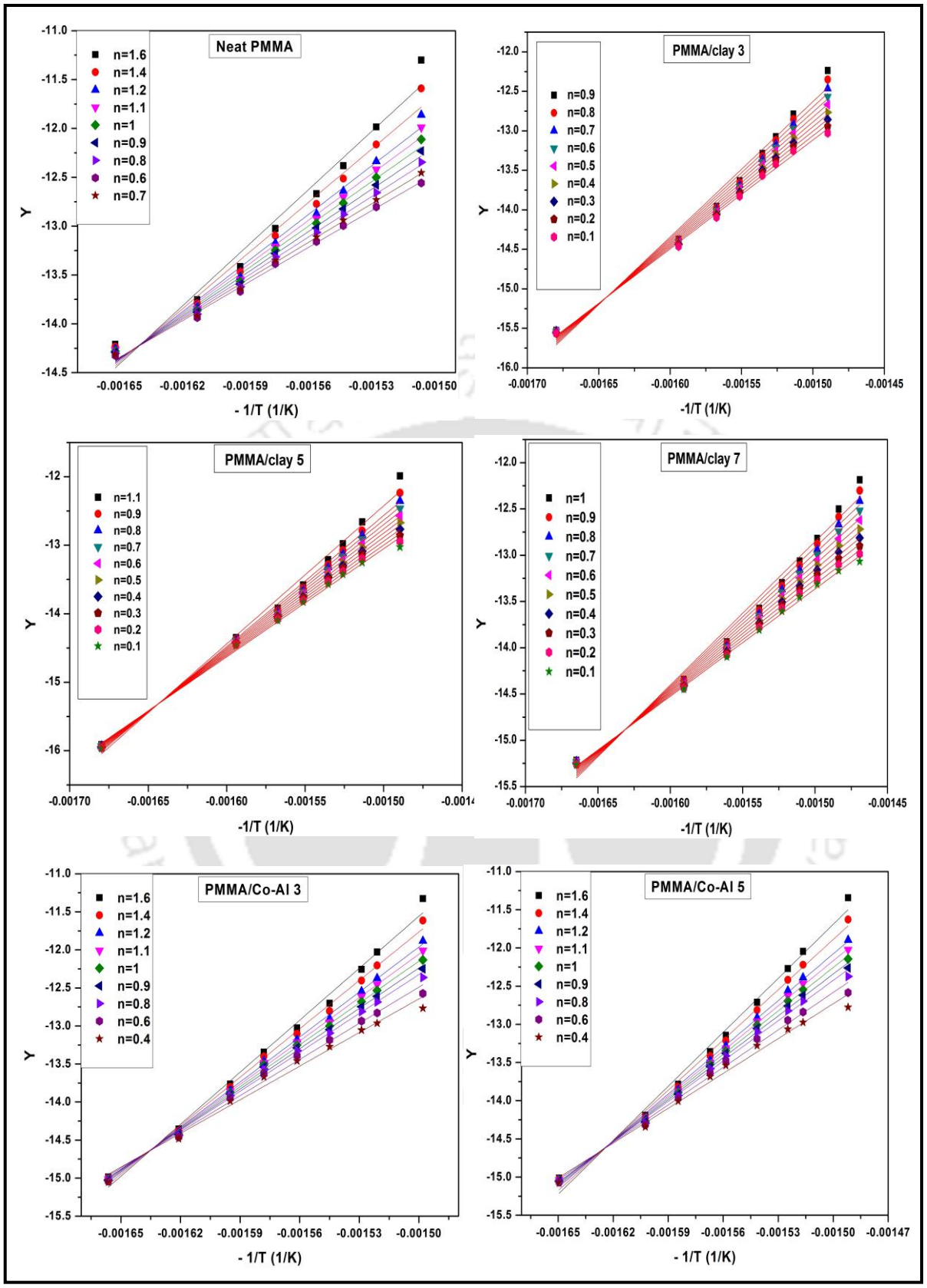
Neat PMMA
n=1.6
n=1.4
n=1.2
n=1.1
n=1
n=0.9
n=0.8
n=0.6
n=0.7
Y
- 1/T (1/K)
PMMA/clay 3
n=0.9
n=0.8
n=0.7
n=0.6
n=0.5
n=0.4
n=0.3
n=0.2
n=0.1
Y
-1/T (1/K)
PMMA/clay 5
n=1.1
n=0.9
n=0.8
n=0.7
n=0.6
n=0.5
n=0.4
n=0.3
n=0.2
n=0.1
Y
-1/T (1/K)
PMMA/clay 7
n=1
n=0.9
n=0.8
n=0.7
n=0.6
n=0.5
n=0.4
n=0.3
n=0.2
n=0.1
Y
-1/T (1/K)
PMMA/Co-Al 3
n=1.6
n=1.4
n=1.2
n=1.1
n=1
n=0.9
n=0.8
n=0.6
n=0.4
Y
- 1/T (1/K)
PMMA/Co-Al 5
n=1.6
n=1.4
n=1.2
n=1.1
n=1
n=0.9
n=0.8
n=0.6
n=0.4
Y
- 1/T (1/K)

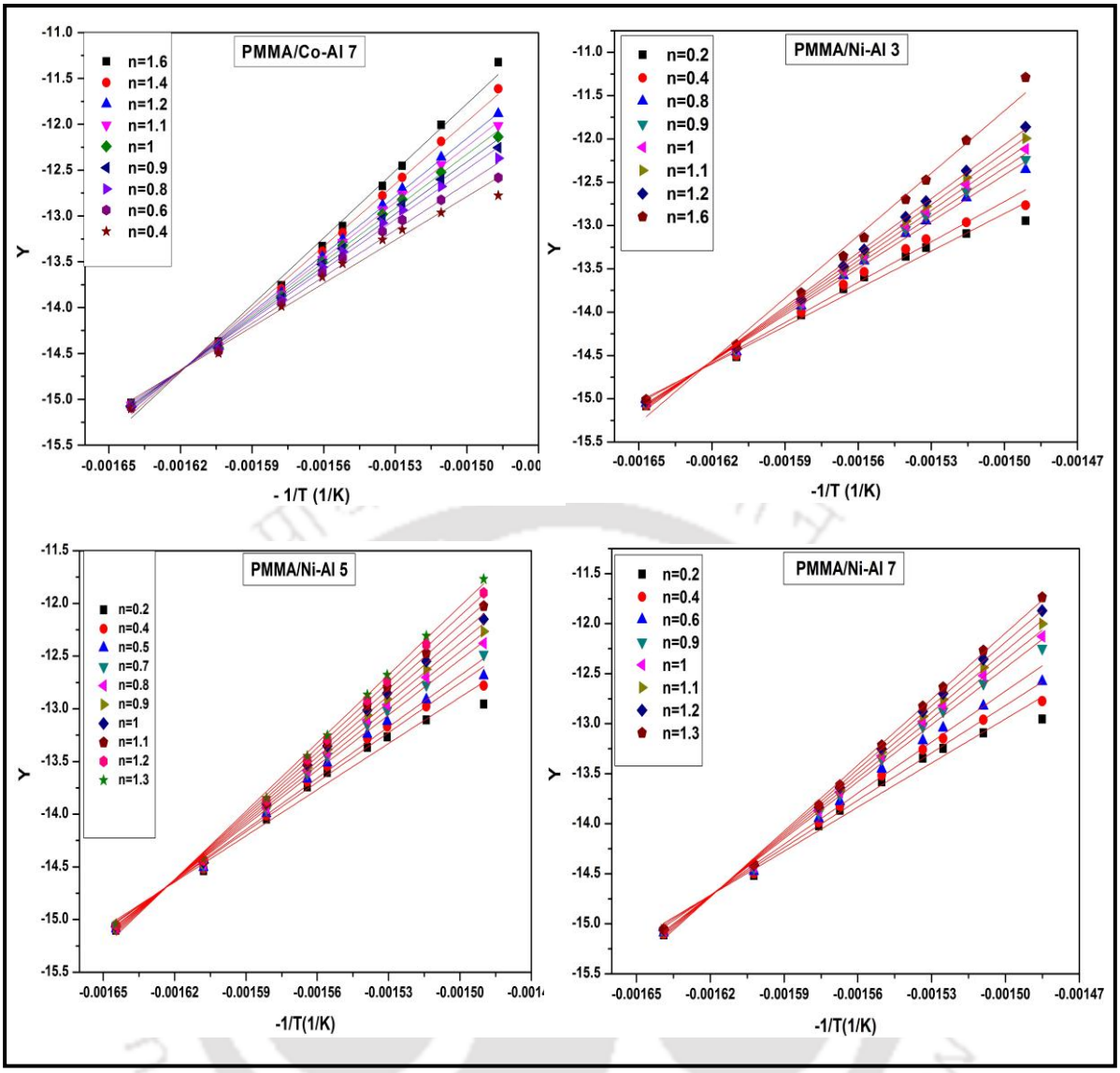

Figure 5.12 Determination of kinetic parameters by plots of the left part in equation 3.10 against -1/T using Coats-Redfern method for various PMMA nanocomposites

The kinetic parameters obtained from Coats-Redfern method are utilized to estimate the different reaction mechanism in Criado method. Figure 5.13 (a-c) displays the Z(α)-α master and experimental curve of neat PMMA and PMMA nanocomposites with 3, 5 and 7 wt.% concentration. It is observed that for neat PMMA, the experimental Z(α)-α curve initially follows F1 reaction mechanism (random nucleation having one nucleus on individual particle) with lower α value (α=0.15-0.4) and then it deviates from F1 reaction mechanism to A4 mechanism (nucleation and growth) at higher α value (α=0.8-0.95). In case of Co-Al LDH and Ni-Al LDH based PMMA nanocomposites, Z(α)-α experimental curves follow F1 reaction mechanism in the entire range of α value.

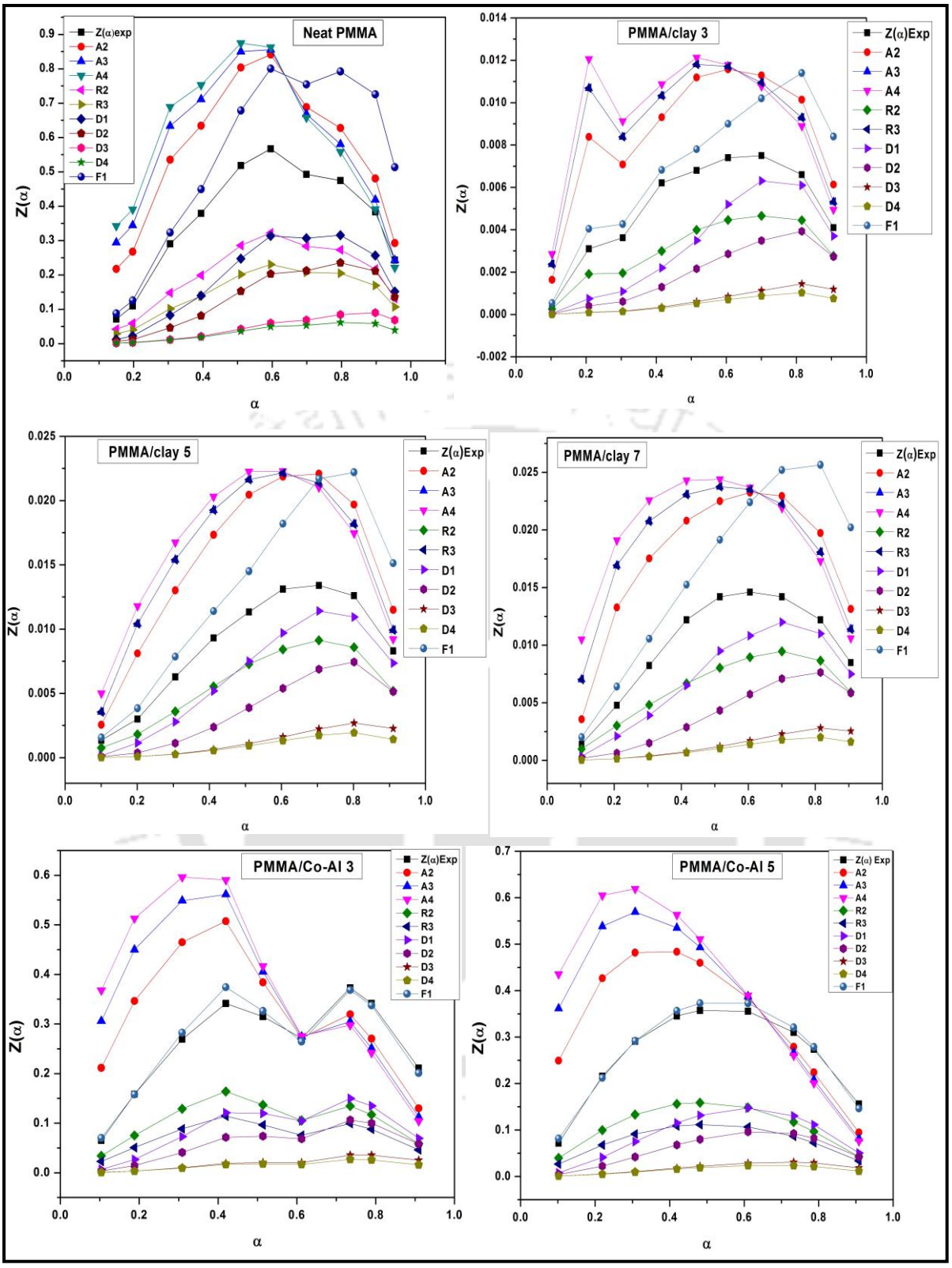
Neat PMMA
Z(α)exp
A2
A3
A4
R2
R3
D1
D2
D3
D4
F1
Z(α)
α
PMMA/clay 3
Z(α)Exp
PMMA/clay 5
PMMA/clay 7
PMMA/Co-Al 3
PMMA/Co-Al 5
Z(α) Exp

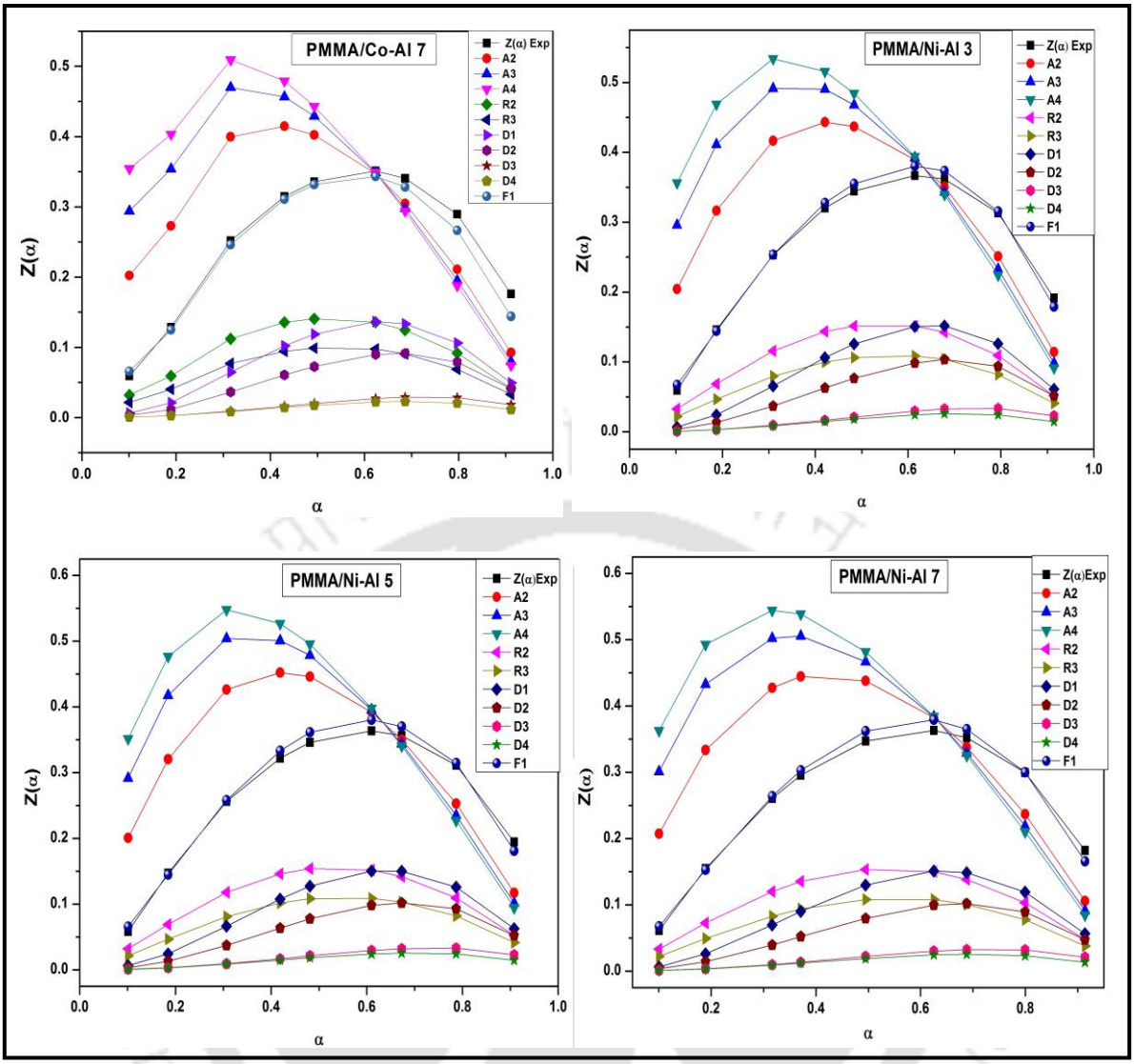

Figure 5.13 Determination of the thermal degradation mechanism by plotting Z(α) versus α using Criado model for various PMMA nanocomposites

The integral procedure decomposition temperature (IPDT) method was employed to estimate the thermal stability of different nanocomposites. All the nanocomposites exhibit higher IPDT value as compared to neat PMMA, which indicates the enhanced thermal stability of the nanocomposites. The IPDT values of neat PMMA and PMMA nanocomposites with 3, 5 and 7 wt.% clay loading are 351.5, 392.3, 401.2 and 405.7 ^{o}C (see, Table 5.5). The PMMA/Co-Al LDH nanocomposites exhibit 397, 412.6 and 421.1 ^{o}C for various compositions. Similar findings are also obtained for Ni-Al LDH based nanocomposites, denoting 399.4, 406.7, 423.6 ^{o}C for 3, 5 and 7 wt.%, respectively.

Table 5.5 IPDT results of different PMMA nanocomposite samples

Samples	Initial Temperature (T_i) ^oC	Final Temperature (T_f) ^oC	IPDT (^oC)
Neat PMMA	50	700	351.5
PMMA/clay-3	50	700	392.3
PMMA/clay-5	50	700	401.2
PMMA/clay-7	50	700	405.7
PMMA/Co-Al LDH 3	50	700	397.0
PMMA/Co-Al LDH 5	50	700	412.6
PMMA/Co-AlLDH 7	50	700	421.1
PMMA/Ni-Al LDH 3	50	700	399.4
PMMA/Ni-Al LDH 5	50	700	406.7
PMMA/Ni-AlLDH 7	50	700	423.6

5.3.13 Rheological properties

The polymer contains both the property i.e. viscous and elastic nature and thus it possesses the viscoelastic characteristic. The storage modulus (*G'*) represents the elastic or stiffness i.e. solid like behaviour and it is associated with energy stored in the material. The loss modulus (*G"*) denotes the viscous i.e. liquid like behaviour of the polymer melts and it is related to energy dissipation. It is essential to analyze the viscoelastic behaviour of polymer nanocomposites as it is very important parameter in processing condition i.e. extrusion, injection. It is also suggested that the mobility and relaxation of macromolecular chains are retarded by the geometric confinement of the organoclay network. Hence, rheological behaviour of nanocomposite melts has been a subject of intensive research and has very high significance in industrial processing of polymer nanocomposites.

(a) Storage modulus

Rheological study of polymer composites is an efficient tool to identify the processing behaviour and nanofiller distribution, concentration of filler and bonding between filler and polymer matrix. Many polymer composites showed the transformation in rheological behaviour from liquid-like to pseudo-solid-like or solid-like with increasing filler concentration. This transition concentration is called the rheological percolation threshold. The storage modulus (*G'*) measured at various angular frequency (190 ^{o}C) for neat PMMA and its nanocomposites containing 3-7 wt.% of clay and LDHs are shown in Figure 5.14. The frequency dependence of storage modulus (*G'*) for the PMMA nanocomposites containing LDH layers demonstrate a liquid-like behavior at the lowest frequency, i.e. below 0.1 s^{-1}. It is distinct from the storage modulus graph that at lower frequency, neat PMMA along with its nanocomposites show similar trend; however, the modulus is higher for nanocomposite samples. As the frequency increases, the storage modulus also enhances and becomes less dependent on the shear rate. This entire phenomenon indicates the behavior from a liquid like to a solid like viscoelastic, i.e. the formation of nanoclay-polymer chain network occurs. As can be directly seen, the moduli of nanocomposites increase with an increase in the LDH concentration; however, this enhancement is greater in the higher frequency region. It is generally observed that both the modulus i.e. storage (solid-like) and loss modulus (liquid like) is affected by the addition of nanofiller as the viscoelastic characteristic changes. At lower loading, the viscosity is changed due to polymer-filler interaction. With the further increase of loading, the viscosity increases which leads to polymer-nanofiller network. Thus, system transition takes place from liquid like to solid like behaviour. It results due to filler-filler and filler-polymer interaction. The increase in the storage modulus is due to the intercalation of clay. At higher frequency, the two moduli soon become equal and display nearly a plateau region having high storage modulus than loss modulus. Similar type of trend is also displayed by clay and Ni-Al LDH based nanocomposites (see Figure 5.14).

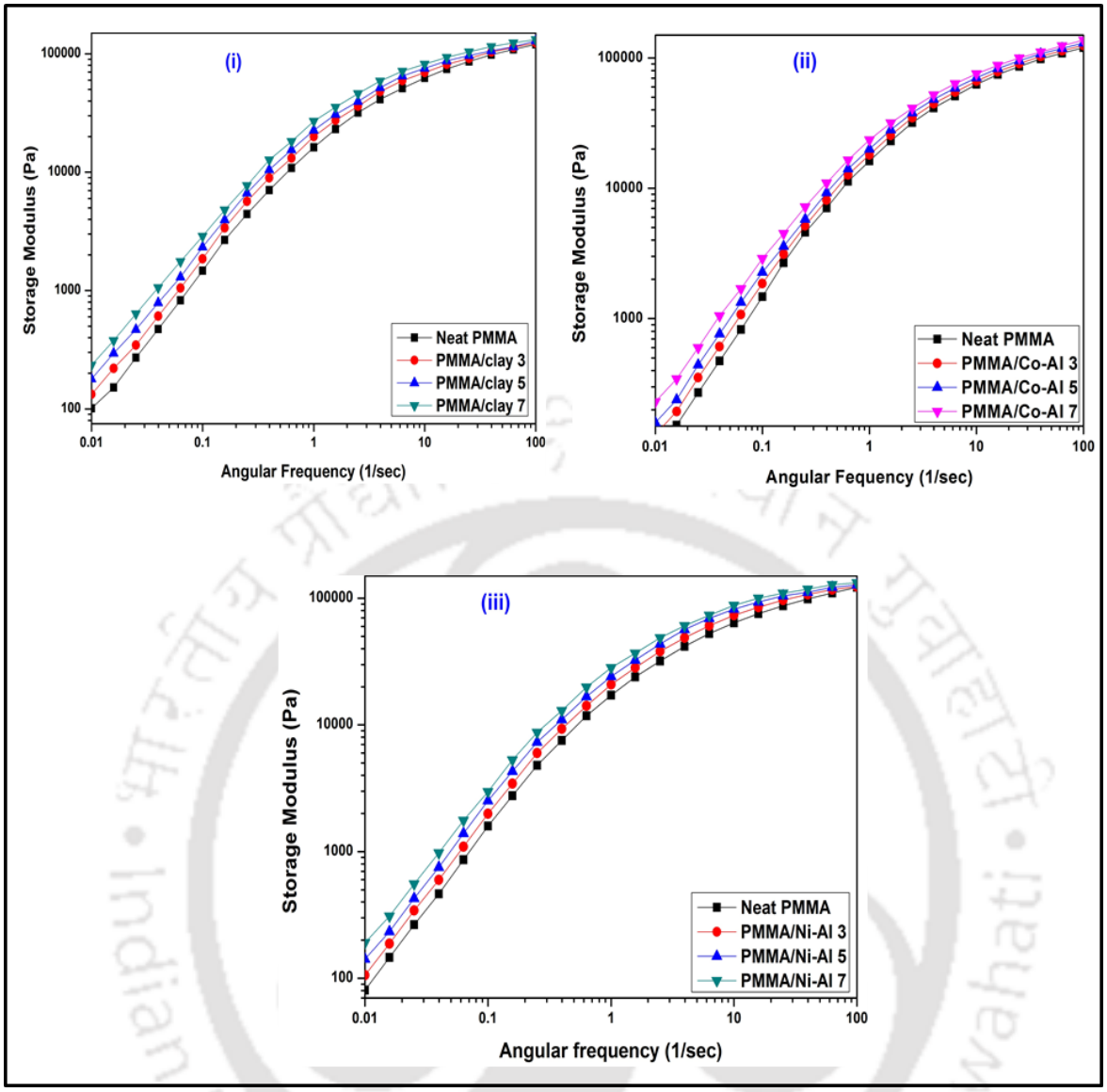

Figure 5.14 Storage modulus as a function of angular frequency at 190 ^{o}C for (i) PMMA/clay, (ii) PMMA/Co-Al LDH and (iii) PMMA/Ni-Al LDH nanocomposites

(b) Loss modulus

Loss modulus is a parameter, which relates the viscous effect of nanocomposites. Variation of loss modulus (*G"*) with angular frequency at 190 ^{o}C is shown in Figures 5.15. It is observed that at lower frequency, PMMA nanocomposites display higher loss modulus with respect to neat PMMA, indicating that LDH layers have pronounced effect on it. At higher shear rate, it is noticed that long-time relaxation for all the samples have perturbed and LDH layers have less effect. A similar type of results is also reported by Zhang and co-authors, **(2012)** for graphene based PMMA composites. PMMA/clay and PMMA/Ni-Al LDH samples also display similar pattern as seen from Figure 5.15 (i and iii).

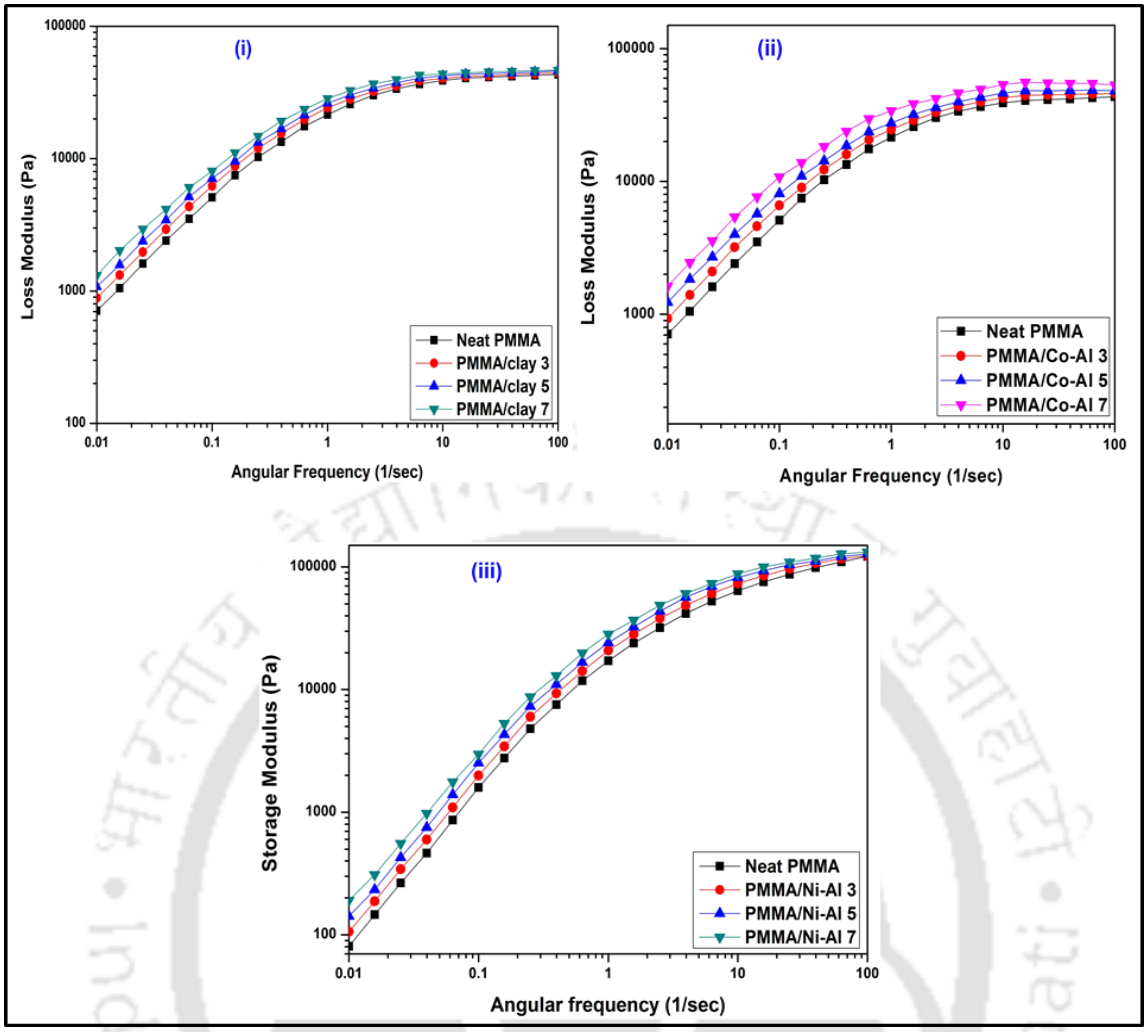

Figure 5.15 Variation of loss modulus with angular frequency at 190 ^{o}C for (i) PMMA/clay, (ii) PMMA/Co-Al LDH and (iii) PMMA/Ni-Al LDH nanocomposites

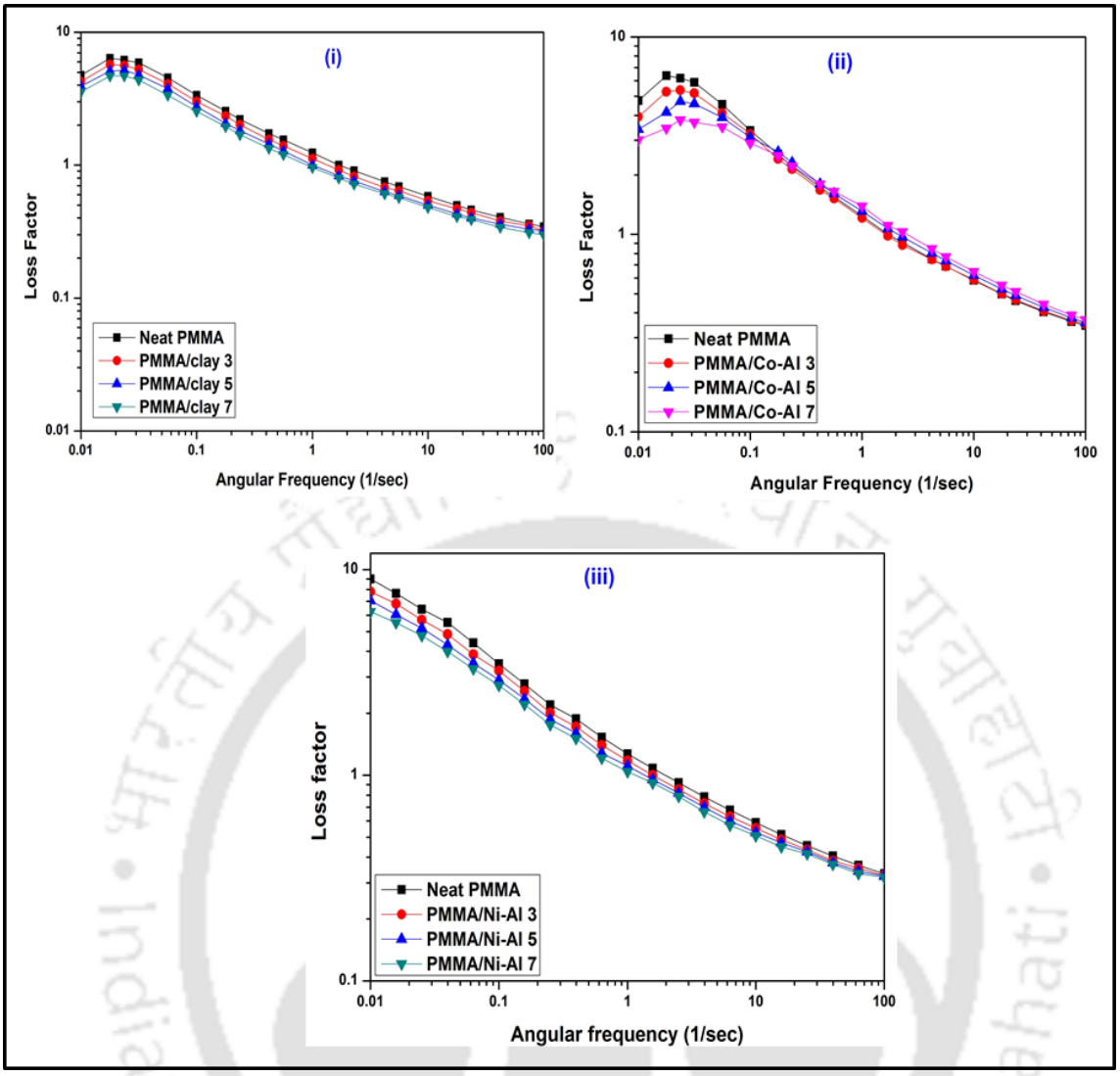

Figure 5.16 Loss factor as a function of angular frequency at 190 ^{o}C for (i) PMMA/clay, (ii) PMMA/Co-Al LDH and (iii) PMMA/Ni-Al LDH nanocomposites

(c) Loss factor

Loss factor (tan δ) arises from the discordance between strain and stress in the polymer when exposed to an external force, which is strongly related to applied frequency. For neat PMMA and along with different nanocomposites, tan δ decreases monotonously with increasing angular frequency (see Figure 5.16). Loss factor (tan δ) of polymer nanocomposites is nearly independent particularly at lower frequency region. This independency arises due to development of material elasticity. This material elasticity decreases with an increase in the nanofiller loading at lower frequency region or in other words, it is higher for neat polymer.

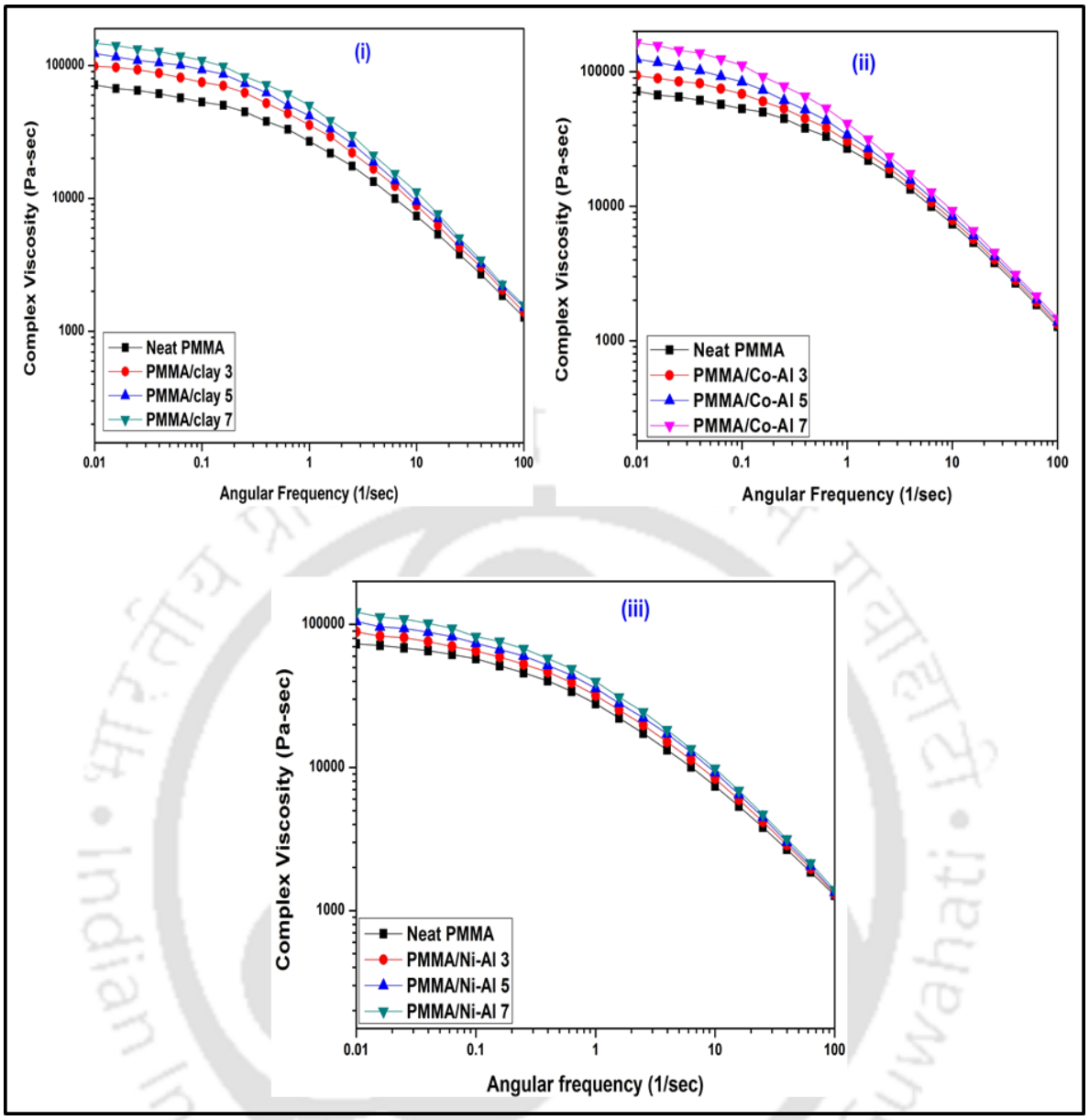

Figure 5.17 Variation of complex viscosity with angular frequency at 190 ^{o}C for (i) PMMA/clay, (ii) PMMA/Co-Al LDH and (iii) PMMA/Ni-Al LDH nanocomposites

(d) Complex viscosity

Figures 5.17 (i, ii and iii) illustrates the complex viscosity (η^*) of neat PMMA and nanoclay, Co-Al LDH and Ni-Al LDH based nanocomposites at various angular frequency. Similar to rheological moduli, there is an increase in the complex viscosity of nanocomposites with an increase in LDH concentration. Moreover, the rheological behaviour of nanocomposites is more sensitive to LDH concentrations at lower frequency. Graphs converge at higher frequencies. This is due to the fact that the rheological response of nanocomposites arises from frictional interactions between the nanofillers (Samyn et al., 2008), and also between

the polymer chains and layers of LDH. Therefore, increasing the LDH content enhances the number of frictional interactions between the nanofillers and matrix. The neat PMMA shows a classical viscoelastic behaviour, which is characterized by a transition from a low frequency Newtonian flow behaviour to a high frequency shear thinning nature (viscosity decreases with an increase of shear rate/frequency). For PMMA nanocomposites, at a lower frequency region, Newtonian flow behaviour is gradually shifted to shear thinning behaviour when the melt shows a transition from a liquid like to pseudo-solid like state. This type of low-frequency rheological response is typical for polymer nanocomposites, where relaxation of the system is strongly lowered due to the tethering of the polymer chains on the particle surface and particle-particle interactions. A similar type of trend is also reported by Costa et al., (2006) for polyethylene nanocomposites containing 1 to 15 wt.% loading of Mg-Al LDH.

(e) Theoretical Prediction of Storage Modulus and Loss Factor

In order to predict the storage modulus, one of the simplest equations for the reinforcement of a material due to an inclusion was given by Einstein, (1956)

$$G_c = G_m (1+1.25\ V_f) \qquad (5.2)$$

Where G is the storage modulus, subscript c and m represent composite and matrix, respectively. V_f is the volume fraction of the nanoparticles inclusions.

Another equation proposed by Einstein was

$$G_c = G_m (1 + V_f) \qquad (5.3)$$

where the terms are same as discussed above. A modification of Einstein's equation was done by Guth, (1945) and the proposed equation was

$$G_c = G_m(1 + 1.25V_f + 14.1\ (V_f)^2) \qquad (5.4)$$

Generally rigid fillers decrease the damping as expressed by mechanical loss factor (tan δ) to an extent predicted by a rule of mixture (Nielsen and Landal, 1994)

$$\tan\delta c = V_f \tan \delta_f + V_m \tan \delta_m \qquad (5.5)$$

In the case of rigid inclusions, the first term can be ignored and the equation becomes (Drzal et al., 1983)

$\tan\delta_c = V_m \tan \delta_m$ (5.6)

where, the subscripts c and m denote composite and matrix, V_m is the volume fraction of the matrix. This equation must have some stiffness parameter because it is assumed that the matrix in the presence of fillers offers a stiffness equivalent to the minimum elastic modulus of the composite; then above equation was modified as (Tung and Dynes, 1987)

$\tan\delta_c = V_f (G_m/G_c) \tan \delta_m$ (5.7)

where, G is the storage modulus of the material.

The plots of theoretical storage moduli *G'* values at 190^{o}C for various loadings of Co-Al LDH by wt.% are presented in Figure 5.18. It can be observed from different model that Einstein model (Equation 5.2) has better agreement with experimental values while the Guth model (Equation 5.4) deviated the most.

The plots of theoretical loss factor (tan δ) values of PMMA/Co-Al LDH with different loadings of nanoparticles are presented in Figure 5.19. It can be seen from the graph that in the case of low concentrations of nanoparticles, both equations agree with the experimental values and equation (5.6) agrees better than equation (5.7). At higher concentration both equations showed deviation as shown in Figure 5.19. The deviation shown by the models from the experimental data may be due to the fact that both equations ignore the localized constraints imposed by the dispersed phase on PMMA matrix deformation. Moreover, the nanofillers had a more significant effect on the elastic effect than the viscous behavior, damping factor graph confirms the fact, as seen there is significant decrease in tan δ values with an increase in nanoparticle content.

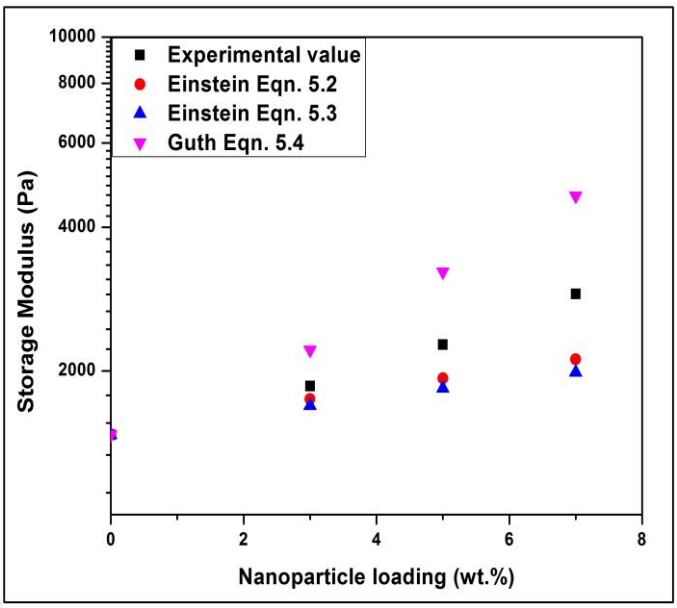

Figure 5.18 Comparison of experimental and theoretical storage moduli values of PMMA/Co-Al LDH nanocomposites against loading of nanoparticles at 190 ^{o}C

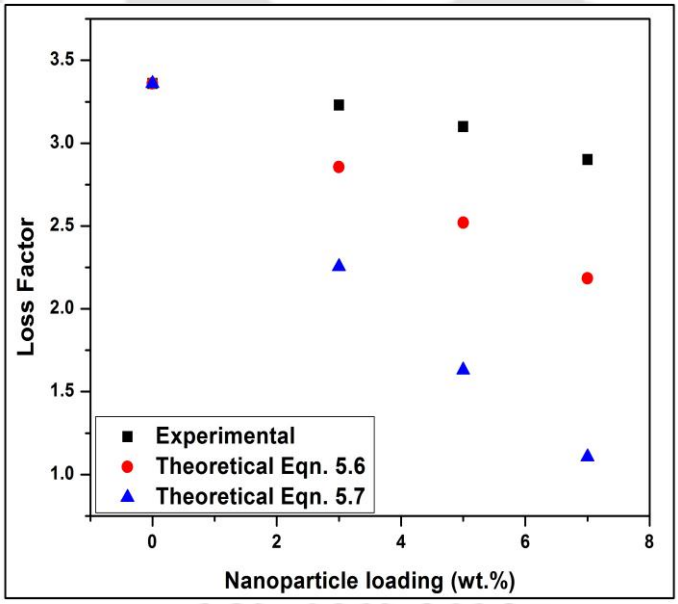

Figure 5.19 Plots of experimental and theoretical loss factor values against loading of Co-Al LDH nanoparticles at 190 ^{o}C

5.3 SUMMARY

A series of PMMA nanocomposites based on clay, Co-Al LDH and Ni-Al LDH have been successfully prepared using solvent blending technique. The XRD results suggested that intercalated morphology is observed for PMMA/clay nanocomposites while the other LDH

based PMMA nanocomposites exhibited exfoliated structure. The partially exfoliated structures of PMMA/clay, PMMA/Co-Al LDH and PMMA/Ni-Al LDH nanocomposites have been confirmed by TEM analysis. The FTIR and FESEM results authenticated the presence of nanofiller in different PMMA nanocomposites. The hardness of different PMMA nanocomposites was also enhanced by the incorporation of clay as it improves the indentation property. At 15% weight loss, the decomposition temperatures of PMMA/Ni-Al LDH nanocomposites are 25-28 ^{o}C higher than that of neat PMMA. T_{max} peaks get shifted to the right hand side for all the PMMA nanocomposites compared to neat PMMA. This is an indication of better thermal stability of PMMA nanocomposites when compared with pure PMMA. The glass transition temperature (T_g) values of neat PMMA, PMMA/Co-Al LDH 3, PMMA/Co-Al LDH 5 and PMMA/Co-Al LDH 7 are 110.5, 112.6, 113.7and 114.6 ^{o}C, respectively. The water vapor transmission rate (WVTR) test was performed for various nanocomposites at 7 wt.% loading and found to be 73, 34.2, 46.9 and 15.2 gm/m^2/day for neat PMMA, PMMA/clay, PMMA/Co-Al LDH and PMMA/Ni-Al LDH, respectively. Various rheological viscoelastic parameters such as storage modulus, loss modulus, damping factor and complex viscosity have been evaluated and the results are quite satisfactory which are also in accordance with the morphology of different nanocomposites. The activation energy of neat PMMA, PMMA/Ni-Al LDH nanocomposite samples containing 3, 5, 7 wt.% LDH was 99.4, 167, 167.1 and 170 kJ/mol, respectively. The thermal degradation mechanism of different nanocomposites was determined by Criado method. In case of PMMA/LDH nanocomposites, Z(α)-α experimental curve followed F1 reaction mechanism in the entire range of α. The IPDT value was also noticed higher for various nanocomposites at 7 wt.% loading.

Chapter 6

Conclusions and Scope for Future work

This chapter summarizes the major conclusions drawn from the research work and scope for further research in the near future.

6.1 CONCLUSIONS

- The PMMA nanocomposites with organically modified montmorillonite (MMT) and layered double hydroxide (LDH) have been successfully prepared by melt-intercalation and solvent blending method.
- The PMMA-5-G nanocomposite exhibits improved tensile strength (40%), Young's modulus (87%), and flexural strength (41%) over PMMA-5 sample. It clearly indicates that grafting is necessary to increase the mechanical properties of PMMA nanocomposites. The thermal stability of PMMA nanocomposites is enhanced by 11 ^{o}C than that of neat PMMA when 50% weight loss is considered as a point of comparison.
- As suggested by XRD analysis, the PMMA nanocomposites containing PP-g-MA, PE-g-MA, PS-g-MA compatibilizer demonstrate intercalated structures. However, PMMA-5-PS nanocomposite has partially exfoliated structure as evidenced by TEM analysis. The tensile modulus of PMMA-5-PP, PMMA-5-PE and PMMA-5-PS samples is found to be 16, 17 and 20%, higher over neat PMMA, respectively. Overall, PMMA-5-PS nanocomposite displays better mechanical properties over other compatibilized compositions.
- Among the nanocomposites prepared by melt intercalation technique, the improvement in tensile strength, flexural strength and impact strength of the PMMA/Co-Al 1% sample over neat PMMA is found to be 24, 25 and 10%, respectively. Similarly, the PMMA/Cu-Cr 1% nanocomposite displays 18 and 21 ^{o}C increment for tensile and flexural strength, respectively. When 50% weight loss is selected as a reference point in TGA profiles, the Co-Al LDH and Cu-Cr LDH based PMMA nanocomposites demonstrate about 31-35 ^{o}C and 26-32 ^{o}C improvement in thermal stability over neat PMMA, respectively. The glass transition temperature is found to be enhanced by 5 ^{o}C for PMMA/Co-Al LDH nanocomposites. The Coats-Redfern and IPDT methods also confirm that the activation energy and thermal stability of nanocomposites increase with an increase in the LDH content. On the whole, PMMA/Co-Al LDH nanocomposites exhibit enhanced mechanical and thermal properties over PMMA/Cu-Cr LDH nanocomposites.

- In the solvent blending method, the PMMA/clay and PMMA/Co-Al LDH nanocomposites demonstrate intercalated structure while the PMMA/Ni-Al LDH nanocomposites exhibit partially exfoliated morphology as confirmed by TEM analysis. The PMMA/Ni-Al LDH nanocomposites prepared by solvent blending method demonstrate higher thermal stability over clay and Co-Al LDH based nanocomposites. At 15% weight loss, the decomposition temperature of PMMA/Ni-Al LDH nanocomposites is 25-28 ^{o}C higher than that of neat PMMA. The rheological studies suggest that storage and loss modulus increase with increasing angular frequency; however, the complex viscosity reduces with increasing angular frequency. The water vapor transmission rate (WVTR) of PMMA/clay, PMMA/Co-Al LDH and PMMA/Ni-Al LDH nanocomposite films containing 7 wt.% filler content is found to be 34.2, 46.9 and 15.2 gm/m^2/day, respectively, which is considerably lower than the neat PMMA (73 gm/m^2/day). Based on the structural and thermal properties, PMMA/Ni-Al LDH nanocomposites demonstrate better properties over Co-Al LDH and clay based nanocomposites.
- The melt-intercalation process has been widely accepted method for industrial process and the PMMA nanocomposite prepared with 1 wt.% Co-Al LDH loading shows improved properties in comparison with other compositions and neat PMMA due to strong interaction between the nanofiller and matrix.

6.2 SCOPE FOR FUTURE WORK

Based on the findings of this thesis work, some recommendations for future research have been presented as follows:

- In order to examine the use of these materials in packaging application, oxygen permeability test can be performed for all the nanocomposites samples.
- Influence of other compatibilizers such as maleic anhydride grafted ethylene propylene rubber (MAH-g-EPR) and ethylene-glycidyl meth acrylate (EGMA) on the properties of PMMA can be investigated.
- Soil burial degradation study can be performed for PMMA nanocomposites.
- In view of biomedical engineering application, influence of other nanomaterials such as graphene, polyhedral oligomeric silsesquioxane (POSS) on the properties of PMMA nanocomposites can be investigated.

References

Acharya, H., Srivastava, S.K. and Bhowmick A.K., Synthesis of partially exfoliated EPDM/LDH nanocomposites by solution intercalation: Structural characterization and properties, *Compos. Sci. Technol*. 67 (13) (2007) 2807-2816.

Ahmadi, S.J., Huang, Y.D. and Li, W., Synthetic routes, properties and future applications of polymer-layered silicate nanocomposites, *J. Mater. Sci*. 39 (6) (2004) 1919-1925.

Artzi, N., Nir, Y., Narkis, M. and Siegmann, A., The effect of maleated compatibilizers on the structure and properties of EVOH/clay nanocomposites, *Polym. Compos.* 24 (5) (2003) 627-639.

Bamfor, C. H. and Tipper, C. F. H., Degradation of polymers, Elsevier, Amsterdam (1975).

Basson, N.C. and Reenen, A.V., The effect of compatibilizer on the properties of impact of poly(propylene)-wood composites, *Macromol. Symp.* 315 (1) (2012) 30-34.

Blumstein, A., Polymerization of adsorbed nanolayers II. Thermal degradation of the inserted polymers, *J. Polym. Sci., Part A: Polym. Chem.* 3 (7) (1965) 2653-2664.

Brostow, W., Nanocomposites of PMMA and montmorillonite (MMT) brazilian clay: A tribological study, *Express. Polym. Lett.* 4 (9) (2010) 570-575.

Cavani, F., Trifiro, F. and Vaccari, A., Hydrotalcite-type anionic clays: Preparation, properties and applications, *Catal. Today*. 11 (2) (1991) 173-301.

Chaiko D.J., Organoclay/polymer nanocomposites: Recent discoveries of new enabling technologies, GSA Resources, Inc., (2006).

Chen, W. and Qu, B., Enhanced thermal and mechanical properties of poly(methyl acrylate)/ZnAl layered double hydroxide nanocomposites formed by in situ polymerization, *Polym. Degrad. Stab.* 90 (1) (2005) 162-166.

Chen, Y. and Wang, Q., Themal oxidative degradation kinetics of flame-retarded polypropylene with intumescent flame-retardant master batches in situ prepared in twin-screw extruder, *Polym. Degrad. Stab.* 92 (2) (2007) 280-291.

Chiu, H.T. and Hsiao, Y.K., Compatibilization of poly(ethylene terephthalate)/polypropylene blends with maleic anhydride grafted polyethylene-octene elastomer, *J. Polym. Res.* 13 (2) (2006) 153-160.

Chow, W. S., Bakar, A. A., Ishak, Z. A. M.., Kocsis, J. K. and Ishiaku, U. S., Effect of maleic anhydride-grafted ethylene-propylene rubber on the mechanical, rheological and morphological properties of organoclay reinforced polyamide6/polypropylene nanocomposites, *Eur. Poly. J.* 41 (4) (2005) 687-696.

Chrissafis, K. and Bikiaris, D., Can nanoparticles really enhance thermal stability of polymers ? Part I: An overview on thermal decomposition of addition polymers, *Thermo. Acta.* 523 (1-2) (2011) 1-24.

Chung, Y., Cho, T.K. and Chun, B.C., Dependence of montmorillonite dispersion in nanocomposites on polymer matrix and compatibilizer content, and the impact on the mechanical properties, *Fiber. Polym*. 9 (1) (2008) 7-14.

Coats, A.W. and Redfern, J.P., Kinetic Parameters from Thermogravimetric Data, *Nature*. 201, (1964) 68-69.

Coiai, S., Passaglia, E., Hermann, A., Augier, S., Pratelli, D. and Streller, R.C., The influence of compatibilizer on the morphology and thermal properties of polypropylene-layered double hydroxide composites, *Polym. Compos*. 31 (4) (2010) 744-754.

Constantino, V.R.C. and Pinnavaia, T.J., Basic properties of Mg^{2+}_{1-x} Al^{3+}_{x} layered double hydroxides intercalated by carbonate, hydroxide, chloride, and sulfate anions, *Inorg. Chem.* 34 (4) (1995) 883-892.

Costa, F.R., Satapathy, B.K., Wagenknecht, U., Weidisch, R. and Heinrich, G., Morphology and fracture behaviour of polyethylene/Mg–Al layered double hydroxide (LDH) nanocomposites, *Euro. Polym. J*. 42 (9) (2006) 2140-2152.

Costache, M. C., Wang, D., Heidecker, M. J., Manias, E. and Wilkie, C. A., The thermal degradation of poly(methyl methacrylate) nanocomposites with montmorillonite, layered double hydroxides and carbon nanotubes, *Polym. Adv. Tech.* 17 (4) (2006) 272-280.

Criado, J.M., Malek, J. and Ortega, A., Applicability of the master plots in kinetic analysis of non-isothermal data, *Thermochim. Acta*, 147 (2) (1989) 377-385.

Cui, L., Tarte, N.H. and Woo, S.I., Effect of modified clay on the morphology and properties of PMMA/clay nanocomposites synthesized by in situ polymerization, *Macromolecules,* 41 (12) (2008) 4268-4274.

Das, R. and Maiti, S.N., Mechanical properties of impact iPP/CSM rubber blend, *Int. J. Polymer. Mater*. 54 (6) (2005) 467-482.

Dayma, N., Satapathy, B.K. and Patnaik, A., Structural correlations to sliding wear performance of PA-6/PP-g-MA/nanoclay ternary nanocomposites, *Wear*, 271 (5-6) (2011) 827-836.

Ding, P. and Qu, B., Synthesis of exfoliated PP/LDH nanocomposites via melt-intercalation: Structure, thermal properties, and photo-oxidative behaviour in comparison with PP/MMT nanocomposites, *Polym. Eng. Sci*. 46 (9) (2006) 1153-1159.

Ding, P. and Qu. B., Synthesis and characterization of polystyrene/layered double-hydroxide nanocomposites via in situ emulsion and suspension polymerization, *J. Appl. Polym. Sci.* 101 (6) (2006) 3758-3766.

Dortmans, A., Batenburg, L.F., Koster, T.P.M., Nelissen, R.G. and Fischer, H., Nanocomposite materials: from lab-scale experiments to prototypes, *e-Polymers.* 2 (1) (2013) 135-144.

Du, B., Guo, Z. and Fang, Z., Effects of organo-clay and sodium dodecyl sulfonate intercalated layered double hydroxide on thermal and flame behaviour of intumescent flame retarded polypropylene, *Polym. Degrad. Stab.* 94 (11) (2009) 1979-1985.

Du, F., Scogna, R.C., Zhou, W., Brand, S., Fischer, J.E. and Winey, K.I., Nanotube networks in polymer: Rheology and electrical conductivity, *Macromolecules*, 37 (24) (2004) 9048-9055.

Du, L., Qu, B. and Zhang, M., Thermal properties and combustion characterization of nylon 6/MgAl-LDH nanocomposites via organic modification and melt intercalation, *Polym. Degrad. Stab.* 92 (3) (2007) 497-502.

Einstein, A., Investigation on theory of Brownian movement. New York: Dover, 1956.

Eng, C. C., Ibrahim, N.A., Zainuddin, N., Ariffin, H., Yunus, W.M. Z. W. and Then, Y.Y., Effect of hydrophilic nanoclay on morphology, thermal and mechanical properties of polylactic acid/polycaprolactone/oil palm mesocarp fiber biocomposites. *Int. J. Inst. Mat. Mala.* 1, (2013) 50-70.

Etiene S., Becker C., Ruch D., Grignard B., Cartigny, G., Detrembleur C., Calberg C. and Jerome R., Effects of incorporation of modified silica nanoparticles on the mechanical and thermal properties of PMMA, *J. Therm. Anal. Calori.* 87 (1) (2007) 101–104.

Ezat, G.S., Kelly, A.L., Mitchell, S.C., Youseffi, M. and Coates, P.D., Effect of maleic anhydride grafted propylene compatibilizer on the morphology and properties of polypropylene/multiwalled carbon nanotube composite, *Polym. Compos.* 33 (8) (2012) 1376 -1386.

Faheem Uddin, Clays, Nanoclays, and Montmorillonite Minerals, *Metal. Mater. Trans.* 39 (12) (2008) 2804-2814.

Favaro, M.M., Branciforti, M.C. and Bretas, E.S., Influence of terpolymer compatibilizer on the nanostructure of poly(trimethylene terephthalate)/montmorillonite nanocomposites, *Polym. Adv. Technol.* 20 (12) (2009) 940-949.

Feitkneeht, W., Zur kenntnis der doppelhydroxyde und basischen doppelsalze III. Uber magnesium-aluminiumdoppelhydroxyd, *Helv. Chim. Acta.* 25 (1) (1942) 131-137.

Fischer, B., Ziadeh, M., Pfaff, A., Breu, J. and Altstädt, V., Impact of large aspect ratio, shear-stiff, mica clay on mechanical behaviour of PMMA/clay nanocomposites, *Polymer*, 53 (15) (2012) 3230-3237.

Flynn, J.H., The 'temperature integral' – its use and abuse, *Thermochim. Acta*, 300 (1) (1997) 83-92.

Fu, J. and Naguib, H.E., Effect of nanoclay on the mechanical properties of PMMA/clay nanocomposites foam, *J. Cell. Plas.* 42 (4) (2006) 325-342.

Galgali, G., Ramesh, C. and Lele, A., A rheological study on the kinetics of hybrid formation in polypropylene nanocomposites, *Macromolecules*, 34 (4) (2001) 852-858.

Gao, Z., Xie, W., Hwu, J.M., Wells, L. and Pan, W.P., The characterization of organic modified montmorillonite and its filled PMMA nanocomposites, *J. Therm. Anal. Calorim.* 64 (2) (2001) 467-475.

Garcés, J.M., Moll, D.J., Bicerano, J., Fibiger, R. and Mcleod, D.G., Polymeric nanocomposites for automotive applications, *Adv. Mater.* 12 (23) (2000) 1835-1839.

Giannelis, E. P., Polymer Layered Silicate Nanocomposites, *Adv. Mater.* 8 (1) (1996) 29-35.

Gross S., Camozzo D., Di Noto V., Armelao L. and Tondello E., PMMA: A key macromolecular component for dielectric low-κ hybrid inorganic-organic polymer films, *Eur. Poly. J.* 43 (3) (2007) 673–696.

Guth, E., Theory of filler reinforcement, *J. Appl. Phys*. 16 (20) (1945) 20-25.

He, F., Zhang, L., Yang, F., Chen, L. and Wu, Q., New nanocomposites based on syndiotactic polystyrene and organo-modified ZnAl layered double hydroxide, *J. Polym. Res*. 13 (6) (2006) 483-493.

He, X., Yang, J., Zhu, L., Wang, B., Sun, G., Lv, P., Phang, I.Y. and Liu, T., Morphology and melt rheology of nylon 11/clay nanocomposites, *J. Appl. Polym.Sci*. 102 (1) (2006) 542-549.

Hellati, A., Benachour, D., Cagiao, M.E., Boufassa, S. and Calleja, F.J.B., Role of a compatibilizer in the structure and micromechanical properties of recycled poly(ethylene terephthalate)/polyolefin blends with clay, *J. Appl. Polym. Sci.* 118 (3) (2010) 1278-1287.

Ho, D.L. and Glinka, C.J., Effects of solvent solubility parameters on organoclay dispersions, *Chem. Mater*. 15 (6) (2003) 1309-1312.

Hong, N., Song, L., Wang., B., Stec., A. A., Hull, T.R., Zhan, J. and Hu, Y., Co-precipitation synthesis of reduced graphene oxide/NiAl-layered double hydroxide hybrid and its application in flame retarding poly(methyl methacrylate), *Mater. Res. Bull*. 49, (2014) 657-664.

Huang, G., Guo, H., Yang, J., Wang, X. and Gao, J., Effect of phosphorus-nitrogen-containing quaternary ammonium salt structure on the flammability properties of poly(methyl-methacrylate)/montmorillonite nanocomposites, *Ind. Eng. Chem. Res.* 52 (11) (2013) 4089-4097.

Huang, G., Zhou, A., Wang, L. and Wang, X., Preparation and flammability properties of intumescent flame retardant-functionalized layered double hydroxides/poly methyl methacrylate nanocomposites, *Mater. Chem. Phys.* 130 (1-2) (2011) 714-720.

Huang, J.C., Zhu, Z., Yin, J., Qian, X and Sun, Y.Y., Poly (etherimide)/montmorillonite nanocomposites prepared by melt intercalation: morphology, solvent resistance properties and thermal properties, *Polymer,* 42 (3) (2001) 873-877.

Huskić, M, Žagar, E. and Žigon, M., The influence of a quaternary ammonium salt and MMT on the in situ intercalative polymerization of PMMA, *Eur. Polym. J.* 48 (9) (2012) 1555-1560.

Hwang, K.J., Park, J.W., Kim, I.I. and Ha, C.S., Effect of a compatibilizer on the microstructure and properties of partially biodegradable LDPE/aliphatic polyester/organoclay nanocomposites, *Macromol. Res.* 14 (2) (2006) 179-186.

Hwu, J.M., Ko, T.H., Yang, W.T., Lin, J.C., Jiang, G.J., Xie, W and Pan, W.P., Synthesis and properties of polystyrene-montmorillonite nanocomposites by suspension polymerization, *J. Appl. Polym. Sci*. 91 (1) (2004) 101-109.

Jeon, H.G., Jung, H.T., Lee, S.W. and Hudson, S.D., Morphology of polymer/silicate nanocomposites high density polyethylene and a nitrile copolymer, *Polym. Bull.* 41 (1) (1998) 107-113.

Jiang, C., Filippi, S. and Magagnini, P., Reactive compatibilizer precursors for LDPE/PA6 blends. II: Maleic anhydride grafted polyethylenes, *Polymer*, 44 (8) (2003) 2411-2422.

Jiang, G.J. and Tsai, H.Y., Preparation and properties of polymethyl methacrylate-clay nanocomposites, *Polym. Prepr*. 41, (2000) 621-622.

Kakati, K., Pugazhenthi, G. and Iyer, P.K., Effect of organomodified Ni-Al layered double hydroxide (OLDH) on the properties of polypropylene (PP)/LDH nanocomposites, *Int. J. Polym. Mater*. 61 (12) (2012) 931-948.

Kalajahi, M.S., Asl, V.H., Razin, S. R., Sadabad, F.B., Mamaqani, H.R. and Najafi, M., Effect of loading and surface modification of nanoparticles on the properties of PMMA/silica nanocomposites prepared via in-situ free radical polymerization, *Int. J. Polym. Mater*. 62 (6) (2013) 336-344.

Kashiwagi, T., Mu, M., Winey, K. and Douglas, J., Relation between the viscoelastic and flammability of polymer nanocomposites, *Polymer*, 49 (20) (2008) 4358-4368.

Kiersnowski, A., Wlazlak, M.T., Dolega, J. and Piglowski, J., One-pot synthesis of PMMA/montmorillonite nanocomposites, *e-Polymers.* 6 (1) (2013) 912-922.

Kim, D.H., Fasulo, P.D., Rodgers, W.R. and Paul, D.R., Effect of the ratio of maleated polypropylene to organoclay on the structure and properties of TPO-bsed

nanocomposites. Part I: Morphology and mechanical properties, *Polymer*, 48 (20) (2007) 5960-5978.

Kim, D.H., Fasulo, P.D., Rodgers, W.R. and Paul, D.R., Structure and properties of propylene based nanocomposites: Effect of PP-g-MA to organoclay ratio, *Polymer*, 48 (18) (2007) 5308-5323.

Kim, T. H., Lim, S.T., Lee, C.H., Choi, H.J. and Jhon, M.S., Preparation and rheological characterization of intercalated polystyrene/organophilic montmorillonite nanocomposite, *J. Appl. Polym. Sci*. 87 (13) (2003) 2106-2112.

Kitayama, T., Nishiura, T. and Hatada, K., PMMA-block-polyisobutylene-block-PMMA prepared with α,ω-dilithiated polyisobutylene and its characterization, *Polym. Bull.* 26 (5) (1991) 513-520.

Kouini, B. and Serier, A., Properties of polypropylene/polyamide nanocomposites prepared by melt processing with a PP-g-MAH compatibilizer, *Mater. Des*. 34, (2012) 313-318.

Krajnc, M and Sebenik, U., Poly (methyl methacrylate)/montmorillonite nanocomposites prepared by bulk polymerization and melt compounding, *Polym. Compos*. 30 (11) (2009) 1678-1686.

Krishna, S. V. and Pugazhenthi, G., Influence of processing conditions on the properties of polystyrene (PS)/organomontmorillonite (OMMT) nanocomposites prepared via solvent blending method, *Inter. J. Poly. Mat.* 60 (2) (2011) 144-162.

Krishna, S.V. and Pugazhenthi, G., Properties and thermal degradation kinetics of polystyrene/organoclay nanocomposites synthesized by solvent blending method: Effect of processing conditions and organoclay loading, *J. Appl. Polym. Sci.* 120 (3) (2011) 1322-1336.

Krishna, S.V. and Pugazhenthi, G., Structural and thermal properties of polystyrene/CoAl-layered double hydroxide nanocomposites prepared *via* solvent blending: Effect of LDH loading, *J. Exp. Nanosci.* 8 (1) (2013) 19-32.

Krishnamoorti, R. and Giannelis, E.P., Rheology of end-tethered polymer layered silicate nanocomposites, *Macromolecules*, 30 (14) (1997) 4097-4102.

Krishnamoorti, R., Vaia, R.A. and Giannelis, E.P., Structure and dynamics of polymer-layered silicate nanocomposites, *Chem. Mater*. 8 (8) (1996) 1728-1734.

Kuan, C.F., Yen, W.H., Chen, C.H., Yuen, S.M., Kuan, H.C. and Chiang, C., Synthesis, characterization, flame retardance and thermal properties of halogen-free expandable graphite/PMMA composites prepared from sol–gel method, *Polym. Degrad. Stab.* 93 (7) (2008) 1357-1363.

Kuila, T., Acharya, H., Srivastava, S.K. and Bhowmick A.K., Ethylene vinyl acetate/Mg-Al LDH nanocomposites by solution blending, *Polym. Compos.* 30 (4) (2009) 497-502.

Kuila, T., Bose, S., Khanra, P., Kim, N.H., Rhee, K.Y. and Lee, J.H., Characterization and properties of *in situ* emulsion polymerized poly(methyl methacrylate)/graphene nanocomposites, *Composites Part A.* 42 (11) (2011) 1856-1861.

Kulia, T., Acharya, H., Srivastava, S.K. and Bhowmick, A.K., Synthesis and characterization of ethyl vinyl acetate/Mg-Al layered double hydroxide nanocomposites, *J. Appl. Polym. Sci.* 104 (3) (2007) 1845-1851.

Kumar, M., Kumar, V., Upadhaya, P. and Pugazhenthi, G., Fabrication of poly(methyl methacrylate) (PMMA) nanocomposites with modified nanoclay by melt intercalation, *Compos. Interfaces*. 21 (9) (2014) 819-832.

Kurahatti, R.V., Surendranathan, A.O., Kori, S.A., Singh, N., Kumar, A.V.R. and Srivastava, S., Defence applications of polymer nanocomposites, *Def. Sci. J.* 60 (5) (2010) 551-563.

Laachachi, A., Ferriol, M., Cochez , M., Cuesta, J. M. L. and Ruch, D., A comparison of the role of boehmite (AlOOH) and alumina (Al_2O_3) in the thermal stability and flammability of poly(methyl methacrylate), *Polym. Degrad. Stab.* 94 (9) (2009) 1373–1378.

Laachachi, A., Ruch, D., Addiego, F., Ferriol, M., Cochez, M. and Cuesta, J. M. L., Effect of nano ZnO and organo-modified montmorillonite on thermal degradation of poly(methyl methacrylate) nanocomposites, *Polym. Degrad. Stab.* 94 (4) (2009) 670–678.

Lai, S.M., Chen, W.C. and Zhu, X.S., Melt mixed compatibilized polypropylene/clay nanocomposites: Part 1- the effect of compatibilizers on optical transmittance and mechanical properties, *Composites: Part A*, 40 (6-7) (2009) 754-765.

Lee, H.G., Sung, Y., Lee, Y.K., Kim, W.N., Yoon, H.G. and Lee, H.S., Effect of PP-g-MAH on the mechanical, morphological and rheological properties of polypropylene and poly(acrylonitrile-butadiene-styrene) beads, *Macromol. Res.* 17 (6) (2009) 417-423.

Lee, J.H., Jung, D., Hong, C.E., Rhee, K.Y. and Advani, S.G., Properties of polyethylene-layered silicate nanocomposites prepared by melt intercalation with a PP-g-MA compatibilizer, *Compos. Sci. Technol*. 65 (13) (2005) 1996-2002.

Li, B., Hu, Y., Liu, J., Chen, Z. and Fan, W., Preparation of poly (methyl methacrylate)/LDH nanocomposite by exfoliation-adsorption process, *Colloid Polym. Sci.* 281 (10) (2003) 998-1001.

Li, H., Chen, H., Shen, Z. and Lin, S., Preparation and characterization of maleic anhydride-functionalized syndiotactic polystyrene, *Polymer*, 43 (20) (2002) 5455-5461.

Li, Y., Zhang, B. and Pan, X., Preparation and characterization of PMMA-kaolinite intercalation composites, *Compos. Sci. Technol.* 68 (9) (2008) 1954-1961.

Li., M., Zhu, J.E., Zhang, L., Chen, X., Zhang, H., Zhang, F., Xu, S. and Evans, D.G., Facile synthesis of NiAl-layered double hydroxide/graphene hybrid with enhanced electrochemical properties for detection of dopamine, *Nanoscale*, 10 (3) (2011) 4240-4246.

Liaw, Jr. H., Hsueh, T.Y., Tan, T.S., Wang, Y and Chiao, S.M., Twin-screw compounding of poly(methyl methacrylate)/clay nanocomposites: Effects of compounding temperature and matrix molecular weight, *Polym. Int*. 56 (8) (2007) 1045-1052.

Lim, J. W., Hassan, A., Rahmat, A. R. and Wahit, M. U., Morphology, thermal and mechanical behavior of polypropylene nanocomposites toughened with poly(ethylene-*co*-octene), *Polym. Int.* 55 (2) (2006) 204–215.

Lin, Z., Guan, Z., Xu, B., Chen, C., Guo, G., Zhou, J., Xian, J., Cao, L., Wang, Y., Li, M. and Li, W., Crystallization and melting behaviour of propylene in β-PP/polyamide 6 blends containing PP-g-MA, *J. Ind. Eng. Chem.* 19 (2) (2013) 692-697.

Liqiang, C., Naresh, T.H. and Ihl, W.S., Effects of modified clay on the morphology and properties of PMMA/clay nanocomposites synthesized by in situ polymerization, *Macromolecules*, 41 (12) (2008) 4268-4274.

Liu, Y.L., Hsu, C.Y. and Hsu, K.Y., Poly(methylmethacrylate)-silica nanocomposites films from surface-functionalized silica nanoparticles, *Polymer*, 46 (6) (2005) 1851-1856.

Liu, Z., Ma, R., Osada, M., Lyi, N., Ebina, Y., Takada, K. and Sasaki, T., Synthesis, anion exchange, and delamination of Co-Al layered double hydroxide: assembly of the exfoliated nanosheet/polyanion composite films and magneto-optical studies, *J. Amer. Chem. Soc.* 128 (14) (2006) 4872-4880.

Logakis, E., Pandis, Ch., Pissis, P., Pionteck, J. and Pötschke, P., Highly conducting poly (methyl methacrylate)/carbon nanotubes composites: Investigation on their thermal, dynamic-mechanical, electrical and dielectric properties, *Compos. Sci. Technol*. 71 (6) (2011) 854-862.

Lonkar, S.P., Therias, S., Leroux, F., Gardette, J.L. and Singh, R.P., Influence of reactive compatibilization on the structure and properties of PP/LDH nanocomposites, *Polym. Int.* 60 (12) (2011) 1688-1696.

Lu, C., Guo, S., Wen, L. and Wang, J., Weld line morphology and strength of polystyrene/polyamide-6/poly(styrene-co-maleic anhydride) blends, *Eur. Polym. J*. 40 (11) (2004) 2565-2572.

Lu, Y. and Larock, R.C., Novel biobased nanocomposites from soyabean oil and functionalized organoclay, *Biomacromolecules*, 7 (9) (2006) 2692-2700.

Madejova, J., FTIR techniques in clay mineral studies, *Vib. Spectrosc*. 31 (1) (2003) 1-10.

Maiti, S.N. and Das, R., Mechanical properties of impact iPP/CSM rubber blend, *Int. J. Polymer. Mater*. 54 (6) (2005) 467-482.

Majid, M., Hassan, E.D., Davoud, A. and Saman, M., A study on the effect of nano-ZnO on rheological and dynamic mechanical properties of polypropylene: Experiments and models. *Composites Part B*, 42 (7) (2011) 2038-2046.

Manjhi, S. and Sarkhel, G., Effect of maleic anhydride grafted ethylene propylene diene monomer (MAH-*g*-EPDM) on the properties of kaolin reinforced EPDM rubber, *J. Appl. Polym. Sci.* 119 (4) (2011) 2268-2274.

Manoratne, C.H., Rajapakse, R.M.G. and Dissanayake, M.A.K.L., Ionic conductivity of poly(ethylene oxide) (PEO)-montmorillonite (MMT) nanocomposites prepared by intercalation from aqueous medium, *Int. J. Electrochem. Sci*. 1, (2006) 32–46.

Manzi-Nshuti, C., Wang, D., Hossenlopp, J.M. and Wilkie, C.A., The role of the trivalent metal in an LDH: Synthesis, characterization and fire properties of thermally stable PMMA/LDH systems, *Polym. Degrad. Stab.* 94 (4) (2009) 705-711.

Mark H. F., Encyclopedia of polymer science and technology, Wiley, New York (1985).

Matusinović, Z., Rogošić, M. and Šipušić, J. Synthesis and characterization of poly(styrene-co-methyl methacrylate)/layered double hydroxide nanocomposites via in situ polymerization, *Polym. Degrad. Stab.* 94 (1) (2009) 95-101.

Meneghetti, P. and Qutubuddin, S., Synthesis, thermal properties and applications of polymer-clay nanocomposites, *Thermochim. Acta*. 442 (1-2) (2006) 74-77.

Mittal, V., Mechanical and gas permeation properties of compatibilized propylene-layered silicate nanocomposites, *J. Appl. Polym. Sci.* 107 (2) (2008) 1350-1361.

Miyata, S. and Okada, A., Synthesis of hydrotalcite-like compounds and their physico-chemical properties - The systems Mg^{2+}-AI^{3+}-SO_4^{2-} and Mg^{2+}-$A1^{3+}$-CrO_4^{2-}, *Clays Clay Miner*. 23 (1) (1977) 14-18.

Mohanty, S. and Nayak, S. K., Effect of organo-modified layered silicates on the properties of poly(methyl methacrylate) nanocomposites, *J. Thermo. Comp. Mat.* 23 (5) (2010) 623-645.

Morgan, A.B. and Gilman, J.W., Characterization of polymer-layered silicate (clay) nanocomposites by transmission electron microscopy and X-ray diffraction: A comparative study, *J. Appl. Polym. Sci.* 87 (8) (2003) 1329-1338.

Motahari, S., Kafashi, B., Taranehjoo, S. and Sarrafi, M., PMMA/polyamide 6/silica ternary nanocomposites; Investigation of dynamic rheology, crystallization and blend phase morphology, *Can. J. Envr.. Cons. Civ. Engg*. 3 (2) (2012) 80-93.

Nielsen, L.E. and Landel, F.L., Mechanical properties of polymers and composites. New York: Marck Dekker; 1994.

Newman, S.P. and Jones, W., Synthesis, characterization and applications of layered double hydroxides containing organic guests, *New J. Chem.* 2, (1998) 105-115.

Manzi-Nshuti, C., Wang, D., Hossenlopp, J.M. and Wilkie, C.A., The role of the trivalent metal in an LDH: Synthesis, characterization and fire properties of thermally stable PMMA/LDH systems, *Polym. Degrad. Stab*. 94 (4) (2009) 705-711.

Nyambo, C., Chen, D., Su, S. and Wilkie, C.A., Does organic modification of layered double hydroxides improve the fire performance of PMMA ? *Polym. Degrad. Stab*. 94 (8) (2009) 1298-1306.

Nyambo, C., Chen, D., Su, S. and Wilkie, C.A., Variation of benzyl anions in MgAl-layered double hydroxides: Fire and thermal properties in PMMA, *Polym. Degrad. Stab*. 94 (4) (2009) 496-505.

Okada, A. and Usuki, A., Twenty Years of Polymer-Clay Nanocomposites, *Macro. Mater. Eng*. 291 (12) (2006) 1449-1476.

Okamoto, M., Morita, S., Taguchi, H., Kim, Y.H., Kotaka, T. and Tateyama, H., Synthesis and structure of smectic clay/poly(methyl-methacrylate) and clay polystyrene nanocomposites via in situ intercalative polymerization, *Polymer*, 41 (10) (2000) 3887-3890.

Oral, A., Tasdelen, M.A., Demirel, A.L. and Yagci, Y., Poly (methyl methacrylate)/clay nanocomposites by photo initiated free radical polymerization using intercalated monomer, *Polymer*, 50 (16) (2009) 3905-3910.

Park, J.H., Lee, H.M., Chin, I., Choi, H.J., Kim, H.K and Kang, W.G., Intercalated polypropylene/clay nanocomposite and its physical characteristics, *J. Phys. Chem. Solids*, 69 (5-6) (2008) 1375-1378.

Park, S.J., Li, K. and Hong, S.K., Preparation and characterization of layered silicate-modified ultrahigh-molecular-weight polyethylene nanocomposites, *J. Ind. Eng. Chem*. 11 (4) (2005) 561-566.

Paterson, W.L., Computation of the exponential trap population integral of glow curve theory, *J. Comput. Phys*. 7 (1) (1971) 187-190.

Pavlidou, S. and Papaspyrides, C., A review on polymer–layered silicate nanocomposites, *Prog. Polym. Sci.* 33 (12) (2008) 1119-1198.

Pereira, C.M.C., Herrero, M., Labajos, F.M., Marques, A.T. and Rives, V., Preparation and properties of new flame retardant unsaturated polyester nanocomposites based on layered double hydroxides, *Polym. Degrad. Stab.* 94 (6) (2009) 939-946.

Pradhan, B., Srivastava, S.K., Ananthakrishnan, R. and Saxena, A., Preparation and characterization of exfoliated layered double hydroxide/silicone rubber nanocomposites, *J. Appl. Polym. Sci.* 119 (1) (2011) 343-351.

Pradhan, S., Costa, F.R., Wagenknecht, U., Jehnichen, D., Bhowmick, A.K. and Heinrich, G., Elastomer/LDH nanocomposites: Synthesis and studies on nanoparticle dispersion, mechanical properties and interfacial adhesion, *Eur. Polym. J.* 44 (10) (2008) 3122-3132.

Qiu, L. and Qu, B., Preparation and characterization of surfactant-free polystyrene/layered double hydroxide exfoliated nanocomposite via soap-free emulsion polymerization, *J. Colloid Interf. Sci.* 301 (2) (2006) 347-351.

Qiu, L., Chen, W. and Qu, B., Exfoliation of layered double hydroxide in polystyrene by in-situ atom transfer radical polymerization using initiator-modified precursor, *Colloid Polym. Sci.* 283 (11) (2005) 1241-1245.

Qiu, L., Chen, W. and Qu, B., Structural characterisation and thermal properties of exfoliated polystyrene/ZnAl layered double hydroxide nanocomposites prepared via solution intercalation, *Polym. Degrad. Stab.* 87 (3) (2005) 433-440.

Quintanilla, M.L.L., Valdes, S.S., Valle, L.F.R. and Miranda, R.G., Preparation and mechanical properties of PP/PP-g-MA/Org-MMT nanocomposites with different MA content, *Polym. Bull.* 57 (3) (2006) 385-393.

Ramaraj, B., Nayak, S.K. and Yoon, K.R., Poly(vinyl alcohol) and layered double hydroxide composites: Thermal and mechanical properties, *J. Appl. Polym. Sci.* 116 (3) (2010) 1671-1677.

Ratinac, K. R., Gilbert, R. G., Ye, L., Jones, A. S. and Ringer, S. P., The effects of processing and organoclay properties on the structure of poly(methyl methacrylate)-clay nanocomposites, *Polymer*, 47 (18) (2006) 6337-6361.

Ray S.S., Okamoto M., Polymer/layered silicate nanocomposites: A review from preparation to processing, *Prog. Polym. Sci.* 28 (11) (2003) 1539–1641.

Ray, S.S., Maiti, P., Okamoto, M., Yamada, K. and Ueda, K., New polylactide/layered silicate nanocomposites. 1. Preparation, characterization, and properties, *Macromolecules*, 35 (8) (2002) 3104-3110.

Ray, S.S., Rheology of polymer/layered silicate nanocomposites, *J. Ind. Eng. Chem*. 12 (6) (2006) 811-842.

Realinho, V., Antunes, M., Arencón, D., Fernández, A.I. and Velasco, J.I., Effect of a dodecylsulfate-modified magnesium aluminum layered double hydroxide on the morphology and fracture of polystyrene and polystyrene-co-acrylonitrile) composites, *J. Appl. Polym. Sci*. 111 (5) (2009) 2574-2583.

Rohlmann, C.O., Horst, M.F., Quinzani, L.M. and Failla, M.D., Comparative analysis of nanocomposites based on polypropylene and different montmorillonites, *Eur. Polym. J*. 44 (9) (2008) 2749-2760.

Sahoo, P.K. and Samal, R., Fire retardancy and biodegradability of poly(methyl methacrylate)/montmorillonite nanocomposites, *Polym. Degrad. Stab.* 92 (9) (2007) 1700-1707.

Sahu, B. and Pugazhenthi, G., Properties of polystyrene/organically modified layered double hydroxide nanocomposites synthesized by solvent blending method, *J. Polym. Appl. Sci.* 120 (4) (2011) 2485-2495.

Samyn, F., Bourbigot , S., and Camino, G., Characterisation of the dispersion in polymer flame retarded nanocomposites, *Eur. Polym. J.* 44 (6) (2008) 1631-1641.

Senum, G. I., and Yang, R. T., Rational approximations of the integral of Arrhenius function, *J. Therm. Analy*. 11 (3) (1977) 445-447.

Shah, V., Handbook of plastic testing and failure analysis of plastic technology. John Wiley and Sons, New Jersey, (2007) 17-93.

Shanks, R.A. and Cerezo, F.T., Preparation and properties of poly(propylene-g-maleic anhydride) filled with expanded graphite oxide, *Composites: Part A*, 43 (7) (2012) 1092-1100.

Shen, Z., Simon, G.P. and Cheng, Y.B., Melt intercalation of PMMA into organically modified layered silicate, *MRS Proceedings*, 576, (1999) 137-142.

Shen, Z., Simon, G.P. and Cheng, Y.B., Nanocomposites of poly(methyl methacrylate) and organically modified layered silicates by melt intercalation. *J. Appl. Polym. Sci.* 92 (4) (2004) 2101-2115.

Silva, A., Soares, B.G., Zaioncz, S. and Dahmouche, K., Poly(methyl methacrylate)-clay nanocomposites prepared by in situ intercalative polymerization: The effect of the acrylic acid. LNLS 2007 Activity Report (2008).

Singh, D., Rai T.J.K.N. and Kumar, A., Preparation of poly(methyl methacrylate) nanocomposites with superior impact strength, *J. Appl. Polym. Sci.* 105 (6) (2007) 3183–3194.

Song, Y. and Zheng, Q., Linear rheology of nanofilled polymer, *J. Rheol*. 59 (1) (2015) 155-191.

Stretz, H. A., Paul, D.R., Li, R., Keskkula, H. and Cassidy, P.E., Intercalation and exfoliation relationships in melt-processed poly(styrene-*co*-acrylonitrile)/montmorillonite nanocomposites, *Polymer*, 46 (8) (2005) 2621-2637.

Trujillano, R., Holgado, M.J., Pigazo, F. and Rives, V., Preparation, physicochemical characterization and magnetic properties of Cu-Al layered double hydroxides with CO_3^{2-} and anionic surfactants with different alkyl chains in the interlayer, *Physica B*, 373 (2) (2006) 267-273.

Tsai, T., Wen, C. K., Chuang, H. J., Lin, M. J. and Ray, U., Effect of clay with different cation exchange capacity on the morphology and properties of poly(methyl methacrylate)/clay nanocomposites, *Polym. Compos.* 30 (11) (2009) 1552-1561.

Tsai, T.Y., Lin, M.J., Chuang, Y.C. and Chou, P.C., Effects of modified clay on the morphology and thermal stability of PMMA/clay nanocomposites, *Mater. Chem. Phys*. 138 (1) (2013) 230-237.

Tung, C.M. and Dynes, P.J., Morphological characterization of polyetheretherketone-carbon fiber composites, *J. Appl. Polym. Sci*. 33 (2) (1987) 505-516.

Unnikrishnan, L., Mohanty, S., Nayak, S. K. and Ali, A., Preparation and characterization of poly(methyl methacrylate)-clay nanocomposites via melt intercalation: Effect of organoclay on thermal, mechanical and flammability properties, *Mat. Sci. Eng.* A 528 (12) (2011) 3943–3951.

Valandro, S.A., Poli, A.L., Neumann, M.G. and Schimtt, C.C., Organomontmorillonite/ poly(methyl methacrylate) nanocomposites prepared by *in situ* photopolymerization. Effect of the organoclay on the photooxidative degradation, *Appl. Clay Sci*. 85, (2013) 19-24.

Wang, B., Zhou, K., Jiang, S., Shi, Y., Wang, B., Gui, Z. And Hu, Y., Poly (methyl methacrylate)/layered zinc sulfide nanocomposites: Preparation, characterization and the improvements in thermal stability, flame retardant and optical properties, *Mater. Res. Bull*. 56 (2014) 107-112.

Wang, D., Zhu, J., Yao, Q and Wilkie, C.A., A comparison of various methods for the preparation of polystyrene and poly (methyl methacrylate)-clay composite, *Chem. Mater*. 14 (9) (2002) 3837-3841.

Wang, D.Y., Das, A., Leuteritz, A., Boldt, R., Haußler, L., Wagenknecht, U. and Heinrich, G., Thermal degradation behaviors of a novel nanocomposite based on polypropylene and Co–Al layered double hydroxide, *Polym. Degrad. Stab.* 96 (3) (2011) 285-290.

Wang, G., Wang, C.C. and Chen, C.Y., The disorderly exfoliated LDHs/PMMA nanocomposites synthesized by in-situ bulk polymerization: The effects of LDH-U on thermal and mechanical properties, *Polym. Degrad. Stab.* 91 (10) (2006) 2443-2450.

Wang, G.A., Wang, C.C. and Chen, C.Y., Preparation and characterization of layered double hydroxides-PMMA nanocomposites by solution polymerization, *J. Inorg. Organomet. Polym. Mater*. 15 (2) (2005) 239-251.

Wang, G.A., Wang, C.C. and Chen, C.Y., The disorderly exfoliated LDHs/PMMA nanocomposites synthesized by in situ bulk polymerization: The effects of LDH-U on thermal and mechanical properties, *Polym. Degrad. Stab*. 91 (10) (2006) 2443-2450.

Wang, K.H., Choi, M.H., Koo, C.M., Choi, Y.S. and Chung, I.J., Synthesis and characterization of maleated polyethylene/clay nanocomposites, *Polymer*, 42 (24) (2001) 9819-9826.

Wang, L., Su, S., Chan, D. and Wilkie, C.A., Variation of anions in layered double hydroxides: Effects on dispersion and fire properties, *Polym. Degrad. Stab.* 94 (5) (2009) 770-781.

Wang, L., Xie, X., Su, S., Feng, J. and Wilkie, C. A., A comparison of the fire retardancy of poly(methyl methacrylate) using montmorillonite, layered double hydroxide and kaolinite, *Polym. Degrad. Stab.* 95 (4) (2010) 572-578.

Wang, M., Zhu, X., Wang, S. and Zhang, L., Surface pattern in thin poly(styrene-maleic anhydride) films, *Polymer,* 40 (26) (1999) 7387-7396.

Wang, N., Gao, N., Jiang, S., Fang, Q. and Chen, E., Effect of different structure MCM-41 fillers with PP-g-MA on mechanical and crystallization performances of polypropylene, *Composites: Part B,* 42 (6) (2011) 1571-1577.

Wang, N., Zhang, J., Fang, Q. and Hui, D., Influence of mesoporous fillers with PP-g-MA on flammability and tensile behaviour of polypropylene composites, *Composites: Part B*, 44 (1) (2013) 467-471.

Wang, Q., Zhang, X., Wang, C.J., Zhu, J., Guo, Z. and O'Hare, D., Polypropylene/layered double hydroxide nanocomposites, *J. Mater. Chem*. 22 (2012) 19113-19121.

Wang, X.D. and Zhang, Q., Effect of hydrotalcite on the thermal stability, mechanical properties, rheology and flame retardance of poly (vinyl chloride), *Polym. Int.* 53 (6) (2004) 698-707.

Wang, Y., Shen, H., Li, G. and Mai, K., Effect of interfacial interaction on the crystallization and mechanical properties of PP/nano-$CaCO_3$ composites modified with compatibilizers, *J. Appl. Polym. Sci.* 113 (3) (2009) 1584-1592.

Wei, S., Sampathi, J., Guo, Z., Anumandla, N., Rutman, D., Kucknoor, A., James, L. and Wang, A., Nanoporous poly(methyl methacrylate)-quantum dots nanocomposite fibers toward biomedical applications, *Polymer*, 52 (25) (2011) 5817-5829.

Wei'an, Z., Xiaofeng, S., Yu, L. and Yue'e, F., Synthesis and characterization of poly(methyl methacrylate) OMMT nanocomposites by γ-ray irradiation polymerization, *Rad. Phys. Chem*. 67 (5) (2003) 651-656.

Wimalasiri, Y., Fan, R., Zhao, X.S. and Zou, L., Assembly of Ni-Al layered double hydroxide and graphene electrodes for supercapacitors, *Electrochim. Acta*. 134 (10) (2014) 127-135.

Xu, S., Zhang, L., Lin, Y., Li, R. and Zhang, F., Layered double hydroxides used as flame retardant for engineering plastic acrylonitrile-butadiene-styrene (ABS), *J. Phys. Chem. Solids*, 73 (12) (2012) 1514-1517.

Yamagata, S., Hamba, Y., Akasaka, T., Ushijima, N., Uo, M., Iida, J. and Watari, F., The effect of enhancing the hydrophobicity of OMMT on the characteristics of PMMA/OMMT nanocomposites, *Appl. Surf. Sci*. 262 (1) (2012) 56-59.

Yano, K., Usuki, A and Okada, A., Synthesis and properties of polyimide-clay hybrid films, *J. Polym. Sci., Part A: Polym. Chem.* 35 (11) (1997) 2289-2294.

Yeom, E., Kim, W., Kim, J., Lee, S.S. and Park, M., Synthesis and characterization of poly(methyl methacrylate)/montmorillonite nanocomposites by emulsifier-free emulsion polymerization, *Mol. Cryst. Liq. Cryst.* 425 (1) (2004) 85-91.

Yoo, S.J., Lee, S.W., Jeon, M., Lee, H.S. and Kim, W.N., Effects of compatibilizers on the mechanical, morphological, and thermal properties of poly(propylene carbonate)/poly(methyl methacrylate) blends, *Macromol. Res*. 21 (11) (2013) 1182-1187.

Zannetti, M., Canuino, G., Reichert, P. and Mulhaupt, R., Thermal behaviour of poly(propylene) layered silicate nanocomposites, *Macromol. Rapid Commun*. 22 (3) (2001) 176-180.

Zhang, H.B., Zheng, W.G., Yan, Q., Jiang, Z.G. and Yu, Z.Z., The effect of surface chemistry of graphene on rheological and electrical properties of polymethylmethacrylate composites, *Carbon*, 50 (14) (2012) 5117-5125.

Zhang, F.A., Lee, D.K. and Pinnavia, T.J., PMMA-mesocellular foam silica nanocomposites prepared through batch emulsion polymerization and compression molding, *Polymer*, 50 (20) (2009) 4768-4774.

Zhang, Q., Wang, K., Men, Y. and Fu, Q., Dispersion and tensile behavior of PP/MMT nanocomposites produced via melt intercalation. *Chin. J. Poly. Sci.* 21 (3) (2003) 359-367.

Zhao, C., Yang, X., Wu, X., Liu, Z., Wang X. and Lu, L., Preparation and characterization of poly(methyl methacrylate) nanocomposites containing octavinyl polyhedral oligomeric silsesquioxane, *Polym. Bull.* 60 (4) (2008) 495-505.

Zheng, X., Jiang, D. D. and Wilkie, C. A., Methyl methacrylate oligomerically-modified clay and its poly(methyl methacrylate) nanocomposites, *Thermochim. Acta.* 435 (2) (2005) 202-208.

Zhou, C., Si, Q., Aa, Y., Tan, Z., Sun, S., Zhang, M. and Zhang, H., Effect of matrix composition on the fracture behaviour of rubber-modified PMMA/PVC blends, *Polym. Bull.* 58 (5) (2007) 979-988.

Zhou, Z., Wang, S., Lu, L., Zhang, Y. and Zhang, Y., Preparation and rheological characterization of poly (methyl methacrylate)/functionalized multi-walled carbon nanotubes composites, *Compos. Sci. Technol.* 67 (9) (2007) 1861-1869.

Zhu, H., Liu, Q., Li, Z., Liu, J., Jing, X. Zhang, H. and Wang, J., Synthesis of exfoliated titanium dioxide nanosheets/nickel-aluminum layered double hydroxide as a novel electrode for supercapacitors, *RSC Adv*. 61 (5) (2015) 49204-49210.

Zhu, J., Start, P., Mauritz, K.A. and Wilkie, C.A., Thermal stability and flame retardancy of poly(methyl methacrylate)-clay nanocomposites, *Polym. Degrad. Stab.* 77 (2) (2002) 253-258.

Zhu, J., Uhl, F.M., Morgan, A.B., Wilkie, C.A., Studies on the mechanism by which the formation of nanocomposites enhances thermal stability, *Chem. Mater.* 13 (12) (2001) 4649-4654.

Zhu, L.P., Yi, Z., Liu, F., Wei, X.Z., Zhu, B.K. and Xu, Y.Y., Amphiphilic graft copolymers based on ultrahigh molecular weight poly(styrene-*alt*-maleic anhydride) with poly(ethylene glycol) side chains for surface modification of polyether sulfone membranes, *Eur. Polym. J.* 44 (6) (2008) 1907-1914.

Research Publications

List of Publications

In Journals:

1. Manish Kumar, Pradeep Upadhyaya and G. Pugazhenthi, Fabrication of PMMA nanocomposites with modified nanoclay by melt intercalation, *Composites Interface*, 21 (2014) 819-832.
2. Vijay Kumar, Manish Kumar and G. Pugazhenthi, Effect of nanoclay content on the structural, thermal properties and thermal degradation kinetics of PMMA/organoclay nanocomposites, *International Journal of Nano and Biomaterials*, 5 (2014) 27-44.
3. Samarshi Chakraborty, Manish Kumar, Kelothu Suresh and G. Pugazhenthi, Influence of organically modified Ni-Al layered double hydroxide (LDH) loading on the rheological properties of poly (methyl methacrylate) (PMMA)/LDH blend solution, *Powder Technology*, 256 (2014) 196-203.
4. Manish Kumar, S. Arun, Pradeep Upadhyaya and G. Pugazhenthi, Properties of PMMA/clay nanocomposites prepared using various compatibilizers, *International Journal of Mechanical and Materials Engineering*, 10 (2015) 7.
5. Manish Kumar, Vivek Chaudhary, Kelothu Suresh and G. Pugazhenthi, Synthesis and characterization of exfoliated PMMA/Co-Al LDH nanocomposites via solvent blending technique, *RSC Advances*, 5 (2015) 39810-39820.
6. Samarshi Chakraborty, Manish Kumar, Kelothu Suresh and G. Pugazhenthi, Investigation of structural, rheological and thermal properties of PMMA/ONi-Al LDH nanocomposites synthesized via solvent blending method: Effect of LDH loading, *Chinese Journal of Polymer Science*, 34 (2016) 739-754.
7. Manish Kumar, Vijay Kumar, A. Muthuraja, S. Senthilvelan and G. Pugazhenthi, Influence of nanoclay on the rheological properties of PMMA/organoclay nanocomposites prepared by solvent blending technique, *Macromolecular Symposia*. 365 (2016) 104-111.
8. Manish Kumar, N. Shanmuga Priya, S. Kanagaraj and G. Pugazhenthi, Rheological investigation of PMMA/clay nanocomposites prepared via melt-blending technique, *Nanocomposites*, 2 (2016) 109-116.
9. Manish Kumar and G. Pugazhenthi, Morphological, mechanical and thermal degradation kinetics of PMMA/Co-Al LDH nanocomposites fabricated by melt intercalation technique, *Composites Science & Technology* (Under Review).

10. Manish Kumar and G. Pugazhenthi, Influence of organically modified Cu-Cr layered double hydroxide (LDH) on the structural, mechanical and thermal characteristics of PMMA nanocomposites (to be communicated).

In Conferences:

1. Manish Kumar, Vijay Kumar, Pradeep Upadhyaya and G. Pugazhenthi, Mechanical properties of PMMA/organoclay nanocomposites prepared via melt intercalation technique, *International Conference on Materials Science and Technology (ICMST 2012)*, 10-14 June 2012, St. Thomas College Pala, Kottayam, Kerala.
2. Vijay Kumar, Manish Kumar and G. Pugazhenthi, Kinetics of thermal degradation of PMMA/organoclay nanocomposites: Effect of nanoclay loading, *2nd International Conference on Process Engineering and Advanced Material (ICPEAM 2012)*, 12-14 June 2012, Kuala Lumpur, Malaysia.
3. Manish Kumar, A. Muthuraja and G. Pugazhenthi, Tribological studies of PMMA nanocomposites with organoclay reinforcements, *First Symposium on Advances in Sustainable Polymers*, 10-11 January 2014, IIT Guwahati, Assam, India.
4. Manish Kumar, S. Arun, Pradeep Upadhyaya and G. Pugazhenthi, Role of various compatibilizers on the properties of PMMA/clay nanocomposite, *International Conference on Advances In Materials and Processing Technology (AMPT-2014)*, 16-20 November 2014, Dubai, UAE.
5. Manish Kumar, Samarshi Chakraborty, Kelothu Suresh and G. Pugazhenthi, Influence of Cu-Cr layered double hydroxide (LDH) on the rheological properties and thermal degradation kinetics of PMMA nanocomposites, *American Institute of Chemical Engineers (AIChE) Annual Meeting*, 08-13 November 2015, Salt Lake City, USA.

Appendix

AFM 2D Images of PMMA Nanocomposites

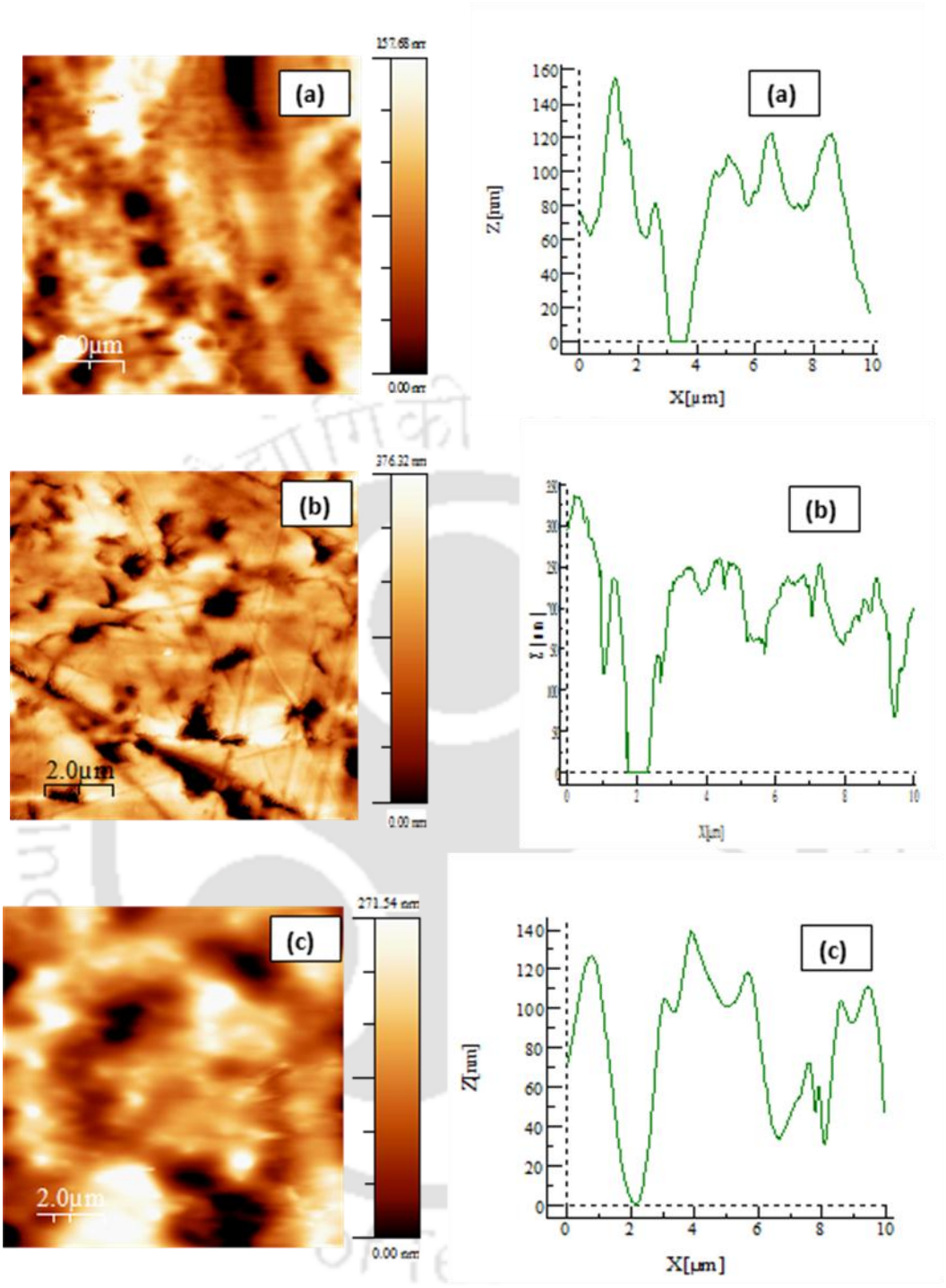

(i) AFM 2-D images of (a) Neat PMMA, (b) PMMA-5 and (c) PMMA-5-G nanocomposites

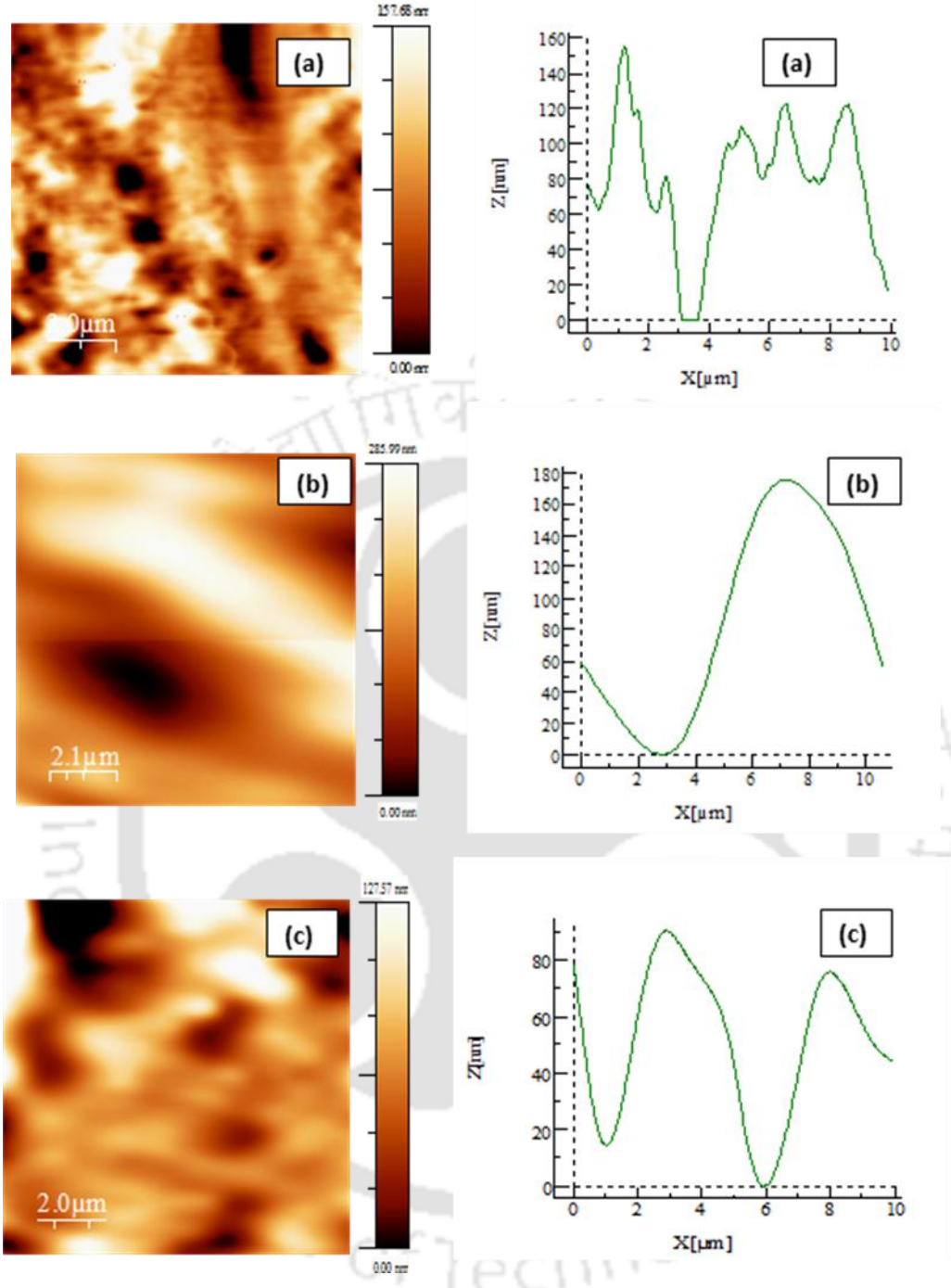
(a)
157.68 nm
0.00 nm
Z[nm]
X[µm]
(b)
285.99 nm
2.1µm
(c)
127.57 nm
2.0µm

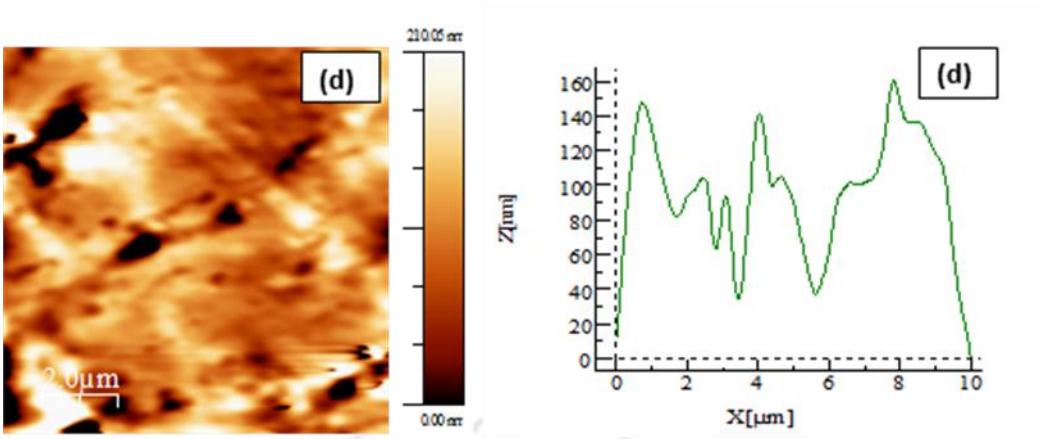

(ii) AFM 2-D images of (a) Neat PMMA, (b) PMMA-5-PP, (c) PMMA-5-PE and (d) PMMA-5-PS nanocomposites

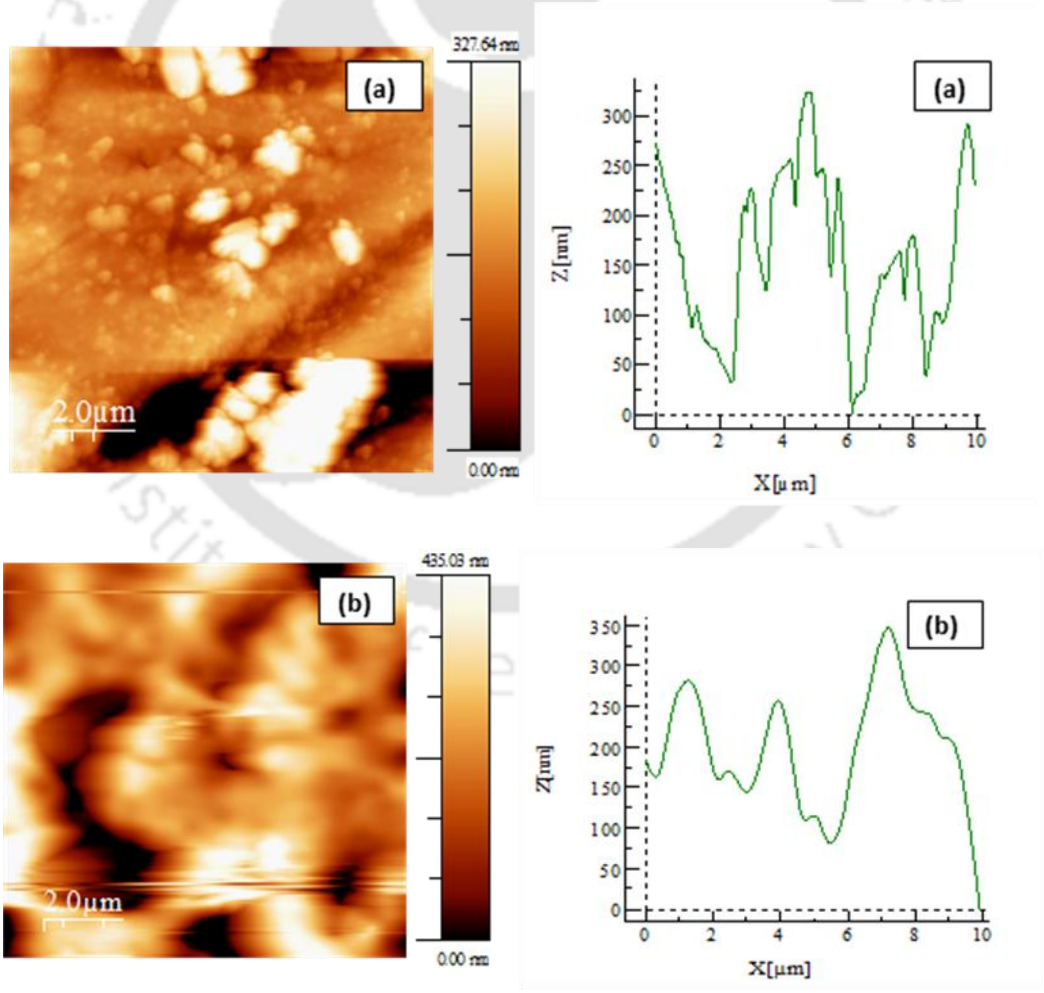

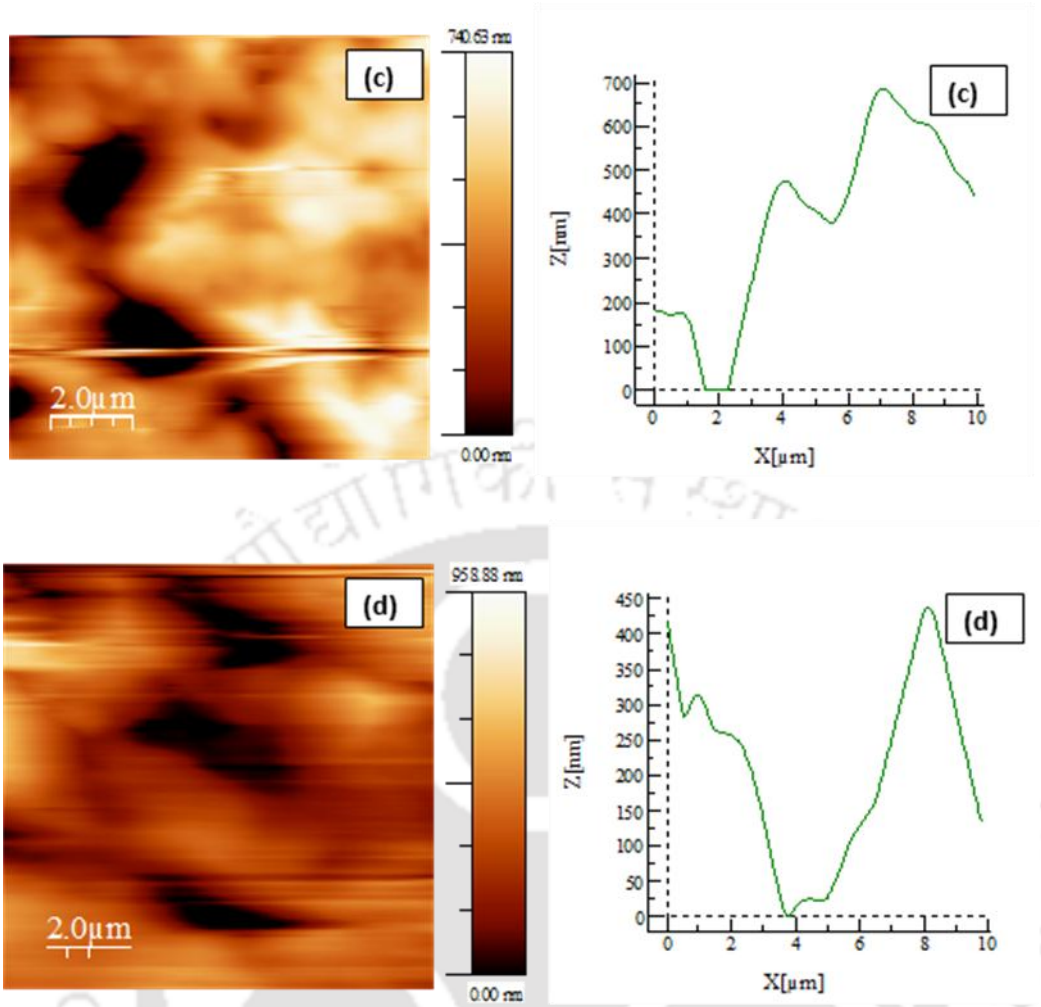

(iii) AFM 2-D images of (a) PMMA/Co-Al 1%, (b) PMMA/Co-Al 3%, (a) PMMA/Co-Al 5% and (d) PMMA/Co-Al 7% nanocomposites

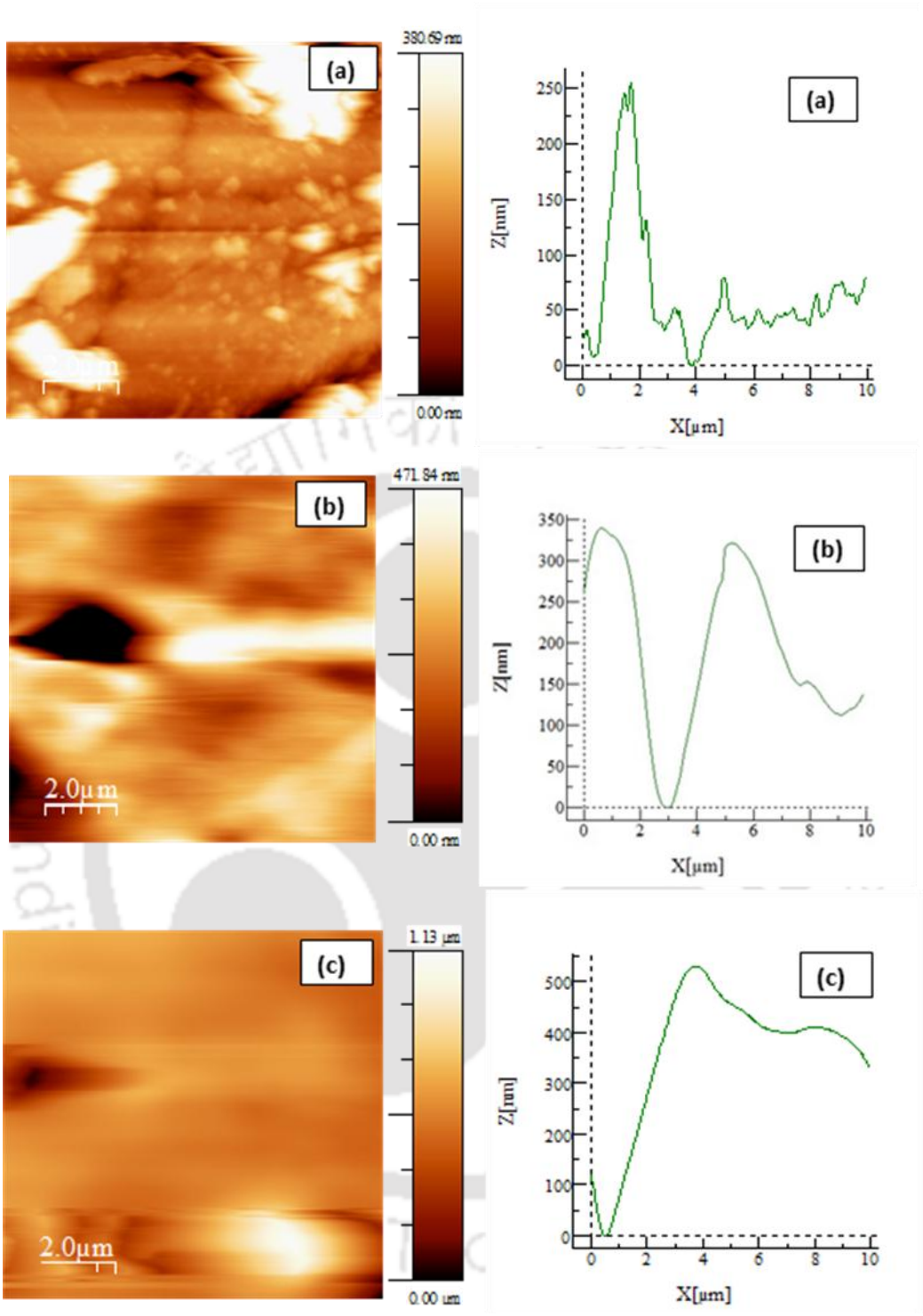
(a)
380.69 nm
0.00 nm
Z[nm]
X[µm]
(b)
471.84 nm
2.0µm
0.00 nm
Z[nm]
X[µm]
(c)
1.13 µm
2.0µm
0.00 µm
Z[nm]
X[µm]

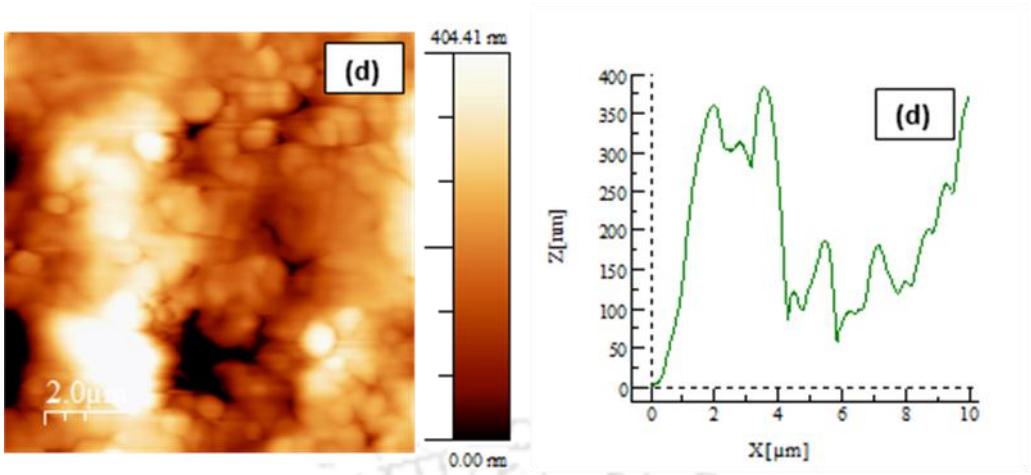

(iv) AFM 2-D images of (a) PMMA/Cu-Cr 1%, (b) PMMA/Cu-Cr 3%, (c) PMMA/Cu-Cr 5% and (d) PMMA/Ni-Al 5% nanocomposites

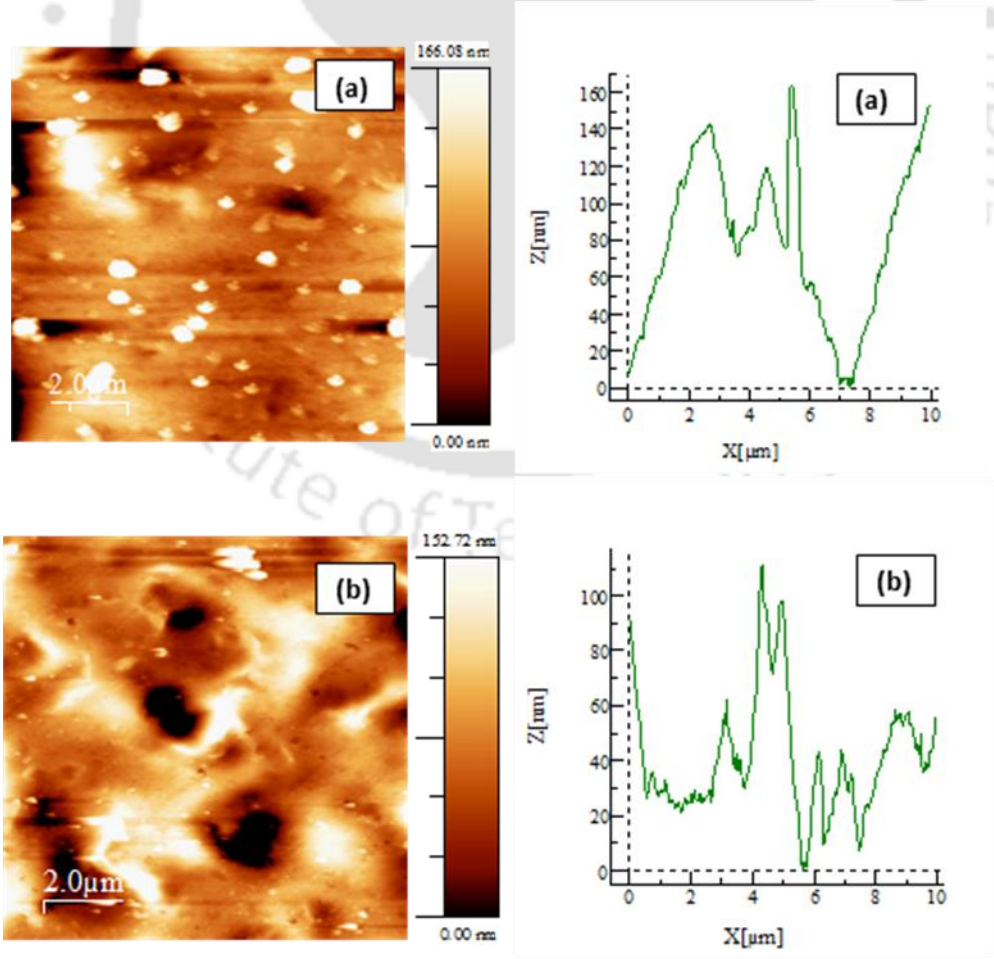

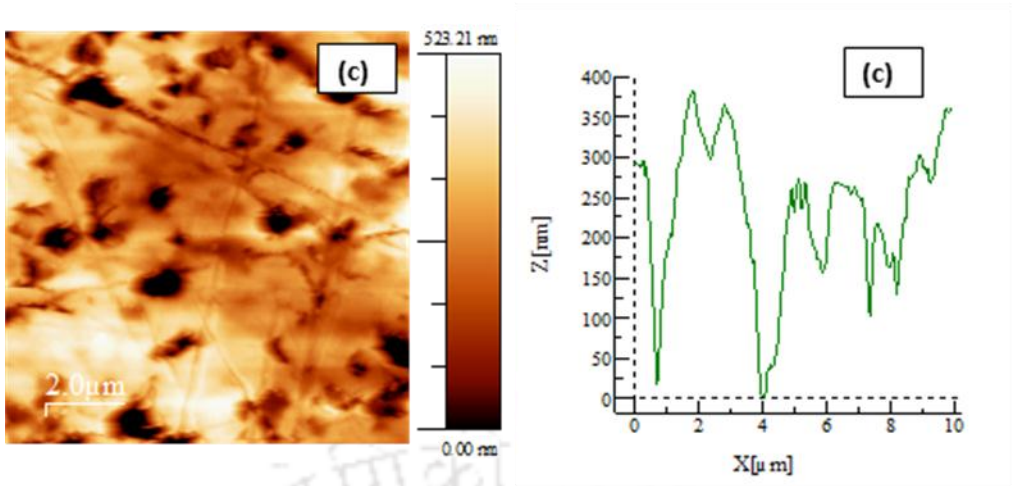

(i) AFM 2-D images of (a) PMMA/clay 3, (b) PMMA/clay 5 and (c) PMMA/clay 7 nanocomposites

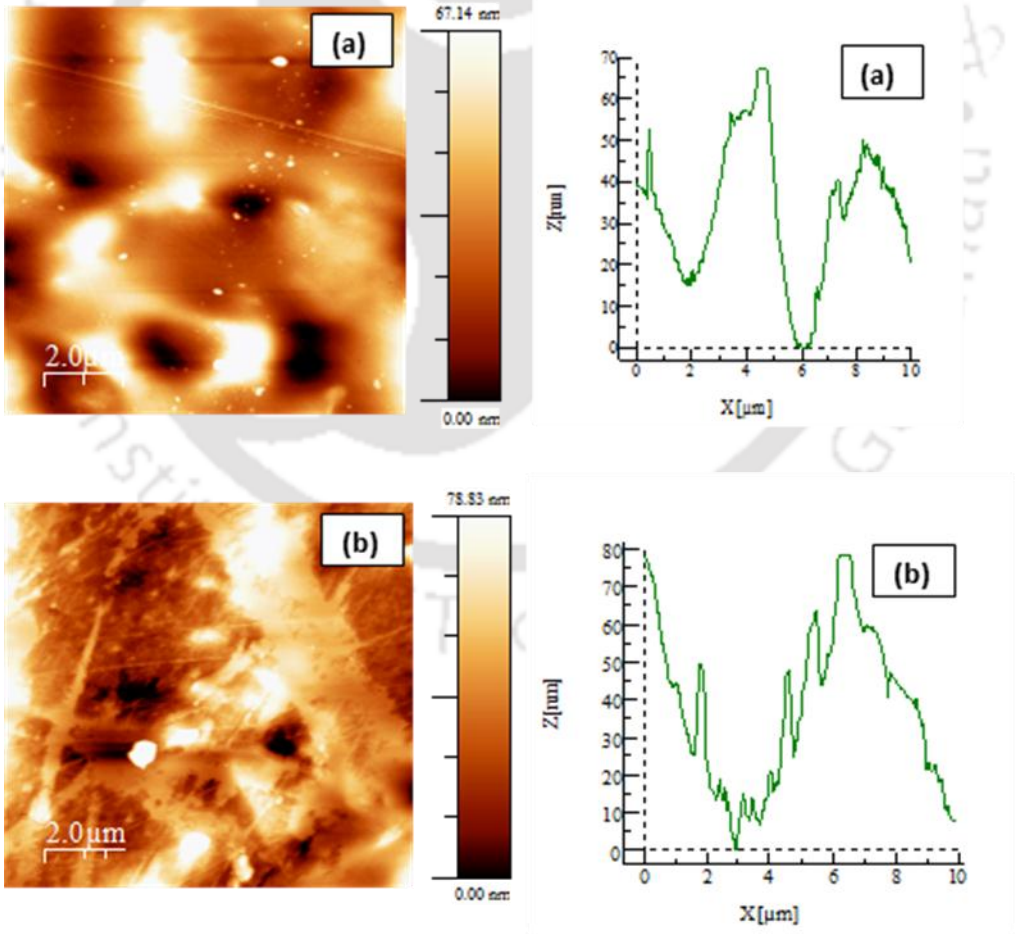

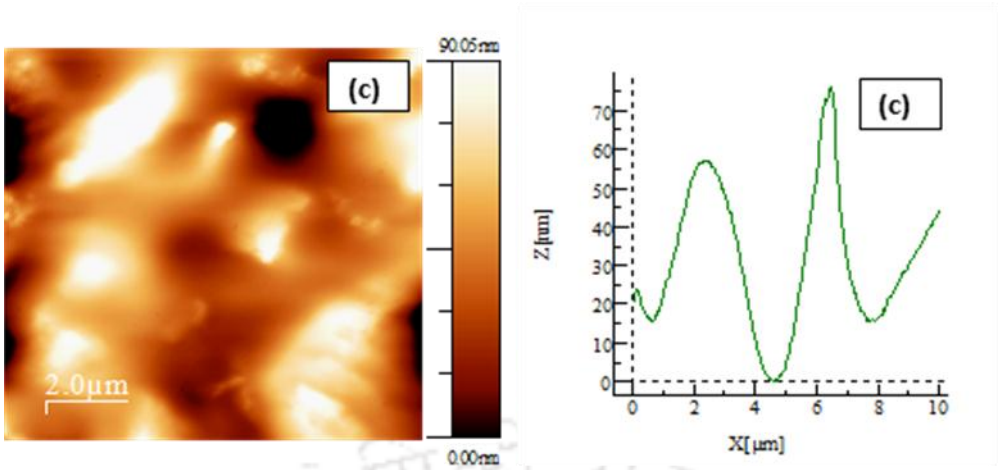

(ii) AFM 2-D images of (a) PMMA/Ni-Al 3, (b) PMMA/Ni-Al 5 and (c) PMMA/Ni-Al 7 nanocomposites

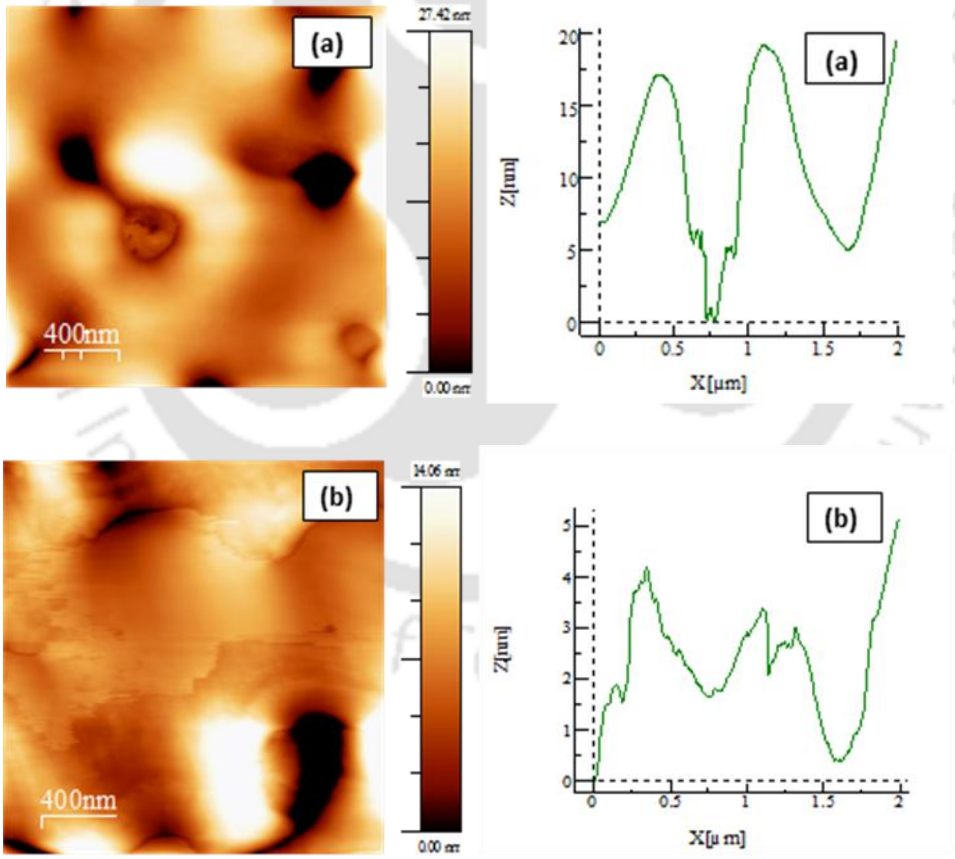

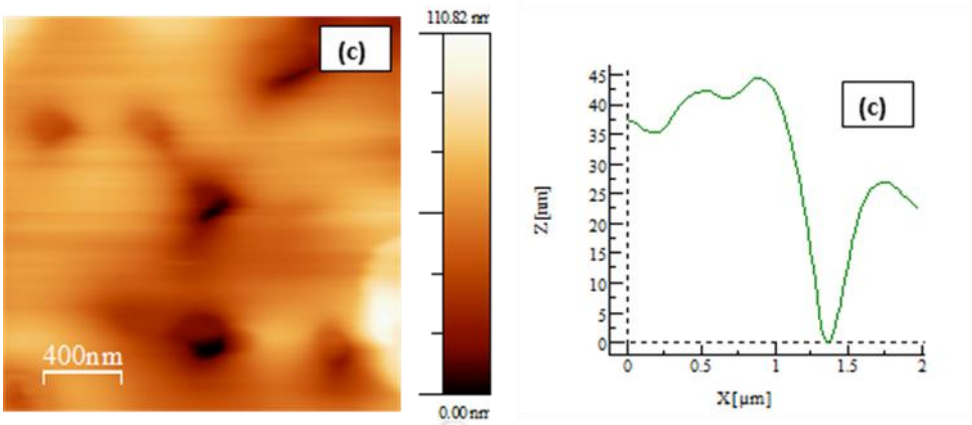

(iii) AFM 2-D images of (a) PMMA/Co-Al 3, (b) PMMA/Co-Al 5 and (c) PMMA/Co-Al 7 nanocomposites

Curriculum Vitae

Manish Kumar

Date of Birth: August 16, 1986

Email: manish.kamal07@gmail.com
manish.kr@iitg.ernet.in

Permanent Address: S/o Sh. Ram Khilawan
House 148, Sector-1,
Jagriti Vihar, Garh Road
Meerut - 250005
Uttar Pradesh, India

Education:

Ph.D. (2016)
Department of Chemical Engineering,
Indian Institute of Technology Guwahati
Guwahati - 781039, Assam, India

M.Tech. (2010)
Plastics Engineering,
Central Institute of Plastics Engineering and Technology
Lucknow, India

M.Sc. (2006)
Polymer Science and Chemical Technology,
Chaudhary Charan Singh University
Meerut, India